A COMPARISON OF THE PERFORMANCE ON NEW AND USED COMMON RAIL DIESEL INJECTORS

Stephen Douglas Grover

A research report submitted to the Faculty of Engineering and the Built Environment, University of the Witwatersrand, Johannesburg in partial fulfilment of the requirements for the degree of Master of Science in Engineering.

Johannesburg, 2012

Declaration

I declare that this research report is my own unaided work. It is being submitted to the Degree of Master of Science to the University of the Witwatersrand, Johannesburg. It has not been submitted before for any degree or examination to any other University.

_____

(Signature of Candidate)

On this ____day of _____2012

Abstract

An investigation was conducted into the effects of wear on the performance of common-rail fuel injectors, in terms of flow and spray characteristics. The investigation conducted involved the testing of four used injectors, and the comparison of the performance of these injectors with that of an identical brand new injector. The used injectors had deteriorated in different ways, with solenoid wear, mechanical wear in the body of the injector, and mechanical wear in the upper section of the injector being identified. All of the manners of deterioration affected the flow characteristics. The solenoid wear and mechanical wear in the body did not affect the spray performance, but wear in the upper section of the body and a combination of wear in the body and solenoid did affect spray performance. A correlation was developed between the spray penetration of the new injector and the spray theories according to Dent and Hiroyasu.

This work is dedicated to my grandfather,

Walter Jardine

A great man and an insightful engineer

Your words of encouragement and advice will stay with me always

Acknowledgments

I would like to thank my supervisor Professor D Cipolat for the opportunity to conduct this research project. Without his ongoing support, patience and guidance this project would not have been possible.

In addition, I would like to thank my family, friends and colleagues for their ongoing encouragement and support throughout the duration of this project.

Contents

List of Figures

Nomenclature

Greek Symbols

θ	Spray Cone Angle
ρ	Density of atmosphere

Variables

A	Area
C_d	Discharge Coefficient
d	Diameter
m	Mass
L	Length
P	Pressure
S	Spray Penetration
t	Time
T	Temperature
U	Velocity

Subscripts

a	Atmosphere
break	Point associated with jet break up time
eff	Effective
f	Fluid
i	Inner
o	Orifice
O	Outter
n	Nozzle
s	Displacement
th	Theoretical

Chapter 1

Introduction

This research is concerned with the comparison of the performance of new and used common-rail injectors, with regard to flow and spray characteristics. Background to the use of common-rail injectors, the reasons for their use, motivation for the research conducted and an outline of the research methodology used is given.

1.1 Background

Over the past two decades much development has taken place into compression ignition injection systems. Injection pressures have been consistently increasing since 1975 [9], and the introduction of the common-rail injector in 1997, by Bosch, marked a major development in the improvement of the compression ignition engine [34].

The development which as been done on compression ignition engines is motivated by two main factors. The reduction in specific fuel consumption, and the reduction in engine emissions. The desire to reduce fuel consumption is driven by increasing oil prices, reduced supply, and the requirements for reduced emissions is driven by guidelines published by the Environmental Protection Agency (EPA)

in America, and the European Unions Environmental Agency (EEA). The EPA's guidelines take the form of Tiers 1 to 3, and the EEA's guidelines take the form of Euro 1-6 [25].

It is challenging to meet the increasingly stringent emissions requirements while maintaining or improving engine performance [24]. Reduction in emissions produced is a balancing act between engine output, noise and fuel consumption , and requires the optimisation of these factors [30].

Increasing the pressure supplied to the injector allows for finer sprays to be producted by the injector, leading to increased entraining of the fuel and air, and thus more efficient combustion and reduced emissions [21]. Developments have also been made as regards the behaviour of the combustion within the cylinder when subjected to more refined injection strategies, incorporating pilot and post-combustion injections. The implementation of these injection regimes requires injection timing to be independent of engine speed and load.

The common-rail fuel injector, as introduced by Bosch, and now in use in most compression ignition engines allows for increased fuel injection pressures, and the removal of the dependence of injection timing and pressures on engine speed and load. This allows the designer of an engine or fuel injection systems to take advantage of the developments described above.

1.2 Motivation

It has been proved that common-rail injection systems produce sprays which are conducive to improved fuel consumption as well as reduced emissions and noise, as required by the EPA and EEA guidelines. However, while these injectors produce consistent and efficient results when new, little is known about the manner in which these injectors wear, and how their performance deteriorates.

In order to sustain the improvements made to performance of engines due to the

application of common-rail injectors across the life span of an engine it is important to understand how these injectors deteriorate, and to understand the drivers for this. An understanding of this could allow for means to be introduced to reduce the likelihood of wear, as well as identifying means to rehabilitate injectors.

1.3 Methodology

The performance of new and used injectors will be compared with regard to both flow and spray characteristics. A selection of four used injections were tested. The factors leading to the deterioration in the performance of the injectors will be determined through looking at the spray characteristics, and the ability of the injectors to deliver fuel effectively will be discussed in the spray analysis.

An analysis was conducted into the theoretical models for spray behaviour. Modifications were made to these theories to improve the compliance of the data acquired during this research. Suggestions were made as to reasons for the differences between the original and modified theories.

Finally conclusions were drawn from the discussions made and recommendations for future research were made.

Chapter 2

Literature Review

2.1 Introduction

The following section provides a review of literature relating to injector design, injector spray behaviour, and injector test facilities. The majority of literature covered was in the form of journal papers, although relevant text books were consulted where available.

Literature largely focuses on the behaviour of the injector with varying injector parameters. Parameters affecting the behaviour of the spray are listed below [25]:

- Injection Pressure
- In-Cylinder Pressure
- In-cylinder Density
- Orifice Geometry
- In-cylinder Swirl
- In-Cylinder Temperature
- Fuel Temperature

- Cavitation
- Fuel Composition

In the literature review, the manner in which the above parameters have been shown to affect the behaviour of the spray is presented.

2.2 Injector Spray Structure

A spray is produced by an injector when pressure is introduced on the inside of the injector's orifices, causing the fuel to flow outward. The flow becomes turbulent as it leaves the nozzle orifice, and becomes entrained with air [13].

Macroscopically, the spray may be descibed in terms of two key parameters: Cone Angle and Spray Penetration. These parameters are illustrated in Figure 2.1.

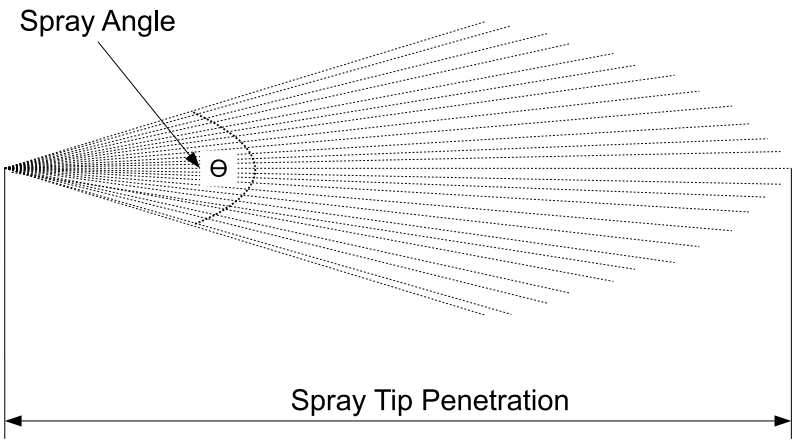

Figure 2.1: Key Parameters in a Spray [13]

The spray structure may be divided into two sections, the steady section and the transient section. These two sections are shown in Figure 2.2. The steady section

of the spray accounts for around 70% of the total spray penetration. Also indicated in Figure 2.2 is the region contained within the spray known as the "Initial Region", or non-purturbed zone. This initial region is what comprises the spray characteristic known as the liquid length, as discussed in Section 2.3 below. [17]

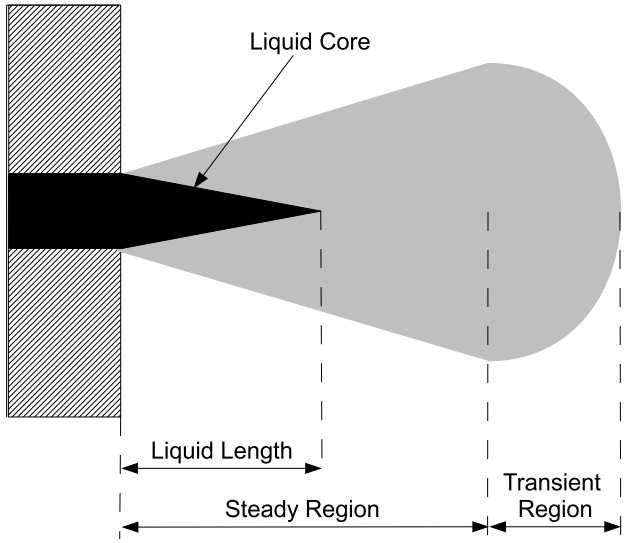

Figure 2.2: Structure of Injector Spray [17]

As the spray develops, vortices are formed at the tip of the spray, as illustrated below in Figure 2.3. These vortices are what gives the spray its mushroom like appearance [14], as well as explaining the effect whereby the spray may be observed to "peel" back upon itself [9] - a phenomenon which is sometimes observed in images of spray formation.

The progression of a spray may be divided into four significant phases [3]:

1. *Opening Transient Phase.*[1]

2. *Propagation of the liquid core into the surrounding atmosphere.*

[1]This phase is governed by the motion of the injector needle, along with the time dependent orifice opening time.

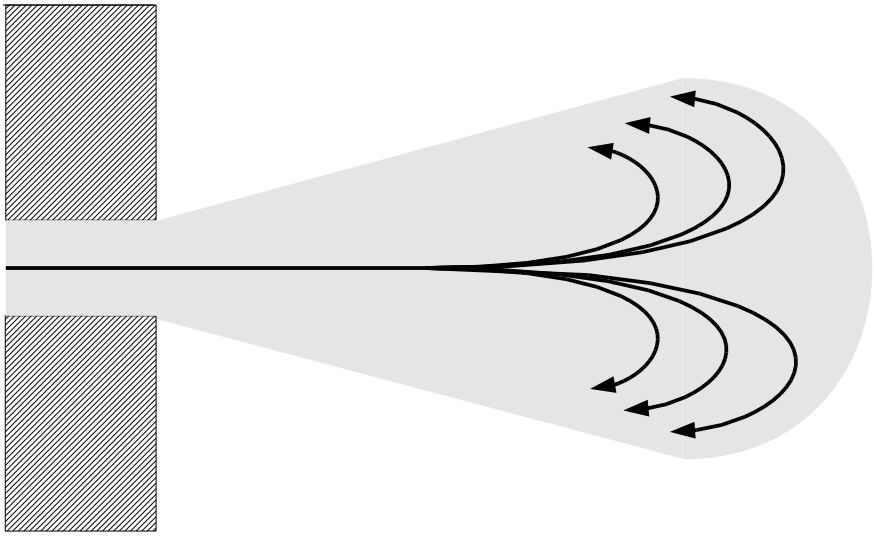

Figure 2.3: Illustration of vortex spray vortex formation [14]

3. *Droplet break-up stage.*

4. *Propagation of droplet clouds.*

The behaviour of the spray in phases 2, 3 and 4 may be described as follows: Initially the velocity of the spray is much faster than the speed of the ambient air, and is thus affected little by it. During stage 3, the velocities of the air and the injected fuel are comparable and during stage 4 the velocity of the agitated air is higher than that of the fuel.

2.3 Spray Penetration

Spray penetration is probably the most researched facet of injector spray structure. Spray penetration, as well as the rate at which the spray penetrates into the combustion chamber are important because they have a direct effect upon the extent to which air within a cylinder is used in the combustion process [13]. The criterion

used to determine the ideal ultimate spray penetration, for a specific application, is whether or not the spray will begin to impinge on the walls of the cylinder or the piston [33]. Whether this impingement is desirable or not is dependent upon in cylinder conditions and temperatures, and may thus be accounted for during the design of the engine [13].

2.3.1 Fundamental Equations

Much research is aimed at attempting to develop an expression, or relationship which effectively predicts the behaviour of the spray, and the manner in which the various parameters detailed in Section 2.1 affect spray penetration.

Through the use of Bernoulli's famous equation [25], along with the application of dimensional analysis the following relationship may be derived [25]:

$$S(t) = k\rho_a^{-\frac{1}{4}}\Delta P^{\frac{1}{2}}t^{\frac{1}{2}}d_o^{\frac{1}{2}} \tag{2.1}$$

In the case where this equation was applied, the coefficient k was found to be 1.895×10^{-3}, and exponents were found to vary slightly from those presented in equation 2.1.

The relationship presented in equation 2.1 bears a strong relationship to that proposed and published by Dent [10], in 1971. This relationship, shown below in equation 2.2, is still used as a benchmark in many technical papers published today.

$$S(t) = 3,07\left(\frac{\Delta P}{\rho_g}\right)^{\frac{1}{4}}(td_n)\left(\frac{294}{T_g}\right)^{\frac{1}{4}} \tag{2.2}$$

Dent's equation remains the only commonly applied relationship which takes into account the effects of the temperature within the combustion chamber [9]. This is important as changes in combustion chamber temperature can result in changes in

penetration of up to 20%.

As a development of equation 2.2, Hiroyasu *et al*, published their proposed relationship, as shown below in equations 2.3 - 2.5 [13]. This relationship divides the spray into two distinct ranges: that before spray break-up, and that after spray break-up. It was found that the spray penetration before break-up increases linearly with time and after spray break-up the penetration is proportional to the square-root of time. The relationship is shown as follows:

$$t < t_{break}: \qquad S(t) = 0.39\left(\frac{2\Delta P}{\rho_l}\right)^{\frac{1}{2}} t \tag{2.3}$$

$$t > t_{break}: \qquad S(t) = 2.95\left(\frac{\Delta P}{\rho_g}\right)(d_n t)^{\frac{1}{2}} \tag{2.4}$$

where:

$$t_{break} = \frac{29\rho_l d_n}{(\rho_g \Delta P)^{\frac{1}{2}}} \tag{2.5}$$

Various researchers have modified the coefficients presented in Hiroyasu's penetration equation so as to achieve results which better fit their data [25], [3], [7].

2.3.2 Modern Application of Fundamental Equations

The generally accepted relationships developed by Dent and Hiroyasu were developed in 1971 and 1980 respectively, well before the advent of the modern common rail. A question thus arises as to whether these theories will accurately predict the behaviour of a common-rail injector, given that the pressures present in a common-rail may be as high as 2500bar [24] in experimental cases and as high as 1800bar in automotive applications [34] [31].

Various researchers have applied these equations to their test results when using common-rail injection systems and have found good correlations [25], [3], [6], [9],

which allows the assumption that the equations developed for use on mechanical fuel injectors may also applied to common rail fuel injectors as well.

Tests have also been conducted to test the validity of these equations at very high injection pressures, up to 2500bar. Good correlation was found [11] especially to Dent's equation.

However, it is noteworthy that there are documented cases of Dent's equation, when applied to common rail injection systems, following the spray penetration trend well, but overpredicting the penetration, in unmodified form [6], [8].

Some common rail injection researchers have achieved good results through the use of only Hiroysau's second equation, as shown in 2.4. This is done since it has been found that in certain cases the region where the spray advances linearly with time does not exist, or at least is not identified [8].

Fluctuations in Spray Penetration found in measured data may be due to spray instabilities where sections of spray are breaking off [21], or due to fluctuations in rail pressure [7]. These situations which were not taken into account when the theories were developed but affect the results achieved, and thus need to be borne in mind when analysing experimental results.

Another factor which needs to be taken into account when one wishes to address common rail injections and compare results, either with other tests, or with published equations, is the effect which the number of orifices the nozzle has on penetration and spray structure in general.

Experimentation has been conducted in this regard, and it was found that there was little difference between the performance of a single-hole injector and a multi-hole injector [18]. The primary motivation for conducting tests using a single-hole injector is that the spray may be more simply analysed due to lack of light interactions, and hole-to-hole interactions present within the injector.

2.3.3 Developments of fundamental equations

If one looks at the parameters which affect the penetration of a spray, as evident in equations 2.2 to 2.5, a strong dependency upon ambient pressure may be noted [25], along with a similar relationship to the change in pressure across the injector nozzle. The proportionality to the change in pressure across the nozzle, as expressed in equation 2.4, means that one should expect less of a marked increase in penetration as the pressure increases[9]. The increased pressure difference has the effect of accelerating the rate at which the spray advances through the spray chamber. This increases the chances of the spray reaching full development [23].

As will be discussed later, the rail pressure also has a positive effect upon atomization [21], droplet size distribution [9] [21] and rate of delivery [21].

As a development of Dent's equation for spray penetration, the following penetration equation was developed:

$$S(t) = \frac{2.95}{\sqrt{\sqrt{2}C_d}}\sqrt{d}\sqrt{U_{s=0}(t)t}\left(\frac{\rho_l}{\rho_g}\right)^{\frac{1}{4}} \tag{2.6}$$

Here the spray velocity at nozzle exit may be defined as:

$$U_{s=0}(t) = C_d\sqrt{\frac{2\Delta P_{inj}}{\rho_l}} \tag{2.7}$$

The above expression is similar to Dent's equation, but the introduction of the spray velocity close to the nozzle is new. This velocity is determined through the use of equation 2.7 which is developed through the use of Bernoulli's equation, and the injector's discharge coefficient, (C_d) [23]. The injector's discharge coefficient may be determined through the use of equation 2.8 below [26]:

$$C_d = \frac{m_f}{A_n\sqrt{2\Delta P\rho_f}} \tag{2.8}$$

The same theory may be used to determine the spray-tip velocity. Equation 2.9 below is found through the differentiation of Dent's Equation:

$$U_s(t) = \frac{2.95}{2}\left(\frac{\Delta P_{inj}}{\rho_g}\right)^{\frac{1}{4}}\left(\frac{d}{t}\right) \tag{2.9}$$

A further documented point of interest regarding spray tip penetration is the rate of increase of penetration. Initially, before 0.3ms after Start of Injection (SOI), the rate of increase of penetration is found to increase with increasing rail pressure, but after this time, the rate of spray penetration increase tends to decrease with respect to rail pressure [7], [6]. This effect is likely to be due to the interaction of the spray with ambient gas, both with regard to aerodynamic drag, as well as heat transfer effects [24]. Turbulent energy, such as that from swirl or squish, also acts to reduce spray penetration [16].

2.3.4 Spray Liquid Length Behaviour

While the above theory all relates to the penetration of the tip of the spray, which is often determined through light intensity, a second field of research within spray penetration is focused on the penetration of the liquid core of the spray. This is most often described as the liquid length of the spray, and is illustrated in Figure 2.2, on page 6.

Studies into the liquid-length are valuable since the liquid core represents a region of the spray where there is little air entrained, and therefore the fuel is unlikely to combust. The size of the liquid core also has an effect on the ability of the fuel to ignite automatically.

The liquid core typically reaches a stable length in an injection, with injection parameters, specifically the injection pressure playing a central role in the time which it takes for a spray to reach this stable state [26]. A relationship linking nozzle parameters with spray liquid-length is presented below in equation 2.10 [23]. As in the case of the entire spray, liquid length penetration rates are elevated

in the case of increased rail pressure.

$$LL = \frac{K_p^2 \left(\frac{1}{4}\right)^{\frac{1}{2}} \left(\frac{\pi}{4}\right)^{\frac{1}{2}} C_a^{\frac{1}{2}} D_o \rho_f^{\frac{1}{2}}}{C_{mv} \rho_a^{\frac{1}{2}}} \tag{2.10}$$

where:

$$K_p = K \left\{ tan\left(\frac{\theta}{2}\right) \right\}^{-\frac{1}{2}} \tag{2.11}$$

The above equations clearly illustrate the effect that spray angle has on the liquid length of a spray and its burning potential, since it may be seen that a greater spray angle indicates a smaller liquid length. Therefore, a larger spray angle leads to more effective burning of the fuel.

2.4 Spray Angle

As the spray leaves the orifice of the injector, it entrains air and expands. At the same time it tends to atomize, as discussed in section 2.5 below. As the spray moves further away from the orifice through which it is being discharged the spray entrains more and more air, and so it expands. This gives rise to the conical shape of the spray. An illustration of the spray angle is shown in Figure 2.1, in Section 2.1. The spray angle gives a good idea of the amount of air entrained in the spray, and is therefore a useful measure of how well one may expect injected fuel to combust [13].

2.4.1 Fundamental Equations

In published research there is little consensus on whether a spray angle reaches a point whereby its development is independent of time. i.e: does it reach a constant steady state value? In cases where the spray was found to reach a constant value, the spray may be found to obey the following correlation [25]:

$$tan\left(\frac{\theta}{2}\right) = K\left(\frac{\rho_0}{\rho_f}\right)^{\frac{1}{2}} \tag{2.12}$$

In a well known equation, the following case is presented [13]:

$$tan\left(\frac{\theta}{2}\right) = \frac{1}{A}4\pi\left(\frac{\rho_0}{\rho_f}\right)^{\frac{1}{2}}\frac{\sqrt{3}}{6} \tag{2.13}$$

Where A is a constant determined by the nozzle geometry, and θ is measured in radians.

Another spray angle equation, also based on the format shown in equation 2.12 known as the evolutionary law, is shown below [11]:

$$\theta = \frac{360}{\pi}arctan\left(B\left(\frac{\rho_g}{\rho_l}\right)^m\right) \tag{2.14}$$

The value of B is given as 0.31 and m as 0.2, in another case B is given as 0.4275 and m as 0.5 [11].

Contrary to what one may expect, the spray angle does not bear any relationship to injection pressure [21], [11]. This is well communicated by experimentation conducted to determine the exponent present in the relationship between cone angle and injection pressure, this exponent was found to be between -0.00967 and 0.0284 [9]. With exponents this low, it is reasonable to say that there is no meaningful relationship between the two parameters.

The trend before the spray reaches a stable cone-angle, if it does at all, follows the following stages:

- **During the early stages of injection:** A large turbulent “Mushroom” is formed at the tip of the spray surrounding the central core. This typically leads to the large measured spray angles during early stages of injection.
- **During the later stages of Injection:** Air entrained in the head of the spray

inflates to form a conical head, with the regions closer to the nozzle having stabilized. This leads to the smaller spray angles associated with the later stages of a spray.

Therefore after an initially wide spray angle, it should steadily reduce [8], [7].

2.4.2 Determination of Cone Angle Optically

A problem arises in the determination of spray angle, and the comparison of spray angles published in various sources becomes difficult since there is no hard and fast rule regarding the measurement of the spray angle. Presented below is a brief outline of different theories regarding spray angle definition:

- **Acute angle of isosceles triangle:** A triangle is generated which has the same overall area, and height as the spray. These two variables allow one to determine the angle at the apex of the triangle - which becomes the injector spray angle. [24]
- **Circular Topped triangle:** An isosceles triangle is combined with a circular top, whereby a similar method is used to that in the *Acute angle of isosceles triangle* method, but instead of the flat top, the top is mathematically matched to fit the shape of the top of the cone. [24]
- **Straight Line Fit:** Two straight lines are fitted through the upstream section of the spray contour. A tangent to the contour may also be taken over which a linear fit is made.[24]
- **Halfway Point Correlation:** The width of the spray is measured halfway through the total penetration, and these two points are traced back to the point where the orifice is known to be. The angle at which these two lines meet is the spray angle. [24]
- **Naber and Siebers Method:** The cone angle is measured from two points where half of the maximum number of liquid pixels are visible, in a similar

manner to that described in the *Halfway Point Correlation* method above. [9]

2.5 Atomization

As a spray is released from the orifice, it moves away from the liquid core, and it breaks up into droplets very much smaller than the size of the orifice in the injector nozzle. This process is referred to as atomization. [13]

The atomization process is partially represented by the spray angle, as discussed above, but some advanced spray visulaisation systems, specifically those using a Doppler Particle Analyser, can masure the size of the droplets within a spray [29]. Visible light techniques are not effective for measuring the degree of atomozation [7].

From the outset, it is worth noting that the mechanisms behind atomization is not yet well understood [16]. Considerable research however, has been carried out regarding the atomization of a fuel spray, as well as investigation into the drivers for good and poor atomization performance.

It has been found that the design of the nozzle has a strong effect upon the atomization of a spray [18]. For this reason it is difficult for one to begin to set an equation to the atomization of a spray, but statements of observations may be made.

Computational Fluid Dynamics (CFD) studies as well as experimentation conducted with injectors manufactured from perspex have been performed so as to better understand how these effects manifest themselves, and how they affect spray performance. These studies, however are largely inconclusive, and provide little useful information for the testing of common fuel injectors.

Atomization is also affected by phenomenons which occur within the injector, such as turbulence, cavitiation, and the velocity profile of the flow [16], [18].

Even with the limited understanding of atomization, the main drivers for good atomization have been identified. The most marked effect on atomization is made by the injection pressure [21], [15]. Another parameter that has a profound effect on the degree of atomisation is the size of the orifices. Smaller orifices result in better atomization.

These two effects are the main drivers in the modern trend of increased common rail/injection pressure and smaller orifice holes.

Better atomization results in faster evaporation rates, and therefore reduced ignition delay [21]. These effects are desirable for good engine performance.

2.6 Cavitation

Cavitation occurs when the pressure in a liquid drops below its vapour pressure, due to flow phenomenon [32]. It is a phenomenon typically associated with processes that involve placing a fluid in a very low pressure situation, such when a pump is trying to pump water from a height far below the height of the pump.

Due to the very high velocity of the flow in an injector nozzle, cavitation has been known to occur. An illustration of cavitation in an orifice is shown below in Figure 2.4.

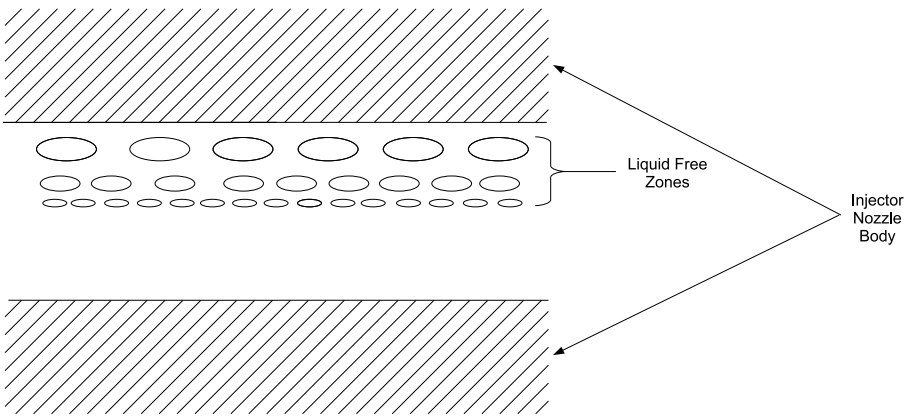

Figure 2.4: Illustration of cavitation occuring in a nozzle orifice

Cavitation in an injector may be identified through the behaviour of the flow-rate with respect to pressure. Cavitation may be said to be occurring when the fuel mass-flow rate does not increase with increasing pressure drop across the nozzle. i.e. as one increases the rail pressure one does not witness an increase in the mass-flow rate [23], as illustrated by equation 2.18 in Section 2.7. This is likely due to the fact that cavitiation has the effect of reducing the area coefficient. As the injecton pressure increases , so too does the level of cavitation, which results in a drop in area coefficient.

As in the case of atomization, it is difficult to analyse cavitation as it requires a knowledge of the flow within the injector nozzle [5]. For this reason some researchers have conducted tests using perspex nozzles, although the high pressures associated with common-rail injection systems present a challenge, and the perspex is often destroyed by the high pressure. This makes cavitation testing difficult and costly.

From research conducted, the following factors were found to have an effect upon the cavitation of an injector [18]:

- Hole Diameter
- Number of Holes
- Entrance shape of holes
- $\frac{L}{D}$ ratio of holes
- Orientation of holes with respect to nozzle axis
- C_d for nozzle
- SAC volume if applicable
- Needle lift

Besides the effects detailed above with regard to identification of cavitation in a nozzle, the following effects are also evident [18]:

- Reduced discharge coefficient
- Decrease in exit area
- Increase in injection velocity
- Reduction in droplet size
- Change in jet turbulence characteristics
- Increase in spray shape oscillation

An argument has been presented which suggests that cavitation may be a desirable effect [1], since the bubbles have a positive effect on breaking up the flow at the wall boundary, thereby reducing the liquid-length and decreasing initial drop-size. However, this is countered by the argument that these effects are only present close to the nozzle, and the detrimental effect that cavitation may have on penetration and especially mass-flow rate act to decrease the efficacy of the injector.

2.7 Injection Nozzle Design

As discussed in previous sections, nozzle design has an effect on the performance of the injector. The nozzle design has a telling effect upon the pressure and velocity distributions within the nozzle and the turbulence energy [19] of the fluid. These in-nozzle parameters have decided effects on the injector characteristics which may then be measured and studied [18].

Common-Rail injector nozzle design may be divided up into two different design philosophies: the Valve-Covered-Orifice (VCO) type, and the SAC or Mini-SAC type. Illustrations of these types of nozzle may be seen below in Figure 2.5.

SAC and Mini-Sac type injectors are typically used for heavier duty applications, and VCO type injectors are more typically used for modern automotive applications. The VCO injector is a relatively new development,and thus most engines

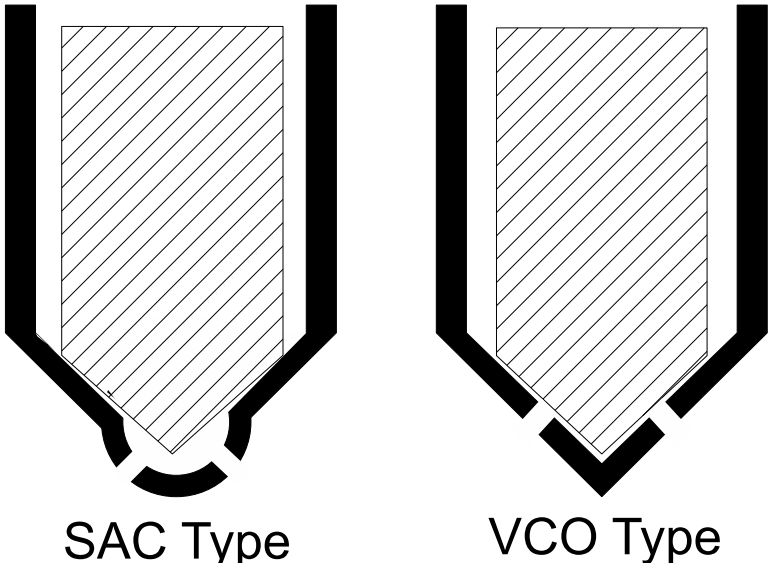

Figure 2.5: Nozzle types

developed before the introduction of the common-rail and some early common rail smaller engines also used SAC type injectors.

The chief advantages of the VCO nozzle design are that it produces finer droplets [16], and avoids dripping of droplets into the cylinder once the needle has closed the orifice [6]. This is because the VCO injectors reduce the parasitic volume in the injector to almost zero [19]. The avoidance of the dripping of droplets into the cylinder has a dramatic effect on reduction of unburned hydrocarbon emissions, since this fuel would be effectively released from the engine without any chemical energy conversion.

A key parameter used when describing the efficacy of an injector is the discharge coefficient, c_d. The discharge coefficient, which may be calculated from equation 2.15 below, is higher in a SAC type injector than in the VCO type injector [16].

$$C_d = \frac{\dot{m}_f}{A_o \rho_l U_{th}} = \frac{\dot{m}_f}{A_o \sqrt{2 \rho_l \Delta P}} \tag{2.15}$$

An effective and relatively simple manner to improve the discharge coefficient is to increase the chamfer of the orifices, however this does have the effect of

narrowing the spray angle [18].

Other important coefficients used to quantify the efficacy of an injector nozzle are [23]:

The area coefficient:

$$C_a = \frac{A_{eff}}{A_o} \tag{2.16}$$

The velocity coefficient:

$$C_v = \frac{U_{eff}}{U_{th}} \tag{2.17}$$

Equation 2.15, presented for the determination of the discharge coefficient, may be rearranged such that:

$$\dot{m}_f = C_d A_0 \sqrt{2\rho_l} \sqrt{\Delta P} \tag{2.18}$$

Further, equation 2.18 maybe shown as follows:

$$\dot{m}_f = k\sqrt{\Delta P} \tag{2.19}$$

Therefore, a plot of $\dot{m}_f$ vs. $\sqrt{\Delta P}$ should reveal a liner relationship, and may be used to identify cavitation as discussed in Section 2.6.

Other differences between the VCO type injectors over SAC type are:

- A VCO injector leads to reduced fuel injection during injection delay period compared to a SAC type injector [6].
- A SAC type injector tends to provide deeper penetration than VCO type injectors, since the geometry of the VCO nozzle results in a reduced ΔP across the nozzle [9].

- VCO injectors result in better atomization, through the development of smaller droplets [9].
- During the injection a SAC type injector provides a more uniform spray [18], and less hole to hole variability than a VCO type injector [8]. This is due to the symmetric pressure field which is generated within the SAC type injector that is not present in the VCO type injector.
- During a similar time period, a SAC type injector will deliver more fuel than a VCO type. This is a reason why SAC type injectors are more common in heavy duty applications than in automotive applications.

Injector orifice design is covered by a term known as concavity, or the K-factor. This K-factor is determined through the application of the following equation [23]:

$$K - factor = \frac{D_i - D_o}{10} \tag{2.20}$$

where D is measured in μm.

The effect of the K-factor is to increase the level of atomization within the spray and thereby decrease the penetration of the spray. This is done through the smaller cross-sectional area at the outlet of the nozzle acting to increase the fluid concentration.

The desired K-factor, as well as other finer aspects of injector finishing are achieved, certainly by Bosch, through a process of Hydro-grinding [18].

2.8 Test Facilities

Many academic institutions and companies in industry are currently conducting research into the performance of injectors. For this reason there is a relative wealth of information available on injectors and their performance, but this information

is of little use if one does not understand the nature of the apparatus used in the testing. This section aims to provide an insight into what experimental apparatus is currently being used in testing.

2.8.1 Types of Injection Chambers

A major element which identifies different test rigs is the nature of the atmosphere into which they inject. A test rig may inject into either a pressurised or un-pressurised environment. Further, this environment may either be stationary, or in motion. The use of a test rig which provides an atmosphere which is at a higher pressure, with moving air, as well an elevated temperature will produce results which are more representative of what would occur within an actual engine. The inclusion of these facilities, however, makes the test rig more complex, and therefore more expensive [26].

Some test rigs are comprised of a high pressure test chamber, generally consisting of a cylinder with windows for optical access [25]. These are limited, however, by window dimensions which often do not allow one to see the full development of the spray. Testing with diesel at pressures representative of a combustion chamber also introduces the chance of the fuel igniting. Because of this reason high pressure testing is often conducted using a non-flammable gas. For instance, Nitrogen is often used [24] as an atmosphere to inject into.

Other experimental set-ups use gases which are more dense than air as an environment into which to inject, such as sulphurhexaflourine. Such gases have densities comparable to that of a charge in a diesel engine, even at atmospheric pressure [2].

In the case of a injection into a heated environment, an autoclave may be employed [3], which heats the air before it enters the modeled combustion chamber.

In the cases where testing is conducted in an environment where the air is in motion, a model engine is created. In this design, the cylinder-head often has to

feature optical access, since a piston moves to generate the motion of the air and would obstruct any sidewards vision [26]. In these test-rigs the engine is driven by an electric motor, and the injector is mounted quite high up in the cylinder head so as to ensure that the piston does not interfere with either the injector or the spray.

2.8.2 Types of Imaging systems

Injector testing may generally be done in one of two manners. The first, and the less common, involves actually capturing a high speed video of the spray. This then provides a clear illustration of what a particular spray is doing during its formation process [24]. In this type of testing resolution is a problem, due to the high speed at which images are required to be captured. The camera used in one such set of tests operated at a frequency of 450Hz, with an exposure time of 22μs [24].

The other popular means of testing injectors is a method knows as strobing. In this means of imaging one image is taken per injection and these images are then assembled to form a comprehensive image of how the injector is behaving with time.

The advantage of the former method is that one may get an idea as to how the injector behaves in a specific injection. Short lived dynamic phenomenons are visible, known as injection-to-injection variability may be identified in this type of imaging [24].

The process of strobing is the simpler means of testing. It allows one to capture still images, which are easier to capture and possess better image quality. The process has the disadvantage of not allowing one to see variability during a specific spray event. Contrasted to this it does give a good idea as to how a spray behaves on average, and therefore is useful for the comparison of different injectors. It also has the benefit of being cheaper to run, in that a very high frame rate camera is not required. An additional cost associated with the process of strobing

is the software required to process the data so as to arrive at averaged, sequential images.

2.8.3 Types of Injectors used in testing

All of the injectors discussed in Section 2.7 are tested in various forms of research. Generally the injectors tested are identical to those used in practical applications. In some cases, however, injectors with just a single nozzle orifice are tested. These provide better definition for spray analysis, as having a single orifice simplifies both the lighting and the image analysis process [2], [3], [24].

2.8.4 Types of imaging systems

Various techniques are used for the effective imaging of sprays.

Shadowgraphy

Shadowgraphy is the most commonly used visualisation technique for spray analysis. It shows an image in which the desnity of the medium is indicated by shadow against a uniformally lit background. In the case of a fuel injector spray, the darkness of the shadow indicates the air-fuel mixture ratio. The disadvantage of shadowgraphy is that it may only be used for the study of macroscopic spray characteristics, and is typically used with high speed video imaging, and not with strobing.

Laser Electric Scattering

Laser Electric Scattering allows one to develop a two dimensional image of the spray, from a region within a very thin sheet of light. This provides an image of the spray which indicating the density of the scattering medium and provides the

ability to evaluate the temperature of the rapidly evaporating medium.

Phase Doppler particle analysis

Phase Doppler particle analysis uses a laser light source, and optical arrangements which generate images of the sprays. Doppler Particle analysis is the most effective means of analysing atomization within a spray, and may be used for measuring droplet diameters up to 500μm. The disadvantage related to this method of imaging sprays is that it is much less effective than other spray imaging processes when sprays are dense [15].

Mie-scattering

Mie-scattering is a process which relies upon the intensity of the light reflected from the spray so as to determine the location of the spray. The process identifies light above a certain concentration threshold [6] and this threshold may be varied through the image post-processing software.

The mie-scattering imaging process is not good for the determination of the level of atomization which has ocured within a spray. The intensity of the scattered light is directly proportional to the particle number density multiplied by the square-root of the liquid drop diameter [7]. This effectively means that as droplets get smaller, less light is reflected. This explains why mie-scattering image processes are not good for atmoisation, as not enough light is reflected.

2.8.5 Types of Injection Regimes used

Injection regimes, refers to how an injector is controlled. This occurs by one of three means:

1. Time Based Injection Duration Variation

2. Injected-Volume Based Duration Variation

3. Crank-Angle Based Duration Variation

In testing the regime used most often is the *Time Based Injection Duration Variation*, because it is the easiest to control. However, in the case of a functioning engine, the *Crank-Angle Based Duration Variation* regime is employed.

2.8.6 Injector Flow Analysis

Little experimental work appears to be carried out with regard to the nature of the flow from an injector. In the literature reviewed, reference was made to a test-rig which operated by injecting into a sealed hollow tube, within which the pressure was measured by a pressure transducer. The resulting increase in pressure may be used to determine the injected mass of fuel. The results obtained from this apparatus was then used to determine the discharge coefficient for the injector.

2.9 The common-rail system

The literature presented this far in this chapter has been related to both mechanical and common-rail injectors, and where appropriate reference has been made to common rail systems. However, given that the research to be undertaken is related exclusively to common rail injectors, it is appropriate to present details of the common rail system here.

2.9.1 Principles of common rail injection

In a conventional injection system, where a mechanical injector is being employed, the injector is actuated by a sharp increase in the pressure supplied by the high pressure fuel pump. Since this high pressure fuel pump is driven by the

crankshaft, the increase in fuel pressure may be timed so as to inject at the correct moment in the engine's cycle - much like a distributor transfers high voltage from the coil to the spark plugs in a traditional spark ignition engine.

In a common-rail injection injection system, a functional separation is introduced between the pumping and injection systems [28]. An illustration of how a common-rail injection system works is shown below in Figure 2.6.

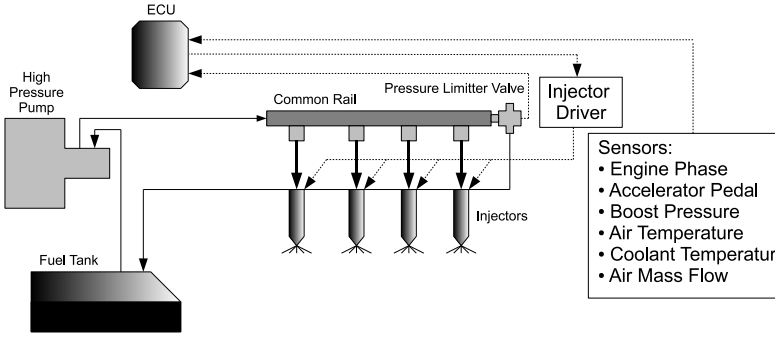

Figure 2.6: Common Rail Injection System [28]

The separation of the pumping and the injection functionality is accomplished by the common-rail, which acts as a pressure accumulator in the system. An identical pressure is then supplied to all the injectors at the same time. The injections are effected by triggering a solenoid in the injector. The duration and timing of the injections may be controlled through changing the current which is placed on the injector solenoid.

2.9.2 Advantages of Common Rail Injection

By providing the injector with a constant pressure supply and controlling the injector's behaviour through the solenoid, the dependency of the injection system on the engine's speed is removed. This allows the timing and duration to be varied

completely independently of engine speed. This functionality enables the designer of the injection system to provide the engine with several injection events per cycle. For instance, it is not unusual for an engine to have a pilot injection, a main injection, followed by a post-injection. Details regarding these injections is given in Section 2.9.3.

Through varying the timing, and quantities of fuel injected in the above mentioned injections, various conflicting requirements may be traded off against each other. The main injection may also be modulated in accordance with time and space related transformation of the fuel within the combustion chamber, i.e. mass flow rate and spray formation in terms of penetration and cone angle. [28]

Through the development of the engine 'map', which is a set of data which contains the optimum injection conditions for any particular state, the above details may be varied constantly so as to provide the optimum injection, in terms of:

- Injection Start Time
- Injection Rate Characteristic
- Quantity of fuel injected

The development of such a 'map' enables the manner in which fuel is introduced into the combustion chamber to be set for various engine speeds and load conditions.

2.9.3 Types of Injections

As discussed above a single injection event may consist of various different types of injections, including:

- Pilot Injection
- Main Injection

- Secondary Injection

These are discussed below:

Pilot Injections

The pilot injection serves to initiate combustion, so as to encourage more complete combustion of the main injection, through the reducting the ignition delay. The pilot injection also serves to reduce the rate of pressure rise in the combustion chamber resulting from of the main injection. [4]

These effects serve to reduce combustion noise, fuel consumption, and generally reduce emissions as well. Since the pilot injection acts to reduce the ignition delay of the main injection, it indirectly contributes to the generation of torque from the engine. [4]

Three sources of pilot injection volume were identified during the course of this literature survey:

The "Technical Instruction" manual published by Bosch defines the delivery of the pilot injection as varying from 1mm^3 to 4mm^3 [4]. The textbook edited by Cornel Stan, *Direct Injection Systems*, provides values for pilot injection volume varying from 2.6mm^3 at 2000rpm to 3.3mm^3 at 1200rpm, with injection timing varying from 11°C to 14°C BTDC [28]. A third source of information regarding pilot injection durations is based on a paper published detailing tests run on a 1929cc Fiat TDI engine, where it is stated that energizing times of between 50 and 250μs were used - with 50μs referring to an injection where no fuel was delivered. With regard to the volume of the pilot injections, they suggest that a quantity of 1-2mm^3 is suitable to reduce combustion noise, however, tests were run with pilot injection quantities of up to 5.6mm^3, this representing 18% of the total injected volume of 31mm^3 [22].

Main Injection

The main injection is where the fuel is provided from which the majority of the energy will be liberated, and is thus responsible for the development of the majority of the engines torque.

Secondary Injection

A secondary injection is employed in engines with exhaust gas recirculation(EGR). Here exhaust gases are fed back into the engine so as to reduced emissions, and fuel is injected during the exhaust cycle.

The secondary injection does not combust upon injection, but rather vaporises. Some of this fuel is later combusted after the exhaust gas is recirculated, and the remainder of the fuel is used to act as a reduction agent in the catalytic converter and lowers the levels of NO_x.

In order for a secondary injection to be effective, it is required that the catalytic converter fitted to the car be compatible with the reduction technique.

2.9.4 The Common Rail Injector

In the mechanical injector, the injection is initiated by an increase in pressure, resulting from the fuel pump directing pressure toward the injector, acting against the spring which holds the injector in a normally closed position. Thus the opening and closing of the injector is entirely a result of the pressure variation in the fuel line to the injector. With the common rail injector the injection is initiated by a current placed upon a solenoid contained within the injector, which allows the pressurised fluid in the common rail to flow into the combustion chamber.

Common Rail Injector Design

A cut-away schematic of a common rail injector is shown in Figure 2.7. The opening and closing of this type of injector is based on the pressure differential across the injector needle.

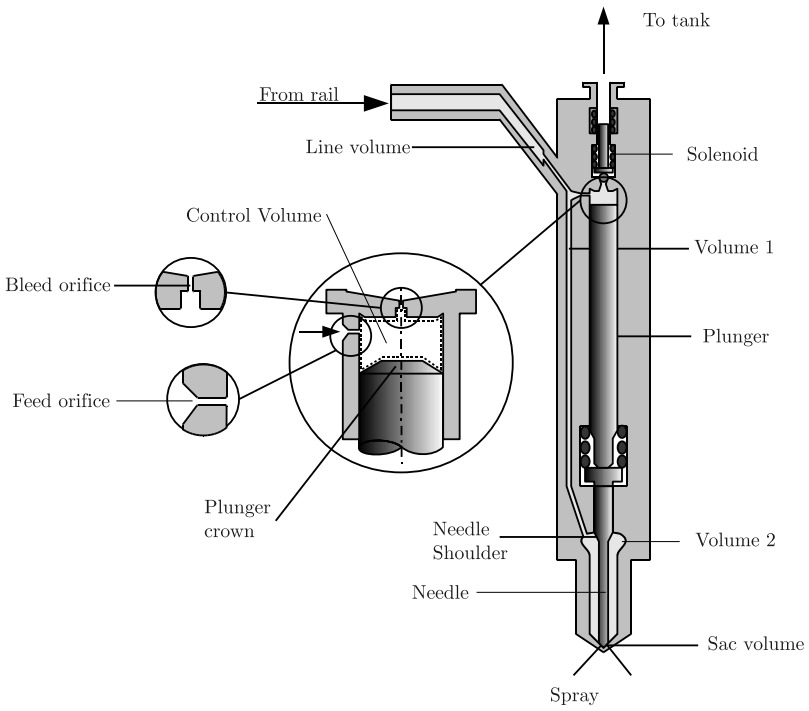

Figure 2.7: Schematic cut-away of a common rail injector [27]

Common Rail Injector Operation

When the injector is closed, that is, there is no current on the injector's solenoid, the control volumes on the top and the bottom of the injector plunger and needle are both subjected to the pressure in the common rail. Since the area at the top of the plunger is larger than the area at the base of the needle, the resultant force on the injector is downwards, and the injector remains closed.

The region above the plunger, designated the control volume in Figure 2.7, has an inlet and an outlet. The inlet, known as the *Feed Orifice* takes the form of an I-throttle, and the outlet known as the *Bleed Orifice* takes the form of an R-throttle.

It is the pressure in this control volume which determines the behaviour of the injector with regard to opening and closing.

When current is passed through the solenoid, the valve ball on the R-throttle on the *Bleed Orifice* rises, and this exposes the control volume to the pressure in the return line away from the injector. As a result of this, the pressure in the control volume above the injector is much lower than the pressure on the surface below the injector. This reduction in pressure causes an upward resultant force to act on the needle against the nozzle spring and moves the injector the needle upward. This results in the injector opening and fuel being injected.

Upon closure of the injector the ball valve seals the control volume above the injector, and the pressure in the control volume returns to that in the common rail, the same as that below the needle. This results in the return of the original state described above and the cessation of injection.

Effects of Varying Orifice Parameters

As would be expected, the discharge coefficients in the feed and bleed orifices will have an effect on the flow rate from the injector. The effects of varying characteristics within the bleed and feed orifices are discussed below.

Bleed Orifice: A higher discharge coefficient for the bleed orifice will have the effect of decreasing the time taken for the pressure in the control volume to reduce, and this result in a faster opening of the injector[2]. However, an increased discharge coefficient will have no effect on the flow behaviour at the end of injection, since this is controlled by the ball valve, and not the characteristics of the throttle.

Feed Orifice: A decrease in the discharge coefficient of the feed orifice results in a slower drop off in the injection rate profile, since the pressure in the control volume will rise to the pressure in the common rail more slowly. This results in the needle moving down later. However, this decrease in discharge coefficient will

[2]Naturally, the opposite is true of an decrease in the discharge coefficient

also result in a decreased rate of pressure drop within the control volume, leading to sluggish injector behaviour.

Thus, the bleed orifice relates to the opening of the injector only, while the feed orifice relates to both the opening and closing of the injector.

Chapter 3

Experimental Facilities

3.1 Introduction

The following section contains details regarding the equipment used for the testing conducted, upon which this research is based.

The equipment is contained within a test stand located within the thermodynamics laboratory at the University of the Witwatersrand, Johannesburg. The test stand was designed and built, specifically for Wits University, by a firm called INOV8, based in Buckingham, England. The test stand was installed and commissioned late in 2008.

A photograph of the Test Stand is shown in Figure 3.1. The test stand is pictured with its lower side panels removed, allowing one to see the test fuel and cooling fluid tanks along with their low pressure pumps, which are mounted above the tanks.

The test stand allows one to investigate:

- Injector Spray Patterns
- Injector Flow-Rate characteristics

These two systems operate independently, while employing the same common rail.

3.2 Mechanical Components

High pressure fuel is supplied to both the spray visualisation injector, and the flow rate injector by a Siemens automotive common rail, part number 5WS4002. The common rail's design pressure is 1800bar.

A pressure transducer is connected to one of the common rail outlet ports. The signal is amplified by a KISTLER calibrated amplifier, TYPE 4618A0. The transducer is rated for pressures from 0 - 2000 bar, and supplies the test stand control unit with a 0 to 10v signal which is proportional to the pressure in the common rail. The test-stand software then relates this voltage to the rail pressure and this is recorded.

Test fluid or fuel is supplied to the common rail by a Siemens-VDO three node

Figure 3.1: Injector Test Stand

high pressure fuel pump, part number K10_07. An illustration of such a pump is shown in Figure 3.2.

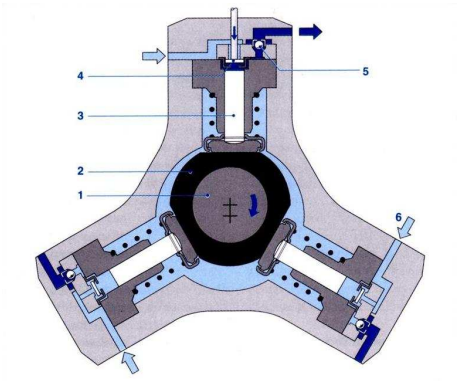

Figure 3.2: A typical three node common rail fuel pump [12]

The common rail fuel pump is driven by an EROY, 380v, 5.4 kw AC motor, the speed of which is controlled by an Emerson Unidrive variable frequency AC drive.

Fuel being used for testing is stored in a 20 litre tank located on the base of the test stand. This fuel is supplied to the high pressure common rail fuel pump by a smaller, low pressure pump which is driven by a 750 watt ABB AC motor.

The flow measurement system, known as the *Akribis*, is cooled through pumping calibration fluid through the flow meter. This calibration fluid is stored in a tank identical to the fuel storage tank, as may be seen in Figure 3.1. The calibration fluid's temperature is regulated to 25^{o}C, and is circulated by the same low pressure ABB motor as is used for the test fuel. A photograph of the storage tanks and pumps are shown in Figure 3.3.

3.3 Test Stand Injection Control System

The actuation of the fuel injectors is controlled through software generated by INOV8, based upon a CAPAC base. This software allows the user to control various aspects of injection, including the injector timing and power parameters. The parameters which the user may vary are listed in table 3.1.

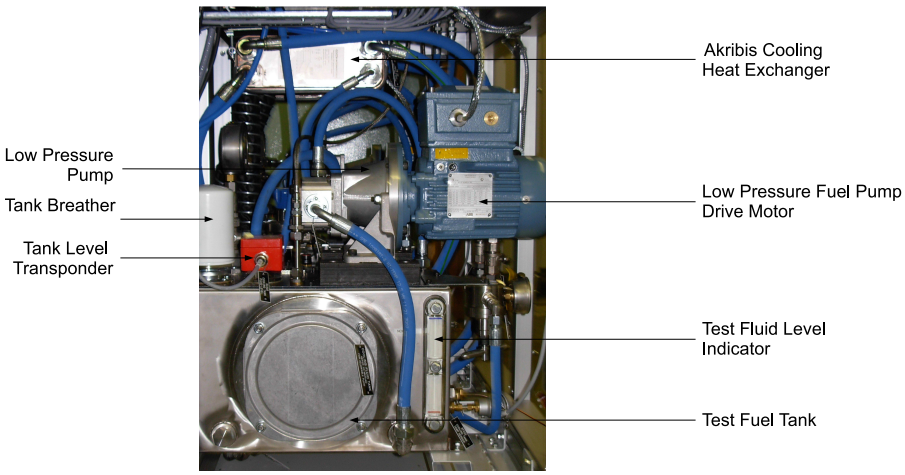

Figure 3.3: Fluid Storage Tanks and Pumps

Table 3.1: Injector Control Input Parameters

Parameter	**Unit**
Boost Voltage	V
Current during Boost phase	A
Length of Pull In Phase	μ s
Low current value in Pull In Phase	A
High current value in Pull In Phase	A
Low current value in Hold Phase	A
High current value in Hold Phase	A

Through the variation of these parameters the test stand may emulate the signals which would be sent to the injector from the ECU and injector driver in an automotive case. This allows the test stand to be customised such that any solenoid actuated injector may be tested.

The control package allows up to five injections per event. The user may set the durations of these injections, as well as the time between these injections. The delay between the start of injection signal being received from the sender unit may also be varied. Since the durations and intervals between injections are variable, the test stand may be set up so as to test multiple injection regimes, or pilot injection conditions.

3.4 Injector Flow Measurement

As mentioned above, the test stand has facility to measure the flow through an injector very accurately. This is accomplished through the use of a flow meter developed by the manufactures of the stand, INOV8, known as an *Akribis*. An image of the Akribis unit is shown, in Figure 3.4.

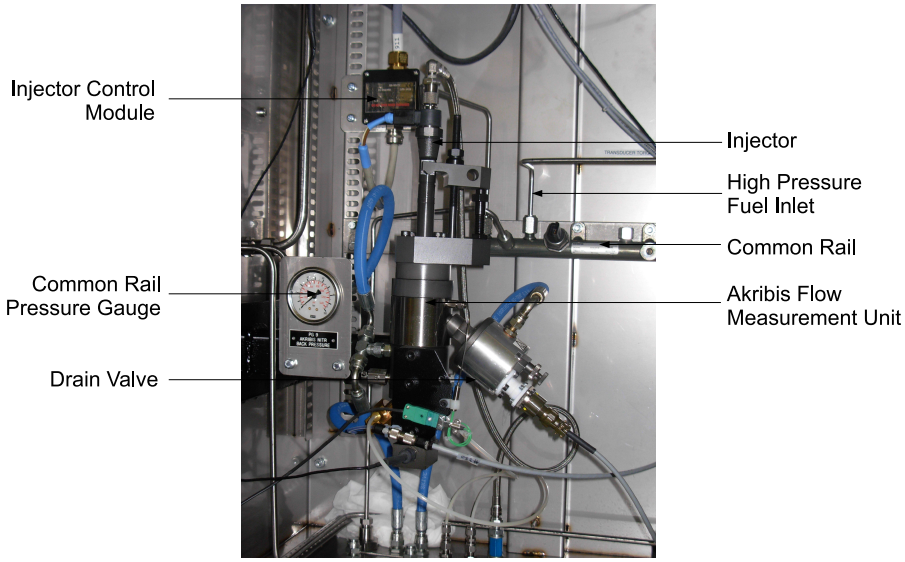

Figure 3.4: Akribis injector flow meter system

The Akribis is a piston operated flow meter. The injector is located above the piston and injects fuel into a region above it. The piston is supported by a bed of pressurised nitrogen. The pressure of this nitrogen may be varied, thus emulating the effects of injecting into various combustion chamber states.

The displacement of the piston is measured during the course of the injection, and related to the rate of injection as well as the volume injected. The pressure in the common rail is also recorded through the course of the injection, along with the profile of the signal sent to the injector. These signals are sent from the Akribis metering unit to a PC, fitted with software also developed by INOV8 on a CAPAC base, which allows one to view, both graphically as well as numerically the nature of the measured details of the injection.

The compartment in which the Akribis is mounted is sealed, and before injection

may be commenced this compartment should be purged with nitrogen supplied by an external source. This is a safety measure to eliminate any chance of ignition of the fuel being tested. Also, the compartment of the test stand which houses the electronic control systems is purged - however, this purging is done with compressed air as opposed to nitrogen.

The specific Akribis fitted to the Test Stand can measure injection events of volume: 0.5 - 150mm^3, with timing increments of 0.02ms.

3.5 Injector Spray Pattern Imaging

3.5.1 Introduction

The test stand also has the capability to collect images of the sprays generated by injectors. This is accomplished in a section of the test stand containing a spray chamber and cameras. The captured images are then sent to a PC contained in the test stand control room, where a software package is used to process the images and produce results.

Details regarding the cameras, spray chamber, and software are presented below.

3.5.2 Cameras

The image capturing system consists of two cameras, located orthogonally to each other. The first camera, designated camera 1, is located underneath the spray injector, and the second camera, designated camera 2, is to the side of the injector. This enables one to see the development of the spray in three dimensions.

The cameras used are supplied by *La Vision*, the same firm who developed the software which is used in the processing of the images. The cameras are *Imager Compact*, a photograph of which is shown in Figure 3.5.

Figure 3.5: Flow visualisation camera

As may be seen in Figure 3.5, the image is projected into the camera through a lens. The lenses are 28mm, 1:2.8 aperture, Nikkor Lenses, which are mounted to the La Vision cameras through an adapter. The aperture and focus of the lens is set and may not be changed during the course of experimentation.

Both cameras are housed within black metal shrouds which serve to minimise light ingress, and reduce noise within the image.

3.5.3 Spray Chamber

The spray chamber consists of a box, 300mm by 300mm, which has glass windows in the sides and base. The windows serve as optical access for both cameras as well as light sources. Schematics are shown below, illustrating the layout of the cameras and light sources for cameras 1 and 2, in Figures 3.6 and 3.7 respectively.

The spray chamber is ventilated to the atmosphere through a duct containing an inline fan, which draws air from within the spray chamber. This duct contains a flow actuated switch which closes when sufficient flow passes through the duct - the test stand will not operate unless the flow is sufficient to close this switch.

High pressure air is routed over the windows in the spray chamber by devices known as air-knives. These air-knives serve to blast air off the windows, thereby

avoiding a build-up of fluid and enabling the system to capture more representative images of the spray development.

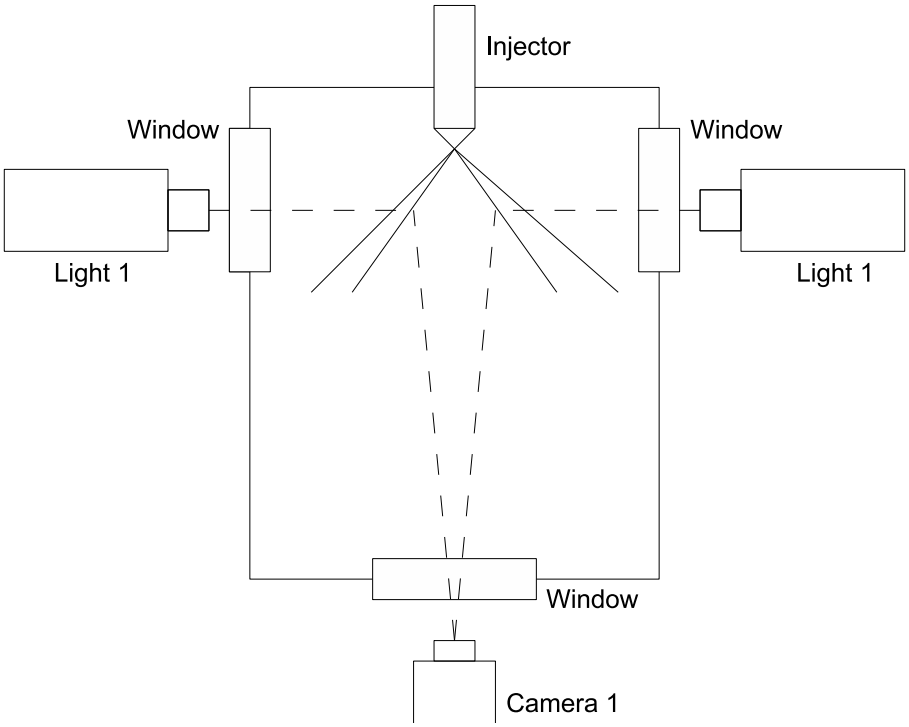

Figure 3.6: Schematic illustration of camera 1 and related lighting

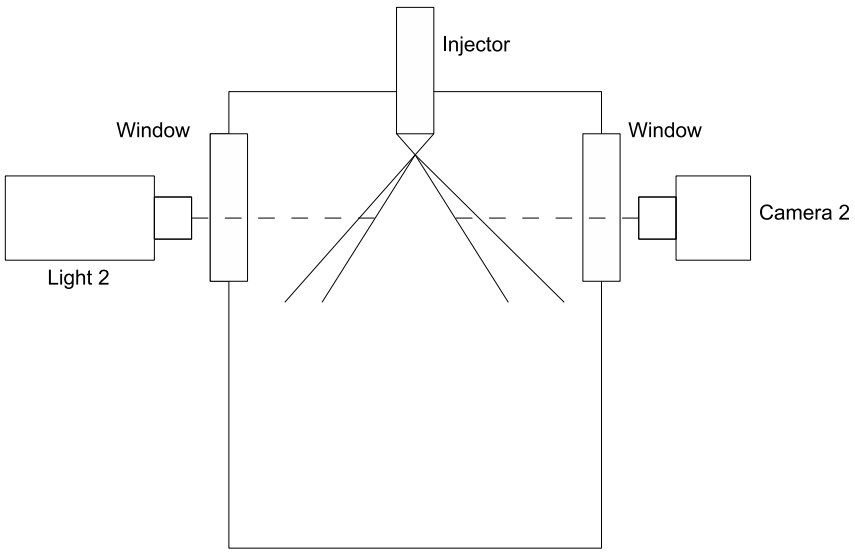

Figure 3.7: Schematic illustration of camera 2 and related lighting

The spray visualisation system is contained within a section of the test stand which is enclosed by three doors, on of which may be clearly seen in Figure 3.1, on page 36. These doors are fitted with solenoid controlled door locks, which prevent the spray chamber from being accessed while injections are in progress, or when there is no power to the test stand.

3.5.4 Injector Imaging Software

The imaging software is developed by the same firm who developed the cameras, *La Vision*. The imaging package is called *DaVis*, and is used for CCD image acquisition and processing.

The spray visualisation system employs a process known as strobing. This process captures one image of the injection per injection. The process which the *DaVis* software employs is to capture a user defined number of images at a given instant during the spray. The user may define the instant at which the system begins acquiring these images, the interval between the images, and the time at which the system stops capturing the images.

Once the system has run through the image acquisition process, there will be a number of sets of images from the various time intervals which have been defined. The sets of numerous images for a given time interval should then be averaged. The averaging is a statistical process which combines the features of all the images captured into one image.

If the background is likely to interfere with the image it may be subtracted. This is done through specifying a background image, generally taken before the process of injection is begun.

Once the images have been averaged, and if necessary the background have been subtracted, the images may now be processed by the DaVis *Geometry Package*. The geometry package, which needs to be set up with regard to the location of the injector nozzle and the sprays, performs analysis of the spray with regard to spray

characteristics. The specific spray characteristics which the package identifies are the spray penetration, cone angle, and spray width at specified distances from the nozzle.

Where the geometry package defines the spray to be is dependent upon the threshold defined by the user. According to the Manual on the *DaVis* geometry package: "*The threshold is a very sensitive parameter of the Geometry Package and must be defined carefully. A bad threshold may be the main reason for strange geometry angles or other bad results.*" This threshold may be defined as either an absolute or a percentage. If it is defined as a percentage, it determines the maximum intensity counts in the source image and defines the edge of the spray where the intensity of the light descends below the user defined percentage of the maximum intensity [20]. The threshold may be defined differently for cone-angle and penetration, and should be recorded and associated with the results.

Chapter 4

Procedures and Precautions

The test apparatus has been described in Section 3, on page 35. The following section describes the manner in which the test stand is operated, as well as the procedures followed during testing.

The operating procedures for the test stand will be divided into three sections

1. General Test-Stand Operation
2. Spray Visualization Procedures
3. Fuel Flow Metering Procedures

4.1 General Test-Stand Operation

Certain procedures need to be followed for test stand use regardless of whether it is to be used for spray visualisation, or fuel flow metering. These procedures are detailed below:

4.1.1 Test Stand Power

The power to the test stand needs to be switched on. This is done by rotating the three phase switch on the side of the power enclose.

4.1.2 Operating Test Stand

The test stand should be switched on by pressing the green push button labeled ”TEST STAND ON” on the test stand power enclosure.

4.1.3 Air and Nitrogen Pressure

The test stand requires high pressure air and nitrogen. The control valves for these need to be opened.

High pressure nitrogen is stored in a cylinder located on the east side of the room in which the test stand is located. It is necessary to open the valve on the top of this cylinder. The pressure regulator should already be set, however it should be checked that the outlet pressure is 40 bar.

Compressed air is supplied to the test stand from air receivers located in the laboratory. The compressed air valve is also located on the east side of the room, and should be opened completely. The pressure may be checked on the pressure receivers on the dehydrate, and should read around 6 bar. If this pressure is not present there is no pressure in the air receivers, and the laboratory compressor should be switched on to supply pressure.

The air and nitrogen pressure gauges on the test stand should now rise to their proper positions. These gauges are indicated as *Gauge 1* and *Gauge 2* in Figure 4.1 below. If these do not rise, the ’Electrical Enclosure Purge’ switch on the front of the test-stand should be turned on and off again, followed by turning the ’Akribis Enclosure Purge’ switch on and off. By enacting the purge systems for a

short time, the line pressures in the test stand should rise to the correct levels.

In the case of *Gauge 1* not rising to 5.5 bar, the pressure may be adjusted by rotating the air pressure regulator, labeled *Regulator 1* in Figure 4.1. It should be noted that typically this regulator does not need to be adjusted.

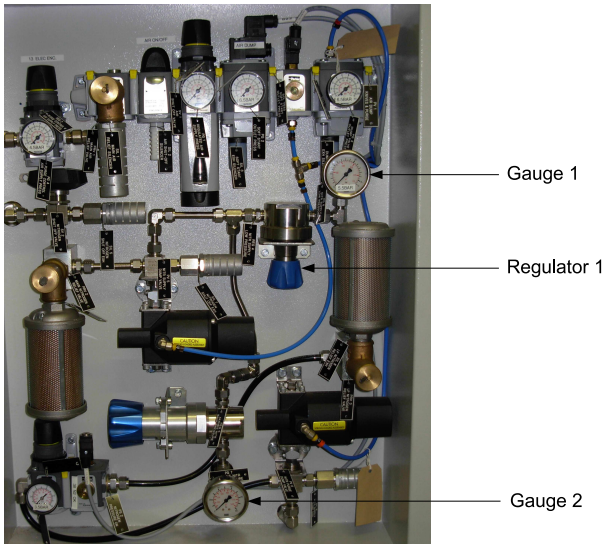

Figure 4.1: Test Stand Pneumatic Control Panel

4.1.4 Operating Water Chiller

The water chiller, which acts to cool the test fluid and the Akribis cooling fluid, needs to be switched on. It should be ensured that the water chiller is on both at the switch on the cooling car and at the wall socket where it plugs into the mains.

Note: No warning is given if one forgets to turn on the cooling car. If either of the fluids rises over its safe temperature then the test stand will shut down, and one needs to wait for the fluid to cool to below its maximum temperature before the stand may be restarted.

4.1.5 Operating Air-Extraction System

The test stand is equipped with an air-extraction system, which removes air out of the LaVision spray chamber. This fan is turned on by a switch located next to the distribution board, on the North Side of the room.

Note: If possible, it is worthwhile turning the extraction fans in room T16. If the extraction fans in room T16 are not on, that room tends to fill with the exhausted gases from the test stand, as both rooms ventilate into the same courtyard. But turning on these fans a relative high pressure is created in the courtyard, and the laboratory remains free from gases.

4.1.6 Opening Injector Control Software

The Stand PC, which is labeled as such, will have turned on when power was supplied to the test stand. At this stage it is necessary to open the software which controls the test stand, and injection profile. This software is launched by double-clicking the ”Launch” icon on the desktop.

The software will open, and a dialog reading ”Initializing” will open. This dialogue will close in a few seconds.

Once the software is initialized, the ”Stand Status” button should be selected on the injector control package. This opens a dialogue box which indicates any errors on the test stand.

4.1.7 Starting Test Stand Pumps

The test stand consists of three pumps, as detailed in Section 3. The first two pumps are switched on first by pressing the ”AK COOL PUMP ON” and ”TEST OIL PUMP ON” push buttons.

Once the above two pumps have been switched on, the test stand will check the

stand for errors. It is important at this stage to check the Stand Status dialogue on the test stand PC. If any errors are detected, these should be addressed - otherwise the Common Rail pump will not activate.

If the Test Stand status is all green, the ”CR PUMP DRIVE ON” button should be pressed. This activates the drive to the common rail high pressure pump.

4.1.8 Setting Injection Parameters

From the stand PC software, the Injection parameters may be set. This is done by clicking on the *”Injector Firing & Pressure Control”* button on the injector Stand PC. This will open the injector control dialogue, where the injection parameters may be set.

These parameters include the number of injections per event, the duration of the injections, and the time between injections. With these parameters an injection may be developed to emulate the an injection in an automotive application.

4.1.9 Setting Common Rail Pump Speed

Again, from the stand PC software, the speed of the common-rail pump may be set. By clicking on the *Pump Speed* button, a dialogue which allows the pump speed to be set is brought up. The pump speed should be set to 1000rpm, which may be done by either selecting the *1000rpm* button, or entering the speed into the appropriate space.

It is good practice not to bring the pump straight up to 1000rpm immediately, an intermediate speed should be selected first, and once the pump has stabilized at this speed then the speed should be increased to 1000rpm.

4.1.10 Setting Common-Rail Pressure

After the common-rail pump has been set to 1000rpm, the pressure demand may set. This is done through the *"Injector Firing & Pressure Control"* dialogue. Once the pressure has been set, the *"Apply"* button should be pressed.

4.1.11 Enabling Injections

Injections are enabled through selecting the *"Enable Injections"* check-box in the *"Injector Firing & Pressure Control"* dialogue, followed by pressing the *"Apply"* button.

Once injections are enabled, one should be able to hear the distinctive sound of the injector injecting.

4.2 Spray Visualization Procedures

The details, beyond that which is detailed above, for the operation of the spray visualization functionality of the test stand are detailed here. For more technical or intricate details regarding the operation of the LaVision software should be referred to.

4.2.1 Setting Test Stand Mode

The rotary switch on the front of the Test Stand power enclosure should be set to *"SPRAY"*.

4.2.2 Spray Injector Current Plug

The injector current plugs may be found in the test stand control enclosure, in the top right corner. There are two plugs, one which sends current to the Akribis injector, and the other which sends power to the spray visualization injector. It should be ensured that the plug marked *"SPRAY"* is plugged in, and the latch around the plug closed firmly. A picture showing the injector current plugs, with the spray injector plugged in, is shown below in Figure 4.2.

Figure 4.2: Test Stand Injector Current Plugs

4.2.3 Activating Air-Knives

As discussed in Section 3, the air-knives are used to ensure that test fluid does not build up on the windows of the spray chamber. The air knives are activated by clicking on the *Air-Knives* button on the test stand PC, and selecting the air-knives for the camera which is to be used for the imaging project.

Note: The air-knives are fed by the same air line as feeds the purge for the electrical enclosure. If this purge is not switched on, the air-knives will not operate. No warning is given if this is the case, and poor images will result.

4.2.4 Starting LaVision PC

Unlike the stand and Akribis PC's, the LaVision PC does not start automatically when the test stand power is turned on.

The LaVision PC, which is located in the control enclosure, needs to be turned on by opening the cover in the front of the PC, and flicking the power switch.

4.2.5 LaVision Application

The LaVision software package; *"DaVis 7.2"*, is launched through selecting the *"DaVis"* icon on the desktop. Various procedures need to be followed to capture images, as detailed in the LaVision Manuals, or the manuals developed by the author as part of a final year Research Project in 2008.

4.2.6 Setting number of Images per time step

In the LaVision software, under the acquisition menu, the user may set how many images per time interval the system captures. This may be set to any number between 1 and 571.

4.2.7 Start, End and Increment Time

Again, in the acquisition menu, the user may set at what point in the injection the image acquisition process begins, and at what point it ceases to capture images. The increment time may also be set, that is, the time between successive sets of images is captured.

The shorter the increment time, the greater the resolution of the injection information will be. The disadvantage of a very short increment is that the tests take a very long time to run, and the data occupies considerably more hard-drive space.

4.2.8 Statistical Imaging Processes

Once the system has captured the spray images, it is necessary to average the images taken at the same time step. This is done through a statistical process built into the DaVis software.

Following the averaging process, it is necessary to subtract a background image from the averaged image. This is done by selecting a background image which is taken without a spray present, and instructing the software to remove the elements of that image from the experimental image.

4.2.9 Geometry Package Use

The *DaVis* software, when operating in *Expert User* mode has a functionality known as the geometry package. This geometry package employs statistical algorithms to determine the geometrical structure of the spray.

Specific items of interest are the cone-angle and penetration of the spray.

Note: The geometry package works by determining the intensity of light in the image, and then finding the cone-angle penetration of the spray by looking for a user defined percentage of the total intensity of the spray. The software identifies the end of the spray where the intensity of the light reaches this value. For this reason, the user intensity which is selected must be kept constant for all tests, otherwise the numerical evaluation of various sprays will not align.

4.2.10 Exporting of Images

The *DaVis* software enables one to export images. Images of interest may be exported, along with videos depicting the spray developing.

4.3 Fuel Flow Metering Procedures

As in the case of the spray visualisation aspects of the test stand, the procedures detailed here should be supplemented by more technical operating instructions as contained in either the Akribis help file, or the Akribis operational manual as prepared by the author.

4.3.1 Setting Test Stand Mode

The rotary switch on the front of the Test Stand power enclosure should be set to *"AK"*.

4.3.2 Spray Injector Current Plug

As in the case of the Spray Visualisation, the Akribis plug shown in Figure 4.2 needs to be plugged in, so that the Akribis injector injects.

4.3.3 Switching on Akribis Drain Valve

Since the Akribis is a piston based flow meter, it is necessary to drain the fuel out of the region above the piston. This is done through the use of a drain valve. This drain valve is switched off when the Akribis is not in operation so as to avoid it running continuously and burning out.

The drain valve is switched by a switch on the back of the drain valve controller. The back of the Akribis drain valve controller may be accessed from the back of the test stand control enclosure, and a picture of it is shown below in Figure 4.3.

Note: If the high pressure Nitrogen supply is turned off the Drain Valve may operate since without the bed of nitrogen the piston will moved down, and the system will believe that there is fuel in the region above the piston and attempt to

drain this fuel.

4.3.4 Akribis Injections

At this point injections into the Akribis unit may start. This is done through enabling injections through the *"Injector Firing & Pressure Control"* dialogue, and selecting *"Apply"*.

4.3.5 Setting Drain-Rate

The drain rate on the Akribis should be set. The drain rate is altered through adjusting the potentiometer on the Akribis drain valve control unit, located in the test stand control enclosure. While the test stand is injecting in free-run mode, one may see what the drain rate is by looking at the graph created on the screen.

The drain rate potentiometer should be adjusted until this drain rate reaches -12 to -15 mm^3/s. Further details regarding the operation of the drain valve may be found in the test stand operating manual.

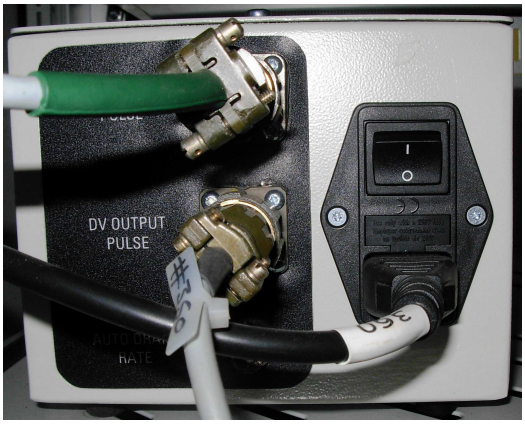

Figure 4.3: Rear of Akribis Drain Valve Controler

4.3.6 Running Tests

Akribis tests are run through taking the Akribis PC out of free-run mode, and then putting it into *"Test"* mode. The number of injections to be recorded, and settings regarding the location of the saved test may be found by selecting the *"Settings"* button.

The settings menu is somewhat self explanatory, but additional detail may be found in the Akribis instruction manual, as mentioned in Section 4.3 above.

4.4 Exporting Results

The results from the spray visualisation my be exported using software eloped in Dev-C++ [27], . The software, may be found on the desktop of the LaVision computer and retrieves the results from the above-mentioned text files and inserts them into a new tab delimited text file.

Note: The program which extracts information from the text files requires information to be entered into the input file in a specific order. If information is not entered into the input file in the correct order then the results will not be exported. The details regarding the formatting of the input file are contained in the "Readme" file in the same directory as the file.

The Akribis results may be exported through the use of Test-Scope, an application developed by INOV8 to allow one to analyse Akribis results. This is done by opening the test, as saved when the test was run, and selecting export from the *"File"* menu.

Note: The exporting function will prompt the user to select from a series of checkboxes what should be exported. The user should select *Waveforms* from this list, as this exports all data.

The files exported through the use of Test-Scope are exported in a manner which

is very difficult to process, since each injection is saved in its own text file. A specifically developed C++ program is then used to combine all the data from a single pressure and duration test into a single text file, consisting of a column for each injection, and a row for each time step. This text file may then be manipulated in a package such as Matlab or MS Excel.

4.5 Deleting Superfluous Images

During the spray visualisation process, the system captures a user specified number of images per time increment, as detailed in Section 4.2.7. Once these images have been averaged, and one images has been produced by combining the characteristics of all these images, there is no need for the multiple images to be stored. By deleting these images, up to 85% of disk space may be saved.

Chapter 5

Injector Flow Analysis: Results and Discussion

5.1 Introduction

The aim of the testing to be conducted was to test and characterise the difference in performance between new and used injectors. To facilitate this a set of seven injectors was obtained for testing, the set consisting of three brand new injectors, and four used injectors of unknown origin. All seven of the injectors were identical Bosch injectors, of part number: 0 445 110 181.

Two of the used injectors were supplied exactly as removed from the engines in which they were operating, and two were supplied after having had their nozzles ultrasonically cleaned. The two injectors which were supplied as run in the engines were naturally coked up, and were cleaned through the use of a buffing wheel before testing so as to prevent dirt carbon ingress into the apparatus.

A simple naming convention was developed for the injectors consisting of two letters and an number. The new injectors were named NI1 through NI3, with the letters standing for “New Injector” and the used injectors were named UI1 through UI4, with the letters standing for “Used Injector”.

This chapter will be structured as follows:

- A brief outline of the testing regime followed will be given.
- The testing of a variety of new injectors will be described.
- A generic comparison of the performance of the used injectors will be made.
- A structured analysis of the performance of all injectors will be made.

5.2 Testing Outline

The testing was conducted using the Akribis test unit, as detailed in Section 3, describing the test equipment. Tests were conducted at pressures of 300, 600, 900, 1200 and 1400 bar, with flow results being taken at durations of between 300μs and 2500μs, at intervals of 100μs, for all pressures. At higher pressures, durations as low as 150μs were tested.

Tests were conducted in accordance with the procedures detailed in Section 4, with the results produced being exported to individual text files through the use of the *Test Scope* software package, as developed by the manufacturers of the test stand. The text files were then combined into a single text file through the use of Dev C++ Software which served to combine the results of the individual tests into a single file.

Code was developed in Matlab which served to read the data from this combined text file, and plot bulk graphs which allowed one to clearly identify patterns and trends which developed in injectors. A full set of graphs showing the results of all Akribis testing is contained in Appendix A.

5.3 Comparison of Performance of New Injectors

As mentioned above, three new injectors were obtained for the research to be conducted. Before it is possible to conduct meaningful analysis into the difference in performance between new and used injectors it is important to establish whether the performance of new injectors is consistent. To check whether the performance of new injectors was consistent all three new injectors were subjected to an identical testing regime. The same tests as were to be performed on the used injectors were carried out on the new injectors.

To facilitate the comparison of results, the total volume of fuel injected during an injection was plotted against duration at all pressures. Figures 5.1 to 5.5 show the volume of fluid delivered against the duration of the injections, at injection pressures between 1400 and 300bar.

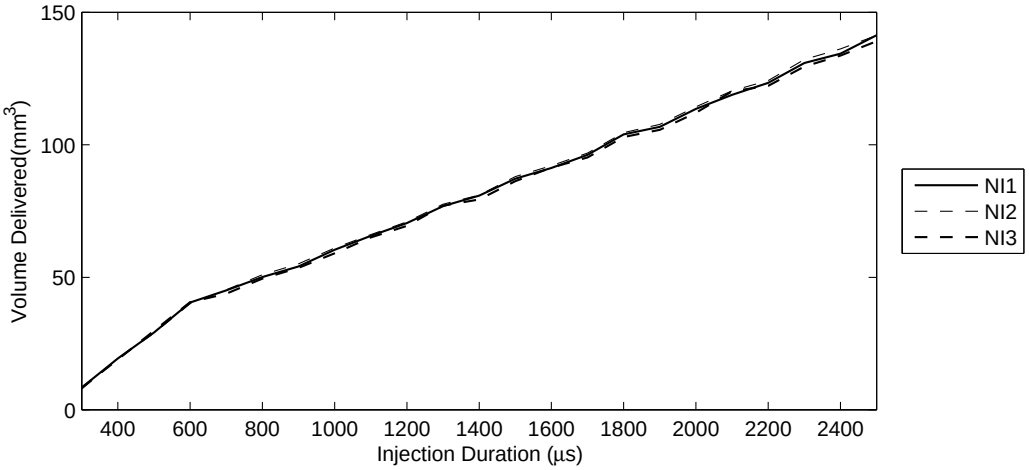

Figure 5.1: Volume of fluid delivered vs injection duration for new injectors at 1400bar

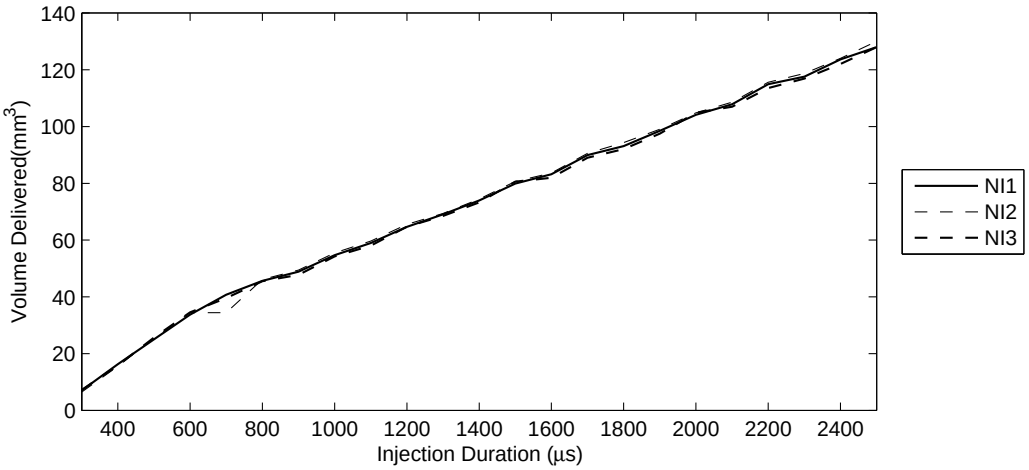

Figure 5.2: Volume of fluid delivered vs injection duration for new injectors at 1200 bar

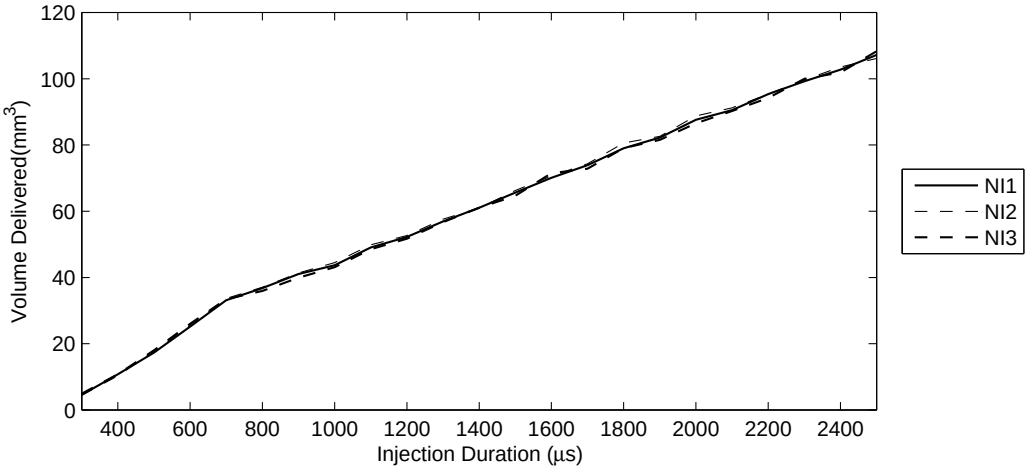

Figure 5.3: Volume of fluid delivered vs injection duration for new injectors at 900 bar

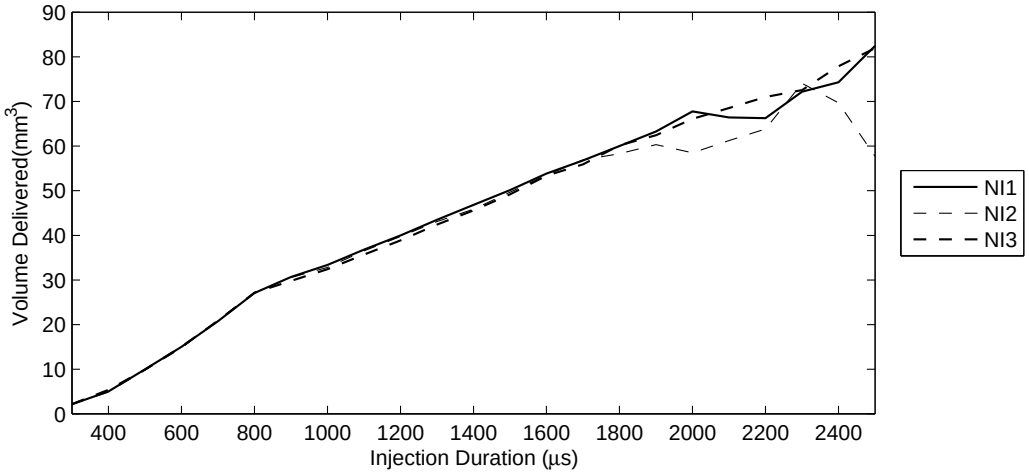

Figure 5.4: Volume of fluid delivered vs injection duration for new injectors at 600 bar

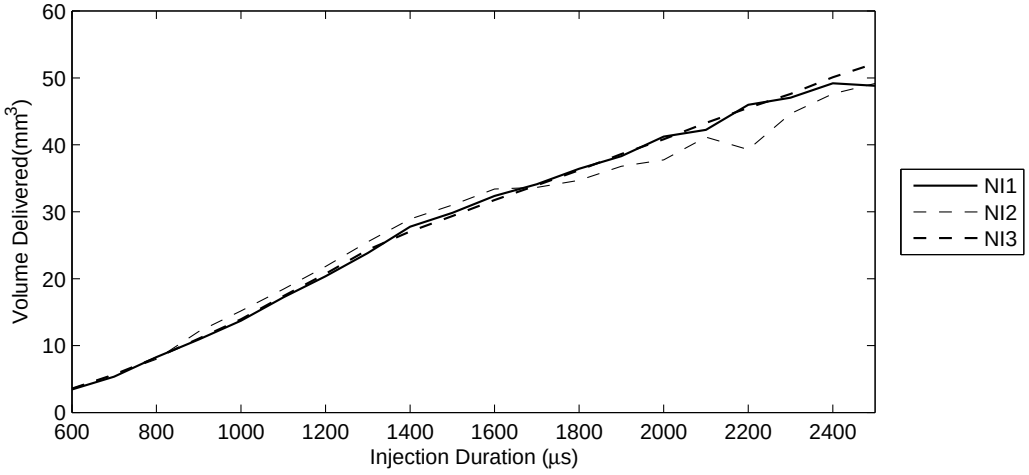

Figure 5.5: Volume of fluid delivered vs injection duration for new injectors at 300 bar

At all pressures a strong correlation may be seen between the volume delivered by all three injectors.

Figure 5.1 shows that the correlation is very close to complete through the entire range of injections, which range from deliveries of 3.7 mm^3 to 138mm^3. This indicates that at the injectors optimum operating pressure of 1400 bar, the new injectors are behaving virtually identically.

If one looks at the behaviour of the new injectors as the delivery pressure is de-

creased, the correlation may be seen to break down. If the plots for delivery pressures of 300 and 600 bar, in Figures 5.5 and 5.4 are examined, it may be seen that a strong correlation of the injectors performance still exists at lower durations, but this is not the case when the durations exceed around 1800μs.

Specifically NI2 does not correlate well with the other two injectors, and does not appear to follow the same linear trend illustrated in all other representations. Since injectors NI1 and NI3 both appear to follow very similar trends, even in the extreme case of low pressure and long durations, it is difficult to argue as to whether one should expect the delivery characteristics of an injector to break down here, however, this difference in performance will be borne in mind during the analysis of the performance of the used injectors.

When critically analysing the performance of NI2, it is noteworthy that the region in which the performance of the injector breaks down is not a region where an injector would typically operate. An injector generally operates at low pressure only while the engine is idling, and as soon as load is applied to the motor the pressure will increase to facilitate better atomisation of the fuel.

The above point regarding the operating region in which the performance of NI2 breaks down is illustrated by the fact that an 1800μs injection at 300bar injects 36mm^3 of fluid, whereas even at the relatively low pressure of 900bar this amount of fuel is delivered in a 800μs injection. Based on that, it would seem unlikely that such a large volume of fuel would be demanded at such a low operating pressure.

In the interests of simplifying the analysis to be done when comparing the performance of new and used injectors, a single new injector is to be chosen for this. Injector NI3 is the most consistent in its performance, as well as possessing the largest data set, and therefore will be used for the analysis to be conducted.

5.4 Injector Comparison

This section begins to look at the performance of the used injectors, upon which this study is based. The results presented in this section aim to look at the performance of all the used injectors and compare their performance to that of injector NI3, the new injector. The detailed analysis of the performance of the used injectors, which is to be conducted below, will be based upon the findings of this section.

While a multitude of results are available from testing, as described above in the testing outline section, it is important to condense these results into a comprehensive and compact set of results. The detailed behaviour of each injector at various pressures and durations will be analysed in Sections 5.6.1 to 5.6.4.

To facilitate this initial analysis the performance of all four used injectors is shown in the same manner as that of the new injectors, as a plot of fluid delivered against injection duration at various pressures. The results for all of the delivery tests at pressures between 300 bar and 1400 bar are shown below in Figures 5.6 to 5.10.

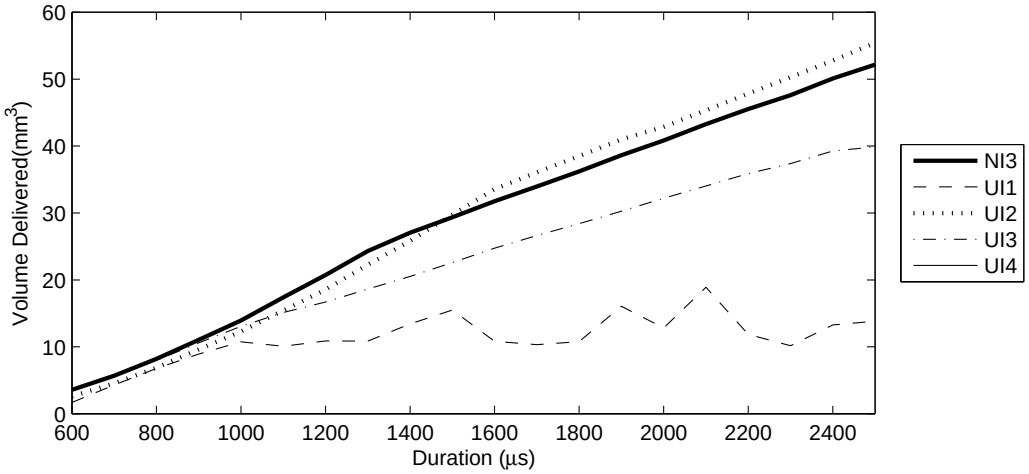

Figure 5.6: Volume of fluid delivered vs injection duration for new and used injectors at 300bar

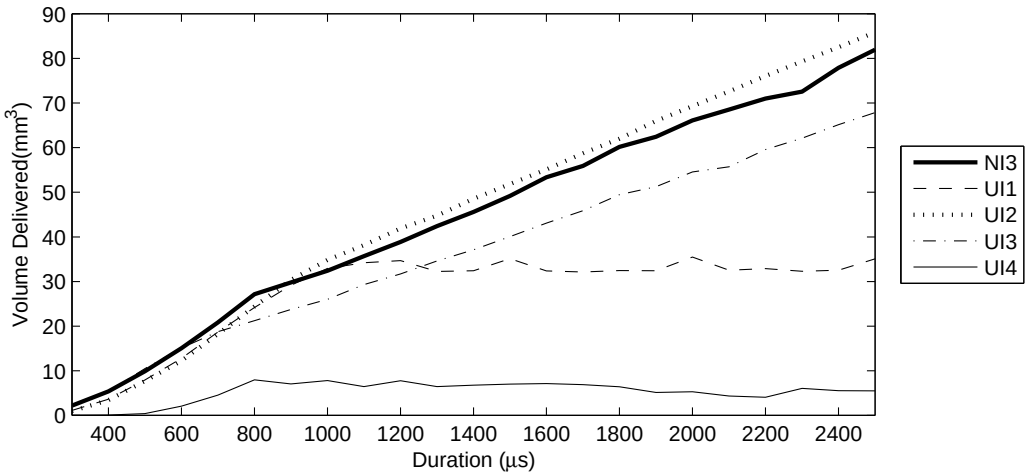

Figure 5.7: Volume of fluid delivered vs injection duration for new and used injectors at 600 bar

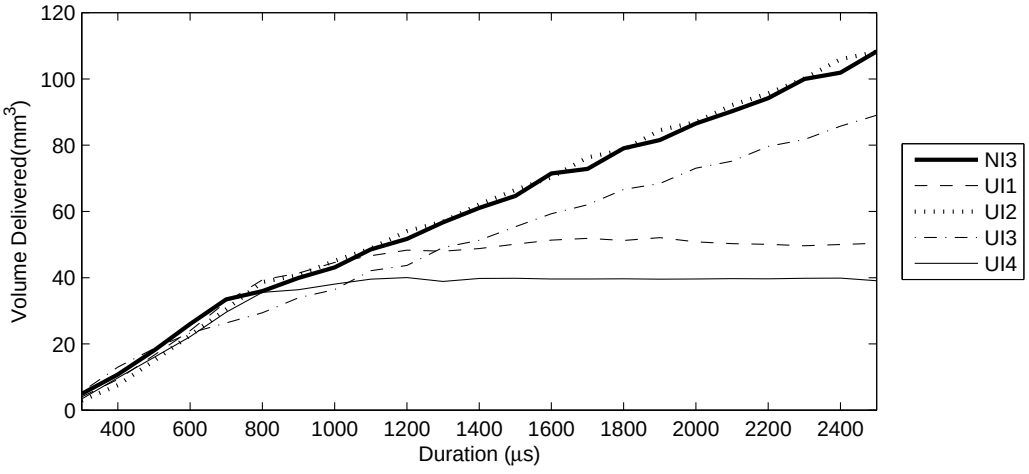

Figure 5.8: Volume of fluid delivered vs injection duration for new and used injectors at 900 bar

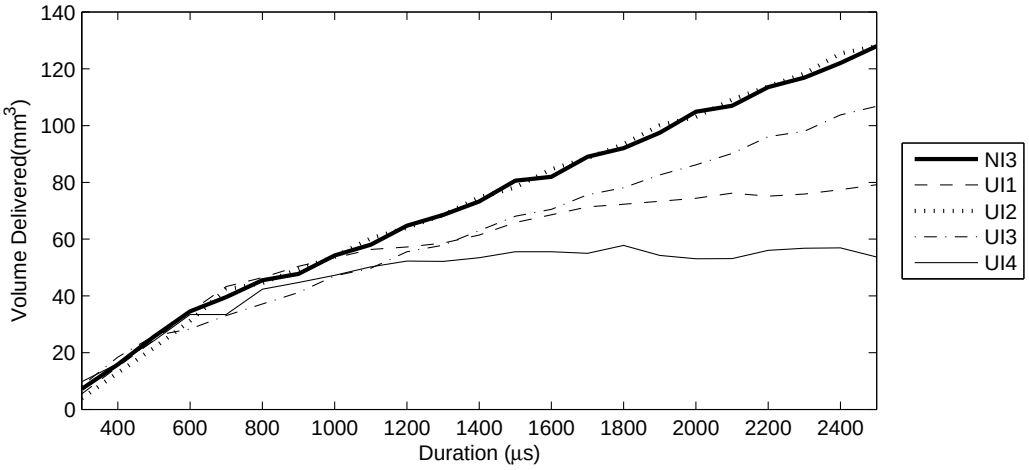

Figure 5.9: Volume of fluid delivered vs injection duration for new and used injectors at 1200 bar

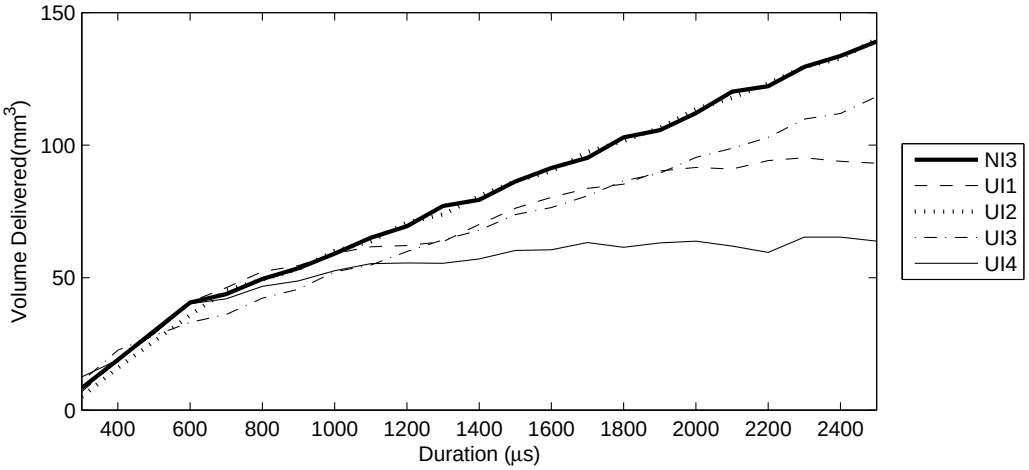

Figure 5.10: Volume of fluid delivered vs injection duration for new and used injectors at 1400 bar

It may be seen from Figures 5.6 to 5.10 that the used injectors do indeed behave differently to the new, control injector. The performance of the injectors varies as the pressure increases, as would be expected. Injector UI2 consistently overfuels slightly across all pressures, while all other injectors tend to underfuel to varying degrees at all pressures.

While the specific behaviour of each injector will be discussed individually in the next series of sections, a few observations may be made at this stage regarding

the performance of the injectors. A note specifically applicable to Figure 5.6, is that injector UI4 fails to deliver any fuel at an operating pressure of 300 bar. This explains why no plot is visible for UI4 in this figure.

Figures 5.6 to 5.10 show that when the fuel delivered by the new injector is plotted against injection duration at constant pressure an almost linear trend emerges. This trend was present in all of the results attained from the new injectors, as illustrated in Section 5.3, on page 60, and illustrated in Figures 5.1 to 5.5.

It seems reasonable that in certain cases a worn injector may behave in a similar manner to a new injector, only delivering more or less fuel, depending on the nature of the wear. If this were to be the case, one would expect to see linear behaviour from the injectors, as witnessed in the new injector results. Figures 5.6 through 5.10 reveal that this linear trend is indeed preserved on two of the used injectors, specifically UI2 and UI3. UI2 may be seen to "Over-deliver" whereas UI3 is evidently "under-delivering" across most pressures. Injectors UI1 and UI4 on the other hand do not follow this linear delivery trend. These two injectors appear to follow a somewhat erratic trend, although both injectors seem to display a notable "knee-point" whereby the delivery appears to level off, and no increase in delivery results from an increase in duration.

All of the above mentioned deviations from the "standard", as established by the control injector, NI3, will be discussed in Sections 5.6.1 to 5.6.4. An attempt will be made to explain the deviations with respect to modes of wear in common rail injectors.

5.5 Cavitation Investigation

As discussed in the literature survey, the phenomenon of cavitation, typically associated with pumps, may occur in fuel injectors. In this section the results obtained from the used injectors will be investigated with regard to cavitation.

It would be reasonable to expect that cavitation may occur in worn injectors due to the fact that wear could influence a number of the parameters which affect the likelihood of cavitation occurring in an injector, as discussed in Section 2.6, on page 17. These parameters include:

- Hole Diameter
- Entrance shape of holes
- C_d for Nozzle
- Needle Lift

Equation 2.19 presented in the literature survey is represented again here for ease of reference:

$$\dot{m}_f = k\sqrt{\Delta P} \tag{5.1}$$

Where $\dot{m}_f$ is mass flow-rate, and ΔP is the change is pressure across the nozzle. The constant *k* is defined below:

$$k = C_d A_0 \sqrt{2\rho_\ell} \tag{5.2}$$

As discussed in the literature survey, the linear behaviour described by equation 5.1 will break down when cavitation occurs. If cavitation occurs during in an injection one would notice that the rate at which fluid is being delivered would not increase with increasing pressure.

The results of the Akribis tests have been processed such that their compliance with equation 5.1 may be verified. This was done by averaging the flow-rate (which may be assumed to be directly proportional to mass flow rate if density is constant), during the period where the injector is injecting at an almost constant flow-rate. To facilitate this, an algorithm was written to determine the average volumetric flow-rate above a threshold of 75% of the maximum flow rate. The results of this algorithm when performed on a single injection are shown below, in Figure 5.11 which indicates how the average delivery rate at steady state was determined. The cacluated avearge steady state flow-rate is indicated by the horizontal line.

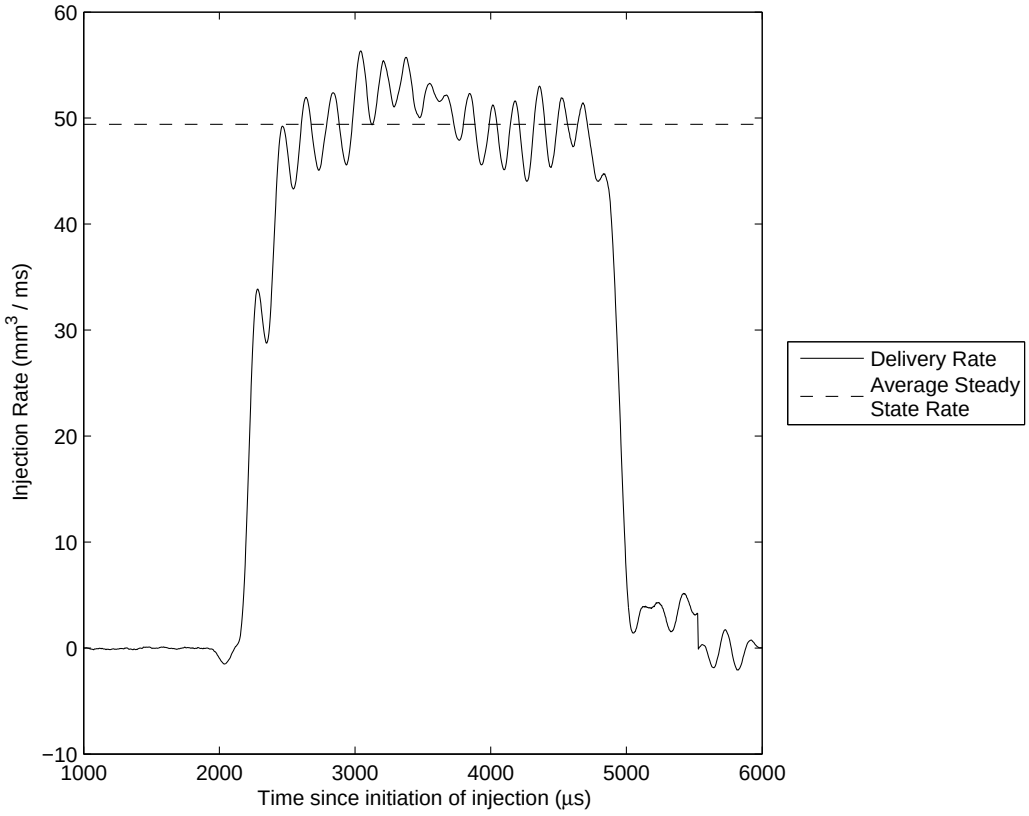

Figure 5.11: Injector delivery rate vs time, indicating average steady state delivery rate

A plot of the performance of all injectors at a duration of 1000μs is shown below in Figure 5.12. The figure shows that all injectors continue to deliver an increasing amount of fuel as the rail pressure increases. It may be seen that four of the injectors, NI3, UI1, UI2 and UI3 all follow linear trends as expected, based on equation 5.1. Only injector UI4 does not follow the same linear trend as evident in the plots of the performance of the other injectors. However, if cavitation were to be occurring one would expect to see a "flat-lining" of the delivery with increasing pressure. This is not the case, instead, the delivery continues to increase, and the rate of increase tends toward a gradient similar to that of the other injectors. Based on this discussion, it may be stated that cavitation is not occurring in any of the injectors tested.

Figure 5.12 indicates that three of the injectors share a similar gradient, and injectors UI3 and UI4 have less steep gradients. This variation in gradient indicates

a difference between the various injector in the 'k' term, as introduced in equation 5.2. This would indicate a difference in either C_d or A_0, as the density term, $\sqrt{2\rho_\ell}$, cannot change. Since the gradient of UI3 and UI4 has decreased significantly compared to the other three injectors, this indicates that either C_d or A_0 has decreased. It would seem unlikely that the area, A_0, should have decreased due to wear. However, the discharge coefficient, C_d may well have altered during the life of the injector.

The injectors with the less steep gradients, injector UI3 and injector UI4, were supplied in the second set of injectors, and were thus supplied after having their nozzles ultrasonically cleaned. There is a significant similarity between the two injectors, and it will be shown in Sections 5.6.3 and 5.6.4 that further performance similarities emerge during analysis of these two injectors.

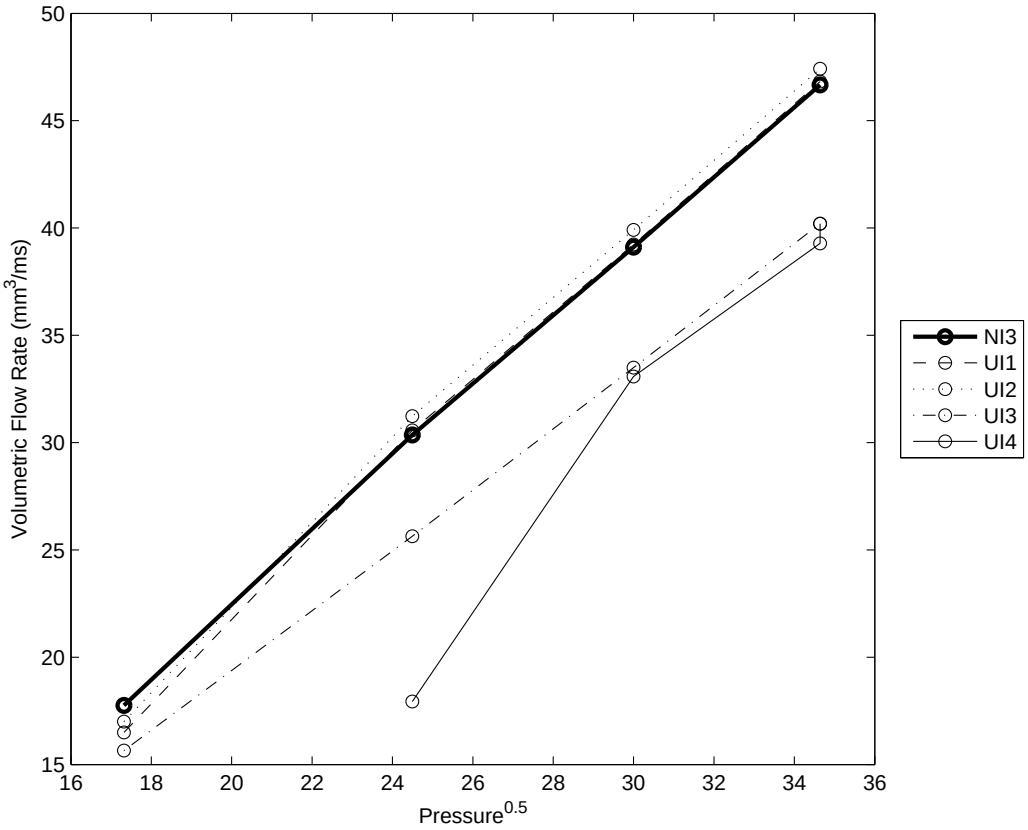

Figure 5.12: Plot of average Volumetric flow-rate vs Pressure$^{0.5}$ for 1000μs injection

It is noteworthy, regarding the above discussion, that the C_d which is discussed above should ideally relate to only the nozzle, but since the control volume for the experiments being conducted is the entire injector, this is not the case. Therefore, the discharge coefficient as discussed refers to the efficiency of the entire injector and not just the nozzle, in converting a pressure differential into a flow of fluid.

5.6 Used injector Performance Investigation

Within this section the performance of each of the four used injector upon which testing was conducted will be investigated. Through comparing the results of the used injectors with those produced by the new injector possible reasons for the disparity between the performance of the injectors will be discussed.

5.6.1 UI1 Investigation

Introduction

Injector UI1 was supplied for the investigation from industry, where the faults present with the injector were described, on the tag, as follows: “Back-leakage Ok. Delivery Characteristic Incorrect (underfueling)”.

From inspecting the performance of injector UI1 in the generic plots of delivery vs duration as presented in section 5.4, it may be seen that injector UI1’s delivery performance is not in line with the performance of either the new injector or the performance of the other used injectors.

Observations

The performance of Injector UI1 is noteworthy in that at shorter durations the delivery characteristics closely follows that of the other injectors. However, at

longer duration the delivery of the injectors appears to reach a steady value, and does not increase in the same manner as the other injectors do, specifically NI3, which is the most consistent injector.

If one inspects the plot of duration against delivery at 900 bar, shown in Figure 5.13 below, it may be seen that a distinct "knee-point" exists on the graph, at around 1100μs and 50mm^3

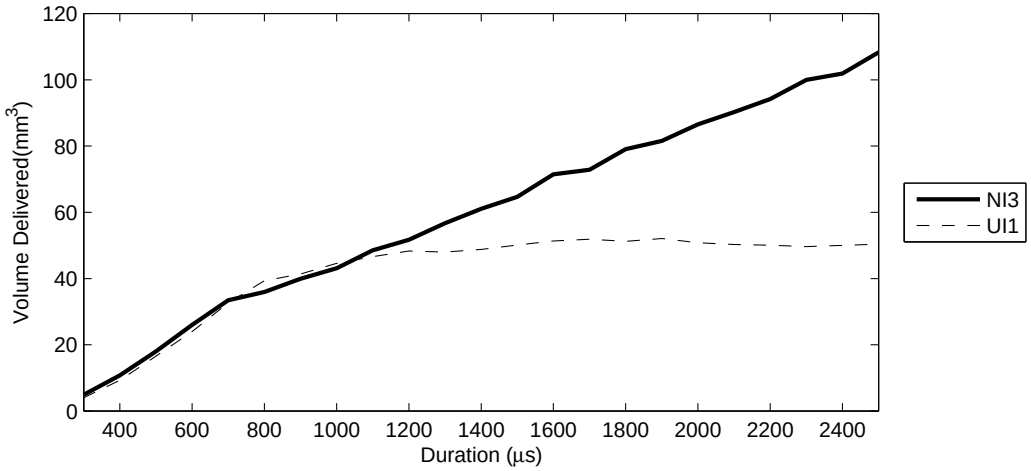

Figure 5.13: Volume of fluid delivered vs injection duration for injectors NI3 and UI1 at 900bar

After the knee-point, the delivery appears to "flat-line". The early stages of delivery closely follows the performance of the new injector, more closely than some of the other injectors, which perform better at later stages of the injection. This close following of the new injector's characteristic curve suggests that wear is not present in either the feed or bleed orifices, the effects of which are described in the literature review, on page 33.

A plot of injector delivery rate is shown alongside the firing pulse sent to the injector from the driver unit is illustrated in Figure 5.14 below. This figure is a plot of the rate at which fluid is discharged from the injector against the signal sent to the injector against time. This plot aims to illustrate the manner in which the injector behaves when subjected to an excitation signal.

Figure 5.14 clearly illustrates the difference in performance between the used in-

jector, UI1, and the control injector, NI3. It may be seen that injector UI1 ceases to deliver fuel before the driver unit stops sending a signal to it, while NI3 continues to deliver fuel.

If one examines Figure 5.14, it may be seen that the firing pulse sent to the injector has two distinct steady levels. The first level is known as the "Pull" phase and is designed to give the injector a high energy pulse to overcome its initial stationary state. The second state is known as the "Hold" state, and is designed to hold the injector in an open position once the injector is open.

The tests run on the injectors were conducted using standard settings, as programmed into the test stand by the manufacturers. These standard settings provide for a 500μs pull phase, which is evident in Figure 5.14.

The control injector, NI3, does not show a significant change in performance when it is receiving either the initial pull signal or the steady "Hold" signal. It may be argued that the rate of delivery is more constant and less oscilitory during the initial phase of the injection. This level of subtlety, however is beyond the scope of this study. In comparison to the control injector, injector UI1 does not appear to react to the hold phase of the injector at all.

In order to verify the that the injector is not responding to the hold phase of the

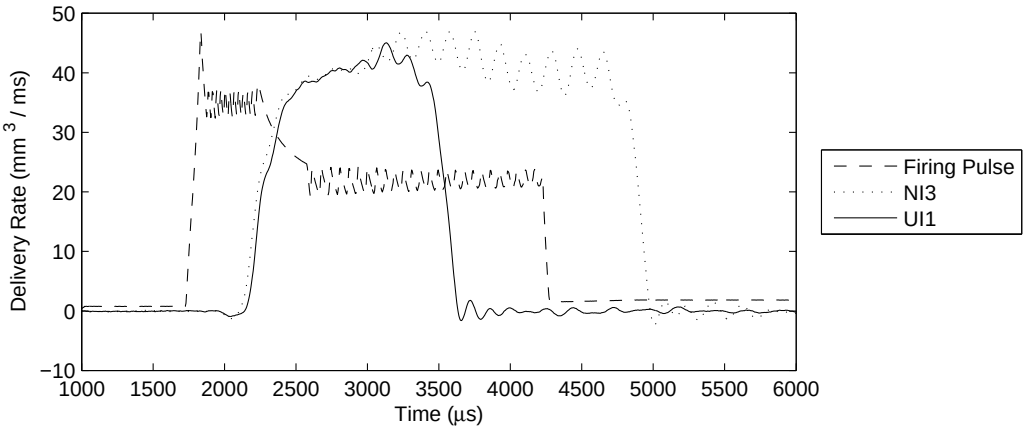

Figure 5.14: Delivery rate and firing pulse vs time for injectors NI3 and UI1 for 300bar, 600μs injection

firing pulse, tests were conducted using identical firing pulse settings but with the duration of the pull phase extended to 1000μs.

The results of the tests conducted for injectors using a 500μs and 1000μs pull phase for injector UI1, and a 500μs pull phase on NI3, are shown below in Figure 5.15.

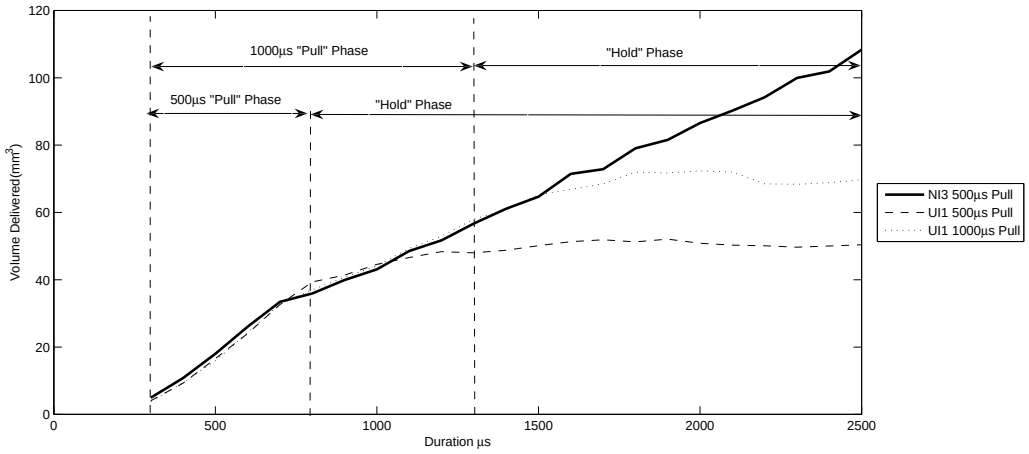

Figure 5.15: Volume of fluid delivered vs injection duration for 500μs and 1000μs Pull Phases, for injectors UI1 and NI3 at 900 bar

Figure 5.15 clearly indicates that injector UI1 behaves differently when subjected to the 500μs and 1000μs duration pull phases. It is immediately evident that the used injector continues to flat line in terms of delivery, but this now occurs approximately 500μs later. This leads one to believe that the firing pulse duration is indeed having a marked effect on the performance of the injector.

In order to verify that the duration of the pull phase of the injector should not affect a properly functioning injector, a plot has been prepared showing the performance of injector NI3 when subjected to both 500μs and 1000μs pull phase durations. It may be seen from Figure 5.16 below that there is no discernible difference between the results for the two pull phase durations.

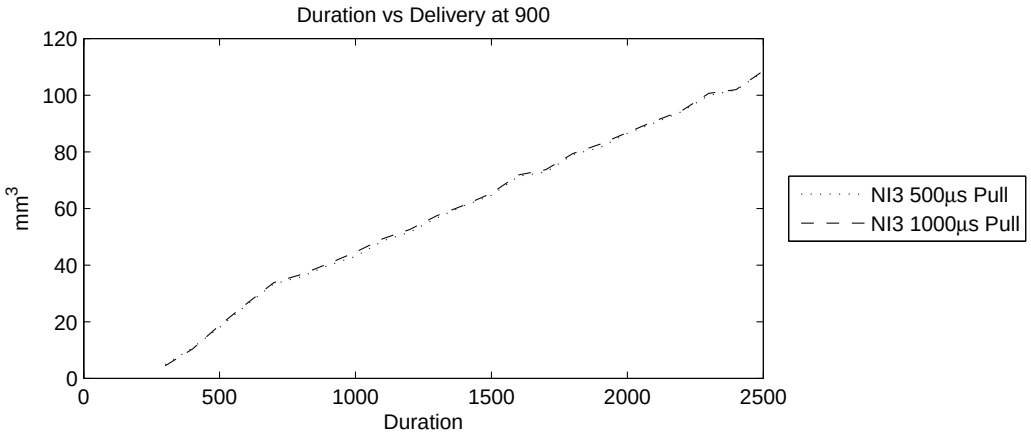

Figure 5.16: Volume of fluid delivered vs injection duration for 500μs and 1000μs Pull Phases, for injector NI3 at 900 bar

Discussion

The following subsection aims to provide rationale for the behaviour of injector UI1, as described in the observations above.

The pull phase duration affects the profile of the signal sent to the solenoid of the injector. Based on the above results it seems reasonable to deduce that a degree of wear has been experienced within the solenoid of the injector, leading to it requiring increased current levels in order to hold the injector open. The results presented in Figure 5.15 provide a clear illustration of the solenoid failing to engage the injector's ball to facilitate the injection. However, at higher pressures the behaviour of the injector becomes less well defined.

An identical plot to that shown in Figure 5.15, but for a rail pressure of 1400 bar, in Figure 5.17. The delivery versus duration plots for 900 bar and 1400 bar injections, as shown in Figures 5.15 and 5.17, are similar in that both closely follow the control injector, NI3, until they reach the end of the pull phase, and then tend to deliver less fuel. A major difference becomes evident at higher pressures, where the injectors do not cease to inject, or "flat-line" as evident in Figure 5.15 at 900 bar, but rather continues to deliver more fuel as duration increases. The

delivery, however is not in line with the performance of the control injector, NI3. This continued increase in fuel delivery as duration increases indicates that the solenoid has not lost all of its effectiveness. When it is assisted by an increase in pressure in the volume beneath the ball, which is operated by the solenoid, it may still deliver fuel. From Figure 5.17 it may be seen that the 500μs pull phase injections experiences a steep gradient followed by a short period where the injector does not deliver more fuel with increasing duration. During this period the gradient of this curve is very similar to that of NI3. The delivery of UI1, employing a 500μs pull phase, then rises to within 70% of that of the same injector using a 1000μs pull phase, before following a similar characteristic to the 1000μs pull phase plot.

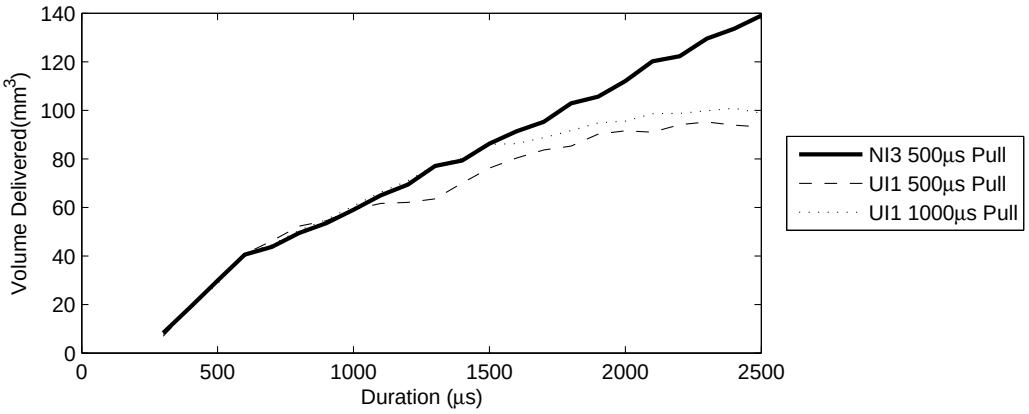

Figure 5.17: Volume of fluid delivered vs injection duration for 500μs and 1000μs Pull Phases, for injectors UI1 and NI3 at 1400 bar

At present there is no explanation for the intermediate behaviour of the injector as described above. The most obvious reason being different behaviour within the solenoid once normal operating current has been restored, in conjunction with the high rail pressure. Regardless of the mechanism behind the unusual intermediate results, the behaviour of the injector would lead to strange performance of the engine to which it was fitted. This is especially so considering the manner in which the delivery picks after a period of not increasing delivery with increasing duration, as displayed in Figure 5.17.

5.6.2 UI2 Investigation

Introduction

The second used injector upon which testing was conducted, designated UI2, was supplied with the following label: “Delivery Characteristic: Over fueling. High Back leakage”. Injector UI2 was briefly discussed in Section 5.4, where the performance of all the used injectors was discussed. There it was stated that injector UI2 possessed the most linear flow characteristics with respect to delivery versus duration.

Observations

The duration versus delivery plots for the lowest and highest pressures are shown below, in Figures 5.18 and 5.19 respectively. The plots also show the performance of the control injector, NI3, for comparative purposes.

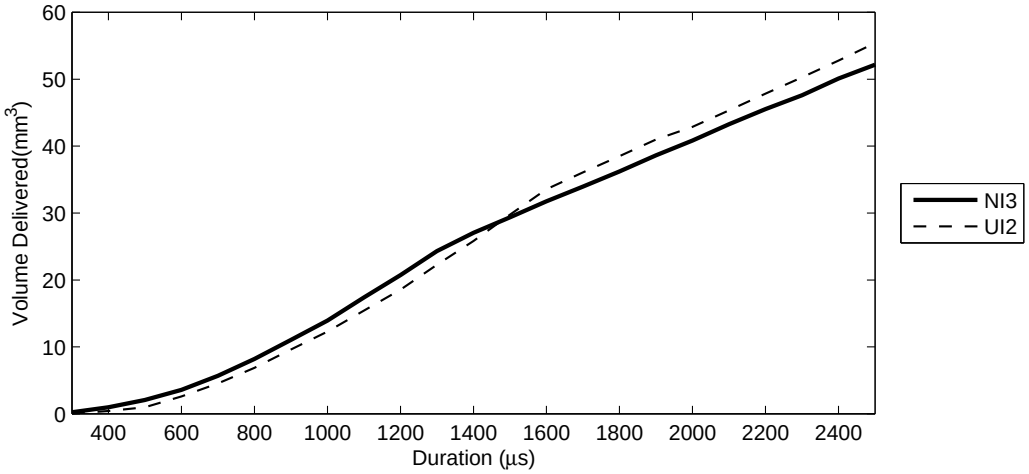

Figure 5.18: Volume of fluid delivered vs injection duration for injectors NI3 and UI2 at 300bar

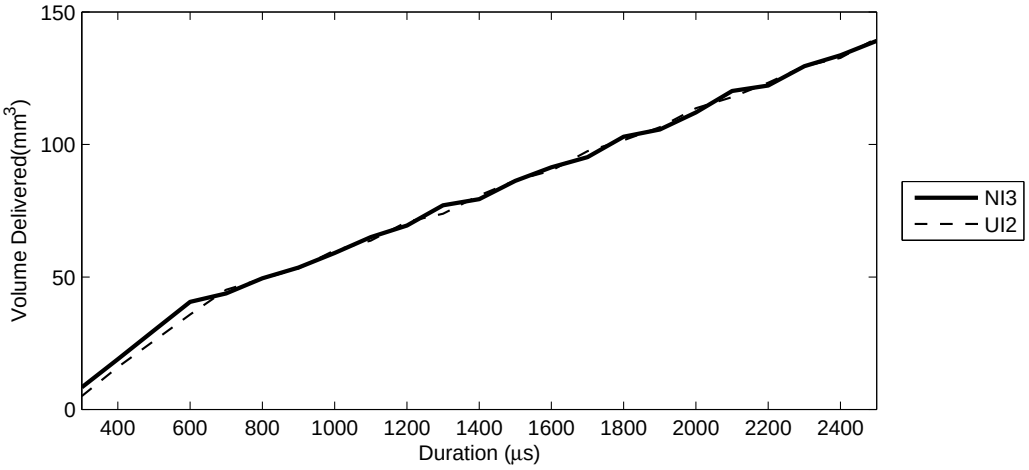

Figure 5.19: Volume of fluid delivered vs injection duration for injectors NI3 and UI2 at 1400bar

From Figures 5.18 and 5.19 it may be seen that injector UI2 follows a delivery characteristic very similar to that of the new injector. At the lower pressure, 300 bar, it may be seen that injector UI2 tends to underfuel, at durations up to 1500μs, after which the injector over fuels by about the same amount as it was underfueling. The injector's delivery at various durations with the rail pressure of 1400 bar is shown in Figure 5.19. At this higher pressure injector UI2 follows the standard as established by NI3 even better than at 300 bar. It may be seen that injector UI2 underfuels initially, as was the case in the 300 bar plot, but at 1400 bar the injector ceases to underfuel at durations longer than 700μs. It then follows the performance of injector NI3 very closely.

Injector UI2 was discarded due to high back-leakage, and since the apparatus employed for testing does not provide data regarding back-leakage this may not be verified. However, the injector characteristics may be investigated so as to attempt to identify what may be wrong with the injector.

The injection specific profile, that is, the manner in which the injector delivers fuel at a specific pressure and duration, may be looked at to provide insight into the performance of the injector. A selection of injections will be shown here in an attempt to investigate the source of the non-standard delivery characteristics of the injector under investigation.

Total fuel delivered was represented at the the lowest and highest test pressures, so the delivery rate and duration specific fuel delivered will initially be represented at these pressures. Presented below, in Figure 5.20, is the delivery rate plot for a 600μs injection at a rail pressure of 300 bar.

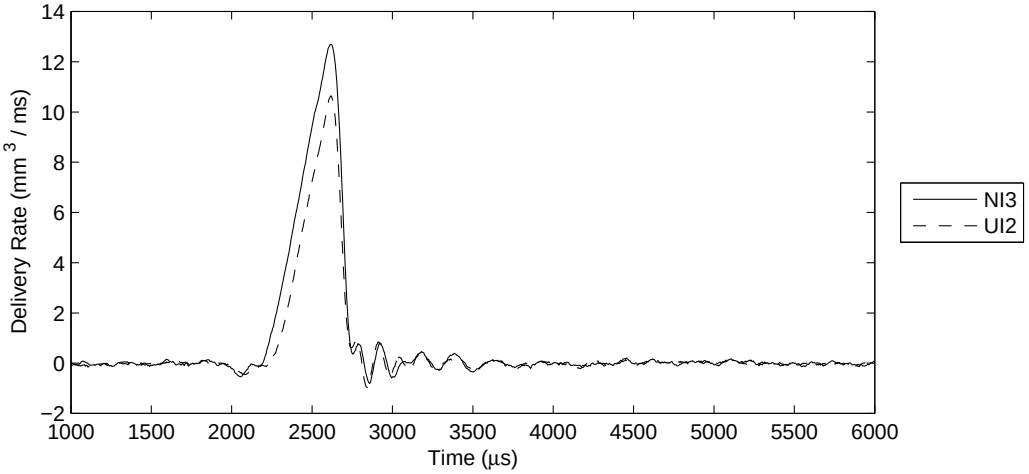

Figure 5.20: Delivery rate vs time for injectors NI3 and UI2 for a 300bar 600μs injection

From Figure 5.20, it may be seen that injector UI2 does not react as rapidly as the new injector. This may be seen by the fact that the gradient of injector UI2 is less steep than that of NI3. The area beneath the rate versus time curve indicates the volume of fuel injected. It may clearly be seen that injector UI2 is indeed underfueling as a result of the slower opening of the injector.

The low pressure analysis may be continued by looking at the details behaviour of injectors at longer durations. To facilitate this, Figure 5.21 below shows the injectors rate profile at 300 bar and 2500μs duration. The delivery rate profile at 2500μs tells a very different story to that of the same injector at the same pressure, but at shorter durations. The increase in delivery rate is still slower than that of the new injector. However, a major difference emerges in the manner in which the injector closes. Injector UI2 is very sluggish in its closing when compared to injector NI3. The area underneath the curves for UI2 and NI3 shows the extent to which injector UI2 is overfueling.

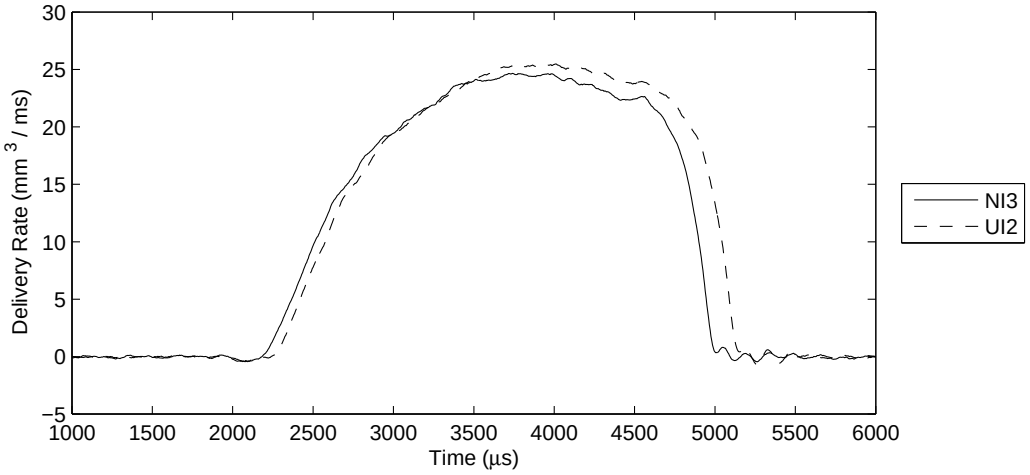

Figure 5.21: Delivery rate vs time for injectors NI3 and UI2 for a 300bar 2500μs injection

In addition to both the short and long duration cases, it is interesting to look at the situation where both the new and the used injector deliver an equal volume of fuel. As discussed above, this occurs at the 1500μs injection. The rate profile for this injection is shown in Figure 5.22 below.

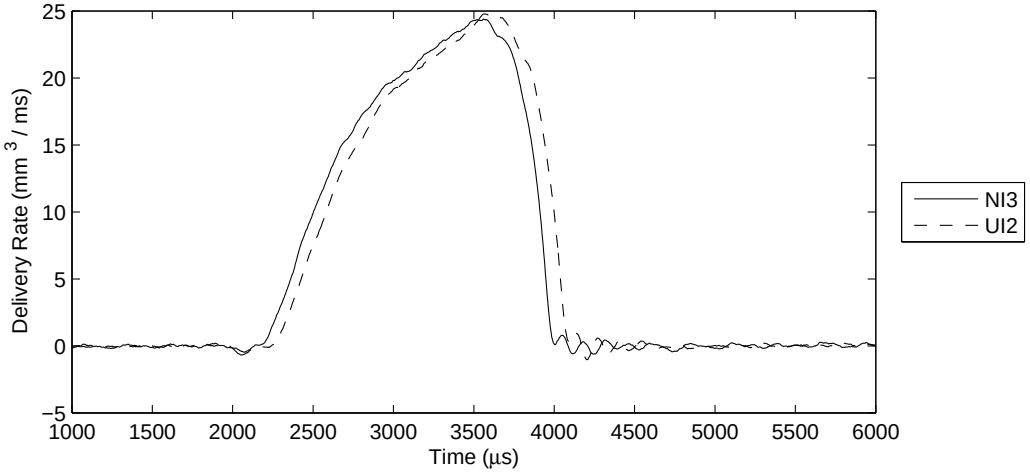

Figure 5.22: Delivery rate vs time for injectors NI3 and UI2 for a 300bar 1500μs injection

Figure 5.22 provides interesting insight into the performance of injector UI2, in that it may be seen that for the initial period of the injection underfueling occurs and later overfueling occurs. At a duration of 1500μs the initial period of

underfueling is matched by the later period of overfueling. This is important to note because, by reading figure 5.18, one may be lead to believe that under these circumstances the injector is functioning effectively. This would be erroneous.

The 1400 bar injections, as discussed earlier, will now be looked at in greater detail, as done in the case of the 300 bar injections. From Figure 5.19, it was seen that at 1400 bar, injector UI2 underfuels initially, after which it closely follows the performance of the standard injector. Figure 5.23 below shows a short duration 1400 bar injection.

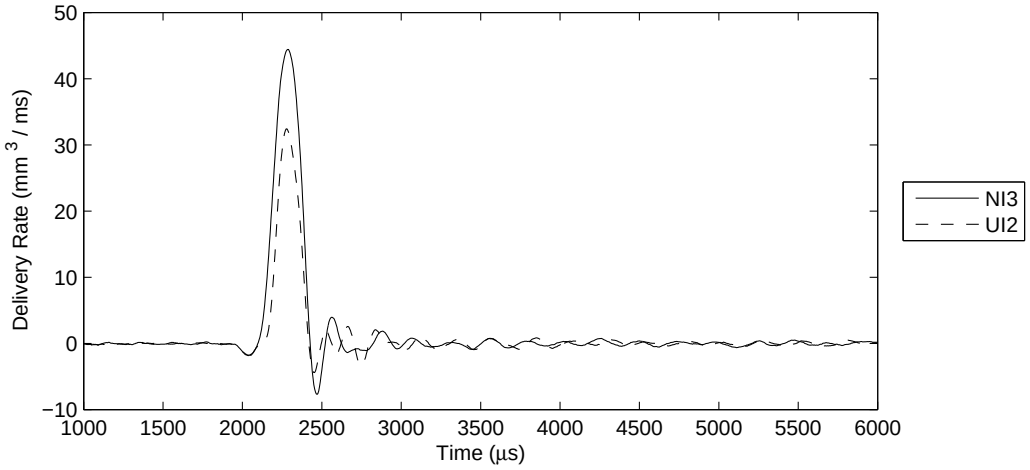

Figure 5.23: Delivery rate vs time for injectors NI3 and UI2 for a 1400bar 300μs injection

By observing the areas underneath the injection rate curves for injectors UI2 and NI3 in Figure 5.23, it is clear that injector UI2 is indeed underfueling. Unfortunately, there is little detail available from Figure 5.23 due to the brief nature of the injection. In order to provide more detail, the worst case of underfueling for injector UI2, occurring at 600μs duration, is shown below in Figure 5.24.

It may be seen from Figure 5.24 that the delivery rate of the injector behaves in a very similar manner during the period of steady state operation, and during the period relating to the cessation of injection as was the case in the 300 bar test. The difference between the new and used injector emerges in the early stages of the injection.

The new injector delivery rate climbs almost linearly to the point where it is delivering steady state flow. The used injector also climbs linearly, but then appears to suffer a kink whereby the delivery rate slows before reaching the new injector's steady state delivery rate.

Previous discussion based on Figure 5.19 indicated that in later stages of the injection both UI2 and NI3 delivered similar amounts of fuel. To provide insight into the behaviour of the injector at longer durations, a 2500μs injection rate profile is shown in Figure 5.25.

Injector UI2's rate profile is interesting in that it is very similar to that presented in the case of the 600μs duration injection presented in Figure 5.24. The description given for that injection holds in this case, and the levels underfueling during the initial phase appears to be about the same.

The underfueling is only occurring during the initial injection phase, and the degree of underfueling does not increase with increasing duration. However, the overall amount of fuel is increasing, so as the duration of the injection increases, the degree of underfueling becomes less and less relevant. This explains why the injectors underfueling is so noteworthy at shorter durations and the injector appears to be functioning properly at longer durations.

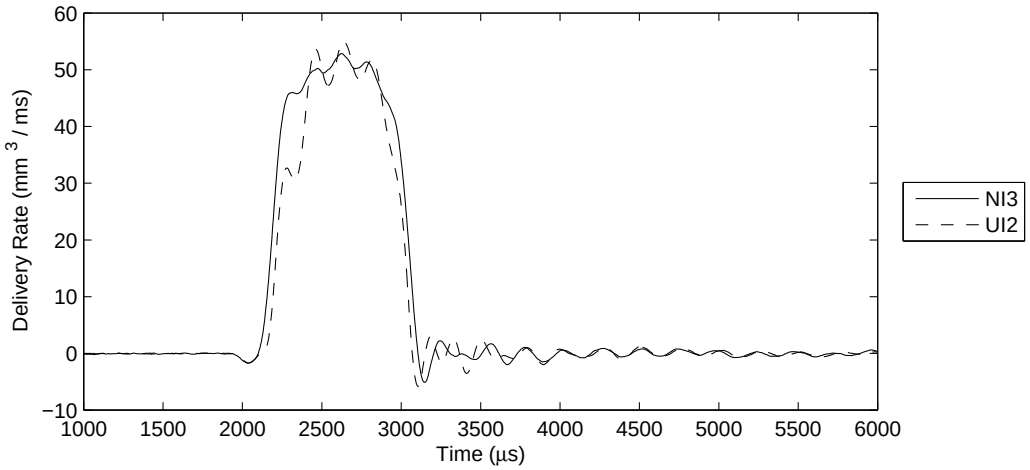

Figure 5.24: Delivery rate vs time for injectors NI3 and UI2 for a 1400bar 600μs injection

Discussion

In the literature survey, in Section 2.9.4, on page 33, a discussion regarding the effects of varying the two main parts of the injector that affect its flow performance. These are the bleed and feed orifice that control the pressure above the plunger which opens and closes the injector.

As an injector wears one would expect a change to occur in the discharge coefficients of the bleed and feed orifices. In addition wear in the injector spring adds to the force effected by the pressure differential resulting from the solenoid and spring closing, and other elements of the injector where flow is present.

Before attempting to isolate problems relating to the injector, it is worthwhile to summarise the behaviour of injector UI2:

1. Poor initial behaviour, at both low and high pressure.
2. Sluggish behaviour at the end of injection, especially at low pressure, leading to overfueling at low pressures.
3. Good steady state behaviour, compared to that of the control injector NI3.

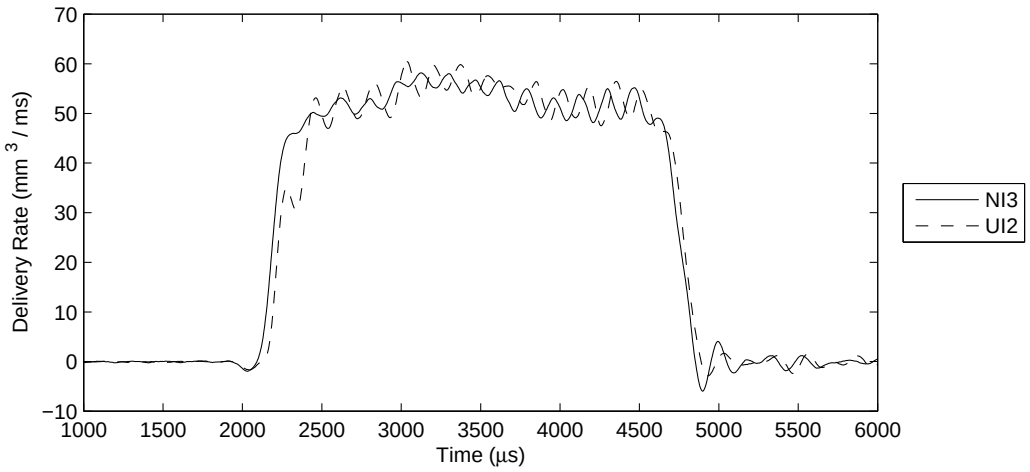

Figure 5.25: Delivery rate vs time for injectors NI3 and UI2 for a 1400bar 2500μs injection

The bleed orifice discharge coefficient controls how fast the pressure in the control volume is reduced when the solenoid releases the pressure on the ball in the valve at the top of the injector. Therefore, wear in the bleed orifice may lead to sluggish opening, as is evident in the observations above. However, due to the fact that the solenoid acts to close the bleed orifice, wear related to the discharge factor generally does not affect the cessation of injection.

Thus the poor initial injection behaviour is very well aligned to wear in the bleed orifice. The bleed orifice discharge coefficient determines how fast the pressure in the volume above the plunger is reduced when the ball above the bleed orifice is removed. A decrease in the bleed orifice discharge factor will result in slower plunger movement, and therefore slow injection.

In order to identify the possible causes for the low pressure overfueling as mentioned in point 2 above it is important to attempt to identify the cause of the overfueling. The nature of the overfueling is evident from Figure 5.21. As discussed above, the closing of the injector at low pressures is sluggish. Figure 5.25 indicates that at the higher pressures this sluggish behaviour tends to not occur.

As discussed in the literature survey, the closing of the injector is caused by the pressure in the volume above the plunger being increased to that of the rail pressure. This leads to a force imbalance between the base of the needle and the top of the plunger, and due to the larger surface area at the top of the plunger, the needle is forced downward. The rate of increase in the pressure above the plunger will naturally have an effect on the speed at which the needle will travel downward, and thus the speed at which the injection is caused to stop. In order for the high pressure fluid to reach this region above the plunger it is required to flow through the feed orifice, as indicated in Figure 2.7, on page 32.

Wear in this feed orifice will result in the fluid taking slightly longer to flow through the orifice, and cause the plunger to travel downward slightly later. Thus wear in the feed orifice may be said to cause the slow closing of the injector.

It may be argued that as the pressure differential across the feed orifice increases,

with increasing rail pressure, that the rate of increase in pressure differential across the plunger/needle assembly will increase. This would mean that, in the event of the discharge coefficient of the bleed orifice decreasing, the injector would indeed close faster at higher rail pressures and slower at lower rail pressures, as is the case in the performance of UI2. One would, however, not expect the slower closing of the injector to be eradicated with increase in pressure. This is confirmed in Figure 5.25, where injector UI2 may be seen to close only slightly slower than injector NI3. The above arguments attributes the incorrect delivery characteristic of injector UI2 to wear in both the bleed and feed orifices. This appears to be logical as whatever mechanism may have been leading to wear in the feed orifice would likely wear the feed orifice as well. In fact, it would seem more unusual if only the one orifice showed signs of wear.

The fault diagnostics sent with the injector detailed that the injector showed high levels of backleakage. Based on the above analysis, which attributes the incorrect delivery characteristics to wear in the bleed and feed orifices, it would seem reasonable that the medium which caused the wear in the bleed and feed orifices could have could have induced deterioration elsewhere. Since the ball is located above the R-throttle which forms part of the bleed orifice, if there was notable wear in this region of the injector, it would be unlikely that the ball would be able to seal effectively. Thus the physical faults originally found with the injector support the theoretical findings of this discussion well.

5.6.3 Injector UI3 Investigation

Injector UI3, the third used injector to be tested was issued in a second batch, along with injector UI4. Unlike injectors UI1 and UI2, UI3 was not issued with a tag detailing the reason for being discarded. Injector UI3 and UI4 also differ from UI1 and UI2 in that their nozzles had been cleaned ultrasonically before being issued for testing.

Observations

Results for the testing of UI3 were presented in Section 5.4, in Figures 5.6 through 5.10 where the total fuel being delivered for injections is shown against the duration of the injections. These results are repeated below, showing only the performance of the new injector NI3 and UI3 at the highest and lowest pressures, in Figures 5.26 and 5.27.

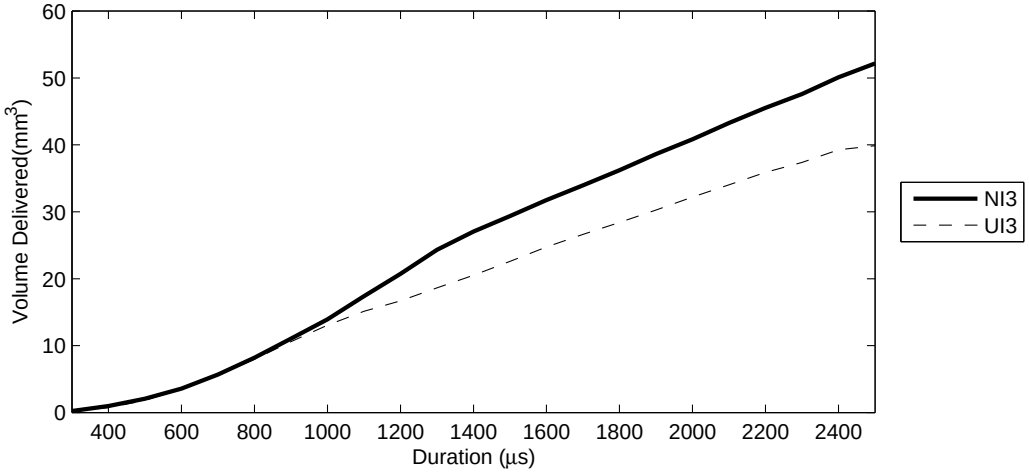

Figure 5.26: Volume of fluid delivered vs injection duration for injectors NI3 and UI3 at 300bar

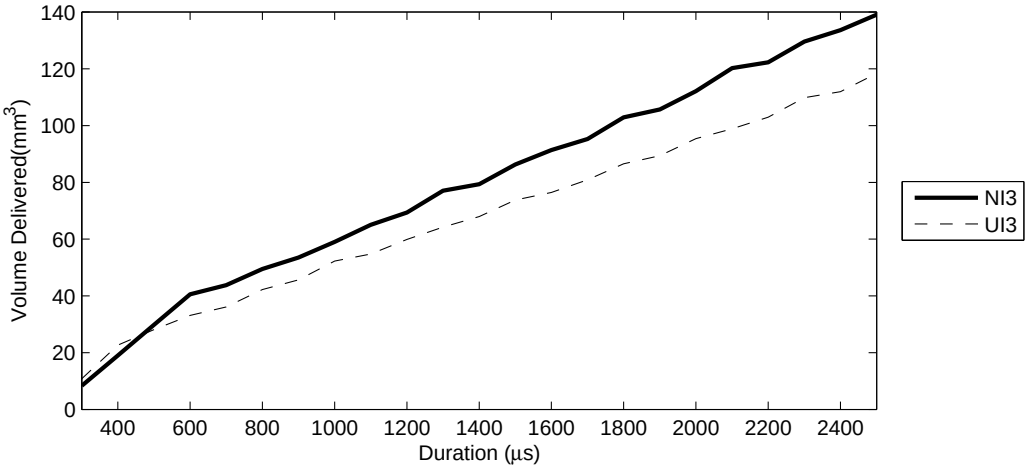

Figure 5.27: Volume of fluid delivered vs injection duration for injectors NI3 and UI3 at 1400bar

From Figure 5.26 and 5.27, it may be seen that injector UI3 underfuels consistently when compared to the performance of the new injector. The results of UI3's performance are interesting in that the manner of the underfueling is consistent at both the lowest and the highest pressure. As durations increase injector UI3 begins to underfuel and continues in a linear fashion from then on. At shorter durations the amount of fuel delivered by injector UI3 is identical to that delivered by the standard injector, NI3.

As in the case of the previous injectors analysed, one hopes that by inspecting the profile of the injection's delivery rate against time at specific durations insight into the mechanism behind injector UI3's underfueling may be gained. The delivery rate for a long, 2500μs, injection at a rail pressure of 300 bar is presented below, in Figure 5.28. This is the low pressure injection with the greatest level of underfueling.

Figure 5.28 indicates three major differences between the performance of injector NI3 and injector UI3. The used injector begins to inject slightly later than the new injector, ceases to inject earlier than the new injector, and delivers considerably less fuel during the steady state period of the injection. As discovered in previous observations, based on the performance of injector UI1 and UI2, it is possible for an injector to behave differently at low and high operating pressures. In order

to investigate the possibility of pressure induced differences in performance, an injection identical to that presented in Figure 5.28, but at an operating pressure of 1400 bar, is shown in Figure 5.29. At higher pressures, and longer durations the injector appears to behave similarly to the new injector during opening and closing periods, however during the typical operating region, the used injector delivers about 20% less fuel.

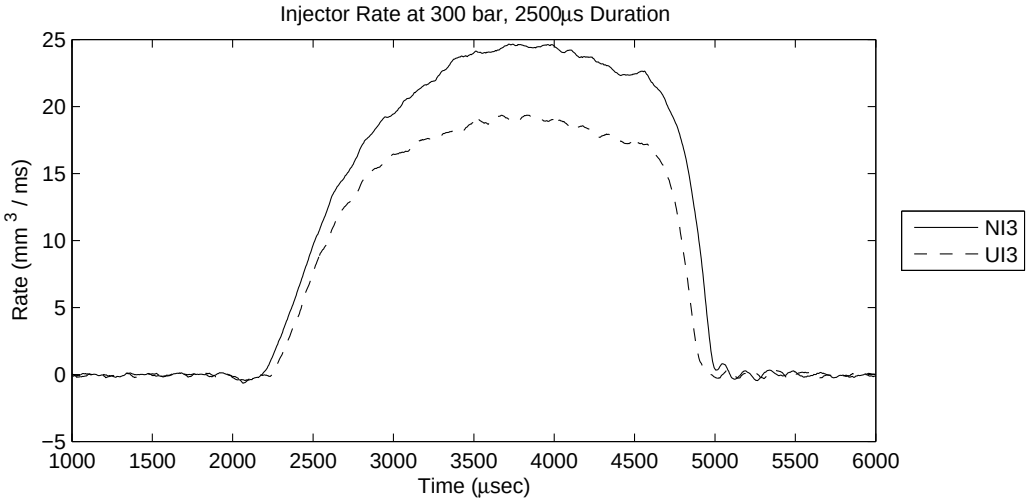

Figure 5.28: Delivery rate vs time for injectors NI3 and UI3 for a 300bar, 2500μs injection

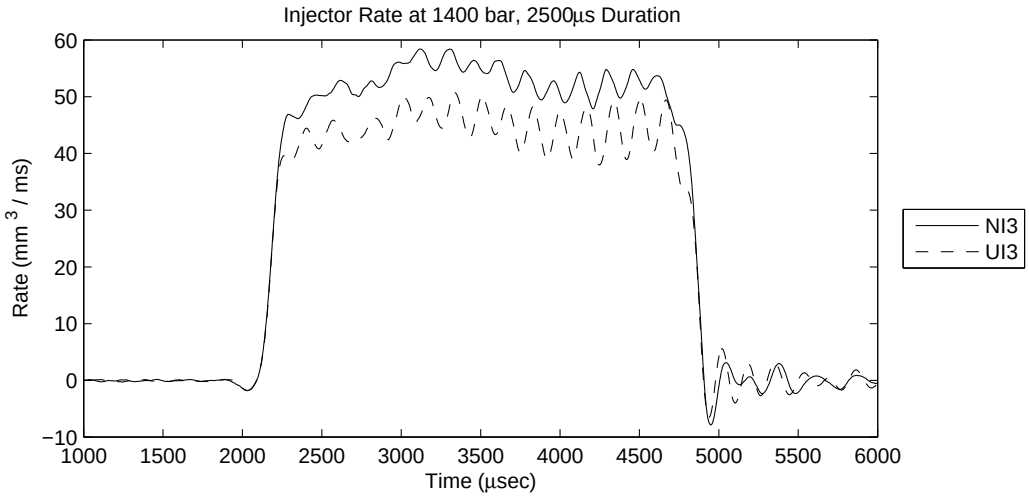

Figure 5.29: Delivery rate vs time for injectors NI3 and UI3 for a 1400bar, 2500μs injection

Discussion

If the opening and closing phases of injector UI3 and NI3 are compared it may be seen that these two injectors perform very similarly. This would suggest that the change in the performance of injector UI3 is not due to deterioration in the bleed or feed orifice. As discussed in Section 2.9.4, as well as in previous analysis of used injectors, wear in the bleed and feed orifices will have a marked effect on the manner in which the injector begins and ceases to inject. However, once the injector has reached steady state operation, steady state conditions will exist in the volume above the plunger, and below the needle shoulder, as illustrated in Figure 2.7 in Section 2.9.4, on page 32. So, regardless of the degree of wear present in the bleed and feed orifices, the steady state behaviours of the two injectors, of identical design, should be the same. The above argument along with the fact that at high pressures, the opening and closing periods of the injections are identical to those of the new injector, leads one to look elsewhere for the fault with injector UI3. It could be proposed that the underfueling is due to a high level of fuel bypass, due to a worn bleed orifice. While it is not possible to confirm or disprove this, it seems unlikely that the injector's opening and closing characteristics would be so similar to the new injector if a significant amount of wear was present in either the bleed or feed orifice.

If one considers an operating common rail injector, fuel enters the injector at the top and flows down the injector to a volume where it applies a pressure to the needle shoulder, as well as the inside of the nozzle, where the fuel exits through the orifices. Thus it may be seen that the flow path of the fuel is relatively simple, and if the actuation system is excluded from the analysis all that remains to be considered is:

1. Injector Nozzle
2. Fuel Line
3. Mechanical Elements

1. Injector Nozzle

Injector UI3 is unique when compared with UI1 and UI2 in that the nozzle was removed and cleaned ultrasonically before being issued for testing. This makes it relatively simple to eliminate the nozzle as a source of underfueling, as any fouling up of the injector nozzle would have been removed by this cleaning process. If the nozzle were to be worn, one would expect material to have been removed from the nozzle and hence the orifices would be larger. The larger orifices would not result in decreased fuel flow, and it may therefore be ruled out as the cause of the underfueling.

2. Fuel Line

It is possible that a blockage may have occurred within the fuel line running down the length of the injector. This initially appeared to be a reasonable source of the injector's underfueling, but it does not make sense that a blockage would become lodged in this fuel line. Firstly the debris would be required to enter the injector through the feed orifice, which is considerably smaller than that of the fuel line. Secondly, the high pressures would likely have forced the blockage down to the nozzle where it would have been removed when the injector nozzle was cleaned. It thus does not seem likely that a blockage could form in this line. Also, if there were to be a restriction in this line, the pressure differential across the needle, which leads to the injector opening, would not be identical to that of the new injector - leading to different opening characteristics. In addition to this analysis, if the fuel filtering system had allowed particulate large enough to constrict the fuel line within the injector, smaller particulate would also have entered the injector which would have lead to wear in the bleed and feed orifices.

3. Mechanical Elements

At this juncture all flow elements have been eradicated as potential sources of the injectors underfueling. The elements remaining are the mechanical components, including the plunger, needle, and spring / ball valve.

The needle forms a component of the nozzle assembly, which would have been cleaned during the nozzle overhaul. It therefore seems reasonable this may be eliminated as a potential source of the underfueling. Should any major wear have been present, it is safe to assume it would have been identified when the nozzle was cleaned. The spring may also be eliminated, because it would naturally become weaker, and would thus lead to overfueling. This would also affect both the opening and closing characteristics of the injector.

Wear in the plunger, however, does seem to be a reasonable cause for the injector's underfueling. During the course of the injection the force imbalance within the injector leads to an upward force on the plunger. If excess friction is present between the plunger and the body of the injector the force balance which results in the plunger's movement will be altered, leading to the evident underfueling of injector UI3. This increase in friction will cause the needle to travel both slower, and a shorter displacement when compared to the new injector. The decreased displacement of the injector's needle is borne out in the lower steady state delivery rate at all pressures, both high and low. However, the sluggish behaviour of the injector which would also result from the friction, is only evident at lower pressures. This may be because the forces involved in accelerating the needle at the lower pressures are that much smaller than those at higher pressures. An alternate reason for change in performance, which also would explain the strange fueling characteristics, would be a physical obstruction preventing motion of the needle. A cause for this may be a blockage or a failure of a mechanical element within the injector. While it is difficult to define a cause for such a phenomenon, it does explain the characteristics of the injector, whereby the transients are as in the case of injector NI3, but the steady state flow is reduced.

The supplier of the used injectors was contacted for background information regarding the injectors, specifically injectors UI3 and UI4, which were provided without descriptions of the faults associated with them. The supplier described the fact that the injector nozzles were cleaned ultrasonically, and that both injectors were removed from relatively high mileage vehicles - having covered between

250’000 and 300’000km. Based on the high mileage of the vehicles, it is possible that the increased friction is simply resultant from excessive use with slightly abrasive fuel, as is frequently found in South Africa. There is no remedy for such a case besides the replacement of the entire injector body, as was determined by the supplier of the injectors, since ultrasonic cleaning did not remedy the underfueling.

5.6.4 Injector UI4 Investigation

Introduction

As in the case of used injector UI3, injector UI4 was supplied without a description of the fault associated with it, but it had been cleaned ultrasonically before delivery.

Observations

Figures 5.6 through 5.10, in Section 5.4, on page 64, show the performance of all five test injectors. From these Figures, and the associated analysis, it was seen that injector UI4 underfuels considerably, and does not delivery any fuel at the lowest pressure, but does deliver at the higher test pressures.

For the sake of clarity, the total fuel delivered against injection duration for the durations that injector UI4 does deliver fuel is shown below in Figures 5.30 through 5.33.

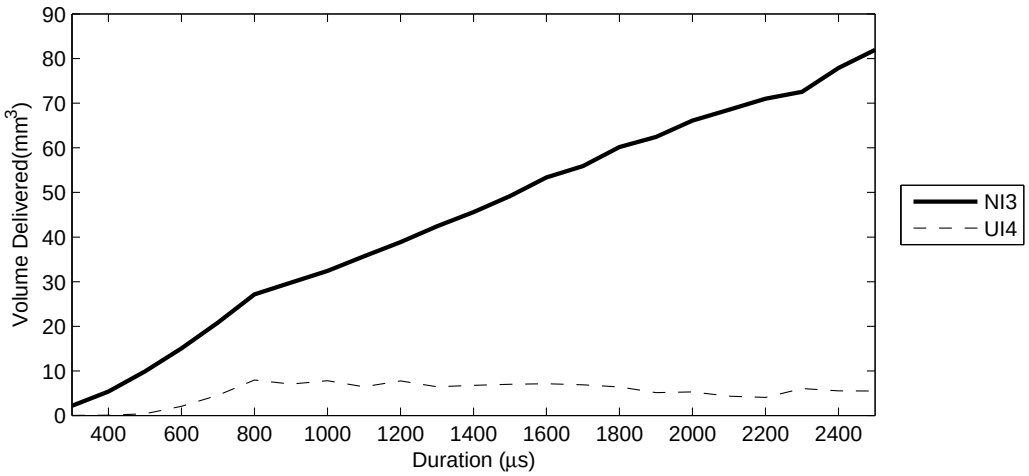

Figure 5.30: Volume of fluid delivered vs injection duration for injectors NI3 and UI4 at 600bar

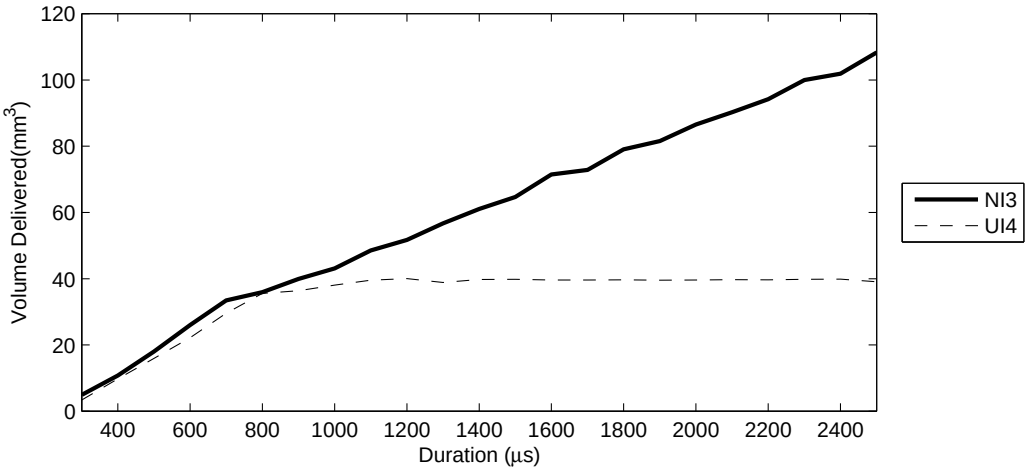

Figure 5.31: Volume of fluid delivered vs injection duration for injectors NI3 and UI4 at 900bar

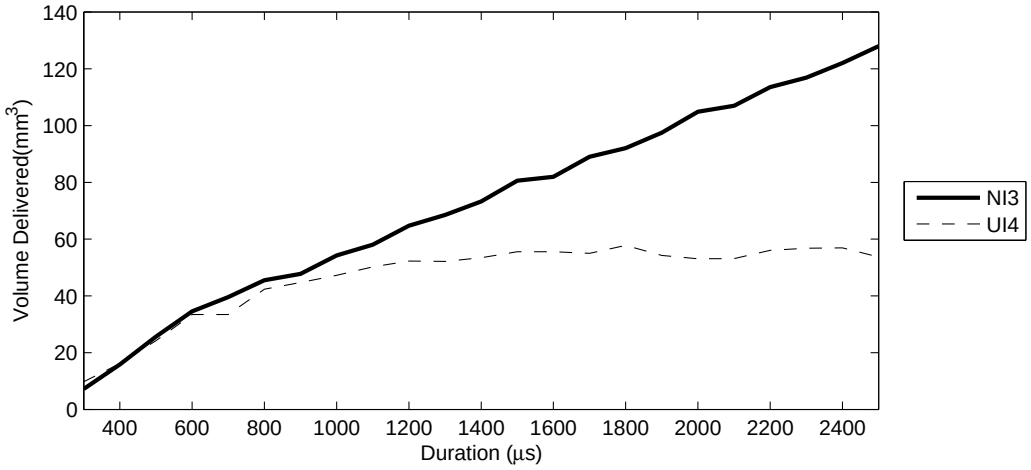

Figure 5.32: Volume of fluid delivered vs injection duration for injectors NI3 and UI4 at 1200bar

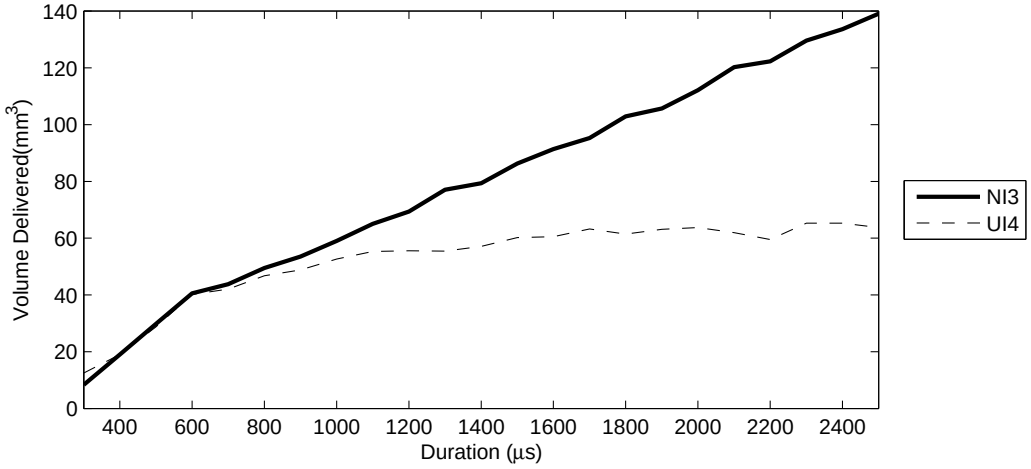

Figure 5.33: Volume of fluid delivered vs injection duration for injectors NI3 and UI4 at 1400bar

If one inspects the performance of UI4 in Figures 5.30 through 5.33 it may be observed that a similar phenomenon to that observed in the results presented for UI2 is occurring. In the three cases where rail pressure is greater than 900 bar a distinct knee point is evident at about 900μs where the injector's delivery ceases to increase with increasing duration.

These results bear more than a passing resemblance to those of injector UI1, which was found to have developed a problem with the solenoid. It would only respond to the "Pull" phase current, and not to the "Hold" phase current.

In order to verify that this was in fact the case, a second set of results was run, as in the case of injector UI1. In this set of results the duration of the "pull" phase of the injection was doubled from 500μs to 1000μs. The results of the 1000μs pull tests are shown below. The results compare the performance of injector UI4 at the standard 500μs pull, and the lengthened 1000μs pull phase. Also shown in these results is the performance of the control injector, NI3, with a 500μs "pull" phase. Figures 5.34 through 5.37 show the maximum delivery of the injectors at various durations, for the pressures at which injector UI4 delivers fuel. A set of tests, employing the 1000μs pull phase, was run at 300 bar but as in the case of the 500μs pull phase injection, the injector failed to deliver any fuel. It should be born in mind from analysis shown in Section 5.6.1, that the performance of the control injector, NI3, does not change significantly with increase "pull" phase duration.

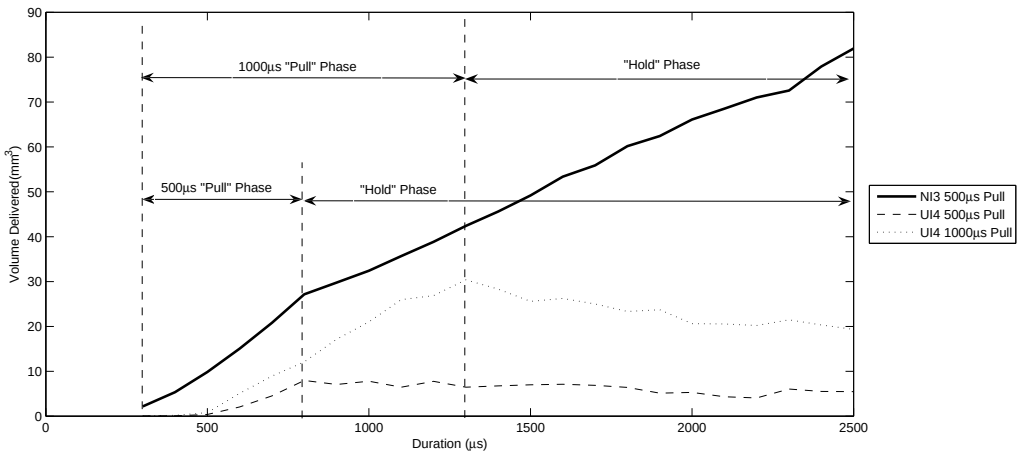

Figure 5.34: Fuel delivery vs injection duration for 500μs and 1000μs pull phases, for injectors NI3 and UI4 at 600 bar

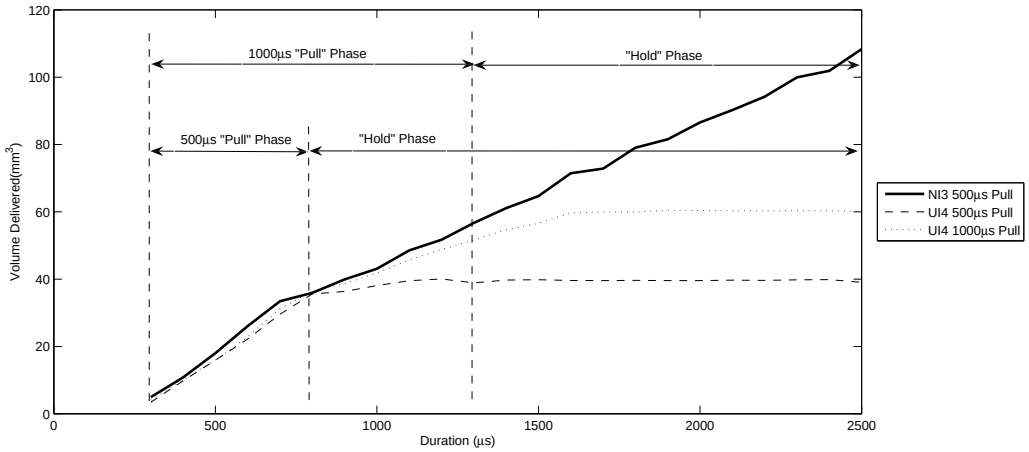

Figure 5.35: Fuel delivery vs injection duration for 500μs and 1000μs pull phases, for injectors NI3 and UI4 at 900 bar

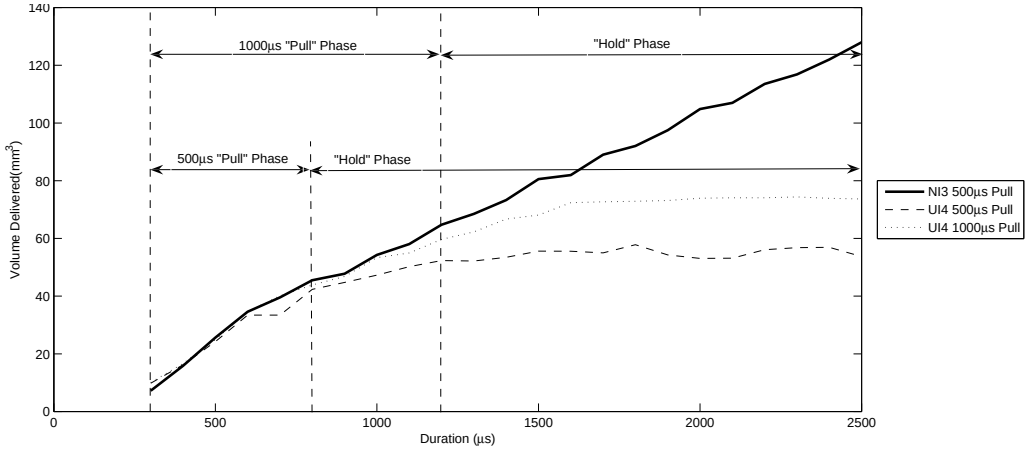

Figure 5.36: Fuel delivery vs injection duration for 500μs and 1000μs pull phases, for injectors NI3 and UI4 at 1200 bar

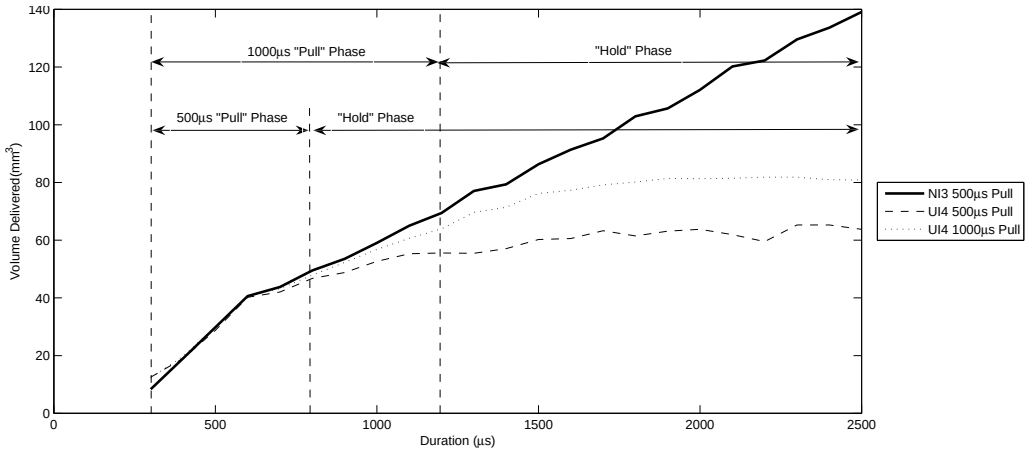

Figure 5.37: Fuel delivery vs injection duration for 500μs and 1000μs pull phases, for injectors NI3 and UI4 at 1400 bar

From Figures 5.34 through 5.37, it may be seen that, as expected, the quantity of fuel delivered is increased with the longer pull phase. As in the results presented for injector UI1, the difference in delivery characteristics based on increased pull phase duration, indicates that there is wear in the solenoid. This is effectively stops the solenoid from operating at the “shorter”, normal, pull phase duration.

The results presented for injector UI4 resemble those of UI1 in so far as there is a decided difference in the performance of the injectors at increased pull duration. However, the results of injector UI4 differ from those of injector UI1 in that if one looks at Figure 5.15, on page 74, it may be seen that the delivery from UI1 only differs from the new injector when the solenoid fails to engage. Up to the point where the solenoid appears to stop working, injector UI1 closely follows the trend established by NI3.

The difference in performance between injectors UI1 and UI4 becomes evident when comparing their performance relative to NI3 after the first 500μs of the pull phase of the injection. If one looks at Figure 5.36, where the results for a rail pressure of 1200bar are presented, a distinct breakaway may be seen in the 1000μs pull phase injection, before it flat-lines. To gain an insight into the nature of the difference in performance a comparison of rate profiles may be made.

Figure 5.38 shows a comparison between injectors NI3 and UI4 when supplied with a 1000μs pull phase. The plot is of in injection where the injector is only the extended pull phase, and not the hold phase current.

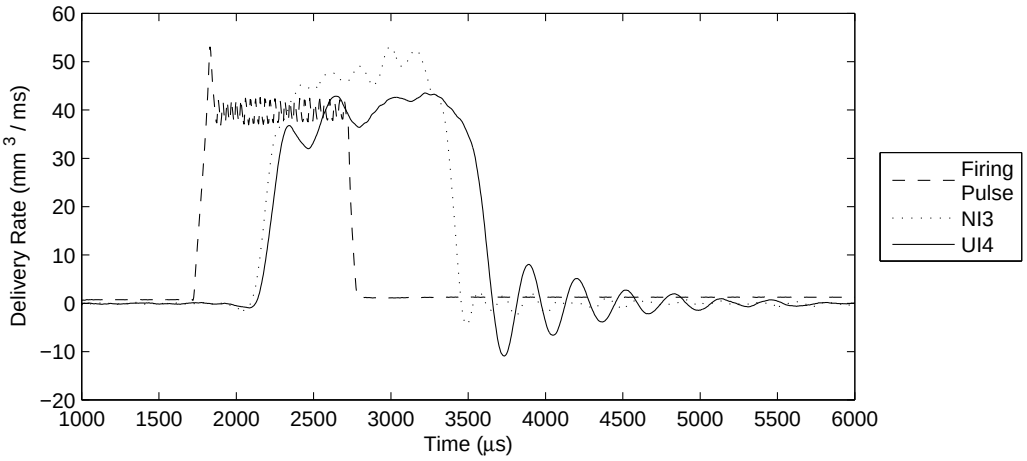

Figure 5.38: Delivery rate vs time for injectors NI3 and UI4 for a 1200bar 1000μs injection

Discussion

The rate plot presented in Figure 5.38 is interesting in that the injector UI4 has a delivery characteristic very different to that of injector NI3. It may be seen that the steady state rate of fuel delivery is considerably lower than that of the new injector. The degree to which underfueling occurs is, however, offset by the fact that UI4's cessation of fuel delivery occurs considerably later than that of the new injector.

The above discussion details the behaviour of injector UI4 for injections of longer durations, however, if one inspects Figure 5.7 through 5.10, in Section 5.4, on page 64, it is worthwhile to investigate the rate of delivery in a shorter injection. One is curious to know whether the deviation from the standard injector only occurs after the first 500μs of the pull phase, or if it was always present and is being masked by some other phenomenon. To facilitate this investigation, a delivery rate plot is presented below, in Figure 5.39, for a 500μs injection. This injection delivers the

same volume of fuel as the new injector, and is still being driven by the original 500μs pull phase current.

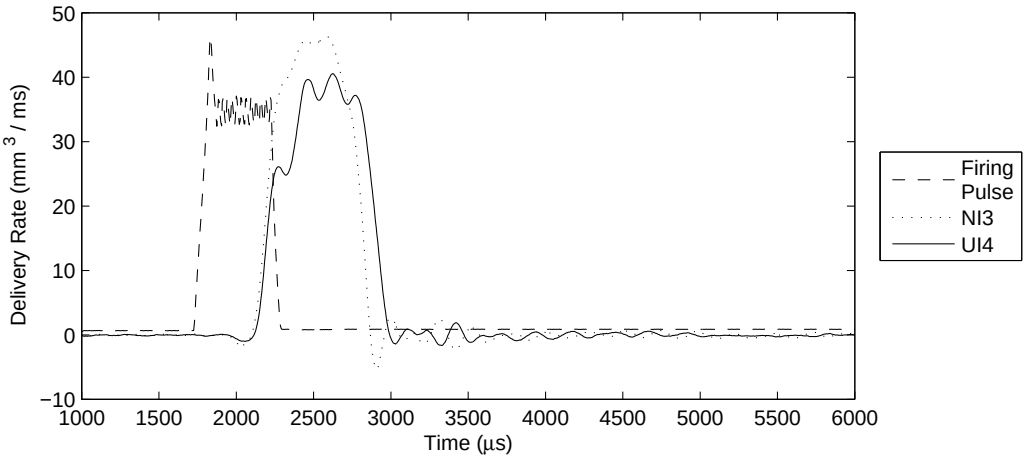

Figure 5.39: Delivery rate vs time for injectors NI3 and UI4 for a 1200bar 500μs injection

The results illustrated in Figure 5.39 clearly show that even though injector UI4 and injector NI3 deliver similar volumes of fuel at shorter duration they have very different delivery characteristics. The trend as discussed above with reference to the 1000μs injection still holds for the 500μs injection. The reason for the similar quantities of fuel being delivered is that at shorter durations the degree of underfueling caused by the lower steady state delivery rate is offset perfectly by the degree of overfueling caused by the slower closing of the injector.

During the discussion relating to injector UI1 it was stated that while differences were present in the performance of that injector compared to the control injector, NI3, these could not be investigated due to their being of a subtle nature. However, in the case of the comparison of the performance of injector UI4 and the control injector NI3 the differences are more than subtle and warrant further investigation.

It has already been determined that the solenoid in injector UI4 is not functioning effectively. This fault will, however, be set aside for the time being, and a flow-based analysis conducted. Figure 5.39, presented above, which showed the performance of a 500μs injection with a rail pressure of 1200bar, may be used to conduct some further analysis.

It may be seen that injector UI4 begins injection very slightly later than the properly functioning injector, NI3. Injector UI4 also ceases injecting considerably later than NI3. These two characteristics lead one to believe that the cause of the incorrect fuelling characteristics are due to wear in the bleed orifice. This would lead to a slower increase in pressure above the needle, resulting in sluggish cessation of the injection.

However, as discussed previously, the steady state rate of fuel delivery is consistently lower than that of injector NI3. This is not explained by wear, or decrease in the discharge coefficient of the bleed orifice. Since it is assumed that even if there is wear in the bleed, or feed orifice, the pressure still reaches the same level. This means that the reduced steady-state delivery rate is not explained by wear in the bleed orifice.

The same logic which was applied in the discussion relating to injector UI3 may be applied to this injector, with regard to the underfueling at steady-state. In the discussion relating to injector UI3 it was stated that the most likely cause of the steady-state underfueling exhibited by the injector was a with level of friction in the plunger section of the injector. Injector UI4 appears to be suffering from the same type of wear as affected injector UI3.The strength of the correlation between the performance of injectors UI3 and UI4 is well illustrated by Figure 5.40.

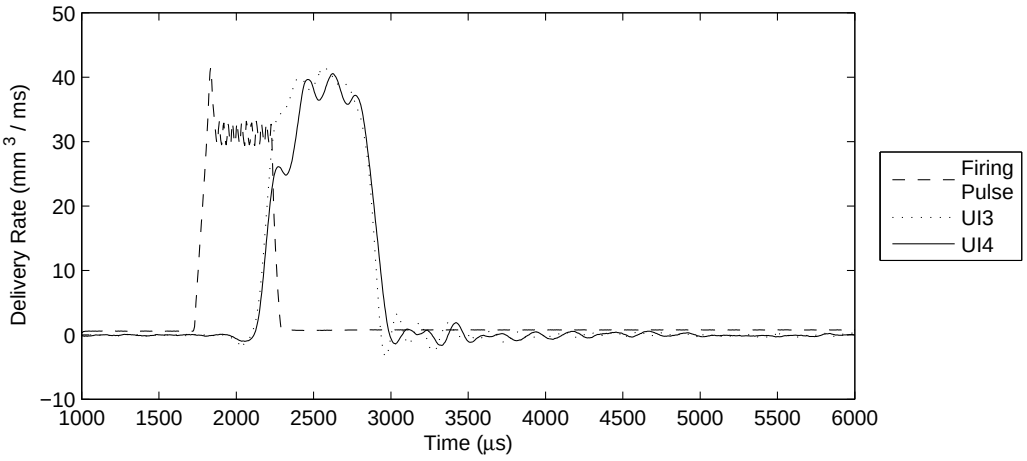

Figure 5.40: Delivery rate vs time for injectors UI3 and UI4 for a 1200bar 500μs injection

Figure 5.40 clearly illustrates the similarity between the performance of injectors UI3 and UI4. Therefore, based on the previous analysis UI4 may be said to be also suffering from increased friction with regard to the plunger movement. A secondary difference between the performance of UI4 and the other injectors tested is that injector UI4 does not deliver any fuel, regardless of injection duration at 300 bar. This observation further supports the theory that friction is present in the plunger. Since the opening of a fuel injector is dependent on that force imbalance on the needle, increased friction and lower operating pressures will cause the injector to fail to open, as is the case with injector UI4.

Injectors UI4 and UI1 both display characteristics which suggest an improper functioning of the solenoid. It is worthwhile to look at whether the delivery of these two injectors differ, as a result of the increased plunger friction that is present in injector UI4 and not UI1. The most obvious differences between the performance of the two injectors will be evident in a longer duration injection. Figure 5.41 below shows the delivery rate of both injector UI1 and UI4 for a 2500μs injection.

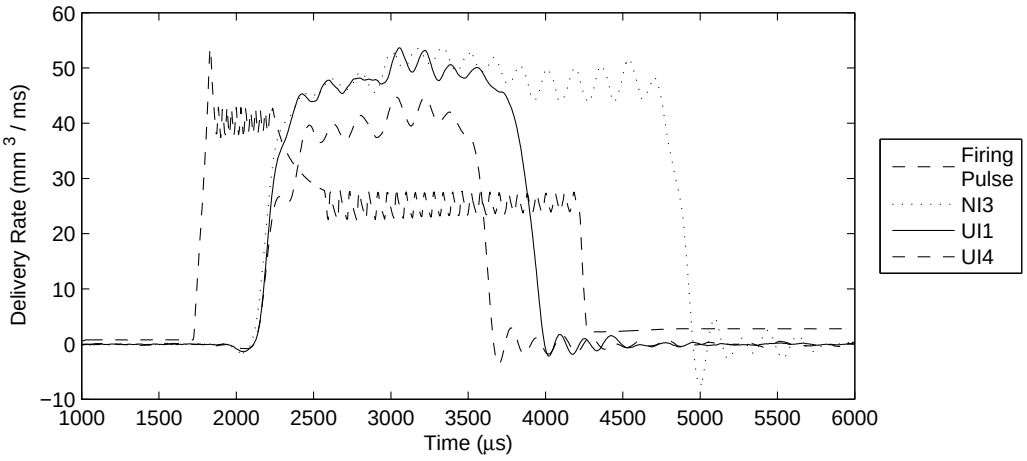

Figure 5.41: Delivery rate vs time for injectors NI3 and UI4, with 500μs and 1000μs pull phases, for 1200bar 2500μs injection

Figure 5.41 clearly illustrates that, although it has been shown that injector UI4 and UI1's performance are both affected by the performance of the solenoid, they behave quite differently. Figure 5.41 illustrates the large difference that the proposed injector wear has had on the performance of the injector even when compared to the results from an injector with an incorrectly functioning solenoid.

If both injector UI1 and injector UI3 were to be used in engines, injector UI1 would function vastly better than UI4, since it only begins to underfuel at longer durations, resulting from high loading of the engine. Injector UI4, on the other hand undefuels much more consistently, and with non-standard delivery characteristics. Therefore, even though injectors UI1 and UI4 both suffer from solenoid wear, the increased friction in injector UI4 means that it would perform very unsatisfactorily in a real-world application.

5.7 Injector Flow Conclusions

5.7.1 Injector UI1 Conclusion

When injector UI1 was supplied for testing it was described as: “Backleakage Ok, delivery characteristic incorrect”.

When the injector was tested it produced strange results in that during short duration injections the results obtained closely followed those of the new injector. However, as the duration of the injections was extended the injector ceased to deliver a comparable amount of fuel, when compared to injector NI3, the control injector.

An investigation was conducted to identify the cause of the cessation of increase in fuel delivery with increasing duration. This investigation revealed that the solenoid was not responding to the “hold” phase of the injector signal, and was only responding to the “pull” phase, which has a larger current rating. This failure of the injector to respond to the “hold” phase of the injection was attributed to the solenoid being faulty.

At lower injection pressures (up to 900 bar), the injector ceased to inject when the “pull” phase ended at 800μs after the start of injection. At higher operating pressure (1400 bar), the injector did not cease to inject entirely, but rather delivered fuel at a reduced rate. The unusual results at the higher pressure were attributed to the mechanical assistance provided to the solenoid by the increased pressure differential across the injector actuation mechanism at higher pressures.

It is noteworthy that all the wear, leading to the substandard performance of injector UI1, appears to stem from the solenoid and if this component were to be replaced, the injector could likely return to service.

5.7.2 Injector UI2 Conclusions

When injector UI2 was supplied for testing it was described as: “High backleakage, incorrect delivery characteristic”

Injector UI2 was found to provide different types of deviations from the new injector at high and low operating pressures, as well as at shorter and longer durations. After looking at the delivery rate profile it became evident that the injector was underfueling during early phases of the injection and overfueling at the longer durations.

Following detailed analysis, it was found that mechanically the injector was performing effectively, with injector UI1 where the solenoid was failing to open the injector properly. The incorrect delivery characteristics were assigned to wear in the bleed and feed orifice leading to initial underfueling and later overfueling during the injection. The high rate of bypass was attributed to wear in the upper section of the injector, in the region where the ball valve seats onto the bleed orifice. Injector UI2 performs better, however, in the range where the injector would typically be operating, at high pressures (900-1400bar) and intermediate durations(300-600μs), the difference between the new and used injector is not very large. In the closely controlled operational environment of the common rail diesel engine, the fuel management system would occasionally expect the injector to perform outside these areas. When the engine management system does expect this performance from the injector poor running will result, due to the engine running lean at low loads and rich at higher load.

The root of the problems would likely be abrasive material entering the fuel system, and possible failure of the fuel filter. It would be interesting to know the history of the injector, so as to attempt to isolate the cause of the wear within the upper section of the injector.

Unlike the suggestion which was made in the conclusion to the study of injector UI1, the wear in injector UI2 is actually mechanical wear within the injector.

However, the top section of the injector, which contains the bleed and feed orifice sections may be replaced, so in a similar manner to that suggested for injector UI1, if this section of the injector were to be replaced, the injector could likely return to service.

5.7.3 Injector UI3 Conclusions

After looking at the results for injectors UI1, UI2 and UI3, it may be seen that UI3 is the only injector thus far where the flow characteristics have indicated a state of mechanical wear.

In the case of the injectors discussed previously the performance problems displayed could possibly be corrected through component replacement on the injector body. Injector UI1 could possibly be corrected through replacement of the solenoid, and injector UI2 may have been corrected through changing the top section above the ball valve.

The only manner in which the performance of injector UI3 may be corrected would be to replace the plunger. While this may help to reduce the level of wear within the injector, and thus the underfueling, the body will likely have worn to a similar degree to the plunger - if not more due to the hardened nature of the plunger material. Therefore, in the event of wear in the manner displayed by UI3 the body of the injector will need to be replaced.

Although the recommended remedy is effectively the replacement of the injector, the injector may be said to have failed due to having operated for its design life. Thus does not represent a particular problem, but it is an economic based decision as to what material should be used in the manufacture of the injector body and needle.

5.7.4 Injector UI4 Conclusions

Upon initial investigation, injector UI4 displays similar characteristics to injector UI1. This is because both of these two injector's solenoid is not functioning effectively. The malfunctioning of the solenoid was illustrated by the increased fuel delivered by the injector when the pull phase duration was increased. There were, however, differences in performance between injectors UI1 and UI4. These difference were attributed to wear in the plunger mechanism, as displayed by injector UI3.

The combination of these two faults leads to an injector that underfuels at longer injection durations, due to the injection being "cut short" due to the solenoid failing to react to the pull phase. The injector also delivers fuel at a decreased steady state rate due to the increased friction within the plunger mechanism. Unfortunately, as in the case of injector UI3, there is no way for the injector to be brought back to service, due to wear in the barrel and plunger assembly. As discussed above, the combination of the two faults will likely lead to most unsatisfactory performance in an engine application.

It is further noteworthy that injectors UI3 and UI4 displayed very similar faults. This was originally identified in the analysis conducted to determine whether cavitation was occurring within the injector, in Section 5.5, on page 67. It was found that the injectors UI3 and UI4 displayed a similar relationship between fuel delivered and $\sqrt{P}$. The reason for this reduction in fuel delivered has been cited as wear being present in the mechanical elements of the injector. This is likely to be more than a coincidence, as it seems reasonable that these two injectors, which were supplied in the same batch, were originally fitted to the same vehicle or engine. If this were to be the case they would have been subject to an identical duty cycle and type of fuel, leading to a similar manner of deterioration. It was considered that these injectors, UI3 and UI4, might be fundamentally different from the other injectors tested, however, the injectors displayed identical part numbers, so this seems unlikely.

Chapter 6

Injector Spray Analysis: Results and Discussion

6.1 Introduction

As described in Chapter 1, the purpose of the research being documented here is to characterise the behaviour of both new and used injectors with regard to fuel delivery, in terms of flow and spray characteristics. Details of the flow characteristics were provided in Chapter 5, and this chapter aims to investigate the behaviour of the injector's spray patterns.

As in the documentation of the research conducted, the injector flow testing was carried out first, followed by the spray testing. Therefore, the decisions documented in Chapter 5.2 regarding the test injector, type of injectors used and the injector naming convention still hold in the following discussion.

The investigation into the spray performance of the injectors will be conducted in the following manner:

- An outline will be given of the operation of the test equipment and the origin of the results. A detailed description of the testing conducted will be given,

with regard to both pressures and injection durations of tests conducted.

- Optimisation decisions which were made during the test program will be highlighted. The limitations of the test equipment, and how these may relate to the results generated by the apparatus, will be discussed.
- A comparison of the performance of the injectors will be made. This analysis will be based on the processed results provided by the apparatus, and specific elements of injector performance will be highlighted.

6.2 Test Equipment and Testing Conducted

6.2.1 Equipment Used

The apparatus used to measure the behaviour of the spray is described in Section 3.5, and the procedures behind the attaining of such results are shown in Chapter 4. However, to aid in the understanding of this section a brief outline of the results, as generated by the test apparatus, will be given.

The test stand captures multiple images of the spray, at many time intervals, in a process known as strobing, as desccribed in section 2.8.2. These strobed images are then averaged by a pre-programmed algorithm, contained within the La Vision Da Vis software geometry package.

It is from these averaged images that key information regarding the behaviour of the spray may be gained. In this specific study, spray penetration and cone angle are the chief characteristics which are of interest, which are acquired from the geometry package. An example of an averaged image, after the geometry pack algorithm has been applied may be seen in Figure 6.1 below.

Figure 6.1 shows a well developed spray, clearly showing the six individual sprays of the injector type being analysed here. It also indicates the injector penetration and cone angles for a well developed spray.

6.2.2 Testing Conducted

As in the case of the injector flow analysis, testing was conducted at various pressures and durations. Due to the amount of time required to run tests as well as the fact that spray behaviour is not expected to change significantly with varying durations, only selected durations were tested, unlike was the case with the flow analysis.

The pressures used for testing were identical to those applied in the injector flow analysis, that is:

- 300 bar
- 600 bar
- 900 bar
- 1200 bar

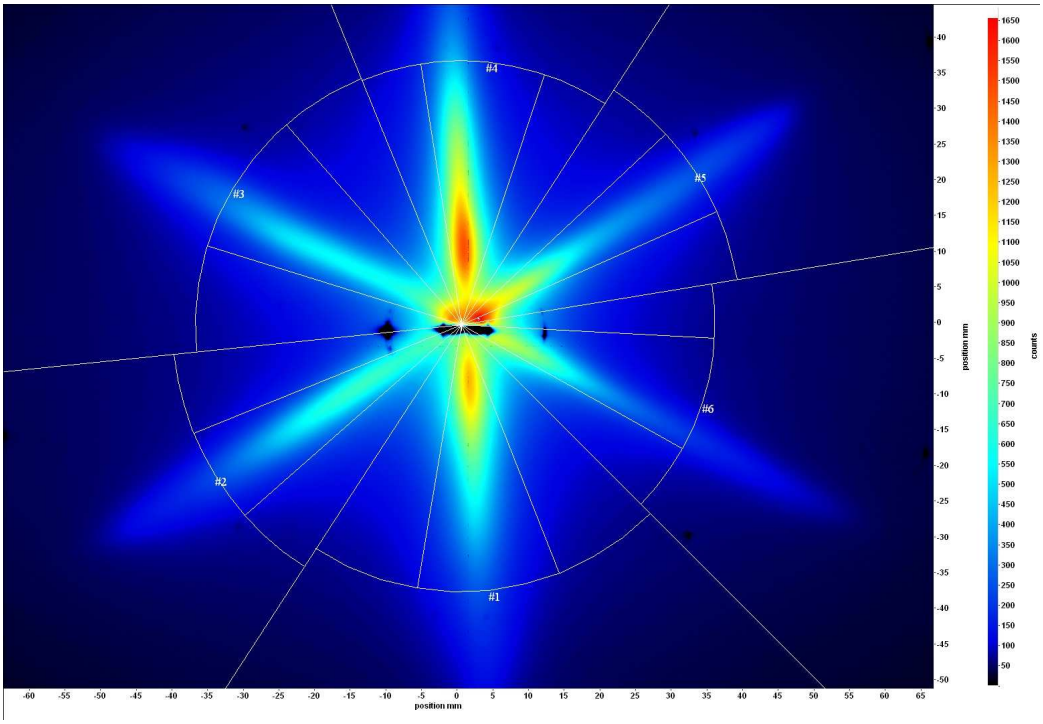

Figure 6.1: Image of Spray 1400bar after processing by La Vison Da Vis Geometry Package

- 1400 bar

Tests were run at the following durations on all five injectors at the pressures indicated above:

- 300 μs
- 600 μs
- 1200 μs

Experimentation was also conducted at durations of 150μs, but results for this duration were not as consistent as those produced at longer durations. While these results are contained in the Appendix A, where all the injector spray results are shown, they are not analysed alongside the other results. Section 6.4.8, containing an analysis of these shorter durations has been included.

The settings for the La Vision spray capturing equipment were as follows:

1. 15 Images per time interval.
2. Time interval of 0.005 seconds.

The initial analysis was conducted using the plots contained in Appendix A. These plots show the penetration and cone-angle development at various pressures and durations, where the penetration and cone-angle values shown are averaged values for all six segments. Further analysis, discussed in this section, was then undertaken on the results as shown later in this chapter.

6.3 Operational Optimisation

6.3.1 Introduction

Before testing could begin, it was necessary to determine the optimal method of operating the injector testing apparatus. The purpose of these tests was to verify that the test stand could provide repeatable test results and to gain the best result resolution.

Due to the new nature of the test equipment, at the time of testing an optimal method of operating the equipment had yet to be developed. Much of the findings of this section have been passed on to other users of the test equipment, for use in undergraduate research projects.

Three factors were investigated during the initial optimisation process. These were:

1. Use of Air-Knives
2. Injection Frequency Rate
3. Spray processing intensity threshold

These factors will be discussed below:

6.3.2 Use of Air Knives

As discussed in Section 3.5.3 describing the spray chamber, the injector analysis equipment is fitted with a set of 'air-knives' which serve to 'blow' air across the glass sections which provide optical access to the spray chamber.

In the process of the injected fuel being removed from the windows, waves are formed. These are visible if one views the imaging system after injecting fuel.

Concern was raised regarding the effect that these 'waves' would have on the quality of the images produced by the system.

For comparative purposes two sets of tests were run, one with the air-knives activated, and a second set deactivated. It was found that while the air-knives may lead to some degree of inaccuracy, due to the fluid flowing over the window without the air-knives, the imaging system saturates almost immediately, rendering the test results meaningless.

It is noteworthy that during the initial period, with the air knives off, the results do show better definition than in the case of later results with the air-knives on. However, the period where good resolution is available is short, with good results only attainable until fluid builds up on the optical window. For these reasons a decision was made to run the tests with the air-knives on at all times.

In addition to running all tests with the air-knives on, before results were taken the test stand was allowed to run for five minutes to ensure that the flow of fluid and air had reached a steady state, to ensure that consistent results were obtained.

6.3.3 Injection Timing

A common rail pump, which is driven by a 5.4kW, 380V motor, provides the high pressures required by a common rail system. In order for the pump to generate such high pressure, it is required to rotate at 1000rpm. At speeds less than 1000rpm, the pump is not be able to generate sufficiently high pressure so as to operate the system effectively.

In an automotive case, the common-rail pump would be coupled to the engine, and therefore would rotate at the same speed as the engine, and thus that of the injector. Because the dynamics of the common-rail pump will influence the performance of the injector it is desirable to have the injection rate and pump speed synchronised, so as to emulate a 'real-world' application.

The results obtained for the section on injector flow testing were run at an injection frequency of 1000rpm. However, in the case of the spray testing it was suspected that if the system was required to inject at a frequency of 1000rpm, too much fluid would be introduced into the spray chamber, too quickly. It was thought that, were this to be the case, the air-knives would be unable to remove the fluid from the windows fast enough, leading to saturation, as was the case when the air-knives were not running.

Tests were run at the synchronised injection frequency of 1000rpm, as well as at a reduced frequency of 100rpm. The results of these tests are shown below in Figure 6.2.

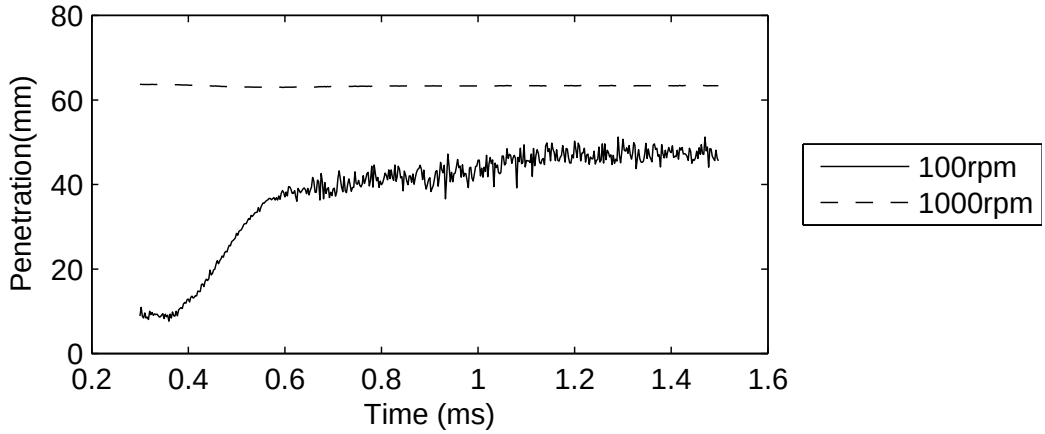

Figure 6.2: Penetration vs time for 100 and 1000rpm injection timing

From figure 6.2 it may be seen that saturation does in fact occur in the case of the 1000rpm injection frequency. The lower injection frequency shows results as one would expect to see.

Due to the undesirable effects of saturation coming into effect at the 1000rpm injection frequency, it was decided that all tests should be conducted with an injection frequency of 100rpm.

An undesirable effect of injecting at a rate different to the speed of the pump is

that the effects of the pump's pressure variation on the rail pressure will not be the same as in a real-world application. However, given that the purpose of the common-rail in an injection system is to provide a buffer between the pump and the injectors, one hopes that this will not have a marked effect on the performance of an injector as regards spray pattern.

It was also considered that given that the engines in which these injectors are typically used, can run up to speeds of 4500rpm, one doubts that the return to steady state is a concern at 1000rpm. Thus, the reduction of injection frequency is unlikely to affect the performance based on deviation from steady-state behaviour.

6.3.4 Spray Processing Threshold

In the section of this report describing the tests apparatus mention was made of the intensity setting when analysing injector spray behaviour. This intensity setting governs the point at which the La Vision Da Vis geomentry package locates the end of the spray.

The La Vision system determines the location of the spray through integrating the intensity of the light reflected by the spray. Setting this threshold alters the level of light required to define the end of the spray. The lower the threshold the more light is required to acknowledge the existence of the spray, and the shorter the Geometry Package defines the spray.

During the preliminary tests it was identified that if the intensity threshold was set to its default value of 95%, and the spray was identified as being rather large. While the development of the spray was found to be well tracked during the initial phases of development its growth appeared to stop prematurely when saturation occurred.

A series of tests were run at the highest pressure for the system, 1400 bar and a duration of 600μs. This duration was selected since, based on the results available, as illustrated in Figure 6.3 below, the spray appeared to have reached its steady

length.

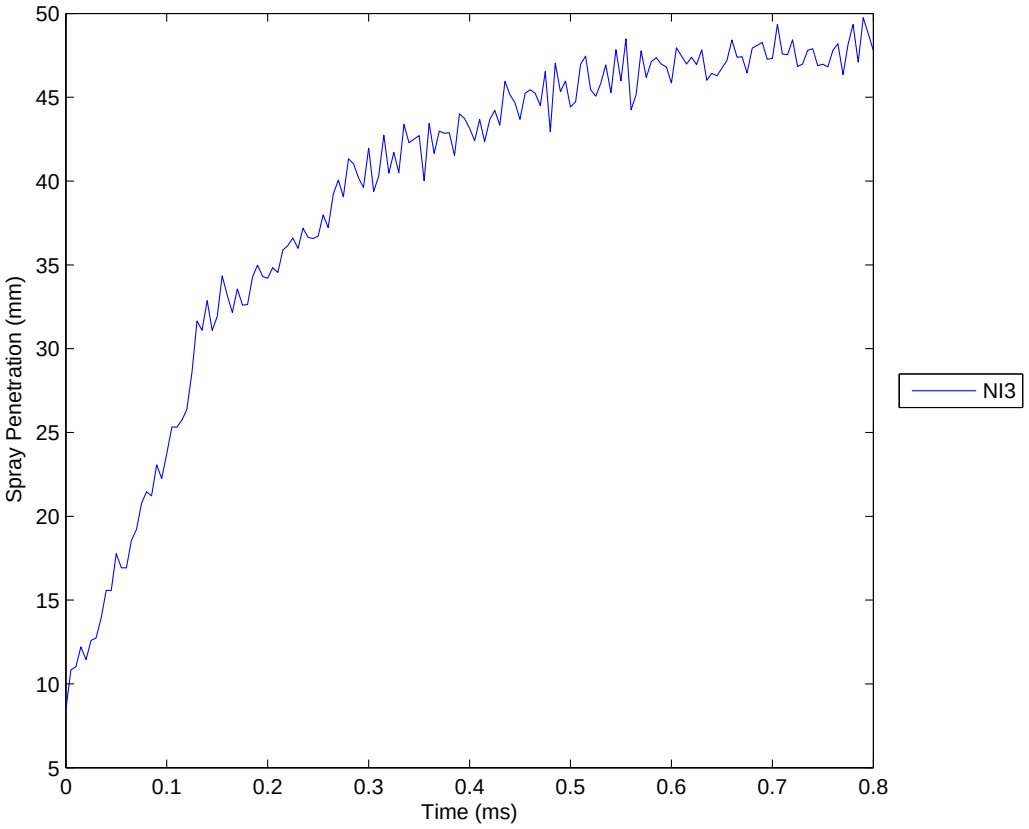

Figure 6.3: Spray penetration vs time at 1400 bar, 600μs duration

During these tests it was observed that while all spray segments initially progressed at the same rate, as the sprays reached a certain length the results indicated that two of the sprays ceased to continue growing, while four did. Figure 6.4 below illustrates an example of an image as processed by the geometry package. It may be seen that the image is rectangular with the injector located centrally.

From the figure it may be seen that there is considerably more “room” for growth in the vertical direction than the horizontal. This effectively means that should saturation begin to occur, spray segments #1 and #4 will appear to be considerably shorter than segments #2, #3, #5 and #6.

Analysis was conducted on the results available, looking at the progression of the difference between the shortest and longest segments for an injector functioning correctly.

The results of this indicated that an intensity threshold setting of 80% allowed the progression of a 600μs injection, at an injection pressure of 1400bar, to be effectivley tracked during the course of its propogation, without the effects of saturation becoming apparent.

While mentioned in the section relating to the test apparatus, this section further serves to emphasise that while the La Vision Da Vis system does provide one with a good indication of the behaviour of an injection, it may not be comparable directly to the results of a different type of imaging system. However, with the intensity threshold set as described in this section good comparative performance measures may be made for different injectors.

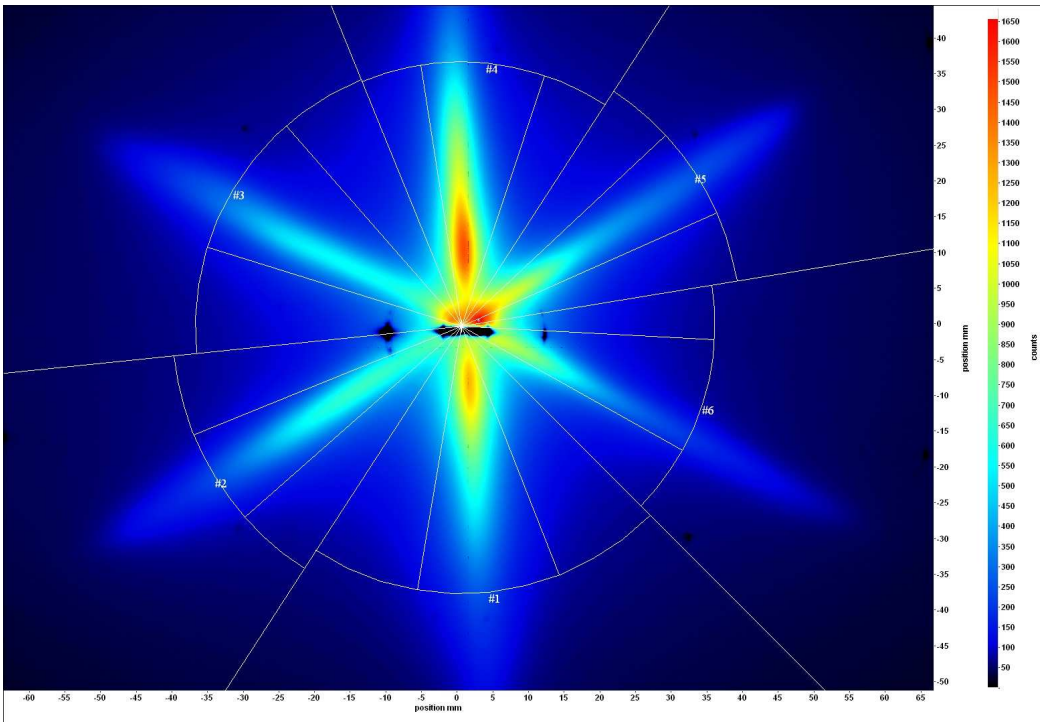

Figure 6.4: Image of spray development, showing spray development by segment

6.4 Spray Results and Discussion

6.4.1 Introduction

The following section contains the analysis and discussion of the performance of new and used injectors, in terms of the behaviour of the spray. Various elements of the behaviour of the spray will be discussed and the section will then be concluded based on the results of all of the elements analysed.

6.4.2 Spray Performance by Segment

Introduction

In this section the observations and analysis of the performance of the new injector will be compared with that of the used injector, based on the variation in the performance of the various segments of the spray.

Observations and Discussion

As discussed previously, the injectors employed for testing were six hole injectors, resulting in the formation of six separate sprays. In a correctly functioning injector it is expected that all six sprays would perform identically, in terms of spray penetration and cone-angle achieved. It is worthwhile to investigate whether this is in fact the case with the new injector, and to what degree the 'per segment' performance of the used injectors has declined.

In previous analysis, as well as in the initial observations, as displayed in Appendix A, the results of a multi-orifice injector have always been displayed as an average of all the sprays. By looking at the variation of the performance of the sprays, it can then be determined whether using an average value for penetration and cone angle for analysis is valid.

To facilitate this comparison an analysis was conducted whereby the coefficient of variation was determined for the sprays, as a percentage, at all pressures and durations. This coefficient of variation was determined through the use of the following equation:

$$C_v = \frac{\sigma}{|\mu|} \times 100\% \tag{6.1}$$

Where,

$$\sigma = \sqrt{\frac{\Sigma(\bar{x} - x)^2}{n}} \tag{6.2}$$

And μ represents the mean, or $\bar{x}$, for the series and Σ represents standard deviation.

Figure 6.5 below indicates the coefficient of variation for a 1400bar 1200μs injection. It does not indicate any major anomalies in the performance of any of the injectors. What Figure 6.5 does indicate is the curious increase in C_v as the time since the onset of the injection, reaches around 0.4ms.

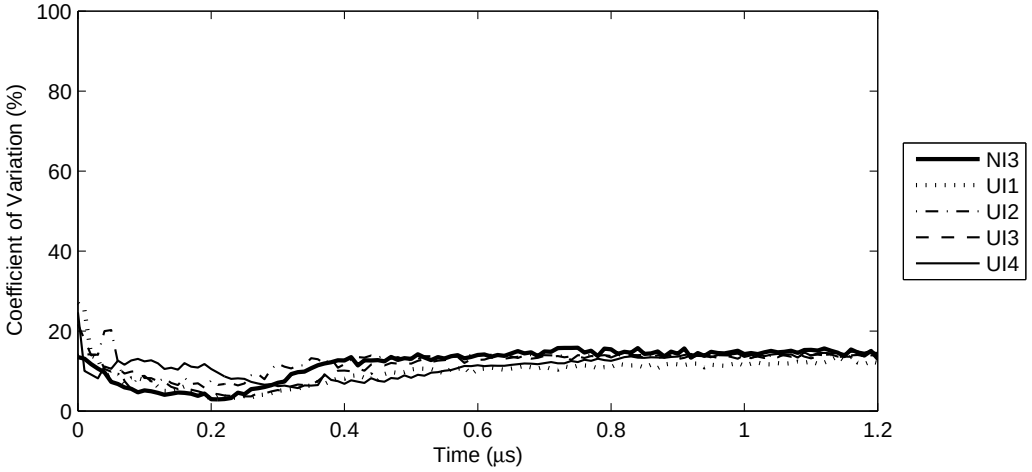

Figure 6.5: C_v vs time for 1400 bar, 1200μs injection

Recalling the discussion made in Section 6.3.4 regarding the varying points at which saturation is likely to occur, it is concerning that the increase in the co-

efficient of variation may be attributed to this. While experimentation was done to try and avoid saturation occuring, that experimentation was based on a 600μs injection, considerably shorter than the 1200μs injection under investigation here. Examples of test images were extracted, for injector NI3, at a time interval of 0.4ms, so as to determine if this was occurring. This spray image is shown below in Figure 6.6.

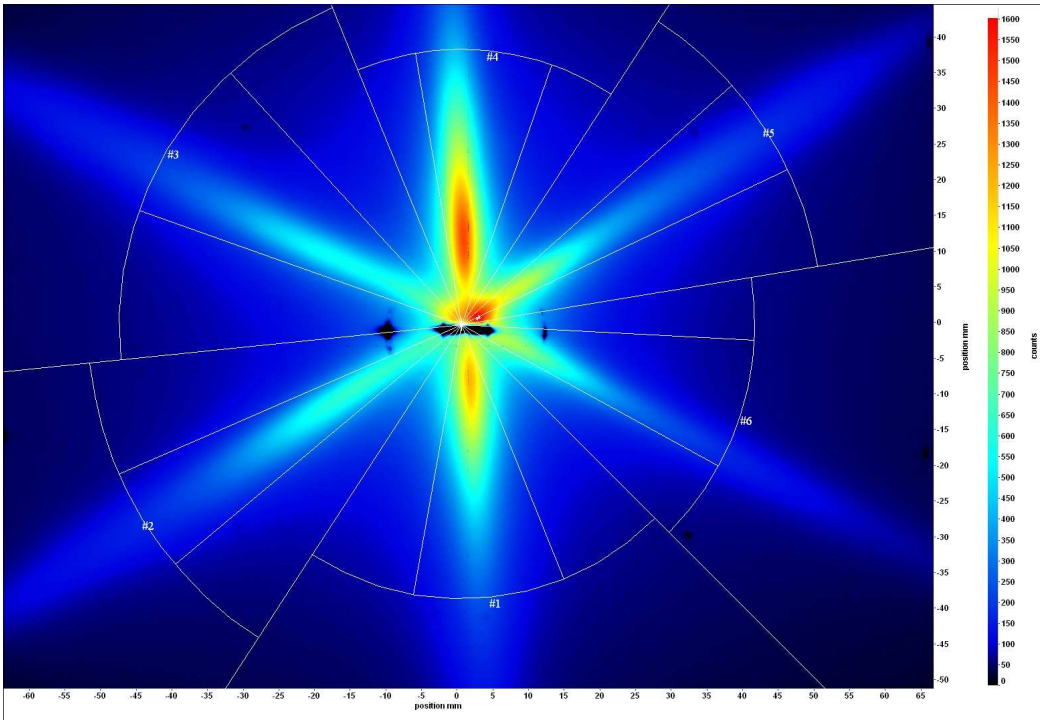

Figure 6.6: Image of spray from injector NI3 at 1400bar with 1200μs injection at 400μs after onset of injection

From Figure 6.6 it may be seen that despite efforts to avoid the onset of irregular saturation, it appears to have occurred nonetheless. In addition to the observations shown above in Figure 6.6, a plot has been prepared showing, in the form of a histogram, the location of the minimum and maximum penetration by segment. This combines information from all tests conducted during the study. The histogram is shown below in Figure 6.7. The segment numbers contained in Figure 6.7 correspond to those shown on Figure 6.6.

Figure 6.7 indicates that the anomalies shown in the image in Figure 6.6 are not unusual, but occur at other pressures and durations as well. According to Fig-

ure 6.7, segments 1 and 4 account for most of the minimum penetration cases, while segments 2 and 5 account for the majority of maximum penetration cases. This would appear to be in line with the theory of saturation corresponding to the rectangular frame in which the spray images are contained.

While considering the variation in the penetration distances, as illustrated by Figures 6.5 to 6.7 there is a second factor which comes into play regarding the physical design of the test apparatus. If one refers to Figure 3.6, on Page 42 in Section 3.5.3 on the experimental facilities it will be noticed that there are lights located on two sides of the spray. This means that certain sprays will effectively be in the shadow of other sprays. Upon inspecting the test rig it may be seen that the lights face into spray segments 1 and 4. Thus sprays 1 and 4 are lit from the 'front' and sprays 2, 3, 5 and 6 are lit from the side.

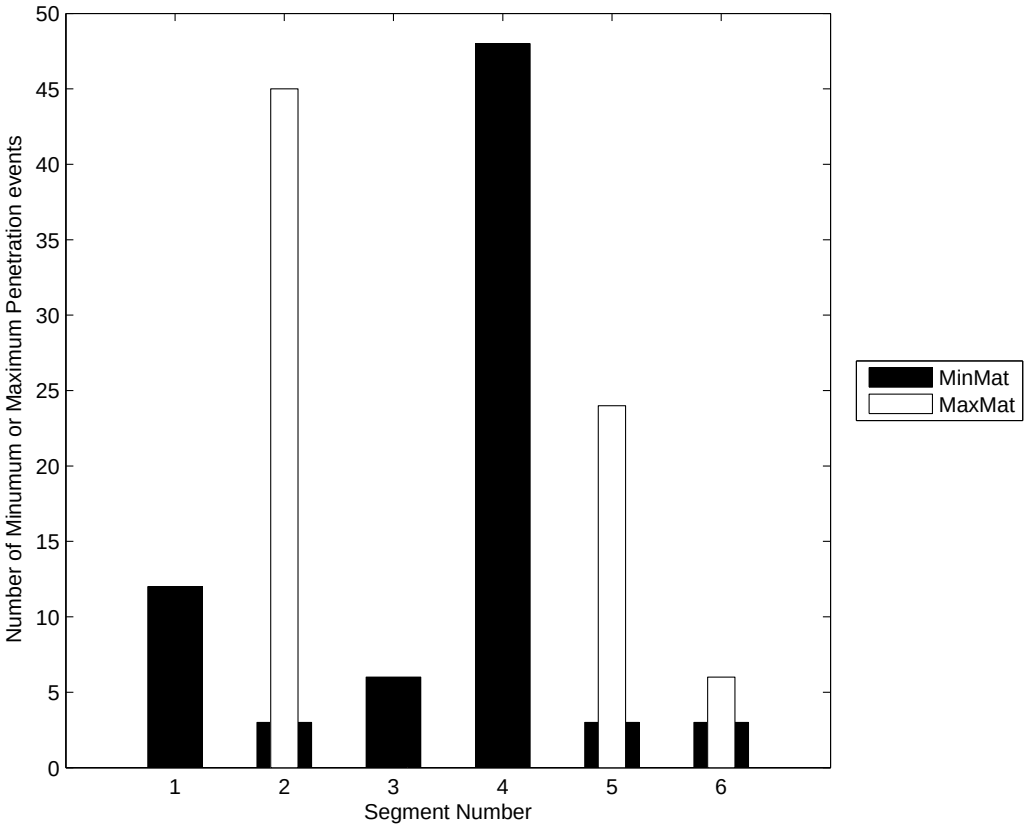

Figure 6.7: Histogram shown the location of the minimum and maximum penetration of injections by segment number

This lighting phenomenon explains why, in a well performing injector, such as injector NI3, the sprays have different shapes, especially close to the injector nozzle.

It is noteworthy that even once saturation has occurred, the location of the spray penetration does not extend to the maximum possible point. It is proposed that the location of the lights and saturation of the imaging work together to develop false results. This is evident by the reduction in the variation of the coefficients of variation for the segments, as presented in Figure 6.1 and the images presented in Figure 6.4.

While considerable discussion has been made into the breakdown of the reliability of the data after results appear to saturate, considerable information may be interpreted before this saturation occurs. If one inspects Figure 6.1 up to the point where the sprays all tend to a similar value for C_v it may be seen that there is considerable variation between the performance of the different injectors.

As would be expected, injector NI3 performs well, with the lowest C_v values. Injectors UI1 and UI3 display similar characteristics to injector NI3. Injectors UI2 and UI4 differ substantially from injector NI3, displaying significantly higher C_v values across the region where the data is valid.

It may prove interesting to note the variation in C_v with changing injection duration. An identical plot to that shown in Figure 6.5 is shown in Figure 6.8, but for a 1400 bar, 300 μs injection.

Figure 6.8 illustrates that the manner in which the injectors behave at high pressure, does not change when the duration of the injection is altered. Figure 6.8 allows one to better identify the trends outlined above regarding the 1200μs injection due to the altered scale used.

As was done regarding the analysis performed on the flow aspects, it is interesting to consider the effects of lower pressures on the coefficient of variation for the performance of the injector. Presented below, in Figure 6.9 and Figure 6.10 are

the plots of C_v for the injections at an injection pressure of 300bar and durations of 300μs and 1200μs respectively.

The most immediate observation from Figures 6.9 and 6.10 is the highly erratic behaviour of injector UI4. However, it may be recalled from the discussion into the flow performance of the injectors, that at 300bar injector UI4 failed to deliver any fuel.

In order to fully appreciate Figures 6.9 and 6.10 it is necessary to show the average spray penetration at this pressure, 300bar, and at these durations. These two plots are shown below in Figures 6.11 and 6.12.

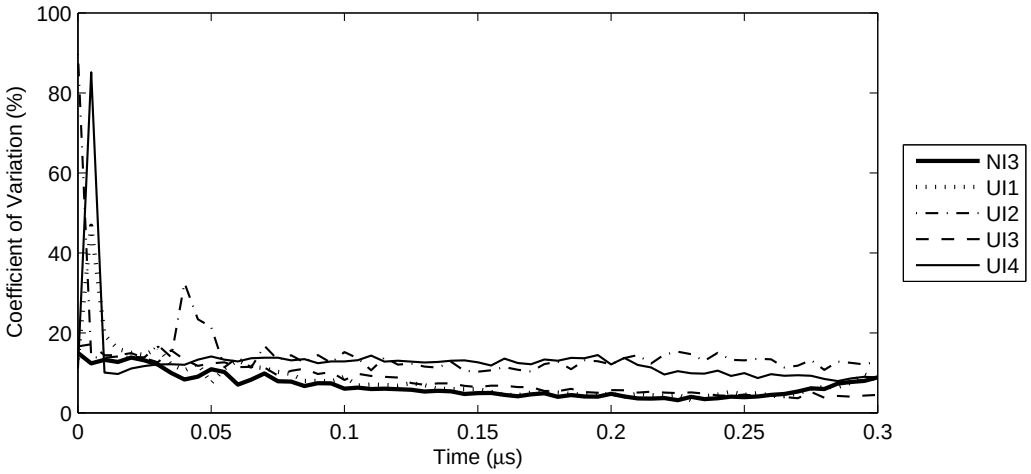

Figure 6.8: C_v vs time for 1400 bar, 300μs injection

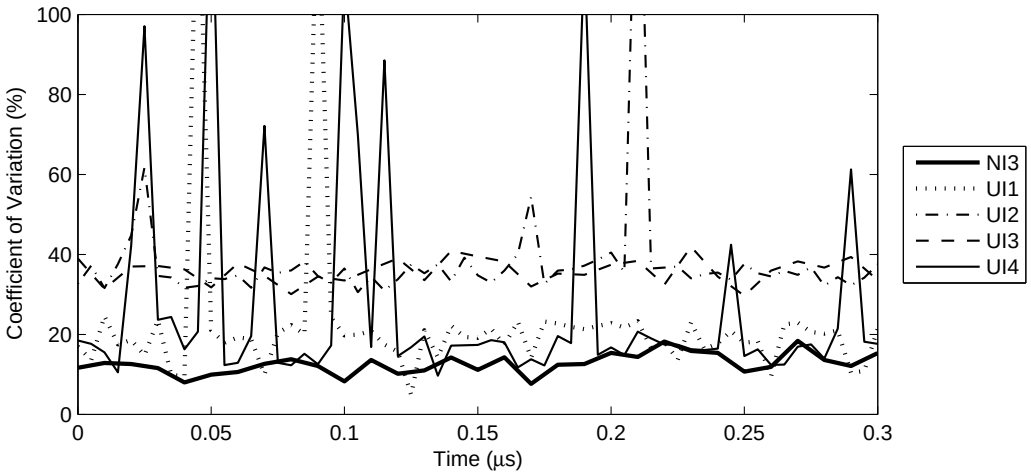

Figure 6.9: C_v vs time for 300 bar, 300μs injection

Figure 6.11 goes a long way to explaining the results shown in the short duration coefficient of variation plot, as seen in Figure 6.9. There is a great deal of variation in the coefficients for all injectors at a duration of 300μs, but this may be attributed to the very low spray penetrations. With such small penetration, three factors come into play. Firstly it is difficult for the apparatus to gain strong definition with regard to the behaviour of the spray, due to the close proximity of the sprays to one another. Secondly, the injector is not behaving as it typically would be, with flow not being fully developed within the injector nozzle. Thirdly, any minor variation, of perhaps one or two millimetres, which would normally go unnoticed if penetrations were longer, will have a marked effect on the C_v if the mean spray

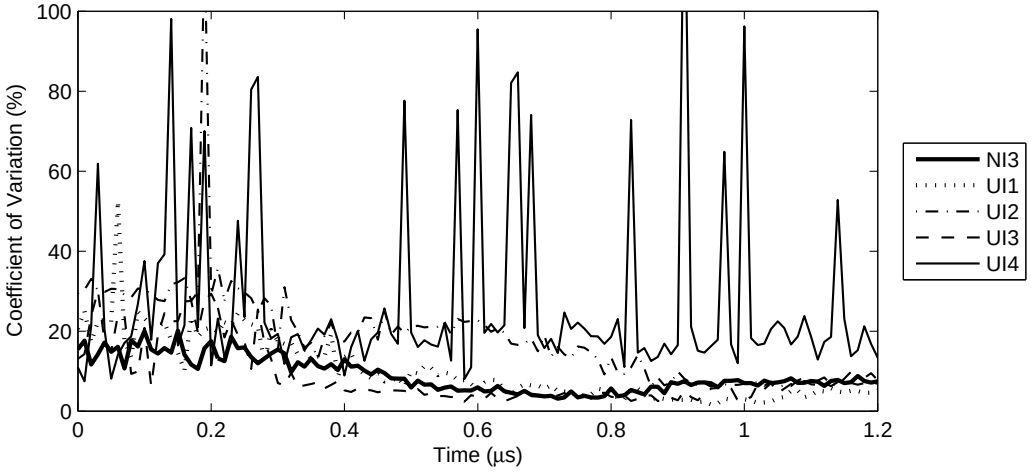

Figure 6.10: C_v vs time for 300 bar, 1200μs injection

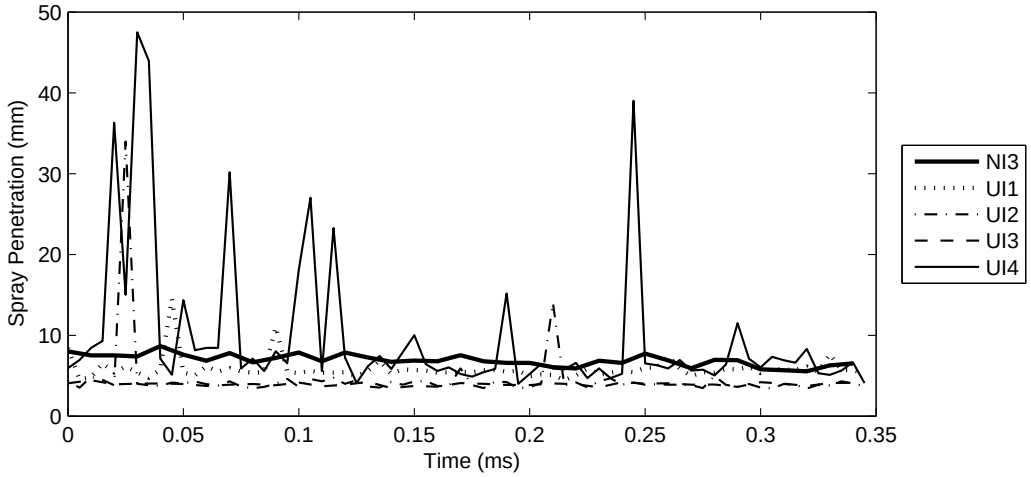

Figure 6.11: Spray Penetration vs. time for 300bar, 300μs injection

penetration is lower since the one or two millimeters represents a much larger proportion of the total spray length.

Figure 6.12 also provides insight on how to interpret Figure 6.10. Figure 6.12 shows the amount of the time that passes before spray begins to provide significant penetration. Based on when the spray at 300 bar and 1200μs duration begins to progress, it becomes clear that the plots of coefficient of variation at 300 bar will only provide meaningful information after 0.4ms have elapsed.

After 0.4ms have elapsed, it may be seen that the injectors behave in a similar manner to the 1400 bar plots shown in Figure 6.7 above. Injectors UI1 and UI3 follow very similar trends to injector NI3. However, injector UI2 has larger variation than any of the other injectors up to 0.9ms, after which it stabilises, possibly as a result of saturation of the test equipment . Injector UI4 is discounted in this low pressure analaysis due to the fact that, as determined in the flow discussion, it does not deliver any fuel at 300bar.

Conclusion

Injector UI1 appeared to perform well under all test conditions. It often compared favourably with injector NI3, and consistently produced lower C_v's than the other

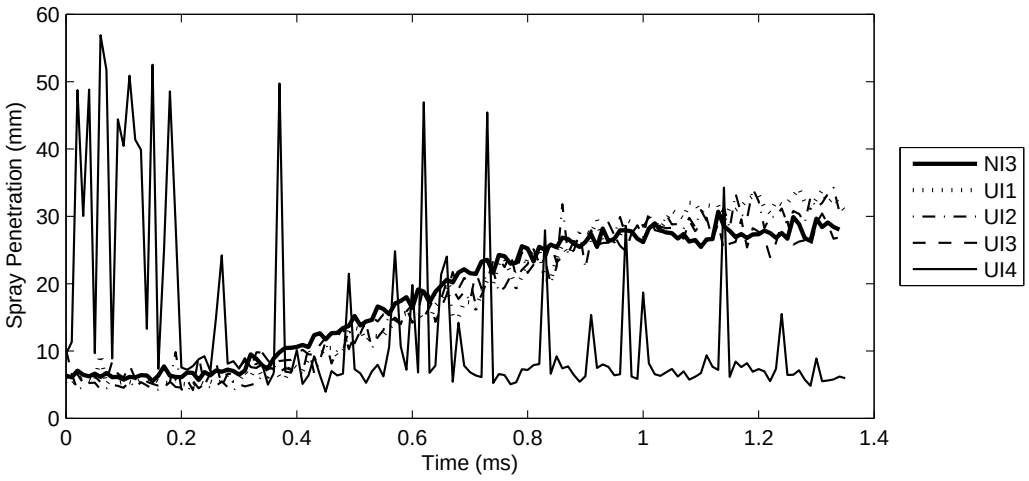

Figure 6.12: Spray Penetration vs. time for 300bar, 1200μs injection

used injectors.

Injector UI2 generally produced poor results compared to the other used injectors as well as the new, control, injector. However, injector UI2 did perform well under low-pressure, short duration conditions.

Injector UI3 generally produced good results, in all circumstances besides the low-pressure short duration case.

Injector UI4 does not deliver any fuel at low pressures, and therefore no results were attained. High pressure results were, however, also not very good when compared to the control injector UI3, or the other used injectors. Two injectors, UI1 and UI3 produced good results, consistent with what would be expected, and to the results displayed by injector NI3. The remaining two injectors, UI1 and UI4 performed poorly.

6.4.3 Injector Spray Behaviour at Various Durations

Introduction

This section will analyse and discuss the behaviour of the sprays at various durations and constant pressure.

During previous analysis, where injector flow was under investigation, it was found that injectors behaved very differently depending on the duration of the excitation signal applied to them. In the analysis of spray, it should be interesting to identify the manner in which duration affects the spray behaviour of a properly functioning injector and to determine whether this characteristic deteriorates with wear.

Observations and Discussions

In order to illustrate the behaviour of the injectors with varying durations, plots have been prepared showing the spray penetration with time for all injectors, NI3 to UI4. These results, taken from injections with rail pressure of 1400bar, are shown below in Figures 6.13 through 6.17. .

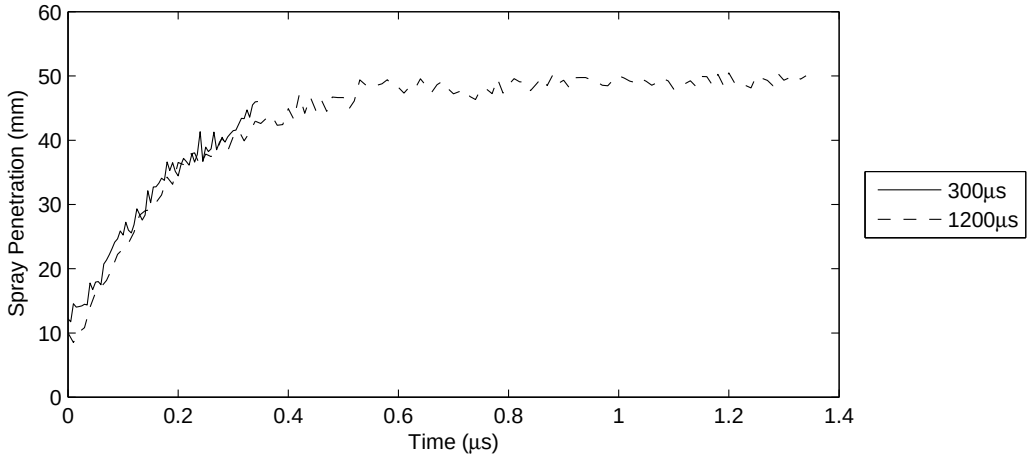

Figure 6.13: Spray penetration vs time for injector NI3, 1400bar injection showing 300μs and 1200μs durations

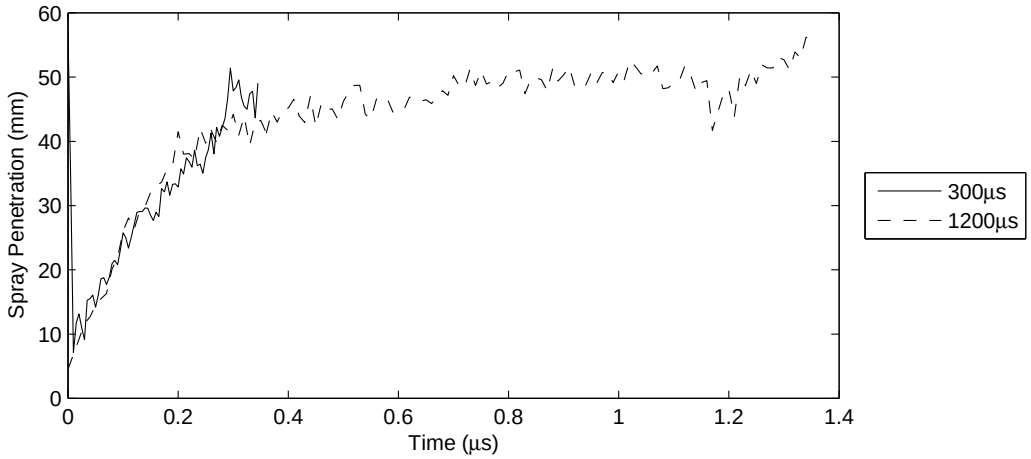

Figure 6.14: Spray penetration vs time for injector UI1, 1400bar injection showing 300μs and 1200μs

From Figure 6.13 it may clearly be seen that in the case of a new, properly functioning injector, there is very little difference in the performance between the shorter and the longer durations.

The results from the used injectors UI1 to UI4 are presented in Figures 6.14 to 6.17. It may be seen that the performance of injectors UI1 and UI3 does not alter much with varying duration, as is expected, based on the performance of injector NI3. Injector UI1 does display a rapid increase in spray penetration toward the end of the shorter duration, but largely performance is similar.

Injectors UI2 and UI4 also perform similarly, however both of these injectors produce lower levels of penetration at shorter durations. The injector flow profile provides additional insight, as shown below in figure 6.18. It is suggested that

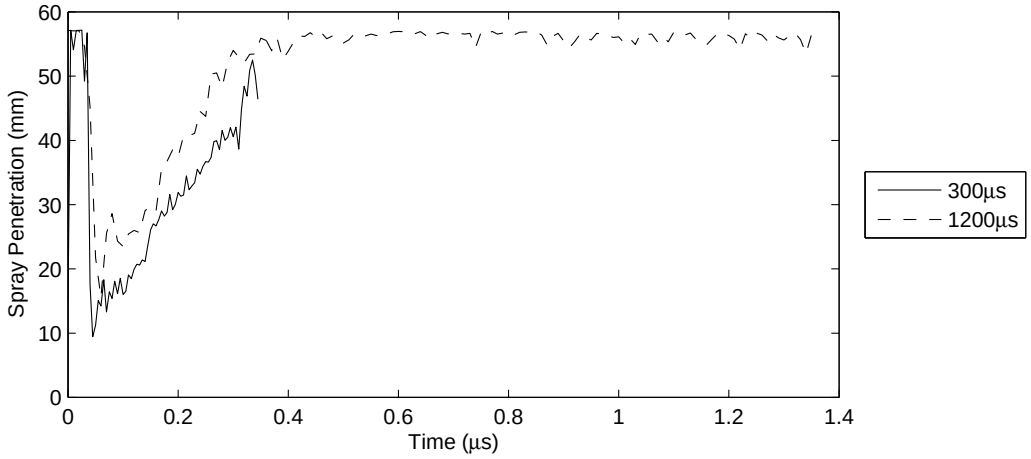

Figure 6.15: Spray penetration vs time for injector UI2, 1400bar injection showing 300μs and 1200μs

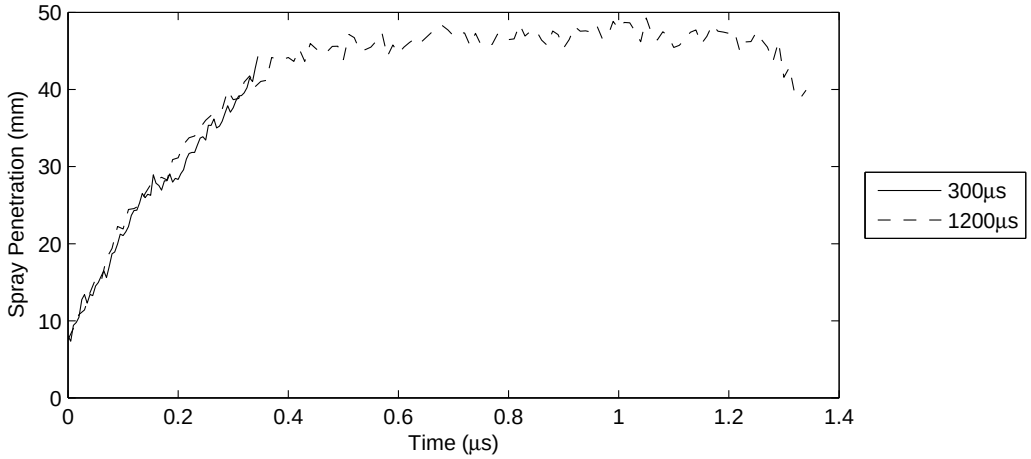

Figure 6.16: Spray penetration vs time for injector UI3, 1400bar injection showing 300μs and 1200μs

these shorter penetrations are due to the fact that the delivery rate of injector UI2 and UI4 peaks below the peaks of the other injections.

Conclusion

The performance on the new injector, injector NI3 indicated that in the case of a properly functioning injector there should be little or no difference between the short and long duration performance.

Two of the four used injectors complied with this expectation, but two of the four

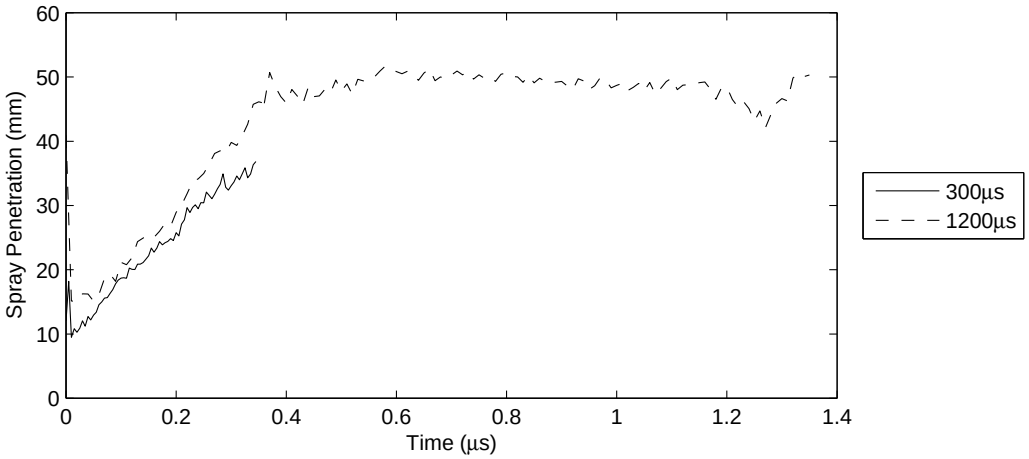

Figure 6.17: Spray penetration vs time for injector UI4, 1400bar injection showing 300μs and 1200μs

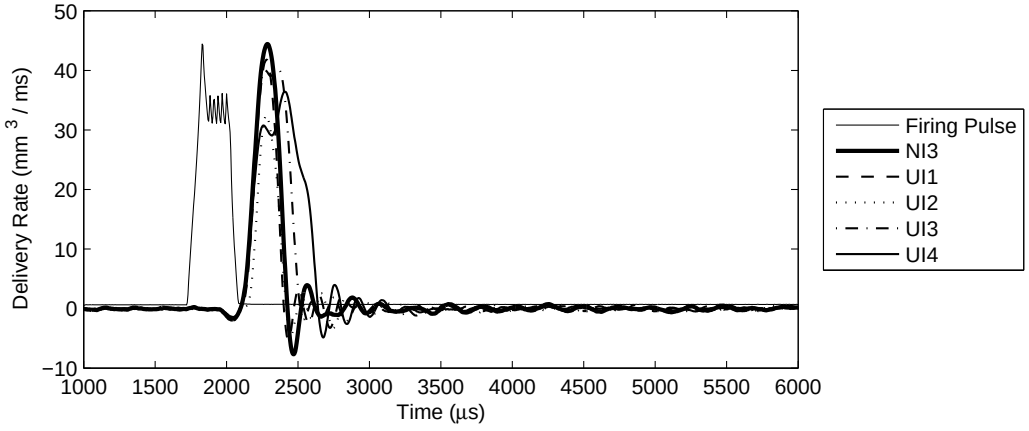

Figure 6.18: Injector delivery rate vs time, for 300μs 1400bar injection

did not. Injectors UI1 and UI3 complied and injectors UI2 and UI4 did not. The failure of injectors UI2 and UI4 to perform as expected was attributed to these injectors having lower peak flow-rates, as discussed in the section on injector flow analysis.

6.4.4 Ultimate Spray Behaviour: Penetration and Cone-Angle

Introduction

As detailed in the literature review, the ultimate spray penetration and cone-angle are key elements in the development of an injector. Cone angle should be maximised so as to increase the degree at which fuel becomes entrained in the air. Penetration is required to be as long as possible, for the same reason as one seeks to maximise cone angle, but should not be so long as to impinge on the cylinder walls.

Observations and Discussions

A straightforward plot has been prepared so as to indicate the ultimate spray behaviour of all injectors, at the various test pressures. The average spray penetration and cone-angle, for the final 100μs of the injection, at various pressures, has been determined. In order to determine the maximum penetration, the longest test duration, 1200μs, has been used in this process.

Figures 6.19 and 6.20 below illustrates the behaviour of the injectors, as described above.

The trend regarding spray penetration may be seen in Figure 6.19. The control injector, injector NI3, shows an almost linear increase in spray penetration with increasing pressure. Two of the used injectors, injector UI1 and UI3 perform in a manner that is almost indiscernible from that of the new injector. The remaining two injectors, injectors UI2 and UI4 tend to penetrate to a somewhat greater

degree than the control injector. It will be recalled from previous discussions that injector UI4 fails to deliver fuel at 300bar rail pressure, and this explains the outlying point visible on the plots at 300bar for injector UI4.

The ultimate cone-angle behaviour indicates strange performance of the control injector, NI3. As outlined in the literature survey, there is a degree of debate as to whether or not the injection pressure should have an effect on the cone angle. The general consensus in the literature is that the pressure should not alter the cone-angle, but injector NI3 does not follow this trend. Also noteworthy in the results for ultimate cone angle is the fact that the overwhelming trend in the data is for

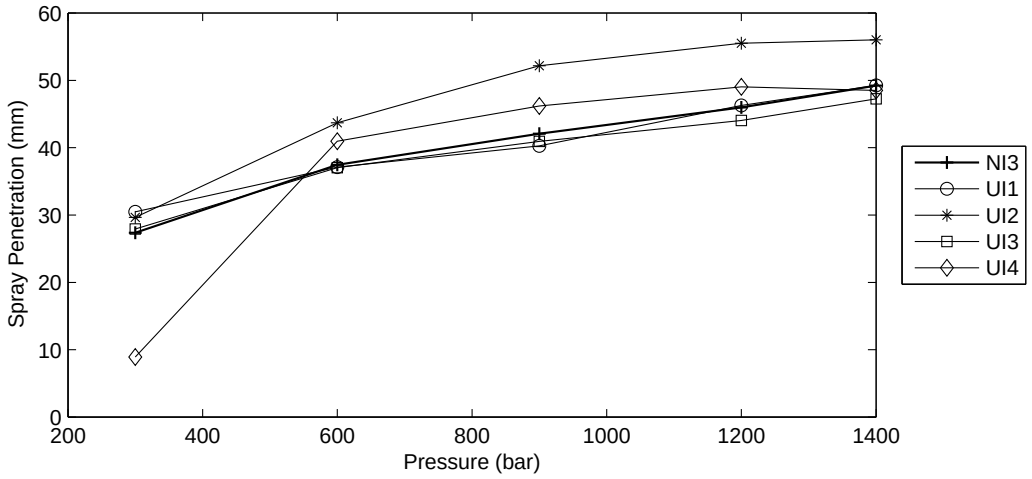

Figure 6.19: Ultimate spray penetration vs pressure for 1200μs injections

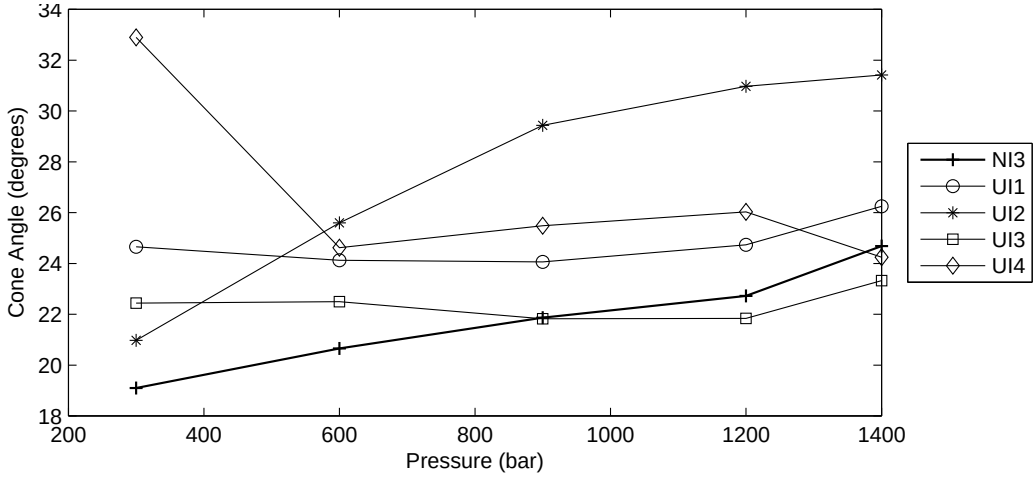

Figure 6.20: Cone-angle vs pressure for 1200μs injections

the used injectors to display larger cone-angles than the control injector. A wide cone-angle is desirable, given that the fuel will then be more spread out, resulting in better entraining with the air, and more effective combustion.

It was mentioned in conversation with the supplier of the used injectors that the running of an engine generally tends to improve after a new set of injectors has been allowed to 'run-in'. The results, as evident in Figure 6.20, provide a very likely reason for this improvement in running, through increased spray area resulting from the increased cone-angle.

Conclusion

The results presented in Figures 6.19 and 6.20 above make for very interesting reading. If anything these results indicate that the ultimate 'macroscopic' qualities of an injector spray behaviour do not deteriorate, but actually improve. A plot has been prepared indicating the spray area, which provides insight into the performance of the spray. This plot is shown below in Figure 6.21.

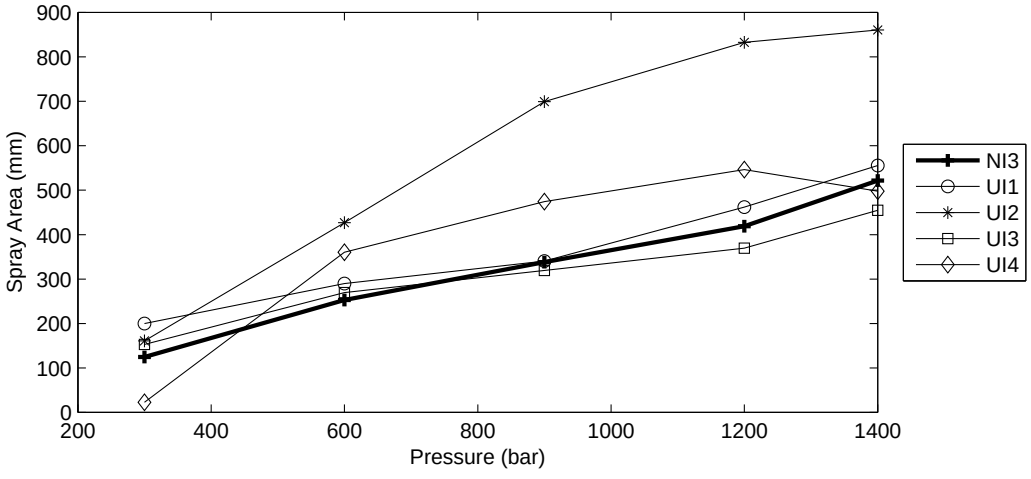

Figure 6.21: Total spray area vs injection pressure for 1200μs injections

The maximum area largely follows the trend as established by the behaviour of the spray penetration seen in Figure 6.19. All the injectors produce larger spray areas than the new injectors except for injection UI3, which drops slightly below the performance of injector NI3.

The results illustrated in Figure 6.21 further indicate that in terms of spray behaviour, the used injectors actually tend to outperform the new injectors.

6.4.5 Transient Behaviour

Introduction

It has been determined how the spray ultimately behaves, but it is important to determine how quickly the injectors arrive at this ultimate behaviour. This section will look at the manner in which the injectors behave during the time before reaching their ultimate penetration.

6.4.6 Observations and Disucssion

An analysis was conducted to determine the time required for an average penetration, across a section of five consecutive intervals to exceed 95% of the ultimate spray penetration, as indicated in Section 6.4.4. Figure 6.22 below is a plot of the time taken for the 1200μs injection to reach 95% of the ultimate spray penetration for that time interval.

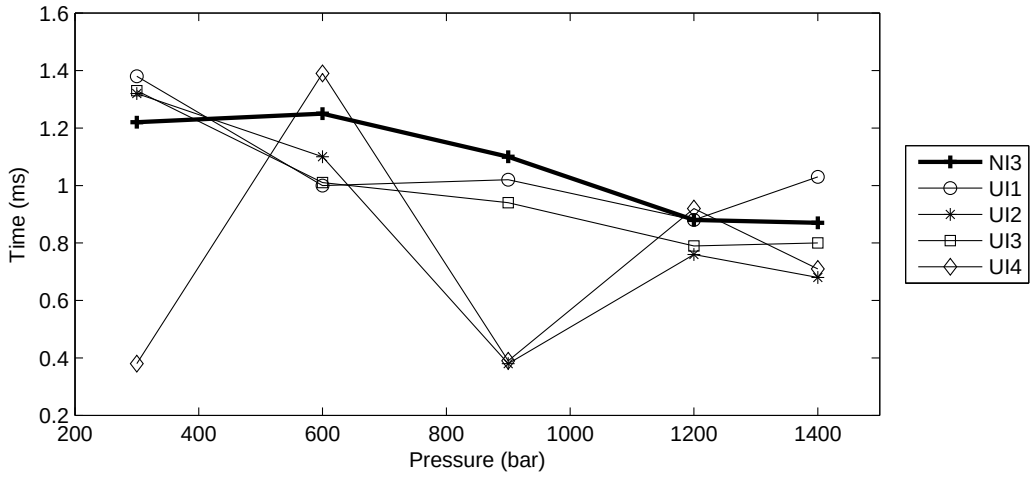

Figure 6.22: Time taken to reach 95% of ultimate penetration vs injection pressure

The behaviour of injector NI3 is largely as expected, where the time for the in-

jection to reach 95% tends to reduce as pressure increases. The other injectors behave in a similar manner, with outliers at 900bar for injectors UI3 and UI4. As was found in the previous section, the used injectors appear to reach their ultimate states earlier than the new, control injector.

Conclusion

As found in the previous section, the used injectors appear to outperform the new injection with regard to the transient performance leading up to the injector's ultimate penetration and cone-angle. This also helps to explain the manner in which engines fitted with new injectors appear to run better once the injectors have been 'run-in'.

6.4.7 Behaviour at early stages of injections

Introduction

The most significant change of state which the injector undergoes is that which occurs when the injector goes from not injecting to injecting. For this reason it is worthwhile to conduct an analysis of the behaviour of an injector at this stage.

Observations and Discussion

To facilitate an analysis of the early stages of an injection, the basic plots showing spray penetration progression over time will be presented below, in Figures 6.23 through to 6.27. The presentation of these figures has the added benefit of allowing one to see the behaviour of the injectors across the entire injection period, enabling one to confirm the results from previous sections. Figures 6.23 through 6.27 are for 1200μs injections, but as presented in Section 6.4.3 the behaviour of the injectors at short and longer durations is largely the same. It may be seen from Figures 6.23 to 6.27 that the performance of the control injector, NI3, is al-

ways progressive, with no unexpected spikes in penetration. This is as one would expect.

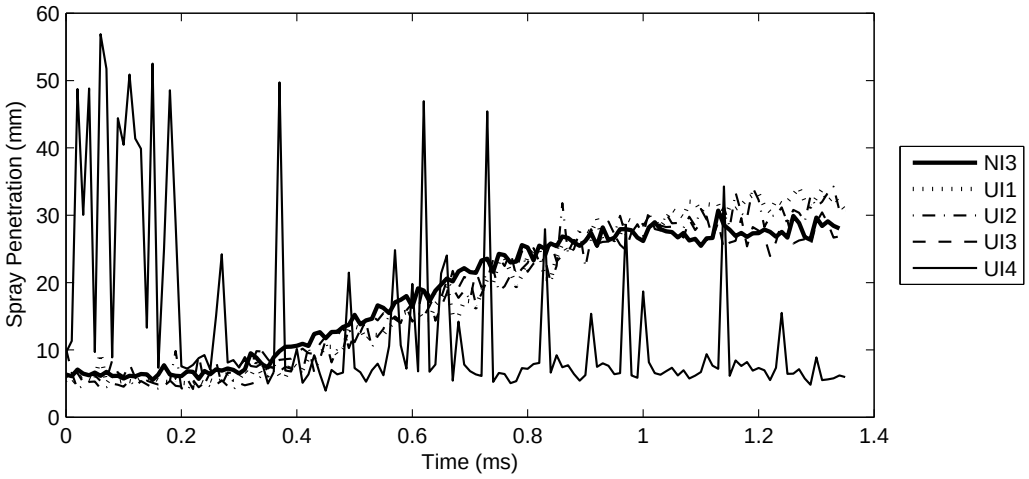

Figure 6.23: Spray Penetration vs Time for 1200μs injection at 300bar rail pressure

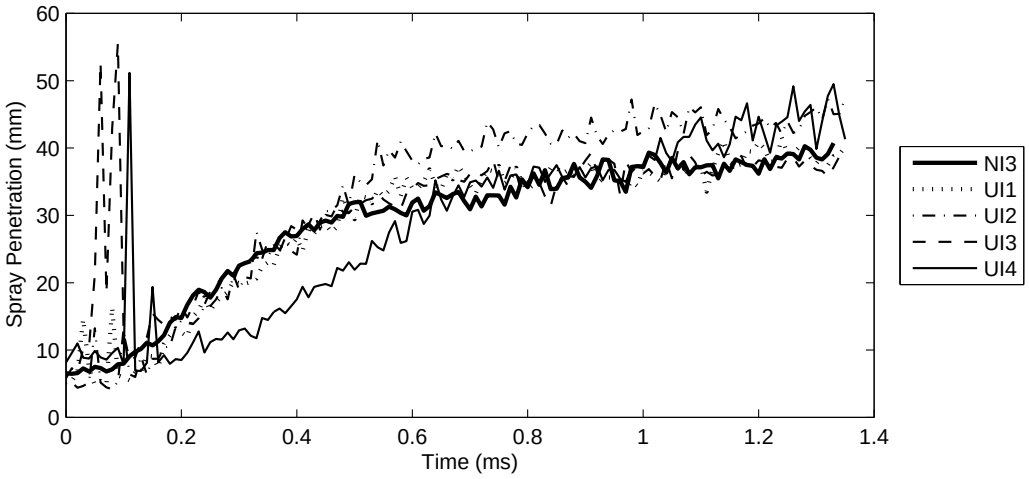

Figure 6.24: Spray Penetration vs Time for 1200μs injection at 600bar rail pressure

At 300bar only injector UI4 gives suspect results, but this is because, as mentioned previously, injector UI4 delivers no fuel at 300bar. When injector pressures increase it becomes evident that the used injectors do not deliver fuel in as stable a manner as the new, control, injector. All of the injectors display their most erratic behaviour at 900bar, whereas their penetrations are lowest at low pressures.

In Figures 6.26 and 6.27 it may be seen that at 1200bar and 1400bar injectors UI2 and UI4 display unusually high initial spray penetration results.

Other interesting results evident in Figures 6.23 through to 6.27 indicate that from pressures of 600bar and upward injector UI2 produces the most advanced spray penetration, as discussed in Section 6.4.4. Again, at pressures of 600bar and upward injector UI4 produces injections which lag behind the other injectors in terms of penetration, before stabilising to a similar ultimate penetration as the other in-

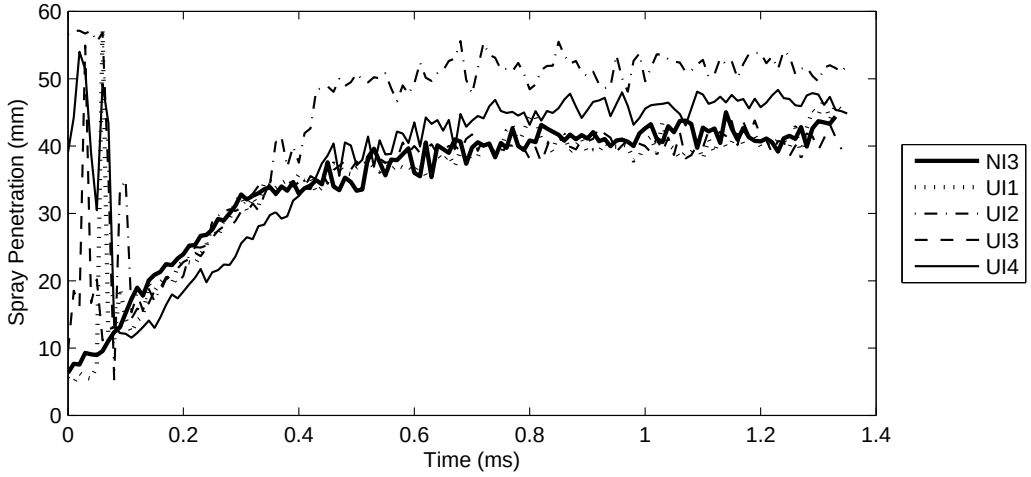

Figure 6.25: Spray Penetration vs Time for 1200μs injection at 900bar rail pressure

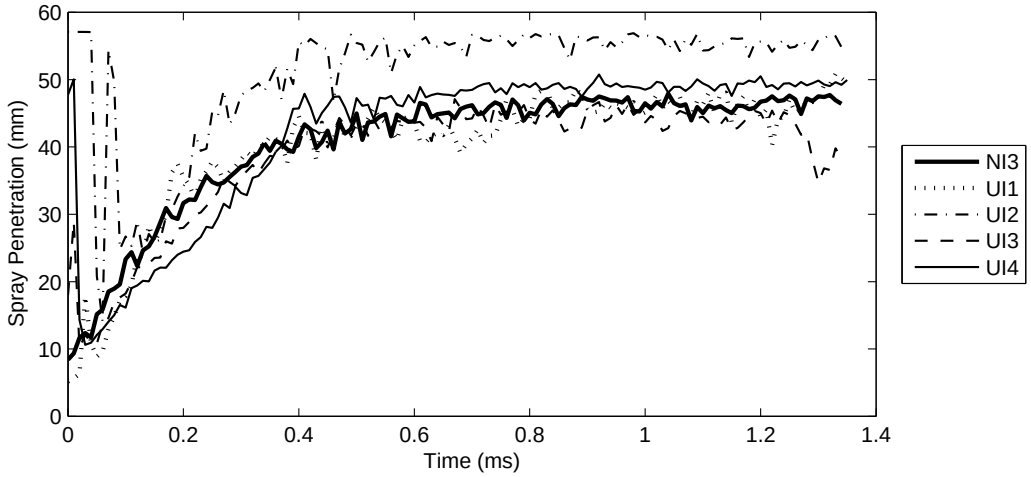

Figure 6.26: Spray Penetration vs Time for 1200μs injection at 1200bar rail pressure

jectors.

Conclusion

Figures 6.23 through to 6.27 show the performance of the injectors. This is not an analysis of the performance of the injectors in terms of some or other derived quality. These images, and this section, serves to illustrate that the performance of the used injectors may look comparable to that of the control injector in many ways. Based on the macroscopic characteristics communicated thus far, however there is a marked difference in the more subtle performance of the injectors.

6.4.8 Short Injection Behaviour

It was mentioned in Section 6.2.2 of this report that testing was conducted at durations shorter than 300μs durations as discussed up to this point. Testing was done at durations of 150μs so as to determine the manner in which injectors perform when a very short injection was simulated. These short injections will be discussed in this section.

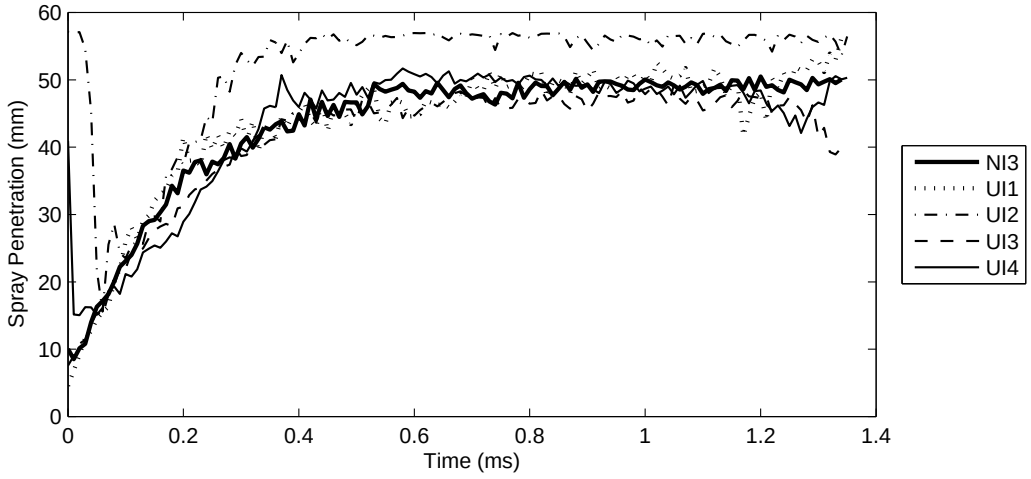

Figure 6.27: Spray Penetration vs Time for 1200μs injection at 1400bar rail pressure

6.4.9 Observations and Discussion

The 150μs injections were conducted at test pressures from 600bar to 1400bar. At 600bar and 900bar the injectors failed to deliver fuel, as evident from Figure 6.28 shown below, illustrating a 900bar plot.

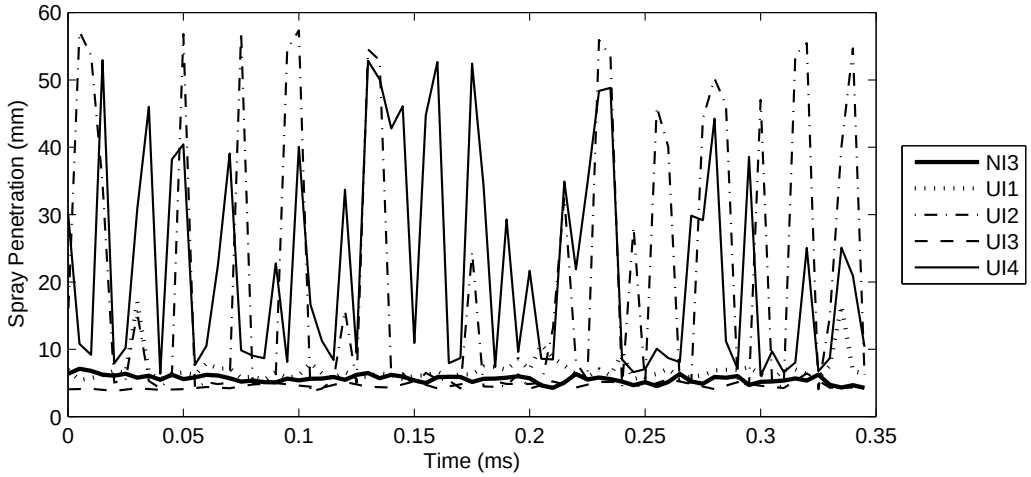

Figure 6.28: Spray Penetration vs Time for 150μs injection at 900bar rail pressure

Injector NI3, the control injector, begins to produce a discernable spray at 1200bar, as is evident in Figure 6.29 below. The sprays produced at 1400bar are somewhat better defined than at 1200bar, as illustrated in Figure 6.30 below.

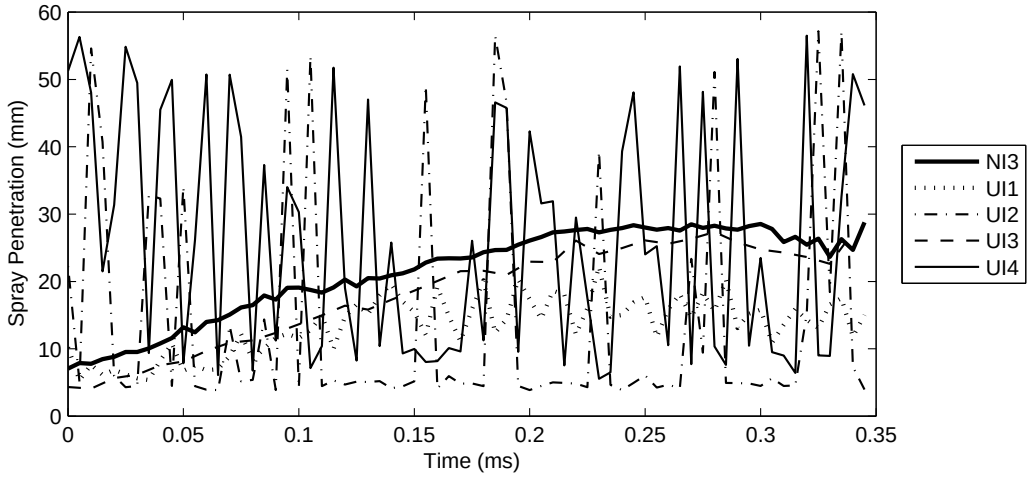

Figure 6.29: Spray Penetration vs Time for 150μs injection at 1200bar rail pressure

The short duration injection behaviour is quite telling with regard to injector deterioration with use. At 1200bar, injector NI3 produces a very well defined spray progression, as does injector UI3. But, injectors UI1, UI2 and UI4 produce poor results, with injections from injectors UI2 and UI4 seemingly producing no spray whatsoever.

At 1400bar, as illustrated in Figure 6.30, it may be seen that all of the injectors produce a result, but these vary widely. Two of the used injectors, UI1 and UI3, produce results very similar to those of the control injector. The sprays of injectors UI2 and UI4 are present, as indicated by the lack of noise, as visible in the performance at 1200bar, in Figure 6.29. That said, the sprays do not appear to advance.

The deterioration of the performance of the spray of the used injectors is most evident in the analysis of the performance of the injectors whilst operating at these shortened durations. In the event of injectors performing in the manner as displayed by injectors UI2 and UI4 being installed in a engine which requires the use of either a brief pilot injection or post-combustion injection the performance of the engine would be adversely affected. Performance, in terms of power produced, smoothness of running and emissions would suffer. The degradation in

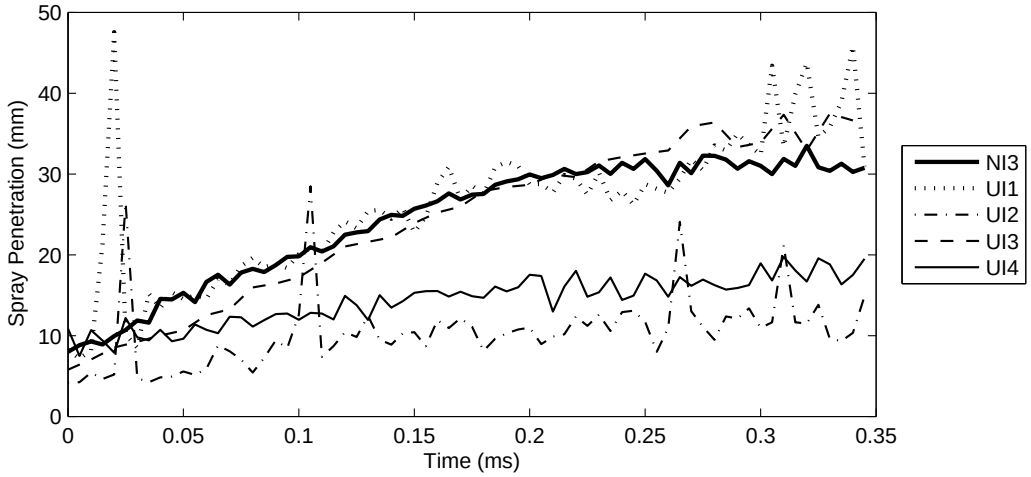

Figure 6.30: Spray Penetration vs Time for 150μs injection at 1400bar rail pressure

performance due to these factors would be sufficient criteria for the discarding of such injectors.

Conclusion

Analysis conducted in previous sections have failed to deliver results which have signaled that any of the used injectors under study should be discarded. The inability of injector UI4 to deliver fuel at low pressure is the exception, as discovered in the analysis of the injectors flow performance. However, when investigating the short duration performance of the injectors, it became clear that some of the injectors would perform very poorly if required to produce a pilot, or post-combustion, injection. This is sufficient discard criteria for an injector, and based on this investigation injectors UI2 and UI4 should be discarded.

6.5 Injector Spray Conclusion

A variety of factors have been considered during the course of the investigation into the spray performance of the injectors. These include:

- Spray performance by segment
- Spray performance with varying durations
- Ultimate spray behaviour
- Spray transient behaviour
- Spray behaviour during early stages
- Spray behaviour during short durations

During the analysis two distinct trends emerged, injectors UI1 and UI3 behaving similarly, and injectors UI2 and UI4 also behaving similarly. Injectors UI1 and

UI3 typically performed similarly to the control injector, while injectors UI2 and UI4 delivered sub-standard performance.

Across most factors analysed the used injectors appeared to perform well. In the cone-angle behaviour, it was found that the used injectors produced larger, and thus more effective cone-angles. This provides justification for the theory that engines run better following a "running-in" period after the installation of new injectors.

The only element of the injectors performance where dramatic deterioration was identified was in the case of the short duration injections. Under simulated pilot-injection conditions, where the injector was subjected to an injection duration of 150 μs, none of the used injectors produced a spray comparable to that of the control injector, NI3. This inability of the used injectors to produce short duration sprays would affect the performance of an engine notably, and in itself are acceptable discard criteria.

While generally the used injectors were found to produce acceptable sprays, their inability to produce short duration sprays renders them ineffective. The alignment between the performance of the injector flow characteristics discussed previously and the spray characteristics discussed here will be discussed in Section 8.

Chapter 7

Injector Spray Analysis: Theoretical Modeling

7.1 Introduction

Within Section 2.3.1, of the literature survey, mention was made of theories which have been developed to predict the behaviour of an injector spray with time. The two principal theories discussed are those developed by Dent and Hiroyasu. In this section these two theories will be investigated, and it will be attempted to align these theories to the performance of the properly functioning injector, NI3.

The results produced by the used injectors will not be considered within this section. This is because of the large number of factors which play a part in the performance of those injectors, and that the original theories were developed using new injectors.

7.2 Spray Theories

The spray theory according to Dent, as stated in Equation 2.2 is repeated here for the sake of clarity.

$$S(t) = 3,07 \left(\frac{\Delta P}{\rho_g}\right)^{\frac{1}{4}} (td_n)^{\frac{1}{2}} \left(\frac{294}{T_g}\right)^{\frac{1}{4}} \tag{7.1}$$

Dent's equation is designed to function effectively over the entire duration of the injection.

The theory according to Hiroyasu is divided into two separate regions, an initial linear region and a second non-linear region. One before, and one after the point defined as t_{break}. This theory is repeated below.

$$t < t_{break}: \qquad S(t) = 0.39 \left(\frac{2\Delta P}{\rho_l}\right)^{\frac{1}{2}} t \tag{7.2}$$

$$t > t_{break}: \qquad S(t) = 2.95 \left(\frac{\Delta P}{\rho_g}\right) (d_n t)^{\frac{1}{2}} \tag{7.3}$$

where:

$$t_{break} = \frac{29\rho_l d_n}{(\rho_g \Delta P)^{\frac{1}{2}}} \tag{7.4}$$

Sample calculations illustrating the use of the above equations are contained in Appendix B, where the variables are assigned and values are given.

7.2.1 Unmodified Theoretical Results

A comparison has been prepared where the results of the performance of the control injector, NI3, have been compared with the predictions based on the Dent and Hiroysau theories. These comparisons are shown for all pressures, in Figures 7.1 through 7.5 below.

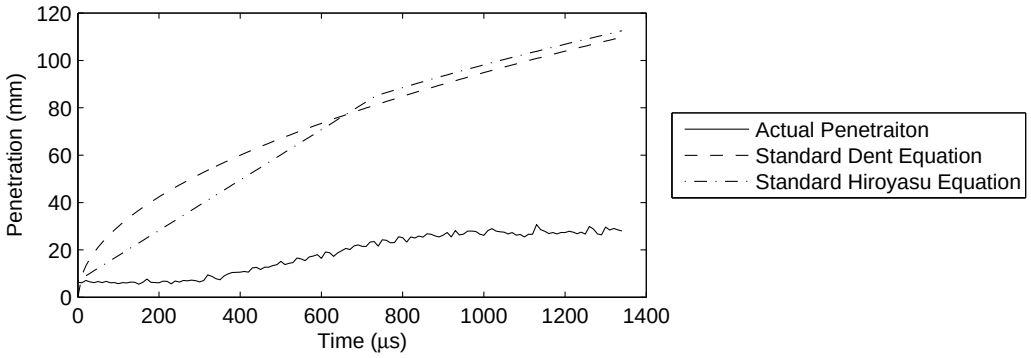

Figure 7.1: Penetration vs time for actual and theoretical spray penetration at 300bar

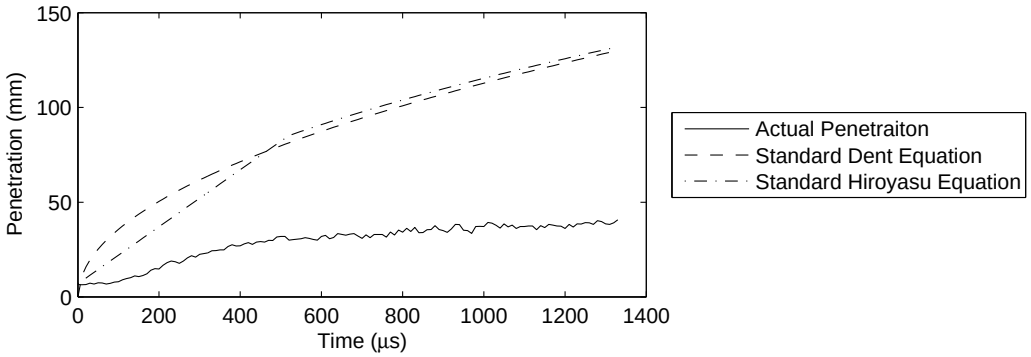

Figure 7.2: Penetration vs time for actual and theoretical spray penetration at 600bar

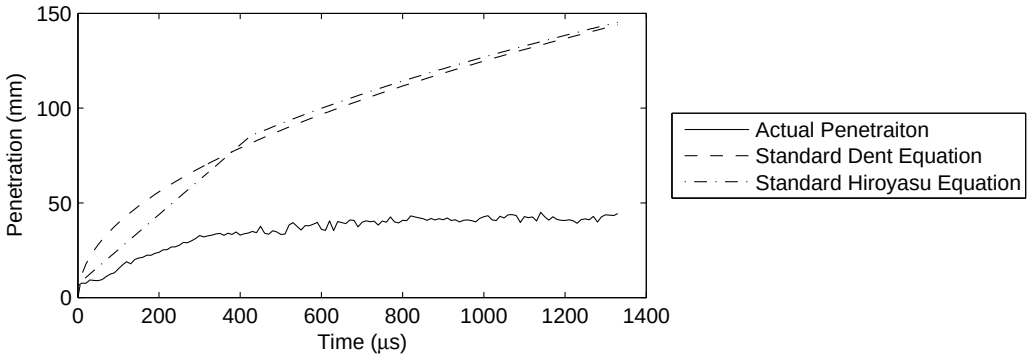

Figure 7.3: Penetration vs time for actual and theoretical spray penetration at 900bar

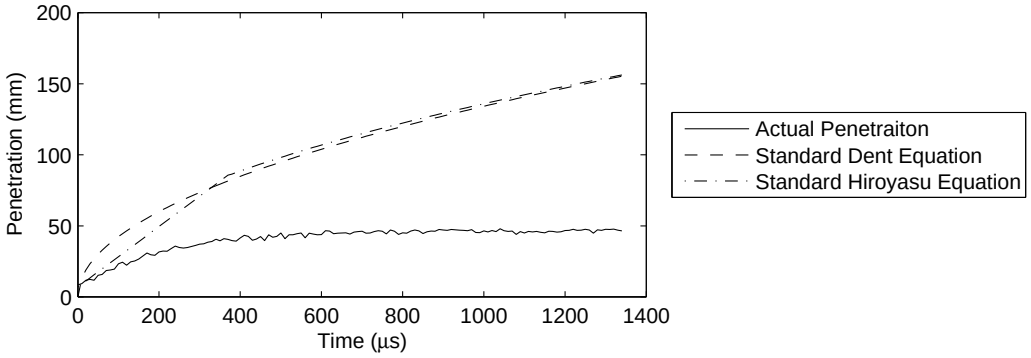

Figure 7.4: Penetration vs time for actual and theoretical spray penetration at 1200bar

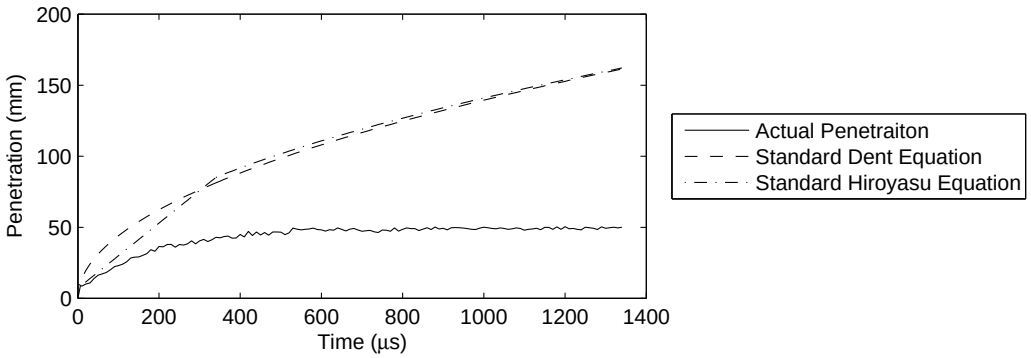

Figure 7.5: Penetration vs time for actual and theoretical spray penetration at 1400bar

It is clear from Figures 7.1 through 7.5 that both theories dramatically over predict the spray penetration when compared to the actual performance of a new injector.

The difference between the theoretically predicted results and those attained by the injectors is so vast that it seems unreasonable that they could align. However, as mentioned in the literature survey, the coefficients contained in the equations developed by Dent and Hiroyasu may be modified to achieve a better fit to data, as has been done by many researchers previously.

7.2.2 Modified Theoretical Results

An empirical process was embarked upon, whereby a series of modifications to coefficients were applied to both Dent and Hiroyasu's theories. At each pressure an iteration was conducted to determine a correlation factor 'k', which would lead to an alignment of the experimental results and the theoretical predictions. The determination of the values of k for the theories according to Dent and Hiroyasu are discussed in Sections 7.2.3 and 7.2.4 respectively.

A set of results identical to those presented in Figures 7.1 through to 7.5 is shown below illustrating predictions when applying the revised, or modified equations, incorporating the various correction factors, which are shown in Table 7.2.2 below. These are shown below in Figures 7.6 through to 7.10 for the modified Dent equation and Figures 7.11 through 7.15 for the modified Hiroyasu equation.

Pressure (bar)	Dent 'k'	Hiroyasu 'k'
300	0.325	0.350
600	0.375	0.350
900	0.450	0.450
1200	0.500	0.550
1400	0.550	0.550

Table 7.1: Values of correlation factor 'k' for theories according to Dent and Hiroyasu

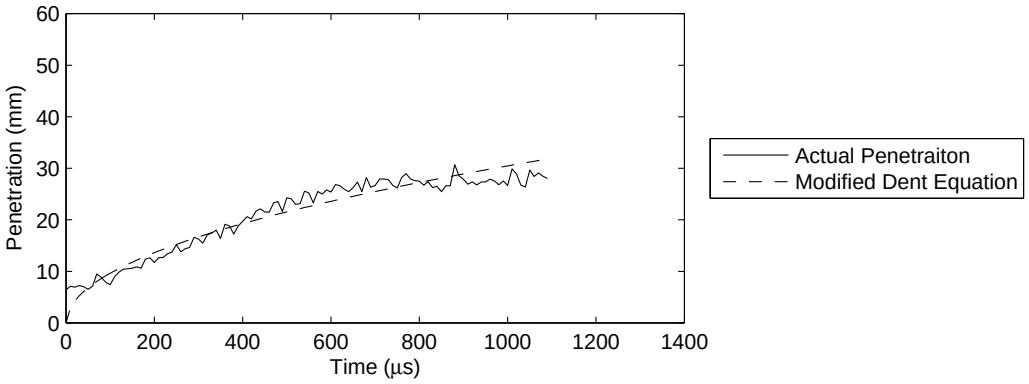

Figure 7.6: Penetration vs time for actual and modified theoretical (Dent) spray penetration at 300bar

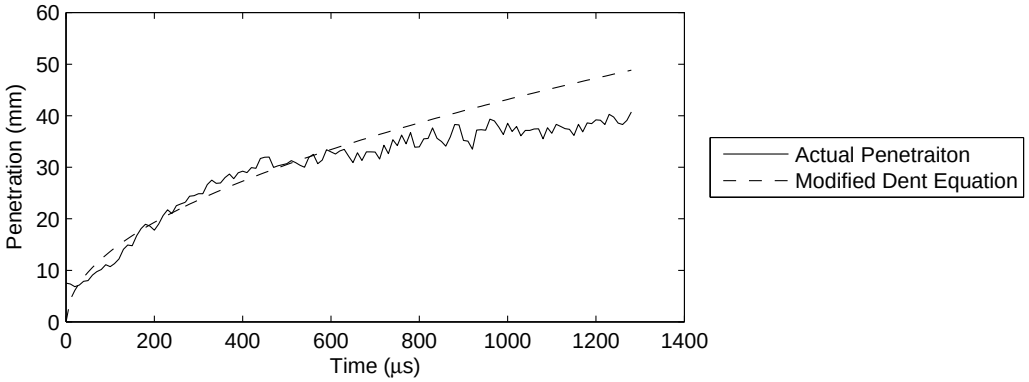

Figure 7.7: Penetration vs time for actual and modified theoretical (Dent) spray penetration 600bar

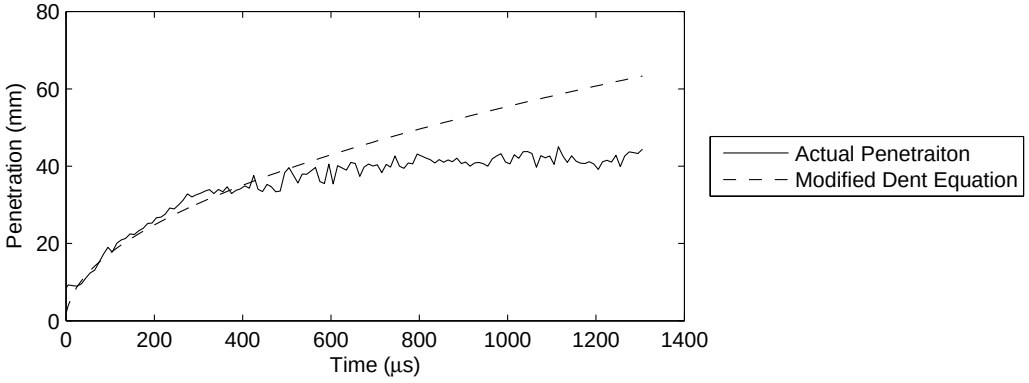

Figure 7.8: Penetration vs time for actual and modified theoretical (Dent) spray penetration 900bar

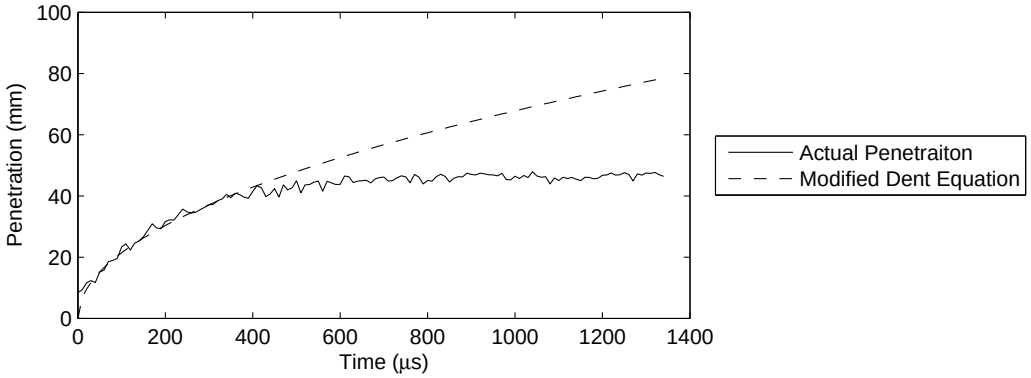

Figure 7.9: Penetration vs time for actual and modified theoretical (Dent) spray penetration 1200bar

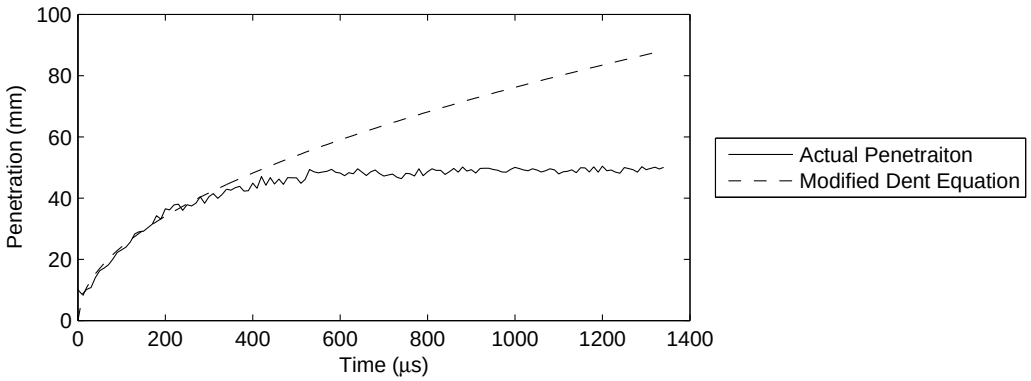

Figure 7.10: Penetration vs time for actual and modified theoretical (Dent) spray penetration 1400bar

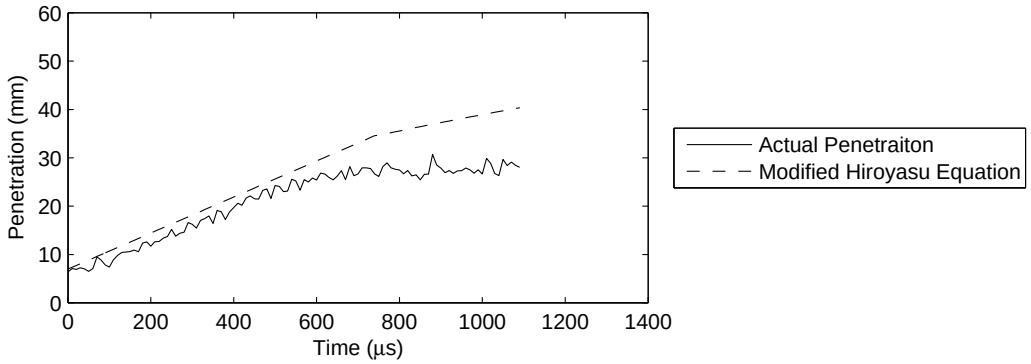

Figure 7.11: Penetration vs time for actual and modified theoretical (Hiroyasu) spray penetration 300bar

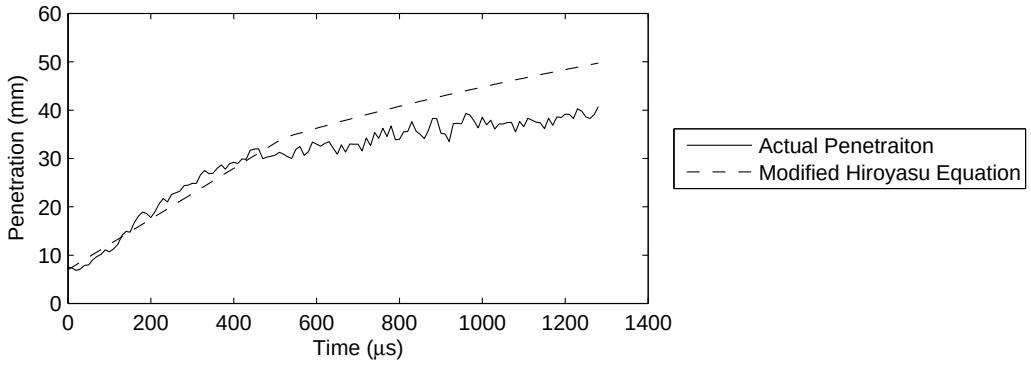

Figure 7.12: Penetration vs time for actual and modified theoretical (Hiroyasu) spray penetration 600bar

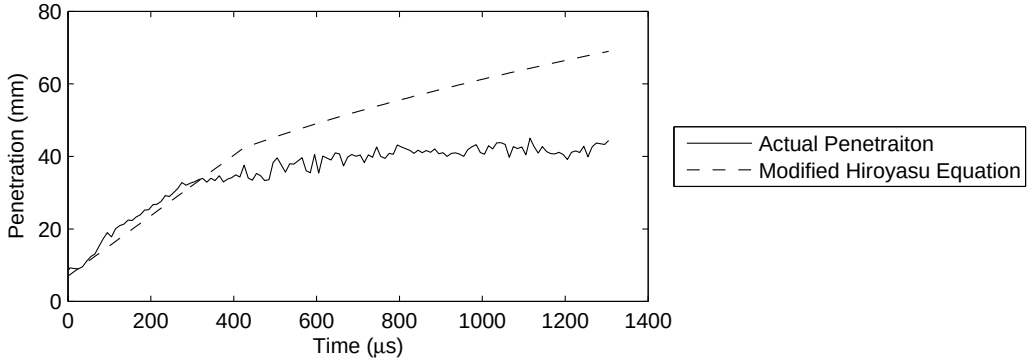

Figure 7.13: Penetration vs time for actual and modified theoretical (Hiroyasu) spray penetration 900bar

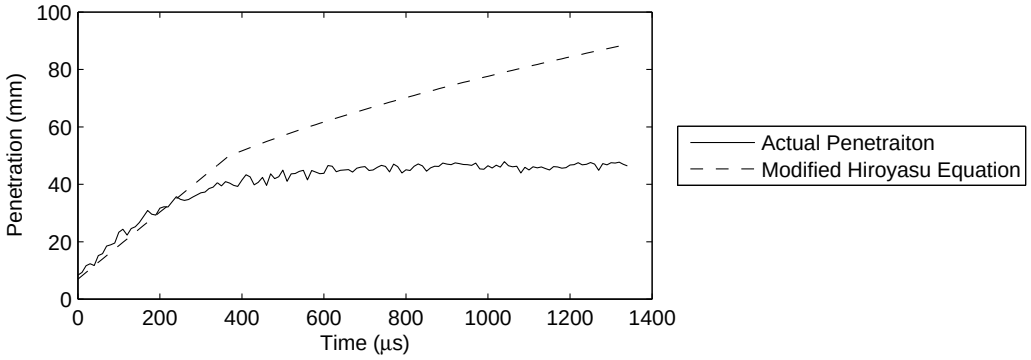

Figure 7.14: Penetration vs time for actual and modified theoretical (Hiroyasu) spray penetration 1200bar

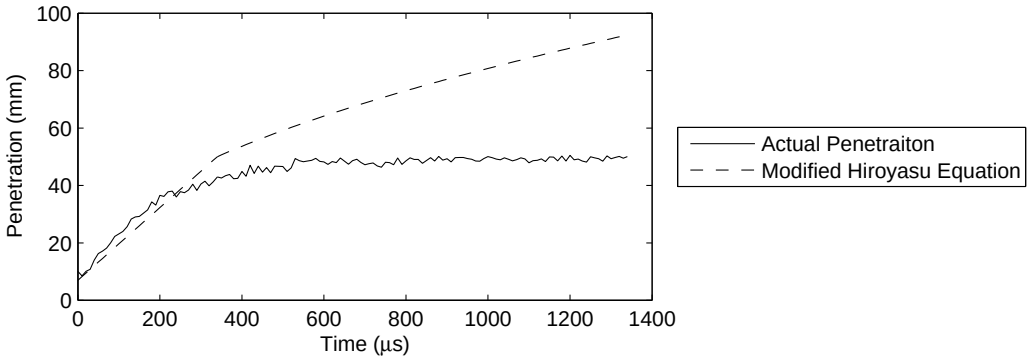

Figure 7.15: Penetration vs time for actual and modified theoretical (Hiroyasu) spray penetration 1400bar

Figures 7.6 through to 7.15 indicate that through the use of an arbitary correction factor a very good correlation may be made between the theoretical and actual spray penetration, during the development of the spray. Since it is difficult to judge the actual performance of the injection at full development, due to the occurrence of saturation, as discussed in Chapter 6, focus was made on the development phase of the injection.

7.2.3 Modified Dent Theory

An analysis was conducted so as to determine the trend present in the 'k'-factors. A plot has been prepared, shown below in Figure 7.16, which indicates the values of these correction factors, with varying pressure.

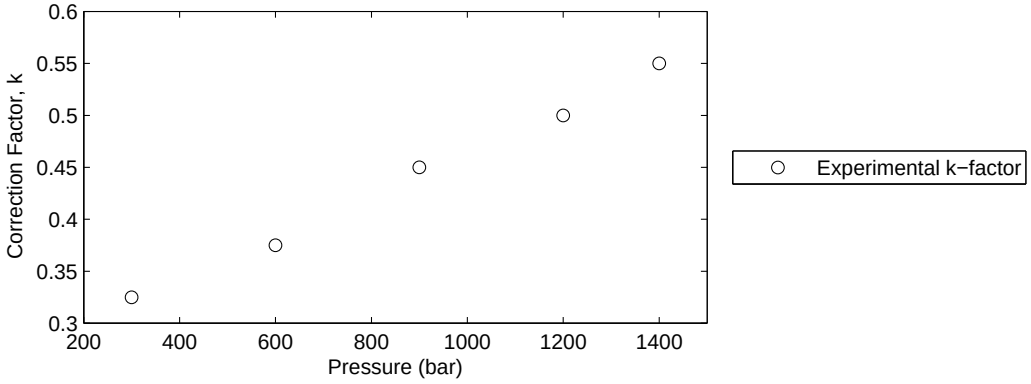

Figure 7.16: Correction factor 'k' vs Pressure for Dent's equation

From Figure 7.16 it may be seen that there appears to be an almost linear trend with the correction factor increasing with injection pressure. The 'Polyfit' function contained in the MATLAB package was used to develop a linear fit equation. Equation 7.5 was developed:

$$k = 0.0002 \cdot P + 0.2596 \tag{7.5}$$

Where P represents the common rail pressure in bar.

If the equation presented above is applied and compared to the experimental results, good results are obtained. the correlation between the theoretical and experimental results are shown below in Figure 7.17.

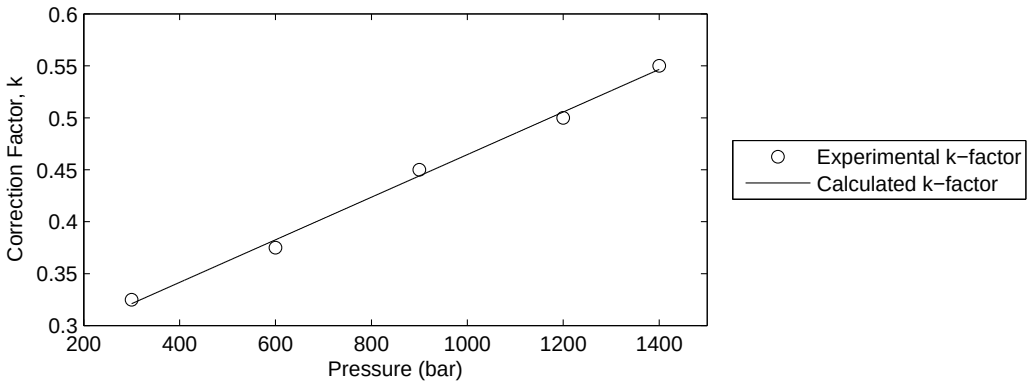

Figure 7.17: Correction factor 'k' vs Pressure for Dent's equation, showing modeled 'k' factor

7.2.4 Modified Hiroyasu Theory

A process similar to that applied to the theory according to Dent was also used on Hiroyasu's theory, and the correction factors 'k' were determined experimentally. The results of Hiroyasu's equations when modified using the correction factor 'k' are shown in Figures 7.11 through 7.15 above. These figures illustrate that a good correlation may be made with the equations through the modification of the equation's constant. The modification factors required are shown below in Figure

7.18. From Figure 7.18 it may be seen that there appears to be an appropriate 'k'-factor for low pressures, 300 - 600bar, an accurate 'k'-factor for high pressure, 1200 - 1400bar, and an intermediate corrector factor at 900bar.

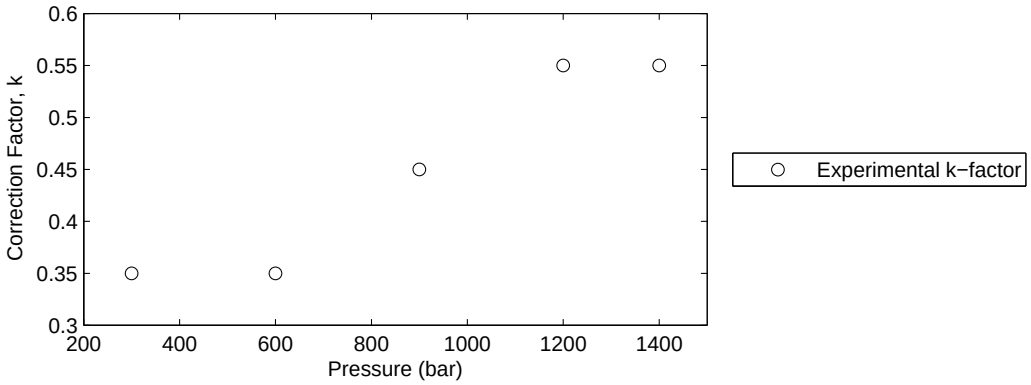

Figure 7.18: Correction factor 'k' vs Pressure for Hiroyasu's equation

An accurate theoretical representation of the 'k'-factors developed and illustrated in Figure 7.18, may be made by fitting a cubic polynomial through the given points, again using the 'Polyfit' function in Matlab. The cubic equation developed is shown below:

$$k = -7.0439 \times 10^{-10} \cdot P^3 + 1.8566 \times 10^{-6} \cdot P^2 - 0.0012325 \cdot P + 0.57213 \quad (7.6)$$

Where P represents the common rail pressure, in bar.

If the equation presented above is applied and compared to the experimental results shown in Figure 7.18, the results as displayed in Figure 7.19 are obtained.

7.2.5 Additional Modification

In addition to the two correction factors, as described in Sections 7.2.3 and 7.2.4, two additional factors were applied to aid the achievement of the correlations illustrated in Figures 7.6 through 7.15. These factors included a time offset in the case of both the Dent and Hiroyasu theories, and a blanket increase in penetration in the case of the Hiroyasu theory.

The offset was a factor included, at lower pressure, to emulate the manner in which the injectors appear to respond later at lower pressures. This offset was applied to neither the 1200bar nor the 1400bar injections, but was introduced at 900bar and below. The factors were 0.25, 0.05 and 0.025ms at 300, 600, and 900bar respectively.

It was also found that in order for the spray theory according to Hiroyasu to fit, the results required a blanket increase of 7mm in spray penetration. This is to offset the fact that at the beginning of the spray development, at t $\approx$ 0, the apparatus registers a spray of approximately 7mm. Since the spray theory, according to Hiroyasu, is linear in nature, it is important to begin the spray development, both theoretical and actual, at the same point. This is so since the linear trend does not demonstrate the rapid growth of an exponential trend at low times, as is the case with the spray theory according to Dent.

7.2.6 Discussion

It has been demonstrated in Sections 7.2.3 and 7.2.4 that a good correlation may be developed between the actual sprays achieved in the testing conducted, and the commonly used theories according to Dent and Hiroyasu. The achievement of this correlation required the adjustment of the equations by factors that varied

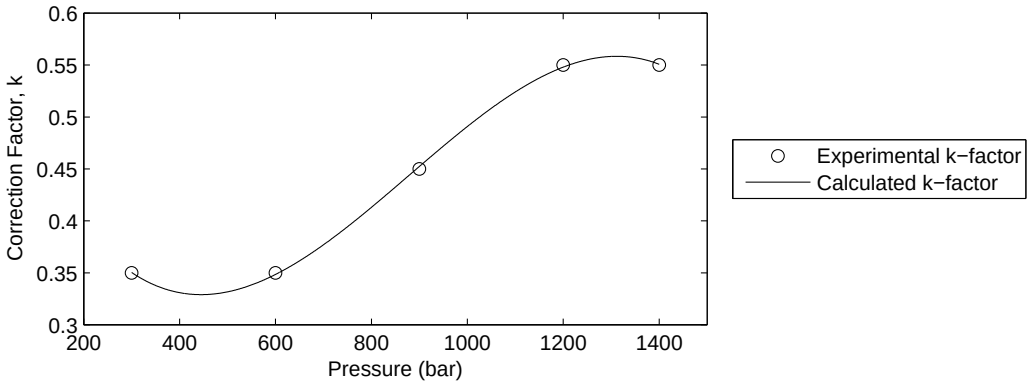

Figure 7.19: Correction factor 'k' vs Pressure for Hiroyasu's equation, showing modeled 'k' factor

with pressure. However, it is noteworthy that in the cases identified in the literature where commonly employed spray theories were applied, most of these cases where shadowgraphy was applied as a means of capturing images. The case under discussion here is unique in its application of the light intensity sensitive imaging.

Factors which come into play in the case being addressed here include the results dependance on the intensity threshold setting, as discussed in Chapter 6, as well as the ability of various liquid droplet sizes to reflect light. It is poignant that even with these factors, a strong correlation may be made between the theoretical results and those achieved with the new common-rail injector, through a relatively simple analysis.

The necessity for a correction factor, which effectively reduces the theoretical predictions, may be introduced by the low setting of the intensity threshold. It may be that the spray is present, but that due to the nature of the test equipment, and the manner in which it is setup, the spray is not detected in the same way that other test equipment does. It also cannot be ruled out that the injector's nature may be such that it performs very differently at high and low pressures, and therefore differently to the predictions made by both Dent and Hiroyasu.

The correction factor increases with increasing pressure. This may be attributed to the manner in which the light reflected by the liquid is inversely proportional to the square of the particle size. Thus the smaller the particle, the less light it reflects. As the rail pressure increases, the droplet size will get smaller, leading to less light being reflected. Therefore, at high pressures the spray may be significantly longer than indicated by the apparatus.

Another reason for the variation of the correction factor with pressure may be due to the amount of fuel being introduced into the spray chamber. As more fluid is in the spray chamber at high pressure this fluid will reflect light. Since more light is being reflected by the atmosphere, it becomes more difficult to discern the actual spray produced, and thus the spray looks smaller, requiring a larger correction factor, as is the case.

Despite the need for correction factors when comparing the theoretical and test results, it is noteworthy that all that was required was a linear scaling factor, which varied with pressure. The shape of the progression of the spray is maintained.

7.2.7 Conclusions and Recommendations

With the application of simple correction factors, a good correlation was achieved between the predictions of Dent and Hiroyasu and the actual test results attained during testing. This is the first time, during the use of the INOV8 test stand, that a good correlation has been achieved between theoretical and empirical results. The achievement of this correlation indicates a similarity between the results attained and those predicted by the theories. The development of a more advanced theory for the prediction of injector spray behaviour when tested with the INOV8 test stand, as well as testing the current theory developed here over a greater spectrum of pressures would be valuable.

Speculation was made as to the reasons for the disparity between the theory and the results achieved, and why there was a need for a correction factor which varied with pressure to be developed. It would be valuable to test a similar injector under the same conditions, using a shadowgraphy technique so as to compare the results achieved and to quantify the differences in spray results from each visualisation technique.

More tests could also be done to investigate the effects of varying the intensity threshold on the ability of the test apparatus to emulate the theoretically predicted results.

Through attempting to quantify the difference in performance between the theoretical results, the results as achieved by other apparatus, and those achieved by the INOV8 - LaVision equipment, considerable future research may be undertaken.

Chapter 8

Conclusion

During the investigation conducted, two separate sets of analysis were performed, comparing the performance of four used injectors to that of a new, control injector, in terms of spray and flow characteristics. Independent of this, an investigation was undertaken to attempt to align two mainstream spray modeling theories to the characteristics displayed by the control injector during testing.

The injector flow analysis was used to examine the detailed performance of the injectors. The differences between the performance of the used injectors and the new injectors were used to identify potential faults in the injectors. These faults were based on an understanding of the manner in which injectors function. A more macroscopic approach was taken with the spray analysis, where differences between the performance of the new and used injectors were highlighted and an analysis of whether the spray produced from the injectors would still prove adequate for use in an engine was done.

The spray results identified that two of the injectors behaved similarly to the control injector, and two behaved quite differently. However, in the case of the short, 150μs injection none of the used injectors delivered significant sprays.

Two of the used injectors produced results with spray and flow characteristics which compared favourably to the control injector. One of these injectors, UI1,

appeared to have suffered from solenoid wear while the other, UI3, appeared to have suffered an increase in mechanical friction.

Another two injectors, UI2 and UI4, produced sprays that did not compare favourably with the control injector. UI2 suffered from wear in the upper section of the injector where the ball valve seats onto the bleed orifice. UI4 suffered from deterioration in the solenoid mechanism, as well as mechanical wear within the injector.

It was hoped that during the course of the investigation a well defined link would emerge between the deterioration in the spray and flow characteristics of the used injectors. The simplest flow-characteristic deterioration was attributed to wear in the solenoid, where the soleniod would only respond to the “pull-phase” signal and not to the “hold-phase” signal. This was experienced on UI1, and it produced sprays which compared favourably with the control injector as was expected. UI3 also produced good spray results. It suffered mechanical wear, which appeared to increase the friction within the injector, leading to poor flow characteristics. However, this wear in the plunger does not appear to have affected the spray characteristics of the injector. This indicates that a deterioration in the flow characteristics will not necessarily manifest in a deterioration in the spray characteristics of an injector.

UI2 was identified to have suffered from wear in the upper portion of the injector, where the bleed and feed orifices are located. This injector produced sub-standard spray performance, due to the injector delivering considerably less fuel than the control injector. UI4 also performed poorly in terms of spray characteristics was subjected to deterioration in the solenoid as well as mechanical wear within the body of the injector.

It is curious that two used injectors, UI1 and UI3, produced efficient sprays with a worn solenoid and increased friction within the body respectively. However, when these two wear characteristics are combined within a single injector sub-standard spray characteristics are delivered. This suggests that the deterioration in the flow and spray characteristics are driven by independent causes. Perhaps

the spray characteristics are affected by deterioration in the shape of the nozzle, or some other mechanical degradation which does not affect the delivery of fuel. However, the deterioration of both the flow and spray characteristics in the case of the injector where the bleed orifice was found to be worn, indicates that there may be alignment between the deterioration of spray and flow characteristic if the wear in question affects the delivery of fuel sufficiently.

Injectors UI3 and UI4 had been ultrasonically cleaned before they were supplied for testing. Since UI3 compared favourably with the control injector, and injector UI4 did not, it may be said that the ultrasonic cleaning does not have a particularly marked effect on improving the spray performance of the injector. However, it would be interesting to run comparative tests of an injector before and after ultrasonic cleaning so as to determine the effect of the process.

It is noteworthy that the used injectors produced improved macroscopic spray characteristics when compared to the control injector. The used injectors produced wider cone angles and thus increased spray areas. This leads to improved engine running after a set of injectors has been “run-in”. Also noteworthy is the fact that none of the used injectors produced sprays at very short durations. This would render the pilot injection ineffective and lead to decreased performance and increased emissions. These observations indicate that there are both positive and negative elements in the characteristics of both new and used injectors. The inability, however, of the used injectors to deliver short pilot-injections could be used as discard criteria, and provide for a quick, real-world, test to determine an injectors efficacy.

A correlation was developed between the spray results displayed by the new injector and the spray theories developed by Hiroyasu and Dent. This correlation was developed by multiplying the results of the spray penetration by a revised constant, which was found to vary with pressure. Additional modifications were introduced in the form of a varying offset from start of injection and a blanket increase in penetration in the case of the theory according to Hiroyasu. The development of a correlation between the two most popular theories indicates a definite

similarity between the theories and the results obtained by the test stand and the La Vision software package.

Future research opportunities based on that conducted here exist. These include expanding the number of used injectors studied in the investigation. This would allow for an analysis in terms of the manner in which injectors wear. Further follow-up could be done on the injectors investigated in this study, in order to verify the nature of the wear as detailed in Section 5.

In terms of the spray, further analysis could be conducted to determine the effects of altering the spray intensity threshold in order to obtain a better visualisation of the spray through reducing the saturation levels. A deeper understanding of the relevance of the results obtained here from the test stand could be obtained if a set of tests were run, with the same injector and injection parameters, using both the test stand and the more traditional shadowgraphy imaging technique. This would allow the differences in the observations from these two techniques to be quantified.

An investigation was done to develop an alignment between the theoretical predictions of both Dent and Hiroyasu and the actual results obtained. Further research may be conducted based on these findings, including running tests at other pressures and different intensity settings within the La Vision environment. Additional tests could be run using the shodowgraphy technique, which is more commonly associated with the above mentioned theories.

In all of the tests, but especially in the case of the new injector, the test stand may be modified such that an alternative fluid may be used for testing, for instance DME as tested before within the same laboratory. This would allow the behaviour of a common rail injector using different fuels to be assessed using the advanced techniques made available in the test-stand, as discussed in Section 3. The test stand may also be adapted so as to actuate a shadowgraphy imaging apparatus, as discussed above.

Bibliography

[1] A. Liepetz A. Fath, K.U. Munch. *Spray break-up processes of diesel fuel investigated close to the nozzle*, pages 513–520. 1997.

[2] et al. Andrew G. MacPhee. X-ray imaging of shock waves generated by high-pressure fuel sprays. *Science*, 295, 2002.

[3] T. Dreier-N.J. Dam J.J. Ter Meulen-T. Gerber B. Bougie, M. Tulej. Optical diagnostics of diesel spray injections and combustion in a high-pressure high-temperature cell. *Springer-Verlag*, 2005.

[4] Bosch. *Electronic engine management for diesel engines: Diesel accumulator fuel-injection system Common Rail. Technical Instruction*, 1999.

[5] A. Fath-A. Leipertz b C. Badock, R. Wirth. Investigation of cavitation in real size diesel injection nozzles. *International Journal of Heat and Fluid Flow*, 1999.

[6] J. Kang C. Bae. Diesel spray characteristics of common-rail vco nozzle injector. Department of Mechanical Engineering, Korea Advanced Institute of Science and Technology.

[7] J. Kang-J. Kong C. Bae, J. Yu. Effect of nozzle geometry on the common-rail diesel spray. *SAE Technical Paper Series*, 2002.

[8] J. Lacoste-M.R. Heikal M.R. Gold N.S. Jackson D.A. Kennaird, C. Crua. In-cylinder penetration and break-up of diesel sprays using a common rail injection system. *SAE Technical Paper Series*, 2002.

[9] M.R. Heikal D.A.Kennaird, C.Crua. Influence of injector parameters on the formation and break-up of a diesel spray. *SAE Technical Paper Series*, 2001.

[10] J.C Dent. Basis for the comparison of the various correlations for spray penetration. *SAE Technical Paper Series*, 1971.

[11] B. Besson E. Delacourta, B. Desmeta. Characterisation of very high pressure diesel sprays using digital imaging techniques. *Fuel*, 2004.

[12] Julian Edgar. Common rail diesel engine management, part 1. *AutoSpeed*, 414, 2007.

[13] John B. Heywood. *Internal Combusiont Engine Fundamentals*. McGraw-Hill Book Company, 1988.

[14] C. Tropea I.V. Roisman, L. Araneo. Effect of ambient pressure on penetration of a diesel spray. *International Journal of Multiphase Flow*, 2007.

[15] M. Heikal-D. Kennaird M. Gold J. Lacoste, C. Crua. Pda characterisation of dense diesel sprays using a common-rail injection system. *SAE Technical Paper Series*, 2003.

[16] Ming-Chia Lai Jian-Rong Qin, Tomohisa Dan. Correlating the diesel spray behaviour to nozzle design. *SAE Technical Paper Series*, 1999.

[17] J.M Garcia-F.J. Salvador J.M. Desantes, R Payri. A contribution to the understanding of isothermal diesel spray dynamics. *Fuel*, 2006.

[18] Xing-Bin Xie Ming-Chia Lai Joong-Sub Han, Pai-Hsui Lu and Naeim A. Henein. Investigation of diesel spray primary break-up and development for different nozzle geometries. *SAE Technical Paper Series*, 2002.

[19] H. Kano M. Kato T. Oya K. Date, M. Manabe. Contribution of fuel flow improvement in nozzle to spray formation. *SAE Technical Paper Series*, 1992.

[20] La Vision GmbH. *Product Manual for DaVis ver 7.2*, September 2007.

[21] D. Kennaird C.Crua J. Lacoste M. Heikal O. Lagnitton, M. Gold. Spray development and combustion characteristics for common rail diesel injection systems.

[22] D. Laforgia P. Carlucci, A. Ficarella. Pilot injection behaviour and its effects on combustion in a common rail diesel engine. 2001.

[23] J. Gimeno L.D. Zapata R. Payri, F.J. Salvador. Diesel nozzle geometry influence on spray liquid-phase fuel penetration in evaporative conditions. *Fuel*, 2007.

[24] L.M.T. Somers W.A. de Boer R.S.G Baert R.J.H Klein-Douwel, P.J.M Frijters. Macroscopic diesel fuel spray shadowgraphy using high speed digital imaging in a high-pressure cell. *Fuel*, 2006.

[25] R. Poola & R. Sekar S. Grupta. Effect of injection parameters on diesel spray characteristics. *SAE Technical Paper Series*, 2000.

[26] J.M. Riesco-Avila A. Gallegos-Munoz S.M. Aceves S. Martinez-Martinez, F.A. Sanchez-Cruz. Liquid penetration length in diesel fuel injection. *Applied Thermal Engineering*, 2007.

[27] Thomas Karl Sprich. Determination of the pressures within an injector - experimentation and model validation. Master's thesis, University of the Witwatersrand, Johannesburg, 2010.

[28] Cornel Stan, editor. *Direct Injection Systems for Spark-Ignition and Compression-Ignition Engines*. SAE International, 1999.

[29] K.H. Lee C.S. Lee S.W. Park, S.H. Bang. Atomization characteristics of common-rail diesel injector witth multi-hole. *SAE Technical Paper Series*, 2003.

[30] Tomoyuki Tsuda Toshiyuki Yoda. Influence of injection nozzle improvement on "di" diesel engine. *SAE Technical Paper Series*, 1997.

[31] J Hammer T. Wintrich-C. Hinrichsen U. Dohle, S. Kampmann. Advanced diesel common rail systems for future emission legislation. Technical report, Rober Bosch GmbH, Stuttgart, Germany.

[32] Frank M White. *Fluid Mechanics*. McGraw-Hill Book Company, sixth edition, 2008.

[33] T. J. Williams. Parameters for correlation of penetration results for disel fuel sprays. *Proc Institute of Mechanical Engineers*, 187, 1973.

[34] G. Ziegler. Euro 4 and beyond role of diesel fuel injection systems. *SAE Technical Paper Series*, 2004.

Appendix A

Complete Spray Observations

This appendix contains the complete results for all used injectors and the control injector NI3.

A.1 300 bar

A.1.1 300μs Duration

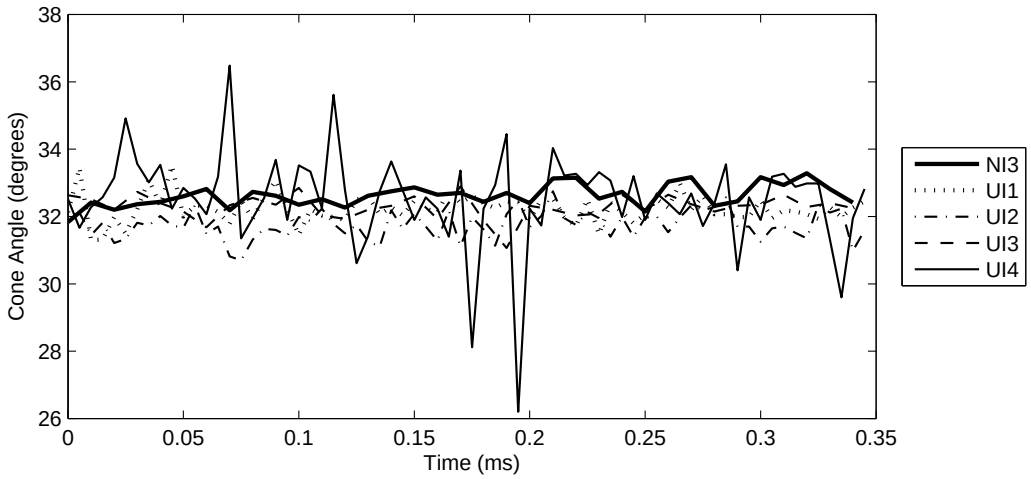

Figure A.1: Cone angle vs time at 300 bar, 300μs duration

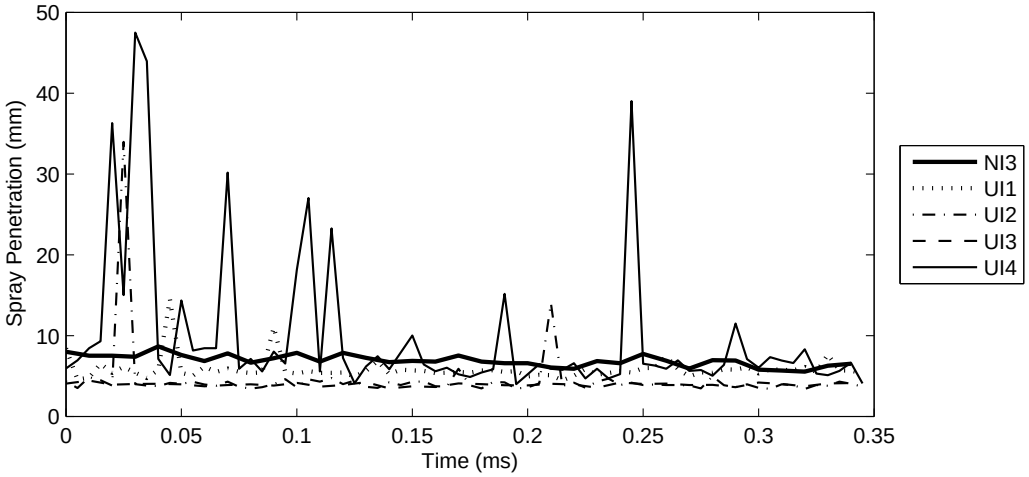

Figure A.2: Penetration vs time at 300 bar, 300μs duration

A.1.2 600μs Duration

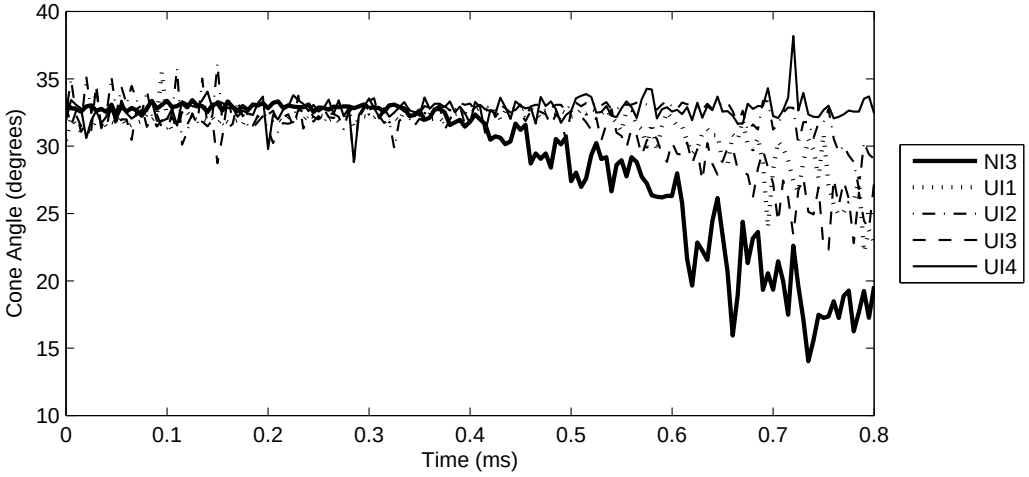

Figure A.3: Cone angle vs time at 300 bar, 600μs duration

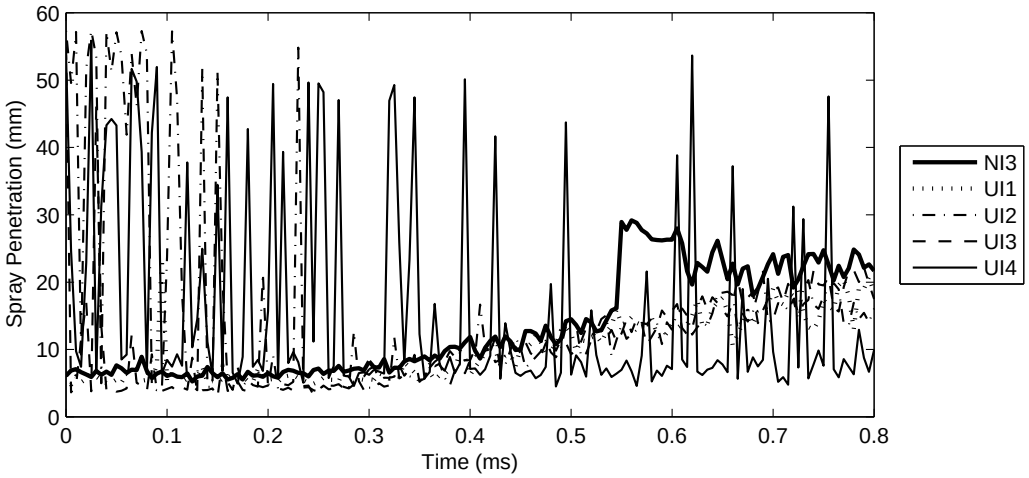

Figure A.4: Penetration vs time at 300 bar, 600μs duration

A.1.3 1200μs Duration

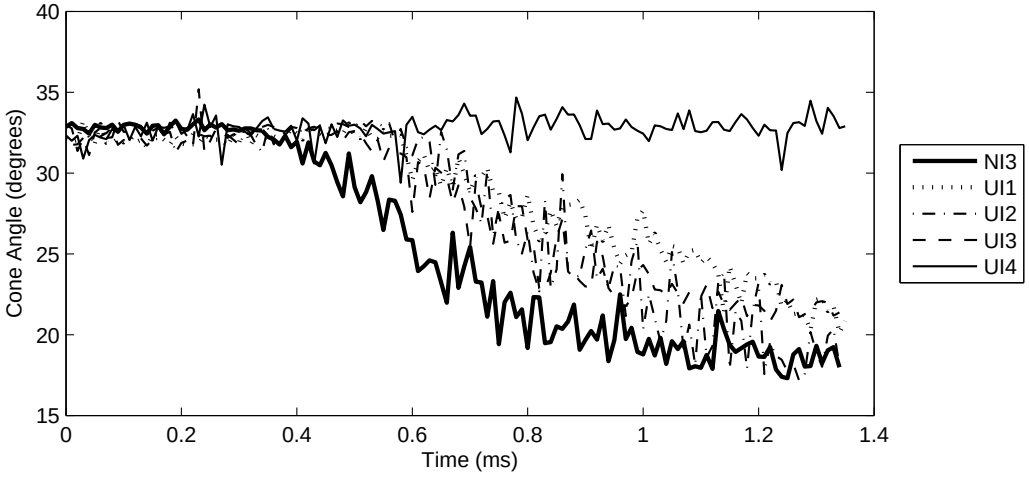

Figure A.5: Cone angle vs time at 300 bar, 1200μs duration

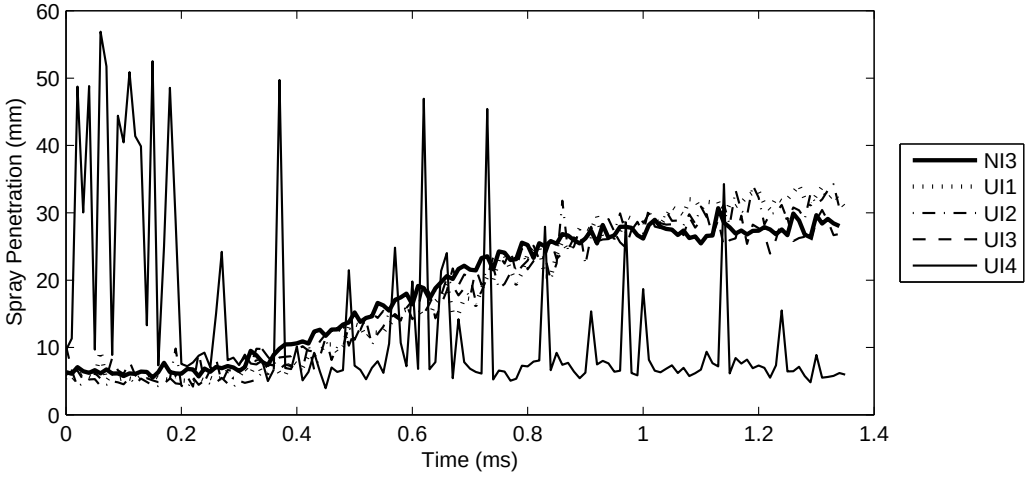

Figure A.6: Penetration vs time at 300 bar, 1200μs duration

A.2 600 bar

A.2.1 150μs Duration

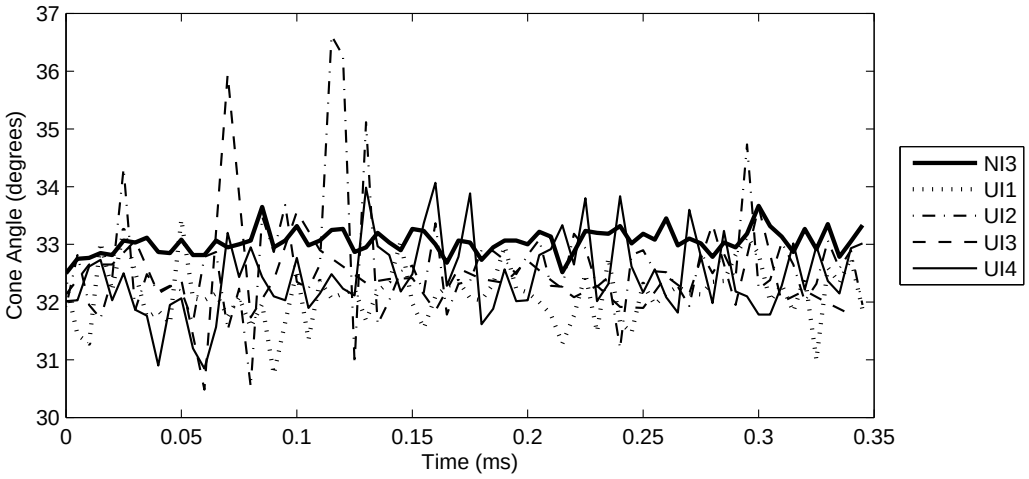

Figure A.7: Cone angle vs time at 600 bar, 150μs duration

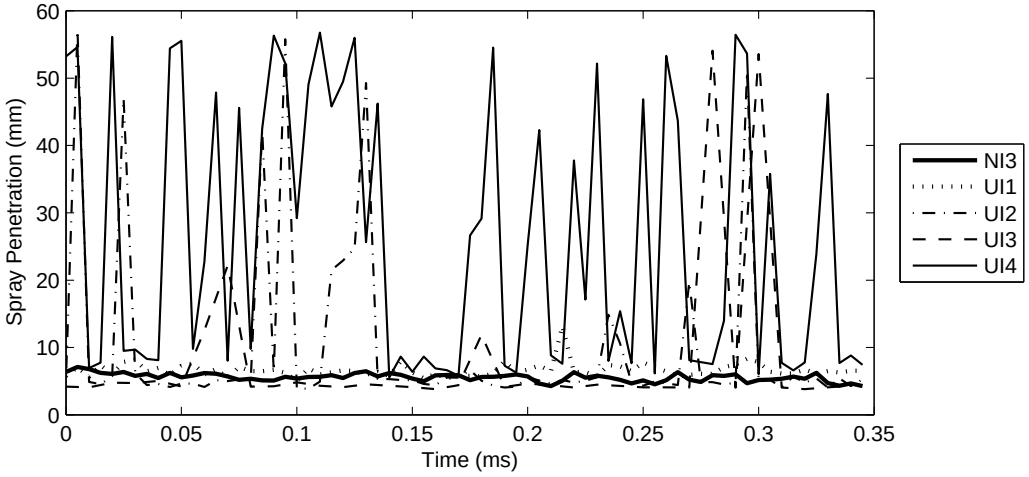

Figure A.8: Penetration vs time at 600 bar, 150μs duration

A.2.2 200μs Duration

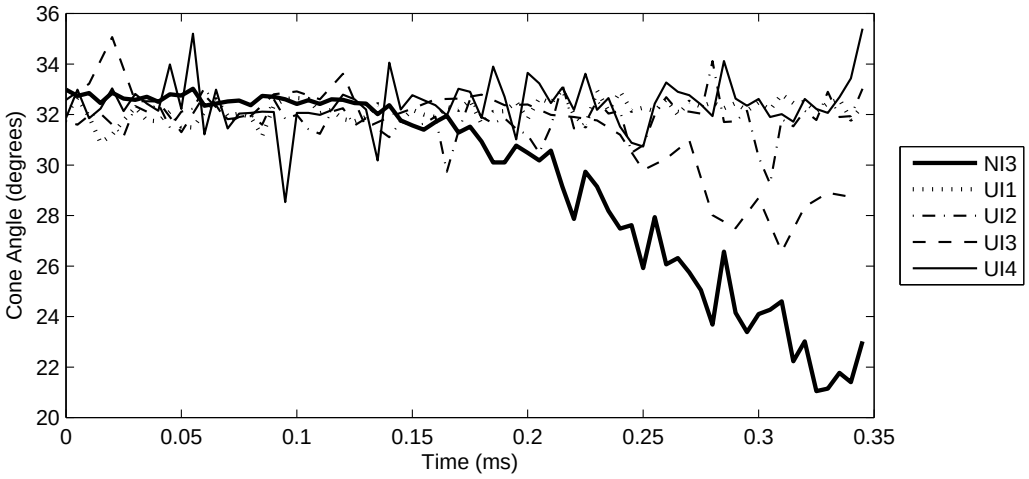

Figure A.9: Cone angle vs time at 600 bar, 200μs duration

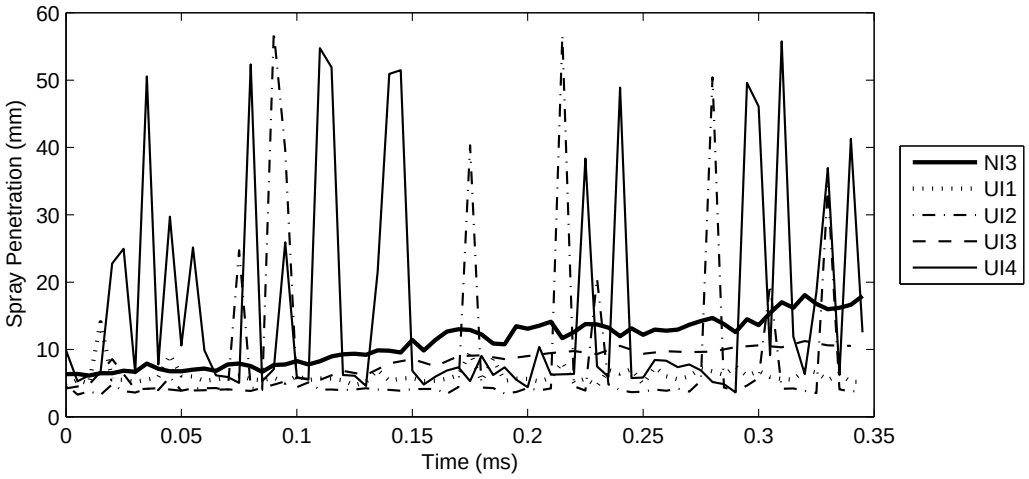

Figure A.10: Penetration vs time at 600 bar, 200μs duration

A.2.3 300μs Duration

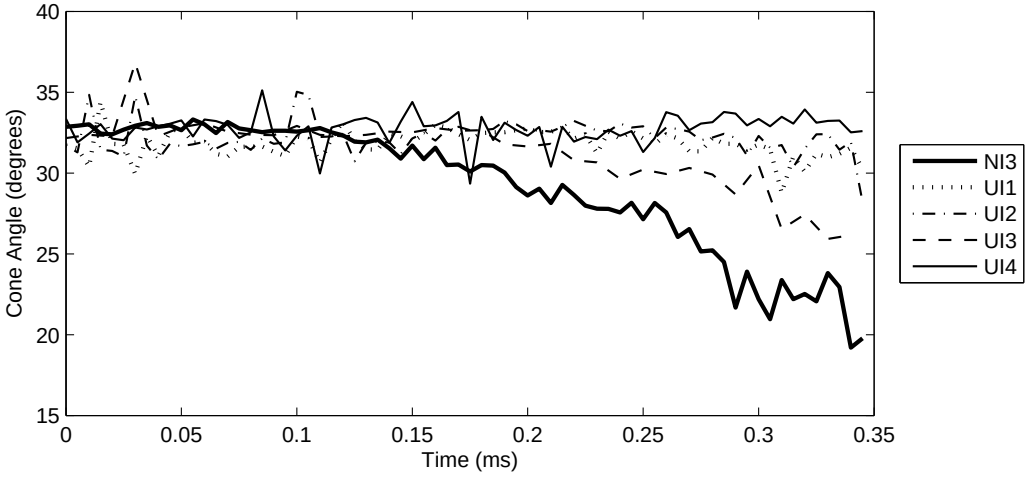

Figure A.11: Cone angle vs time at 600 bar, 300μs duration

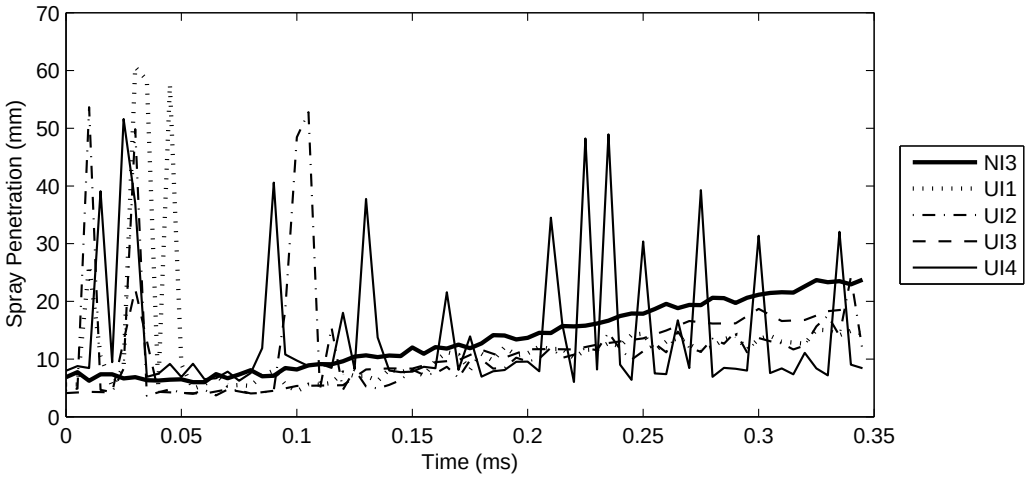

Figure A.12: Penetration vs time at 600 bar, 300μs duration

A.2.4 600μs Duration

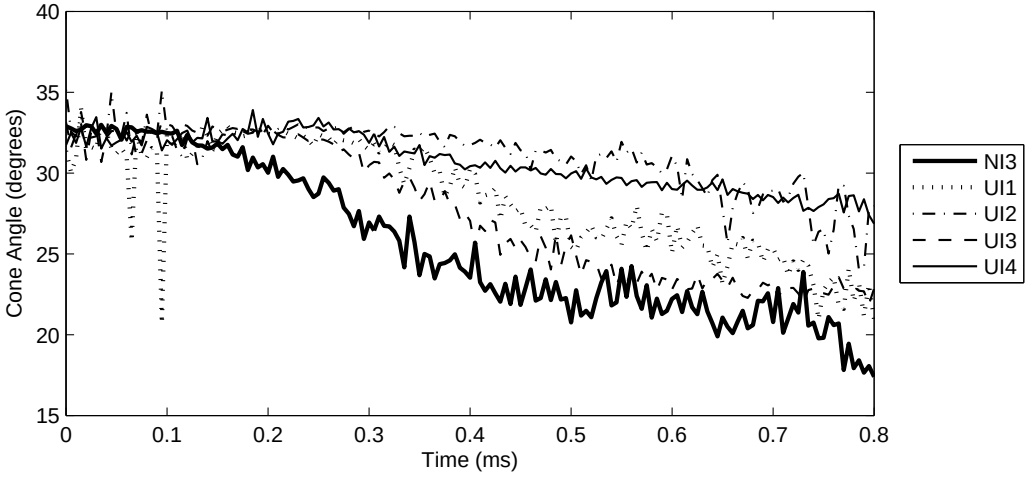

Figure A.13: Cone angle vs time at 600 bar, 600μs duration

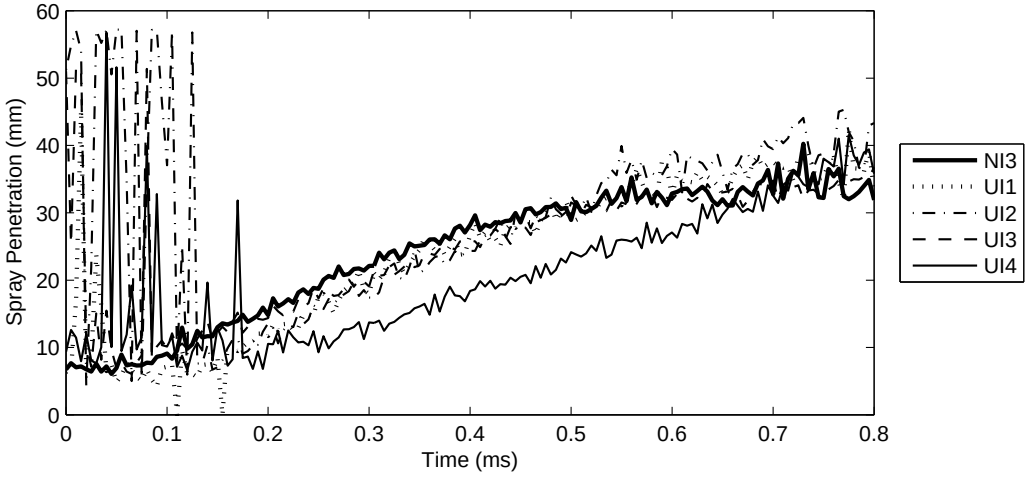

Figure A.14: Penetration vs time at 600 bar, 600μs duration

A.2.5 1200μs Duration

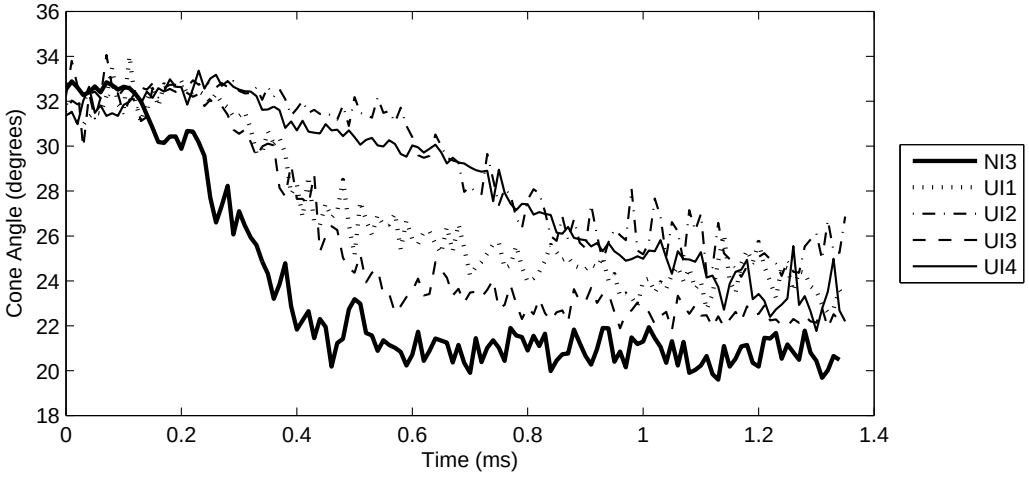

Figure A.15: Cone angle vs time at 600 bar, 1200μs duration

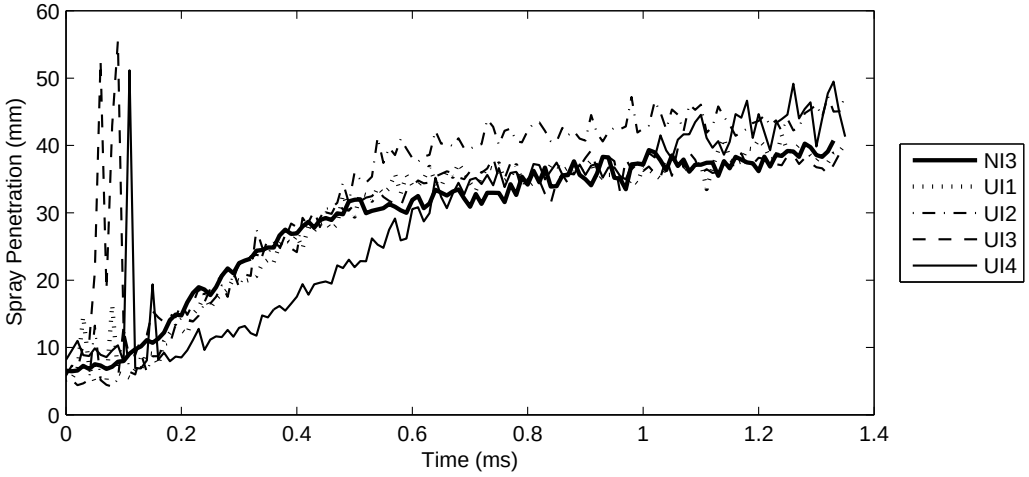

Figure A.16: Penetration vs time at 600 bar, 1200μs duration

A.3 900 bar

A.3.1 150μs Duration

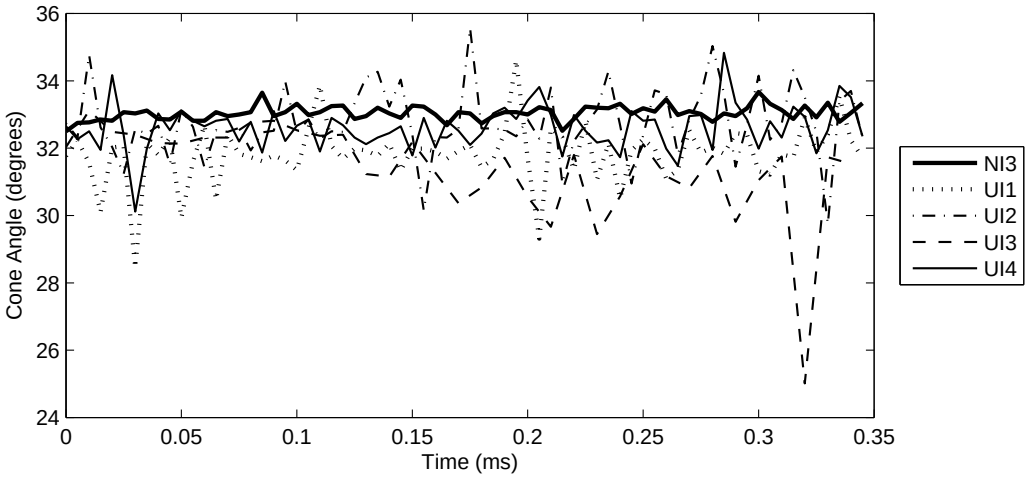

Figure A.17: Cone angle vs time at 900 bar, 150μs duration

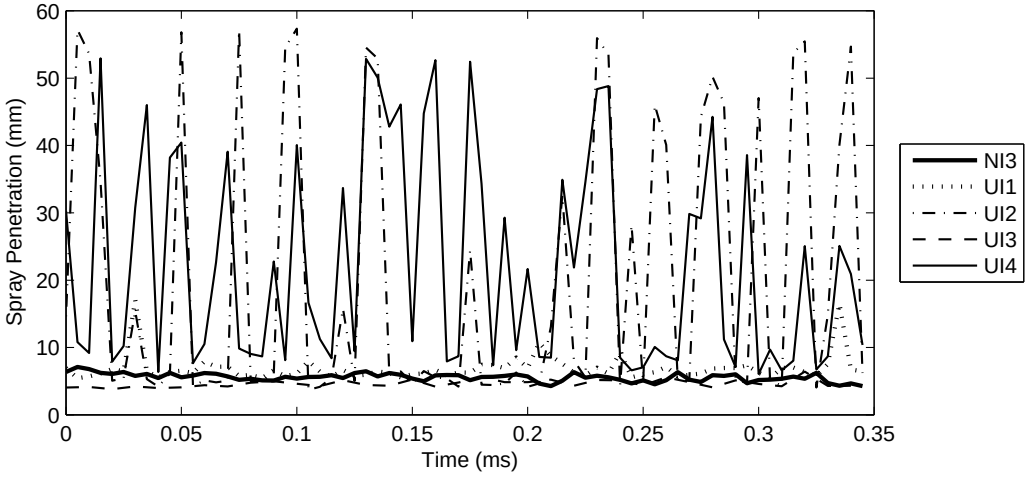

Figure A.18: Penetration vs time at 900 bar, 150μs duration

A.3.2 200μs Duration

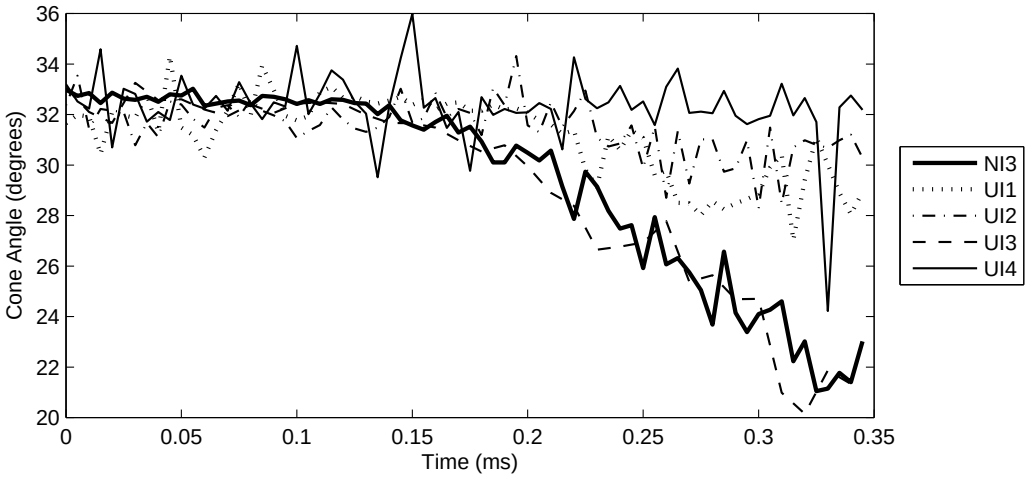

Figure A.19: Cone angle vs time at 900 bar, 200μs duration

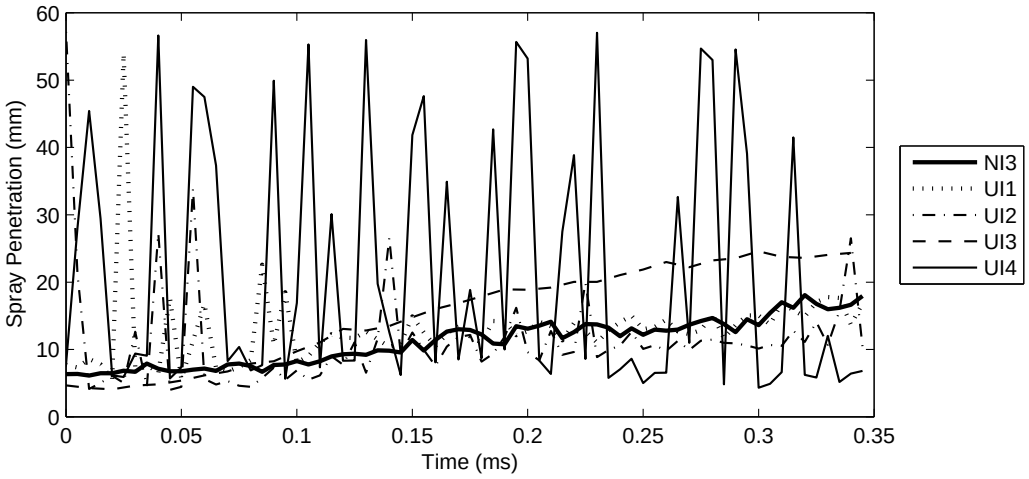

Figure A.20: Penetration vs time at 900 bar, 200μs duration

A.3.3 300μs Duration

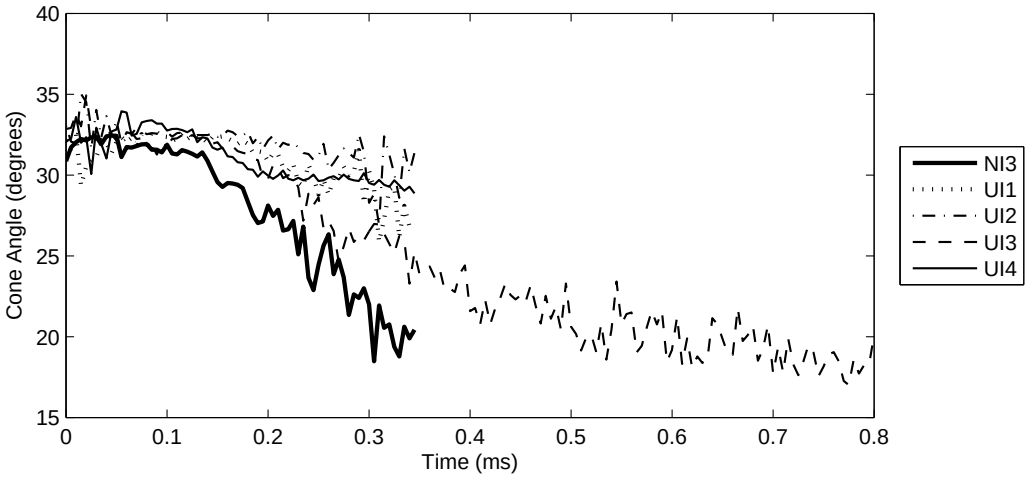

Figure A.21: Cone angle vs time at 900 bar, 300μs duration

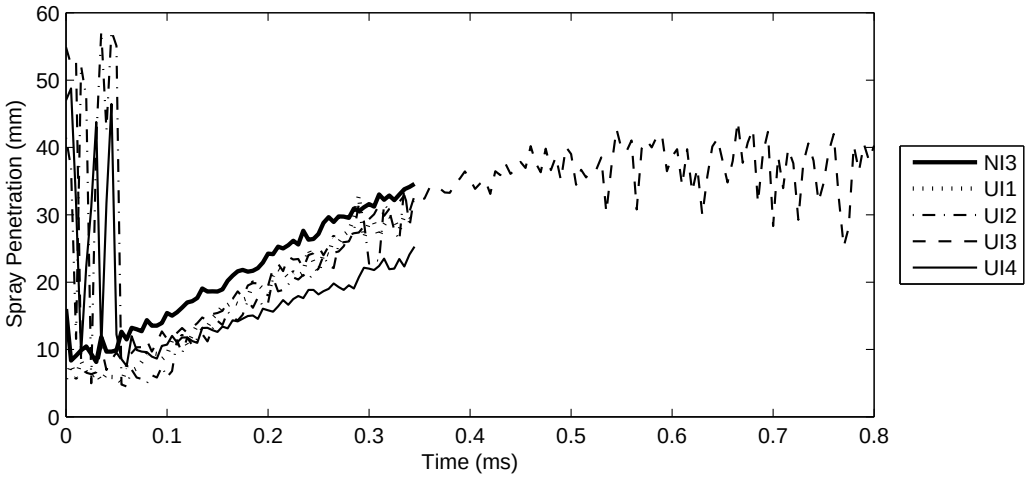

Figure A.22: Penetration vs time at 900 bar, 300μs duration

A.3.4 600μs Duration

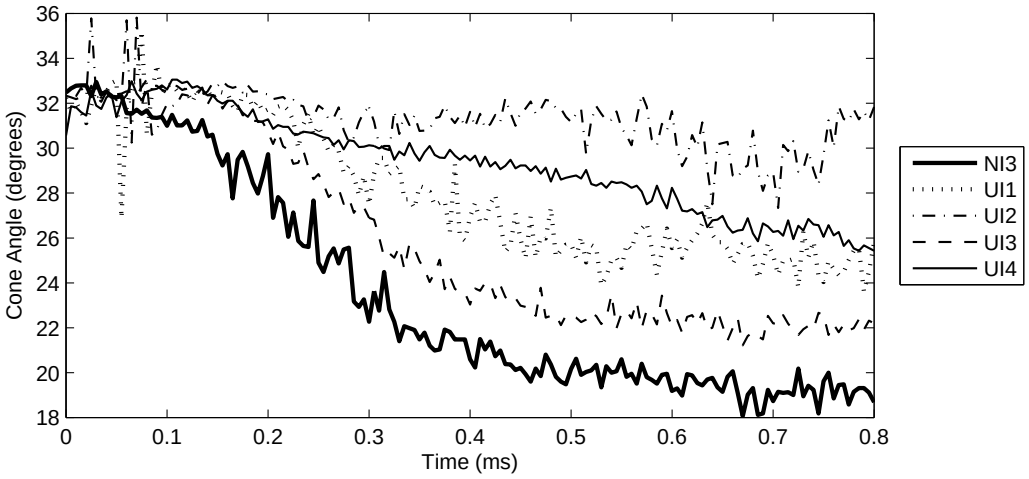

Figure A.23: Cone angle vs time at 900 bar, 600μs duration

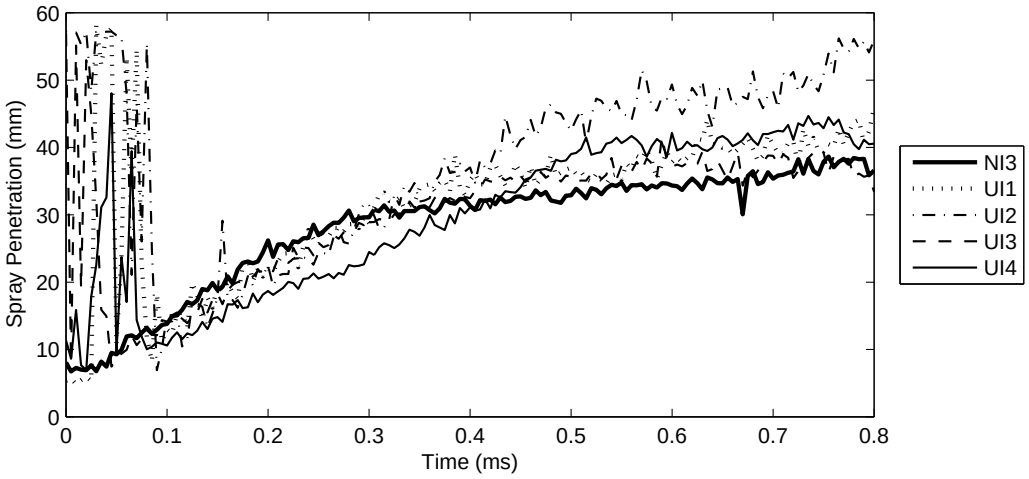

Figure A.24: Penetration vs time at 900 bar, 600μs duration

A.3.5 1200μs Duration

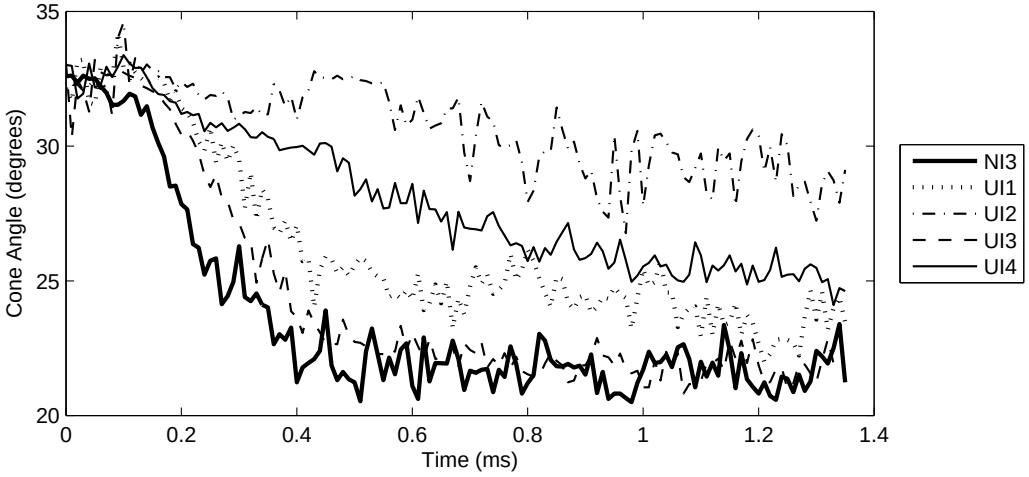

Figure A.25: Cone angle vs time at 900 bar, 1200μs duration

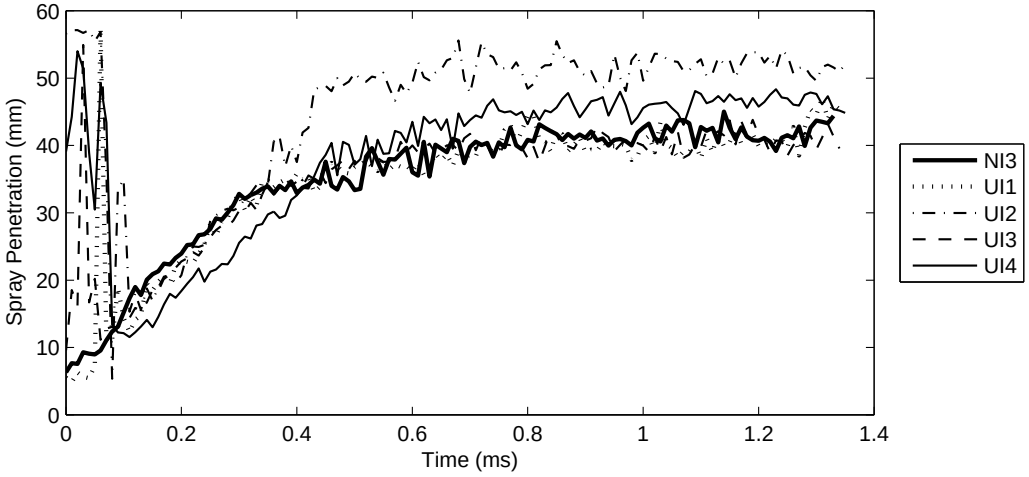

Figure A.26: Penetration vs time at 900 bar, 1200μs duration

A.4 1200 bar

A.4.1 150μs Duration

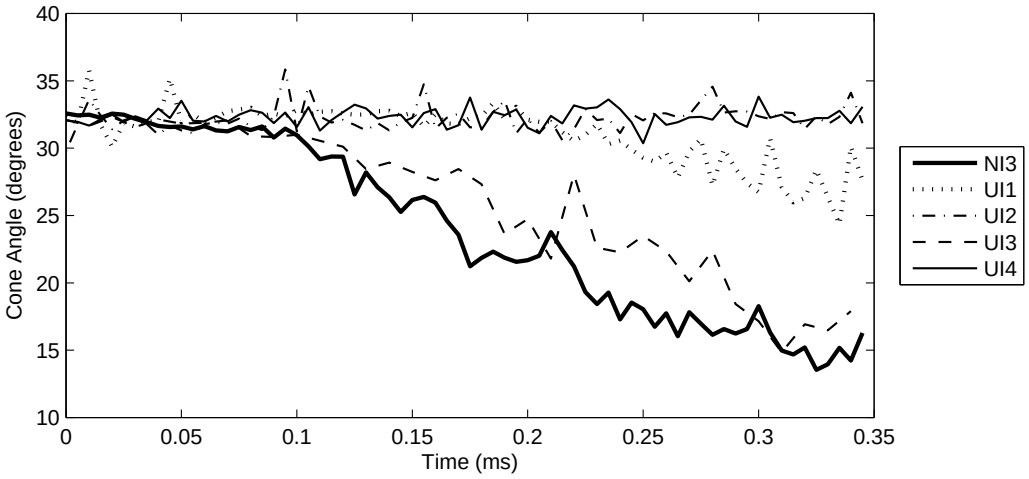

Figure A.27: Cone angle vs time at 1200 bar, 150μs duration

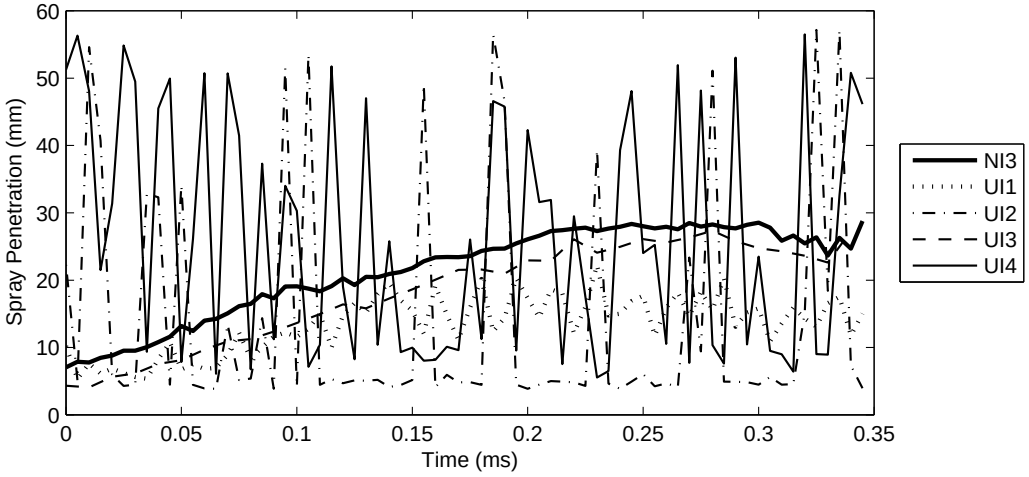

Figure A.28: Penetration vs time at 1200 bar, 150μs duration

A.4.2 200μs Duration

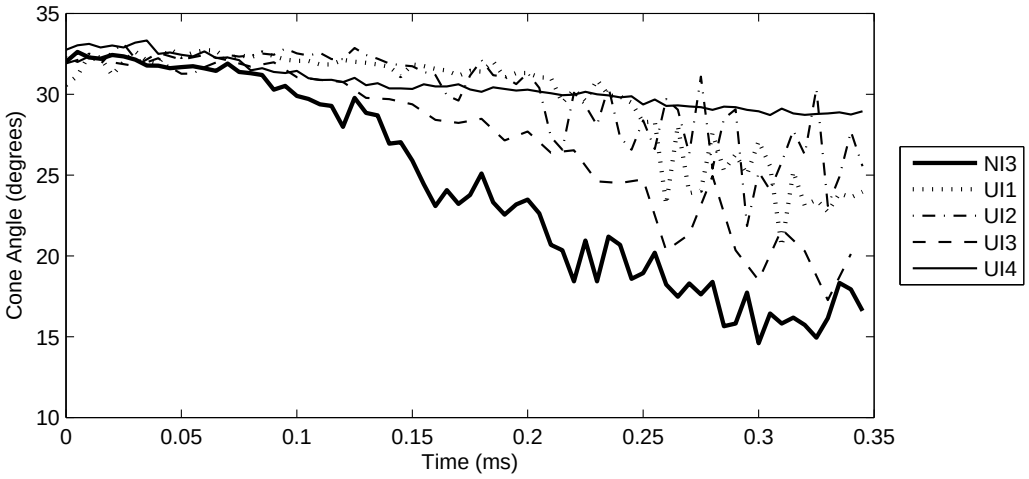

Figure A.29: Cone angle vs time at 1200 bar, 200μs duration

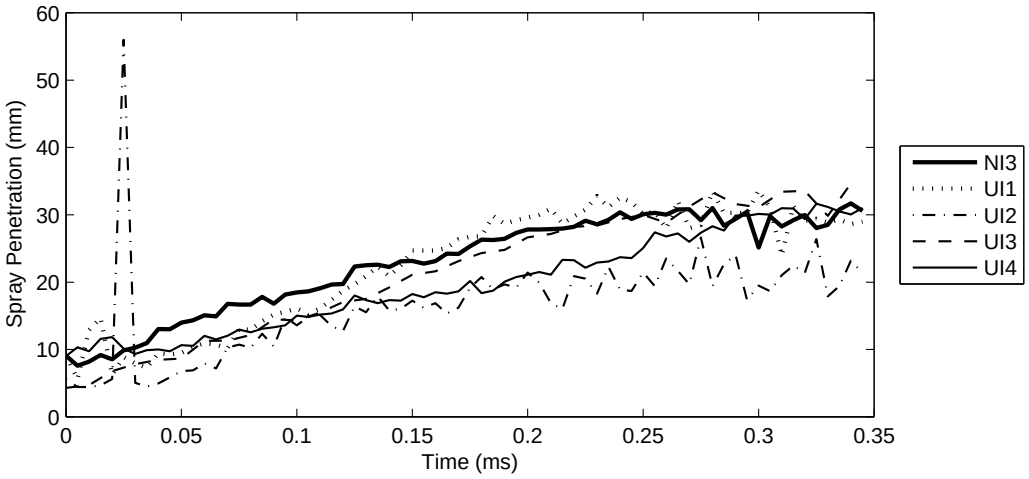

Figure A.30: Penetration vs time at 1200 bar, 200μs duration

A.4.3 300μs Duration

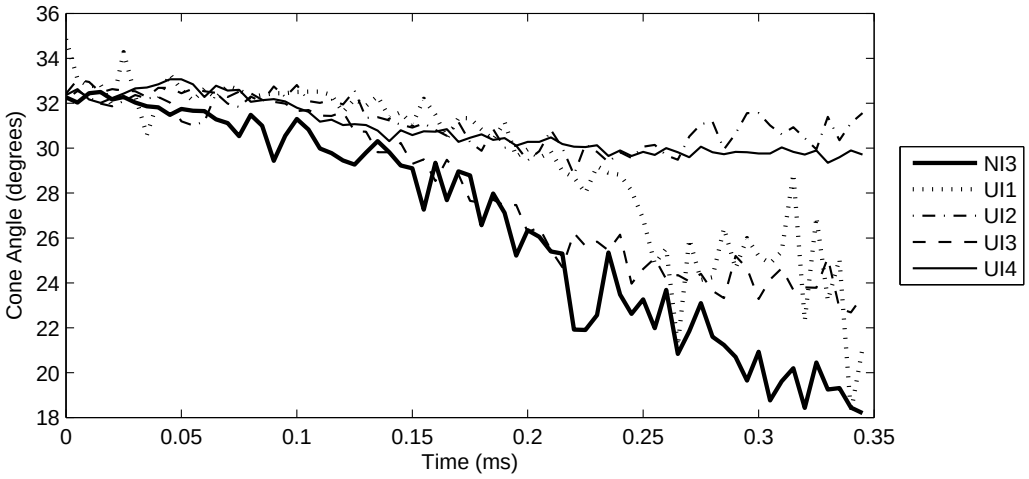

Figure A.31: Cone angle vs time at 1200 bar, 300μs duration

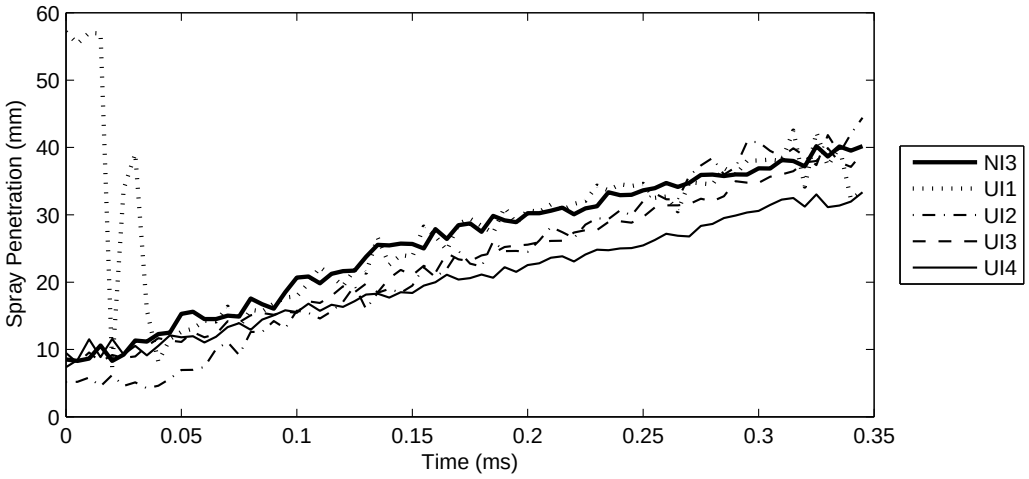

Figure A.32: Penetration vs time at 1200 bar, 300μs duration

A.4.4 600μs Duration

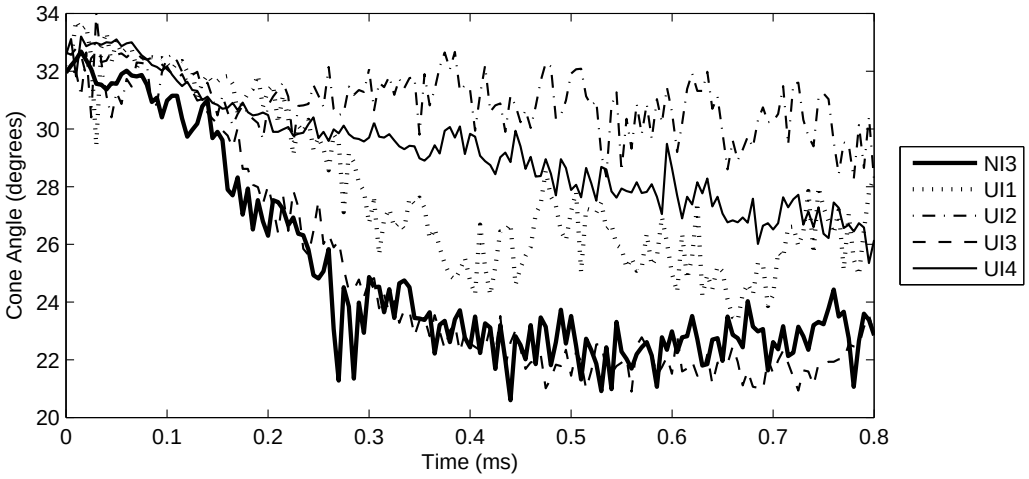

Figure A.33: Cone angle vs time at 1200 bar, 600μs duration

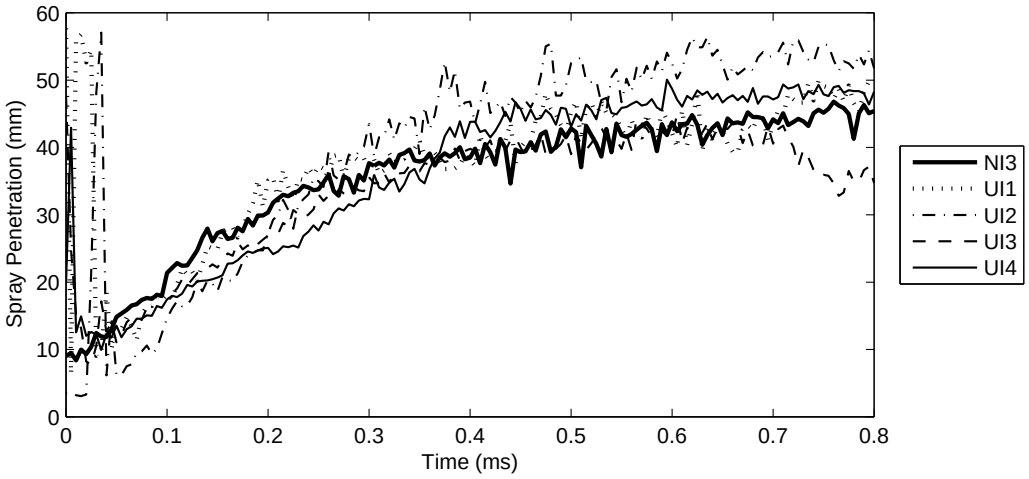

Figure A.34: Penetration vs time at 1200 bar, 600μs duration

A.4.5 1200μs Duration

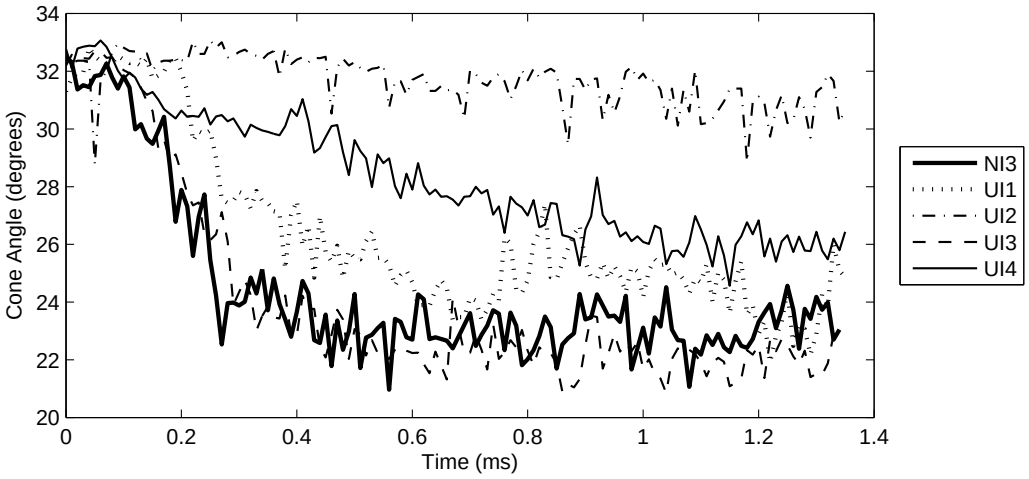

Figure A.35: Cone angle vs time at 1200 bar, 1200μs duration

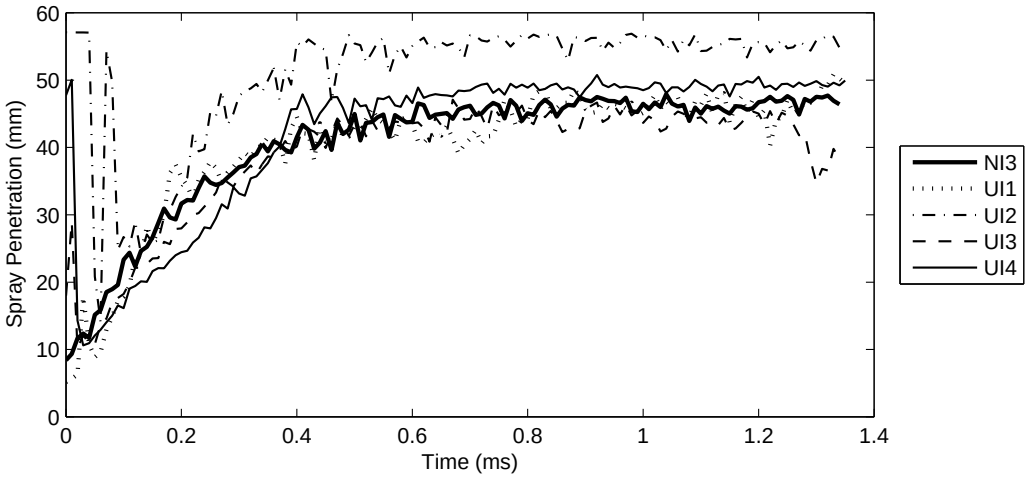

Figure A.36: Penetration vs time at 1200 bar, 1200μs duration

A.5 1400 bar

A.5.1 150μs Duration

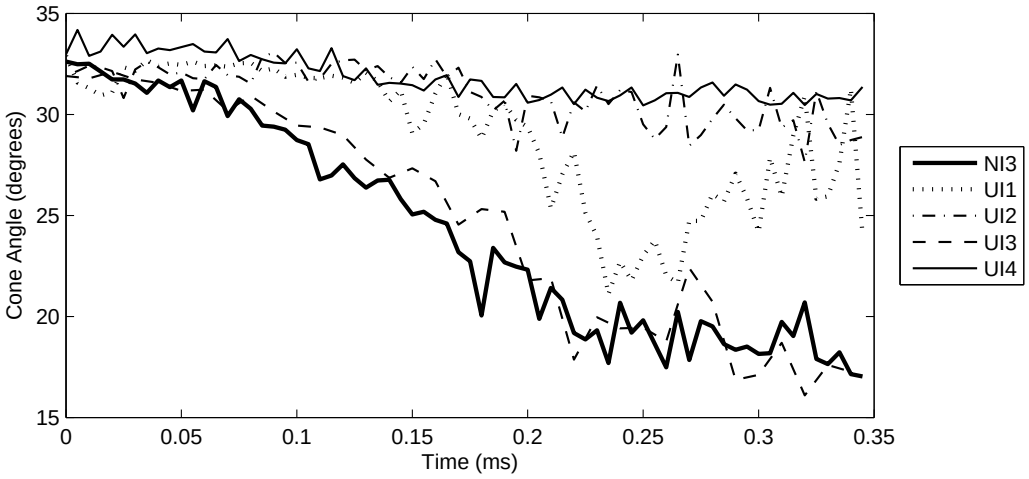

Figure A.37: Cone angle vs time at 1400 bar, 150μs duration

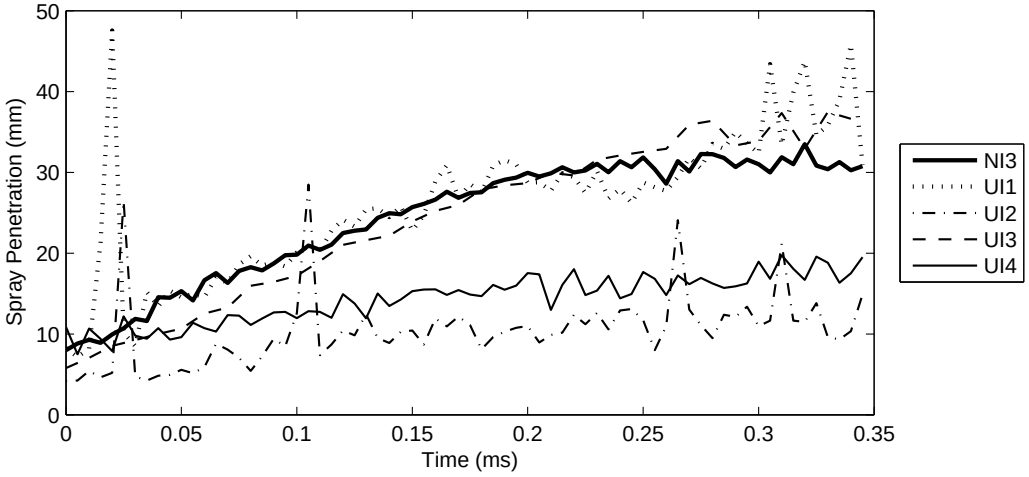

Figure A.38: Penetration vs time at 1400 bar, 150μs duration

A.5.2 200μs Duration

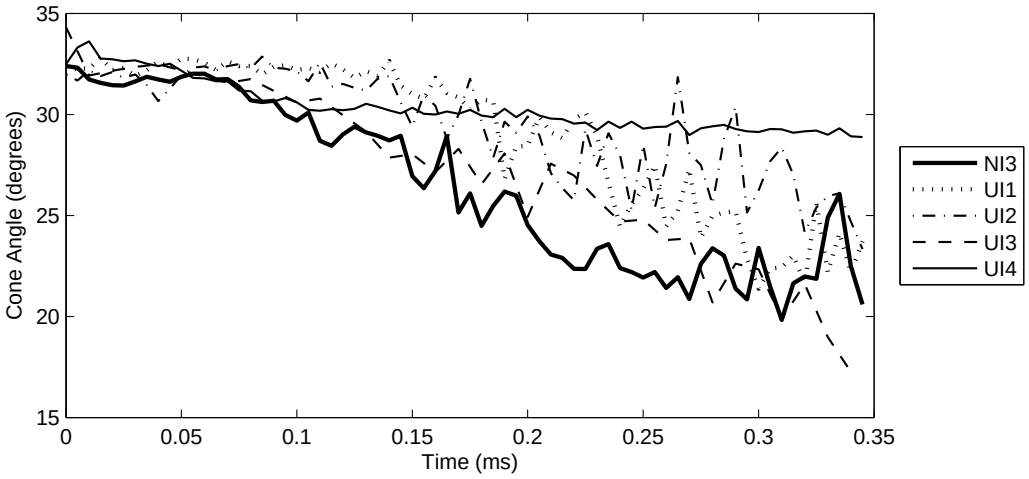

Figure A.39: Cone angle vs time at 1400 bar, 200μs duration

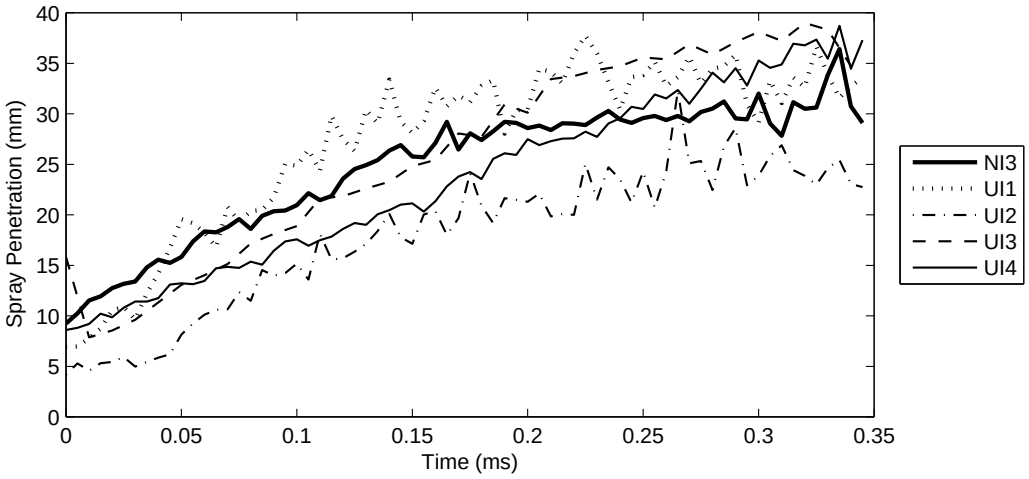

Figure A.40: Penetration vs time at 1400 bar, 200μs duration

A.5.3 300μs Duration

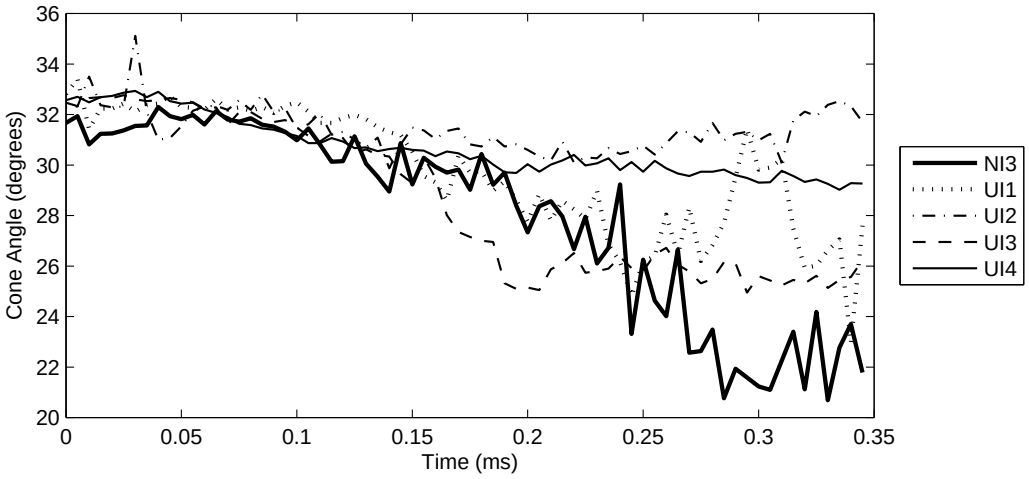

Figure A.41: Cone angle vs time at 1400 bar, 300μs duration

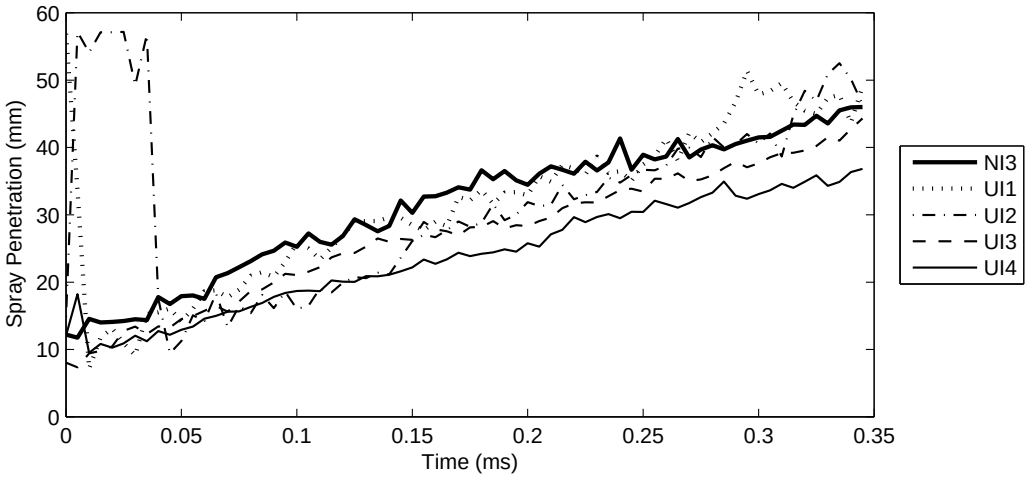

Figure A.42: Penetration vs time at 1400 bar, 300μs duration

A.5.4 600μs Duration

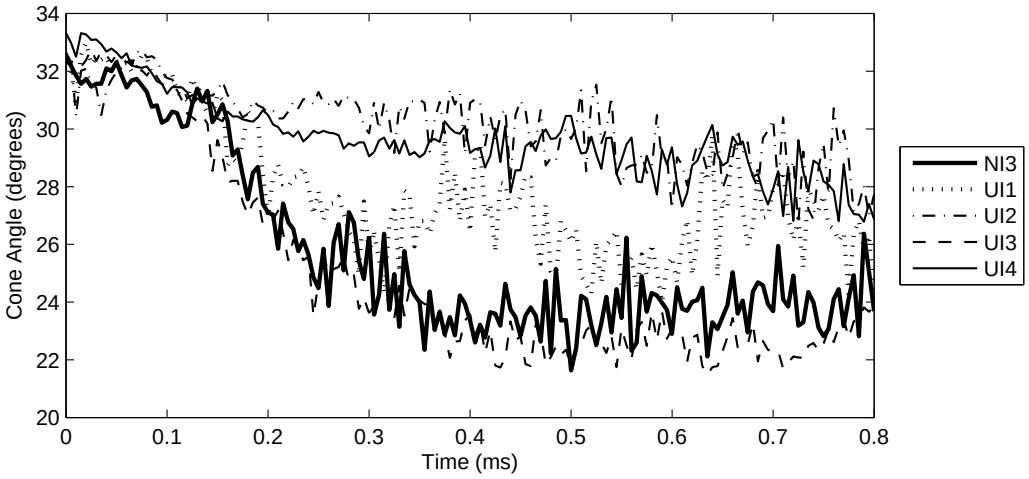

Figure A.43: Cone angle vs time at 1400 bar, 600μs duration

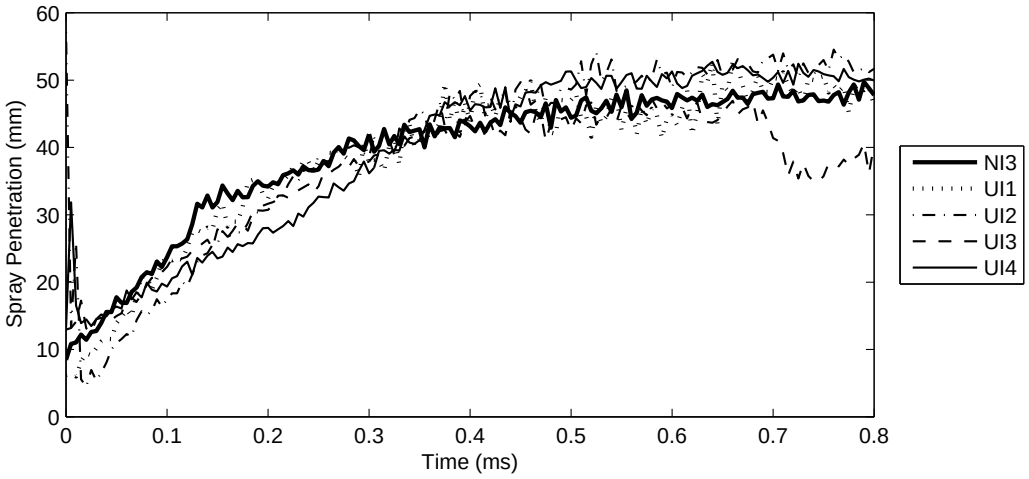

Figure A.44: Penetration vs time at 1400 bar, 600μs duration

A.5.5 1200μs Duration

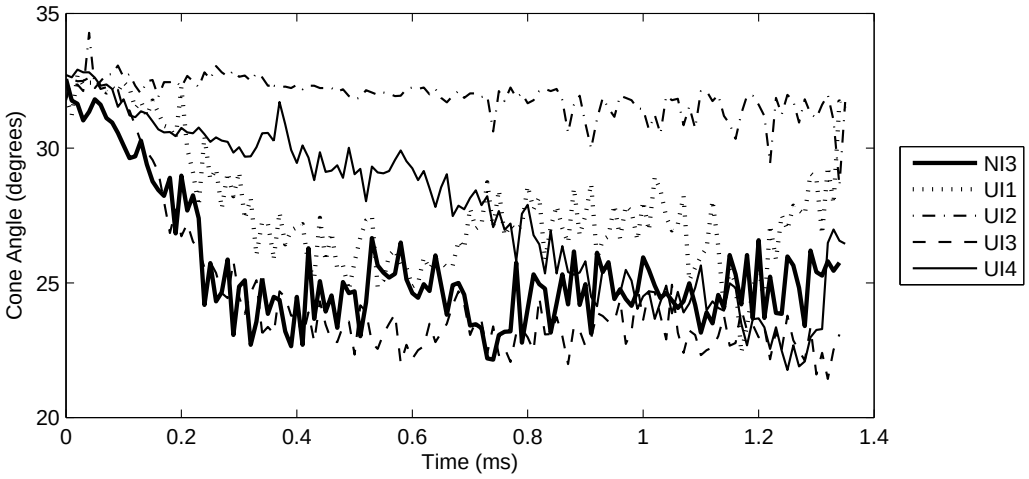

Figure A.45: Cone angle vs time at 1400 bar, 1200μs duration

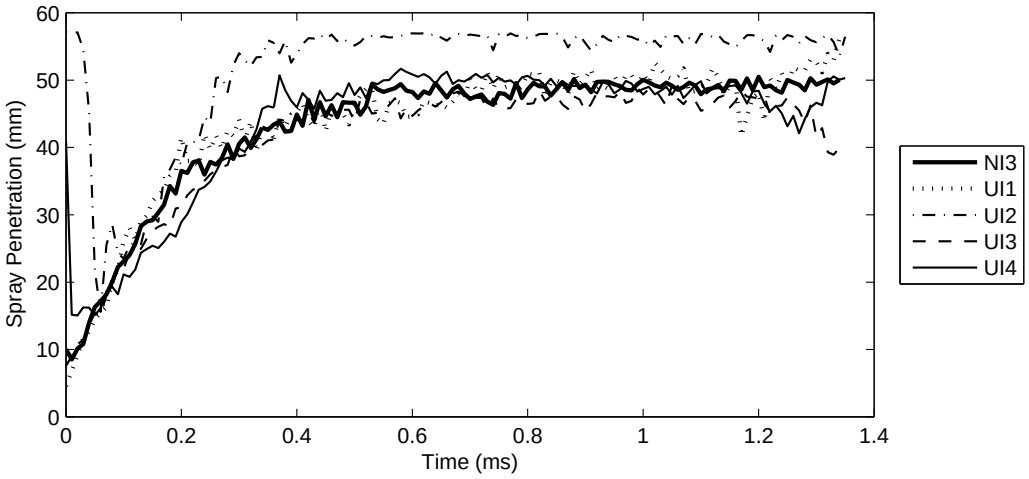

Figure A.46: Penetration vs time at 1400 bar, 1200μs duration

Appendix B

Sample Calculations

B.1 Introduction

In Chapter 7 an analysis was conducted where two principal spray penetration theories, according to Dent and Hiroyasu, were compared to the actual results obtained during testing. During this analysis a series of correction factors, 'k', were developed for the purposes of aligning the theoretical and actual results. The calculations used in determining the theoretical spray penetrations are shown here for demonstrative purposes.

B.2 Paramenter Values

The following values were used for the parameters, in the equations:

ΔP : Differential pressure across the injector, between the common rail and atmosphere

ρ_g : Density of the medium into which injection is taking place (0.985kg/m^3)

ρ_ℓ : Density of fluid being injected (807kg/m^3)

T_g : Temperature of gas into which injection is taking place (294K)

d_n : Diameter of injector nozzle orifice (0.173mm)

B.3 Dent Spray Theory

The equation representing the unmodified spray penetration theory according to Dent is repeated here for the sake of clarity, where the values of the variables listed are as detailed above in Section B.2.

$$S(t) = 3,07 \left(\frac{\Delta P}{\rho_g}\right)^{\frac{1}{4}} (td_n)^{\frac{1}{2}} \left(\frac{294}{T_g}\right)^{\frac{1}{4}} \tag{B.1}$$

For the purposes of a sample calculation a pressure and time after commencement of injection need to be assumed. For the sake of demonstration a 300bar injection, 600mus after the commencement of injection will be used.

$$\begin{aligned} S(t) &= 3,07 \left(\frac{\Delta P}{\rho_g}\right)^{\frac{1}{4}} (td_n)^{\frac{1}{2}} \left(\frac{294}{T_g}\right)^{\frac{1}{4}} \\ S(600\mu s) &= 3,07 \left(\frac{(300-0.985)\times 10^5}{0.985}\right)^{\frac{1}{4}} \left((600\times 10^{-6})(173\times 10^{-6})\right)^{\frac{1}{2}} \left(\frac{294}{294}\right)^{\frac{1}{4}} \\ S(600\mu s) &= 3,07 \left(30.45\times 10^6\right)^{\frac{1}{4}} \left(103.80\times 10^{-9}\right)^{\frac{1}{2}} (1)^{\frac{1}{4}} \\ S(600\mu s) &= 73.14mm \end{aligned}$$

B.4 Hiroyasu Spray Theory

The equations representing the spray theory according to Hiroyasu is presented below:

$$t < t_{break}: \qquad S(t) = 0.39\left(\frac{2\Delta P}{\rho_l}\right)^{\frac{1}{2}} t \tag{B.2}$$

$$t > t_{break}: \qquad S(t) = 2.95\left(\frac{\Delta P}{\rho_g}\right)^{\frac{1}{4}} (d_n t)^{\frac{1}{2}} \tag{B.3}$$

where:

$$t_{break} = \frac{29\rho_l d_n}{(\rho_g \Delta P)^{\frac{1}{2}}} \tag{B.4}$$

For the sake of sample calculations, a pressure of 1400 bar will be assumed.

Beginning with the determination of t_{break}:

$$\begin{aligned}
t_{break} &= \frac{29\rho_l d_n}{(\rho_g \Delta P)^{\frac{1}{2}}} \\
t_{break} &= \frac{29(807)(0.173 \times 10^{-3})}{((0.985)(1400 - 0.985) \times 10^5)^{\frac{1}{2}}} \\
t_{break} &= \frac{4.0487}{11.74 \times 10^3} \\
t_{break} &= 344.98 \times 10^{-6} s \\
t_{break} &= 344.98 \mu s
\end{aligned}$$

Sample calculations are required to be done both before and after t_{break}. Time after injection of 200μs and 400μs will be used.

At 200μs:

$$\begin{aligned}
S(t) &= 0.39\left(\frac{2\Delta P}{\rho_l}\right)^{\frac{1}{2}} t \\
S(200\mu s) &= 0.39\left(\frac{2(1400 - 0.833) \times 10^5}{807}\right)^{\frac{1}{2}} (200 \times 10^{-6})
\end{aligned}$$

$$S(200\mu s) = 32.48 \times 10^{-3}$$

$$S(200\mu s) = 32.48mm$$

At 400μs:

$$S(t) = 2.95\left(\frac{\Delta P}{\rho_g}\right)^{\frac{1}{4}}(d_n t)^{\frac{1}{2}}$$

$$S(400\mu s) = 2.95\left(\frac{(1400 - 0.833) \times 10^5}{0.945}\right)^{\frac{1}{4}}\left((0.173 \times 10^{-3})(400 \times 10^{-6})\right)^{\frac{1}{2}}$$

$$S(400\mu s) = 2.95(110.205)(263.0589)$$

$$S(400\mu s) = 85.6mm$$

B.5 Correlation Factor Equations

In Sections 7.5 and 7.6 equations for the variation of the correlation factors for the spray theory according to Dent and Hiroyasu were presented. The sample calculations illustrating the workings of these equations are presented here.

B.5.1 Dent Theory Correction Factor

The correction factor equation for the spray theory according to Dent is presented below.

$$k = 0.0002 \cdot Pressure + 0.2596 \tag{B.5}$$

Assuming a pressure of 1400bar:

$$k = 0.0002 \cdot Pressure + 0.2596$$

$$k = 0.0002 \cdot (1400) + 0.2596$$

$$k = 0.540$$

If the results of the sample calculation above is compared with the results shown in Table 7.2.2, it may be seen that they compare favourably, within 2%.

B.5.2 Hiroyasu Theory Correction Factor

The correction factor equation for the spray theory according to Hiroyasu is presented below.

$$k = -7.0439 \times 10^{-10} \cdot P^3 + 1.8566 \times 10^{-6} \cdot P^2 - 0.0012325 \cdot P + 0.57213 \quad \text{(B.6)}$$

$$k = -7.0439 \times 10^{-10} \cdot (1400)^3 + 1.8566 \times 10^{-6} \cdot ()1400^2 - 0.0012325 \cdot (1400) + 0.57213$$

$$k = -7.0439 \times 10^{-10} \cdot (1400)^3 + 1.8566 \times 10^{-6} \cdot ()1400^2 - 0.0012325 \cdot (1400) + 0.57213$$

$$k = 0.553$$

Again, if the results of the above sample calculation are compared with the values of the correction factors shown in Table 7.2.2, a correlation of 5% may be seen.

Appendix C

Complete Flow Observations

C.1 Delivery rate vs time Plots

C.1.1 300 bar Results

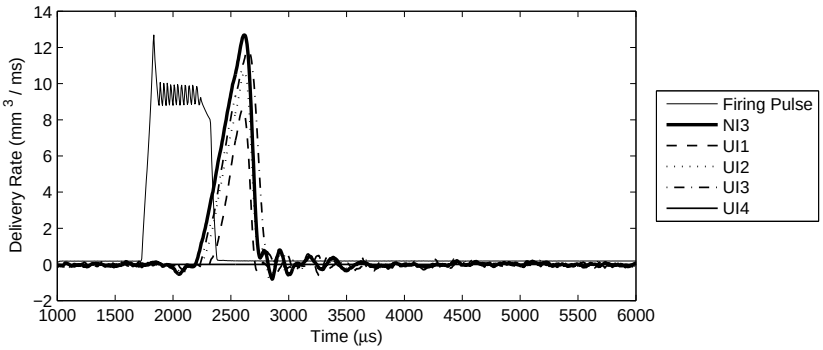

Figure C.1: Delivery rate vs timevs time at 300 bar, 600μs duration

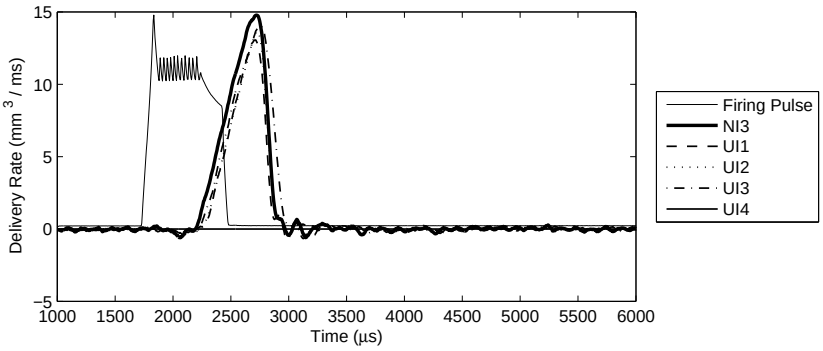

Figure C.2: Delivery rate vs time at 300 bar, 700μs duration

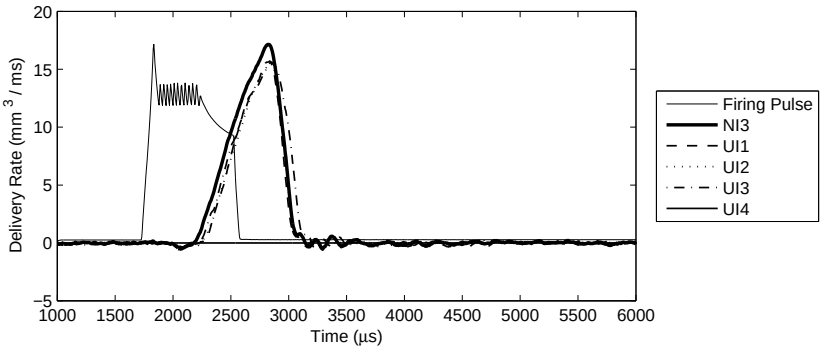

Figure C.3: Delivery rate vs time at 300 bar, 800μs duration

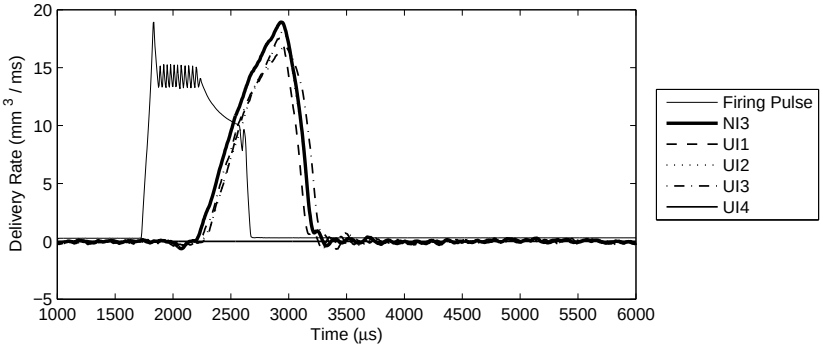

Figure C.4: Delivery rate vs time at 300 bar, 900μs duration

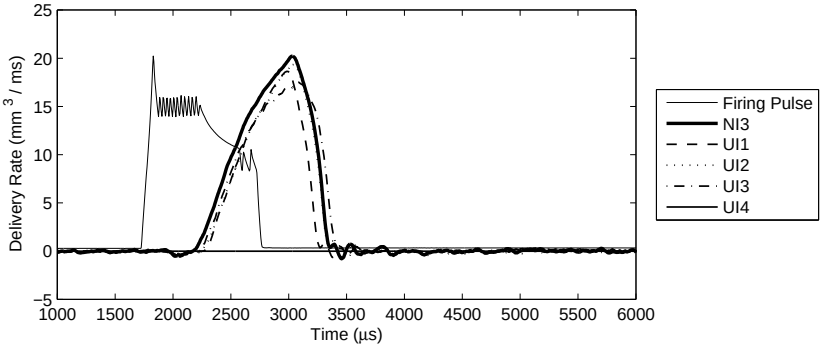

Figure C.5: Delivery rate vs time at 300 bar, 1000μs duration

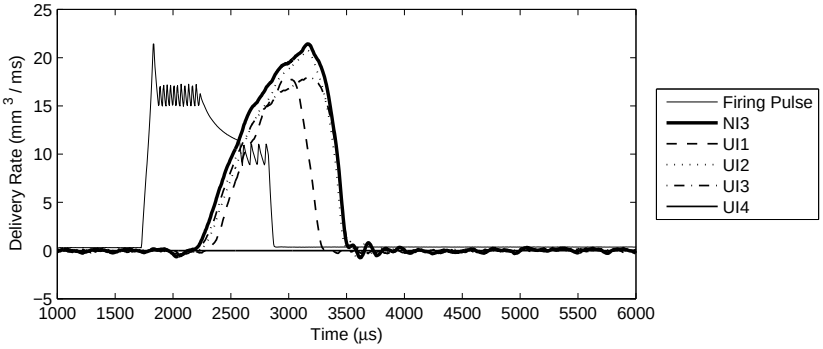

Figure C.6: Delivery rate vs time at 300 bar, 1100μs duration

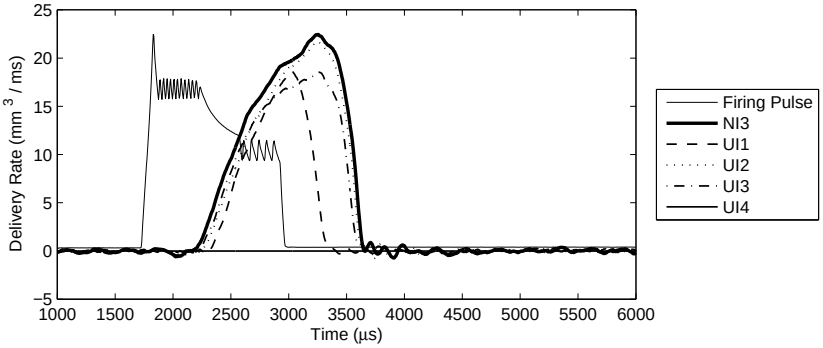

Figure C.7: Delivery rate vs time at 300 bar, 1200μs duration

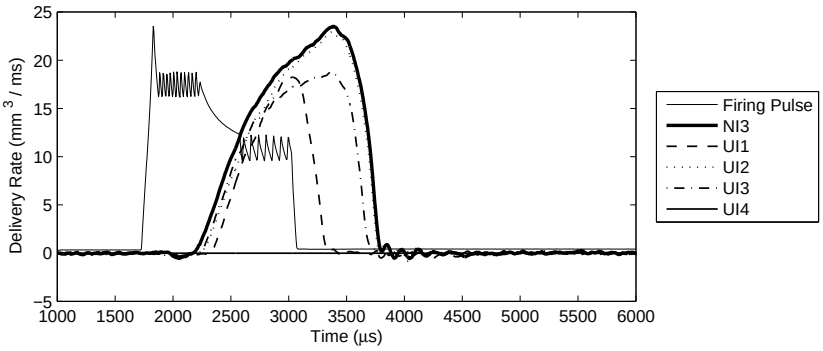

Figure C.8: Delivery rate vs time at 300 bar, 1300μs duration

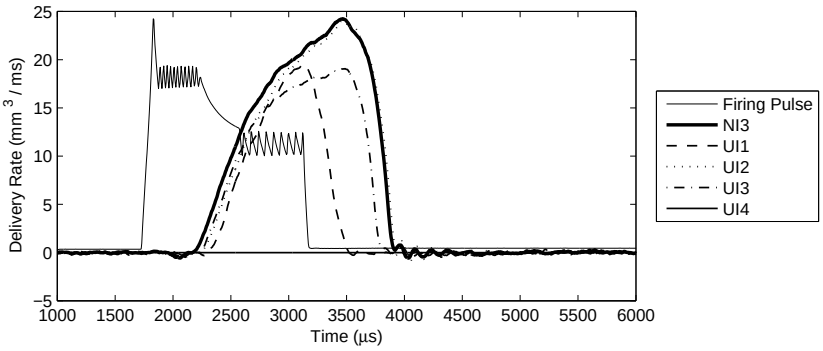

Figure C.9: Delivery rate vs time at 300 bar, 1400μs duration

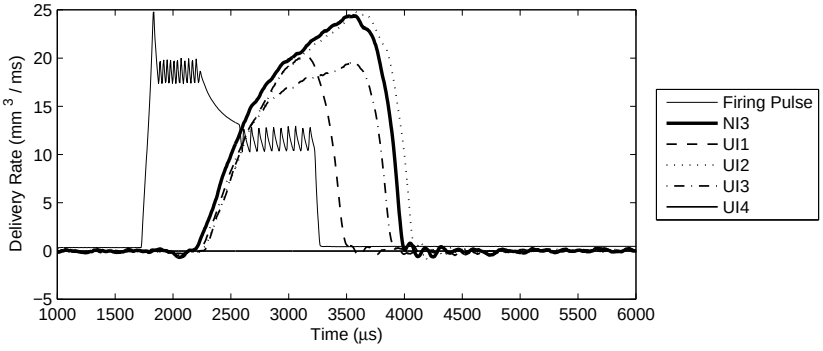

Figure C.10: Delivery rate vs time at 300 bar, 1500μs duration

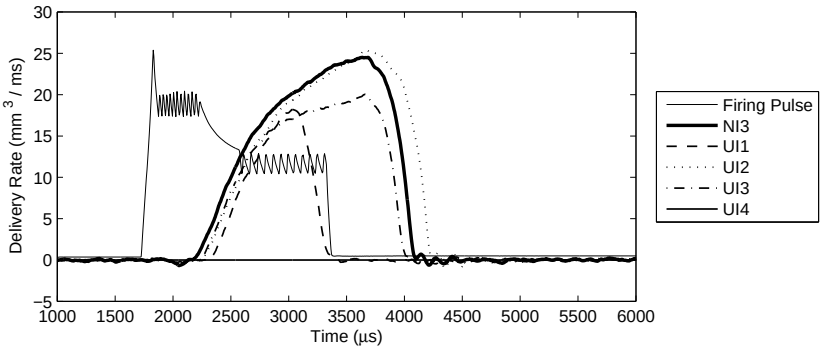

Figure C.11: Delivery rate vs time at 300 bar, 1600μs duration

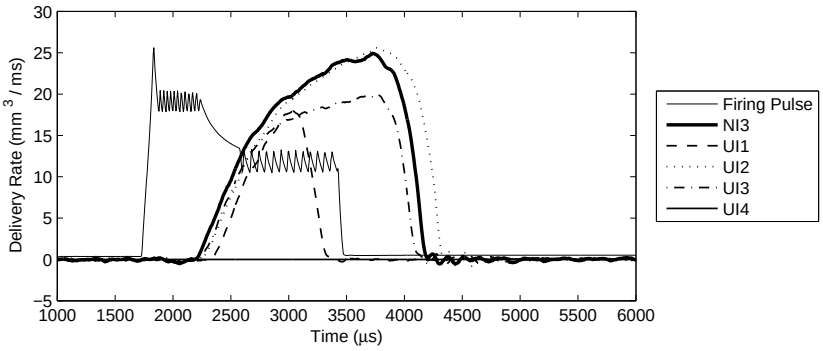

Figure C.12: Delivery rate vs time at 300 bar, 1700μs duration

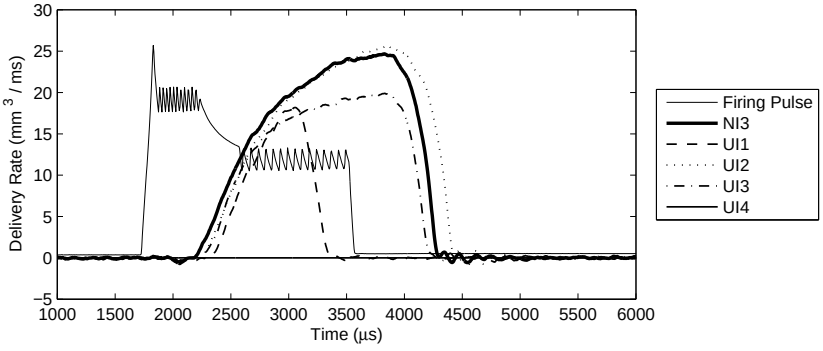

Figure C.13: Delivery rate vs time at 300 bar, 1800μs duration

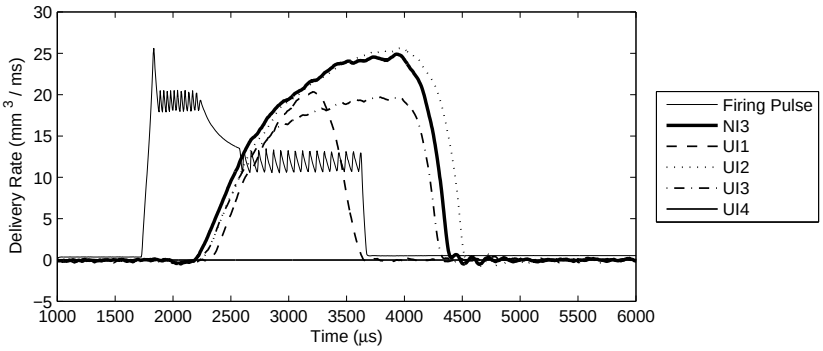

Figure C.14: Delivery rate vs time at 300 bar, 1900μs duration

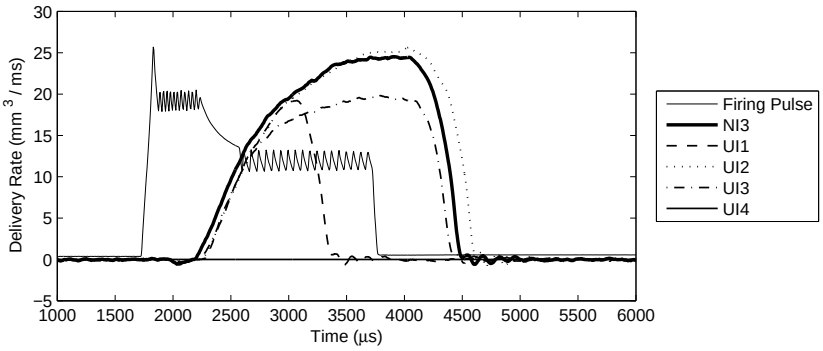

Figure C.15: Injector Delivery rate vs time at 300 bar, 2000μs duration

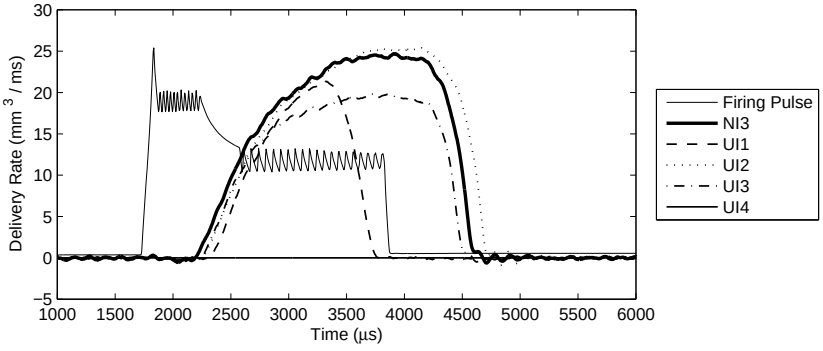

Figure C.16: Delivery rate vs time at 300 bar, 2100μs duration

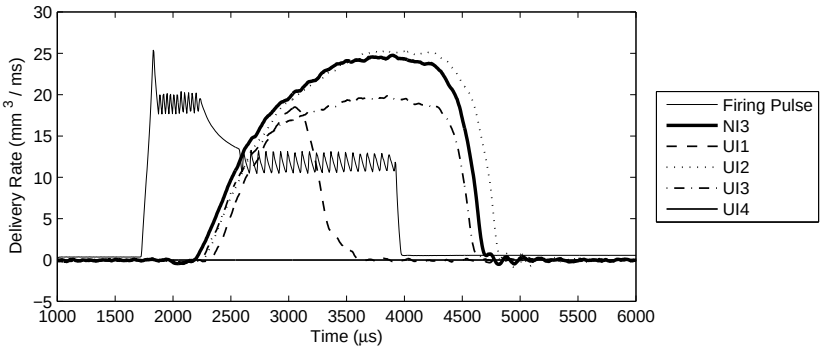

Figure C.17: Delivery rate vs time at 300 bar, 2200μs duration

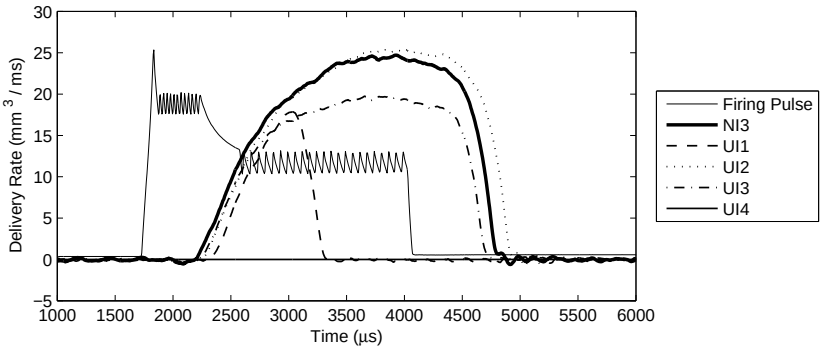

Figure C.18: Delivery rate vs time at 300 bar, 2300μs duration

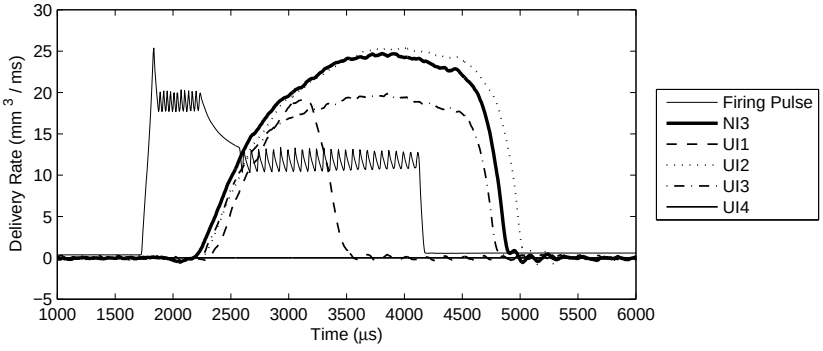

Figure C.19: Delivery rate vs time at 300 bar, 2400μs duration

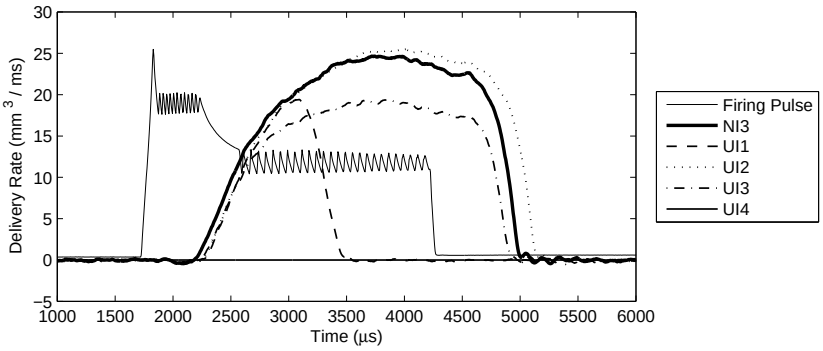

Figure C.20: Delivery rate vs time at 300 bar, 2500μs duration

C.1.2 600 bar Results

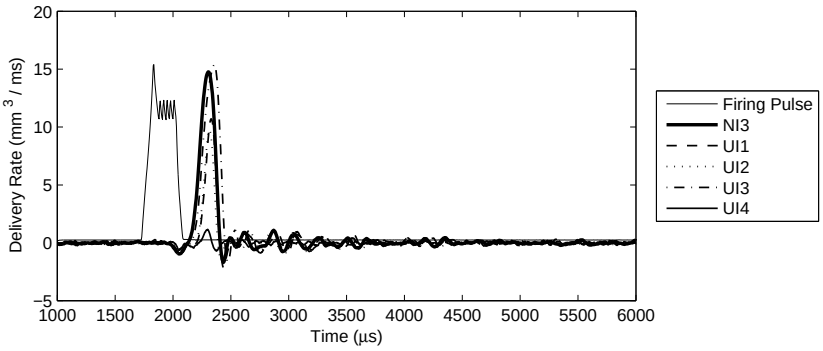

Figure C.21: Delivery rate vs time at 600 bar, 300μs duration

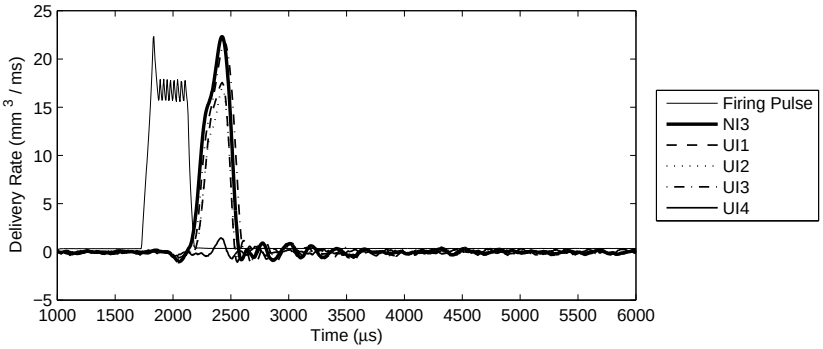

Figure C.22: Delivery rate vs time at 600 bar, 400μs duration

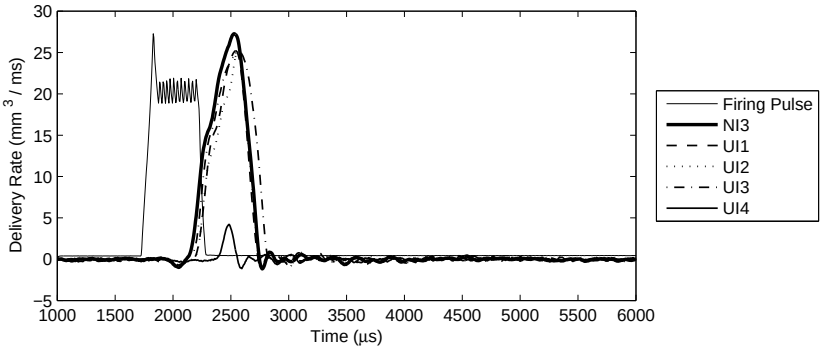

Figure C.23: Delivery rate vs time at 600 bar, 500μs duration

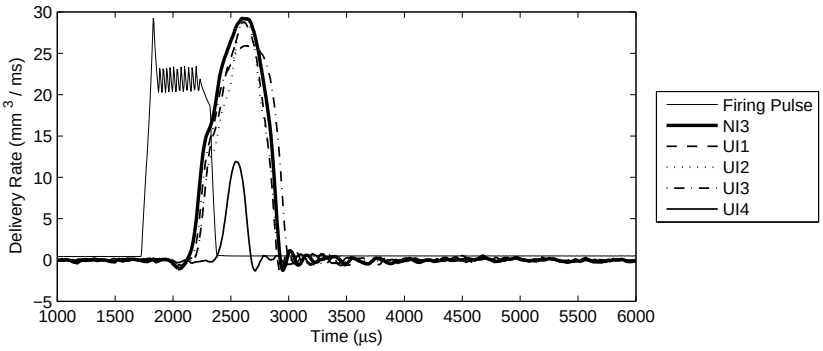

Figure C.24: Delivery rate vs time at 600 bar, 600μs duration

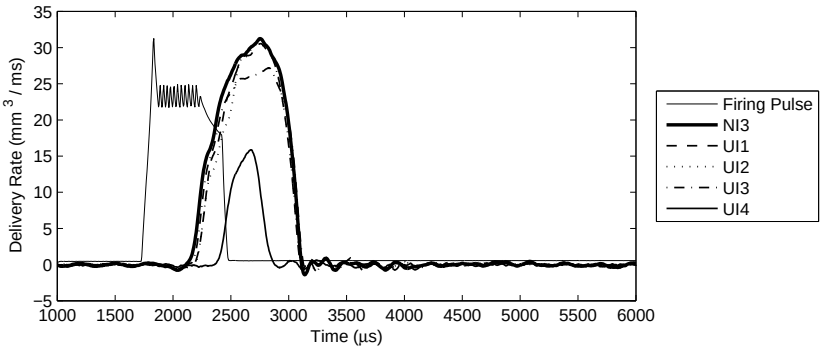

Figure C.25: Delivery rate vs time at 600 bar, 700μs duration

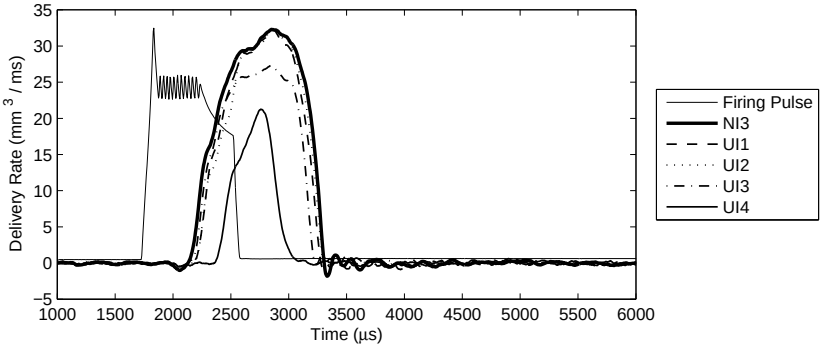

Figure C.26: Delivery rate vs time at 600 bar, 800μs duration

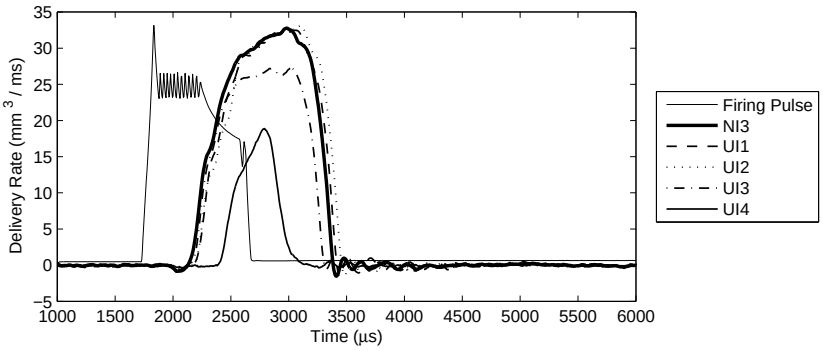

Figure C.27: Delivery rate vs time at 600 bar, 900μs duration

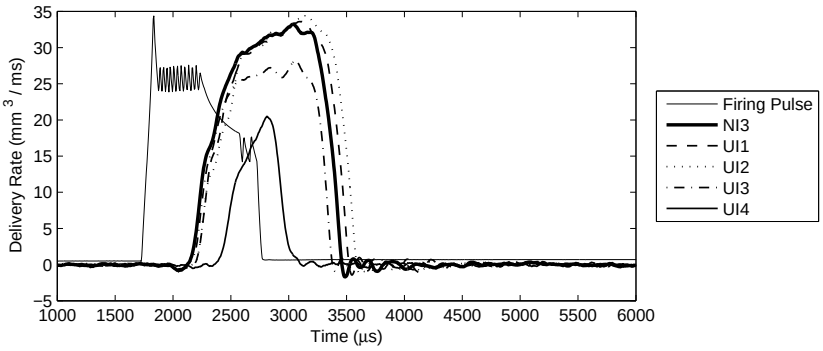

Figure C.28: Delivery rate vs time at 600 bar, 1000μs duration

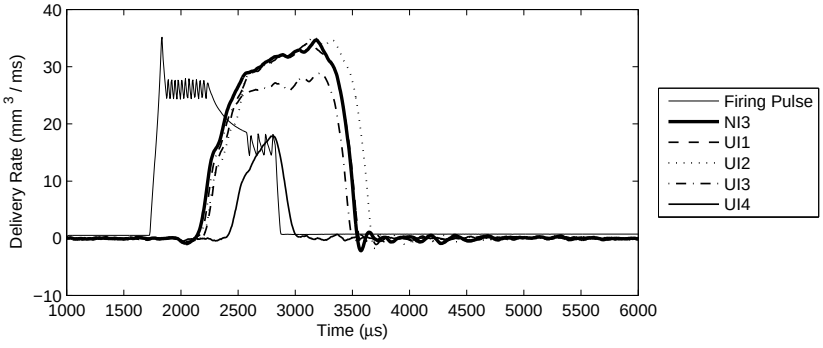

Figure C.29: Delivery rate vs time at 600 bar, 1100μs duration

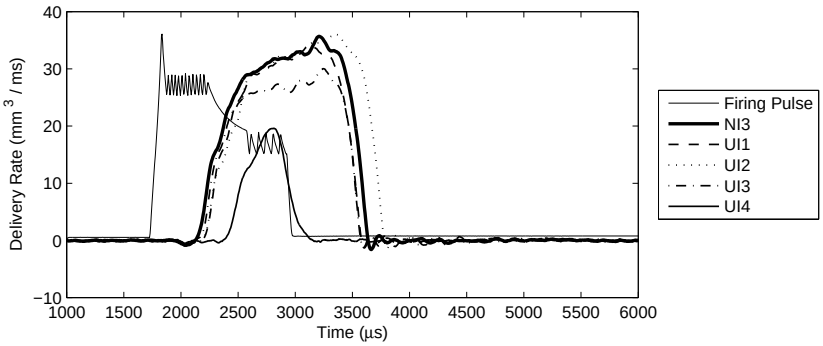

Figure C.30: Delivery rate vs time at 600 bar, 1200μs duration

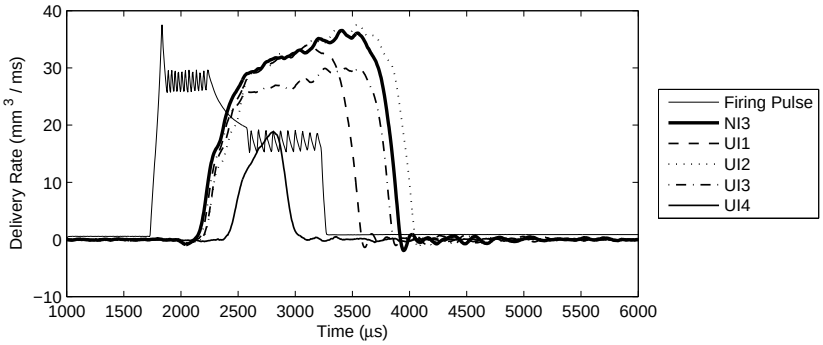

Figure C.31: Delivery rate vs time at 600 bar, 1500μs duration

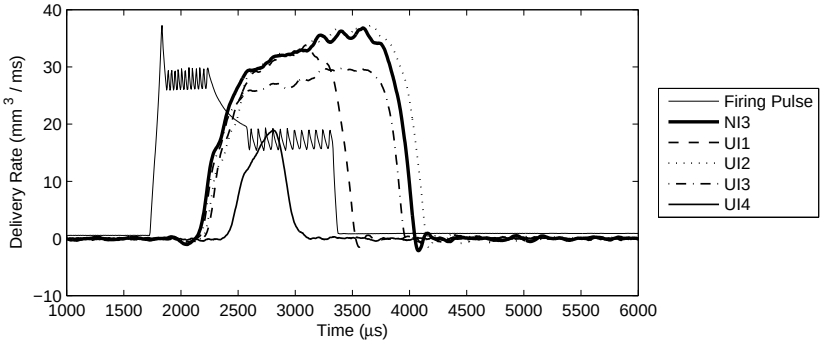

Figure C.32: Delivery rate vs time at 600 bar, 1600μs duration

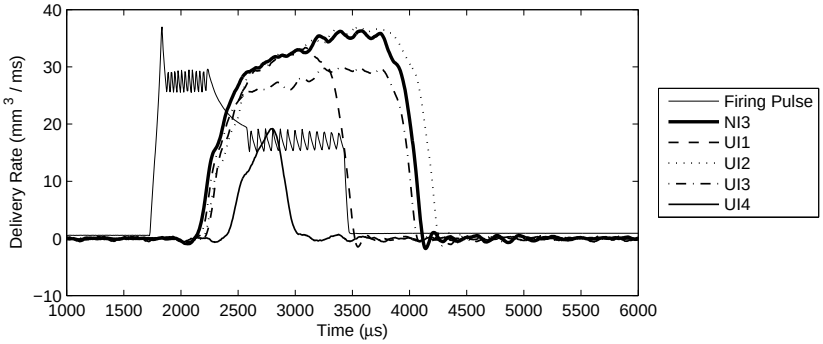

Figure C.33: Delivery rate vs time at 600 bar, 1700μs duration

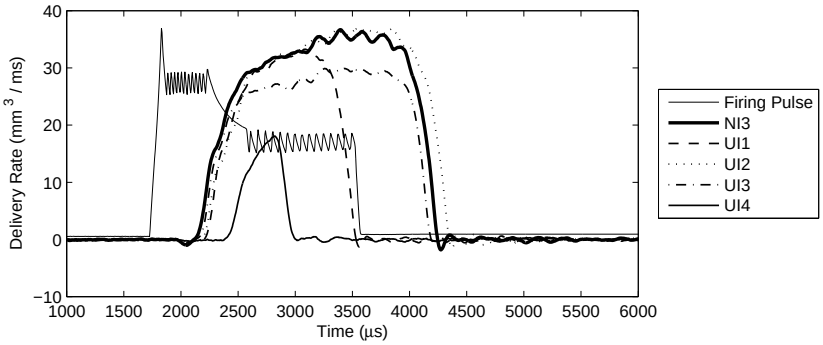

Figure C.34: Delivery rate vs time at 600 bar, 1800μs duration

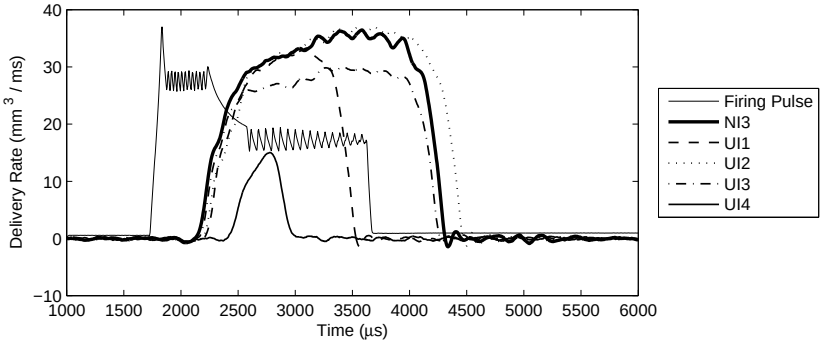

Figure C.35: Delivery rate vs time at 600 bar, 1900μs duration

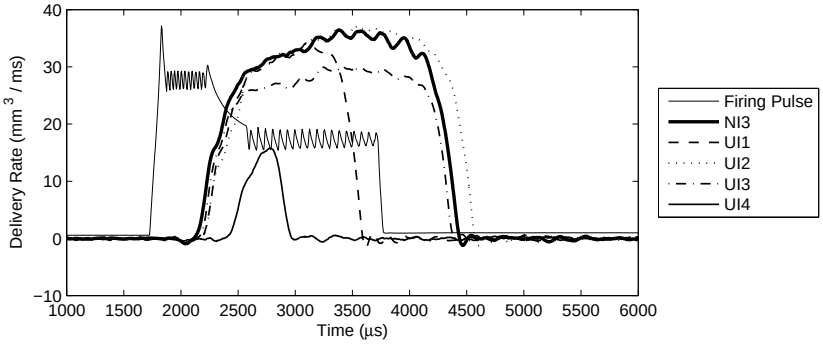

Figure C.36: Delivery rate vs time at 600 bar, 2000μs duration

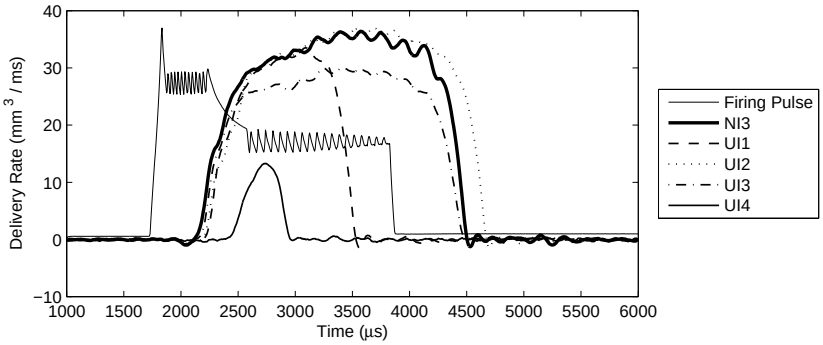

Figure C.37: Delivery rate vs time at 600 bar, 2100μs duration

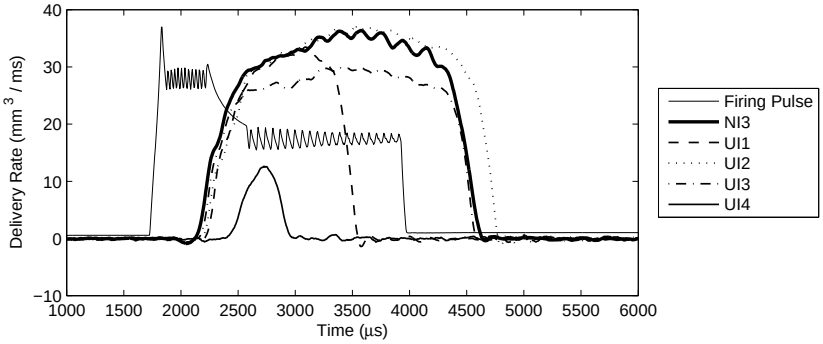

Figure C.38: Delivery rate vs time at 600 bar, 2200μs duration

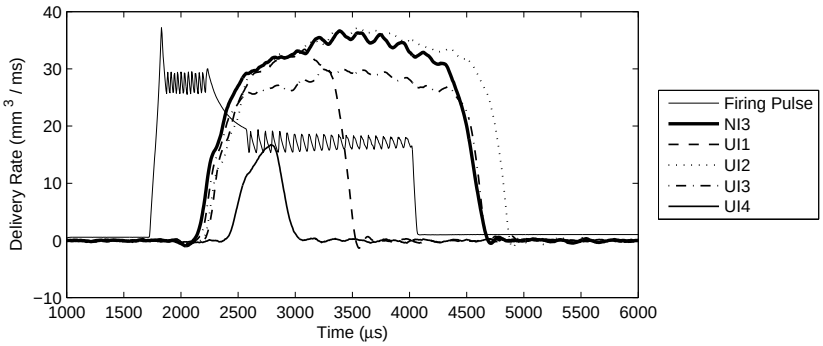

Figure C.39: Delivery rate vs time at 600 bar, 2300μs duration

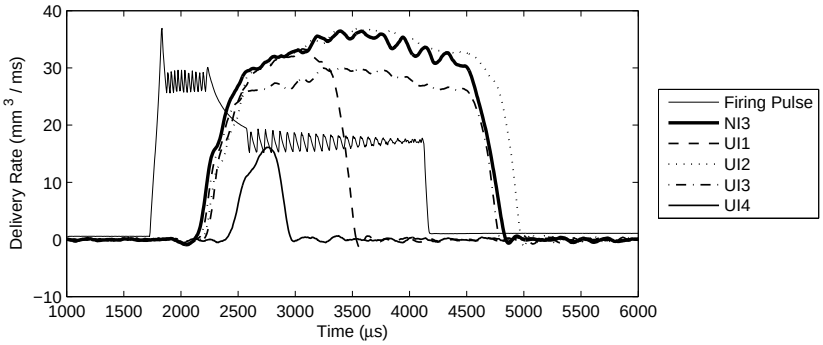

Figure C.40: Delivery rate vs time at 600 bar, 2400μs duration

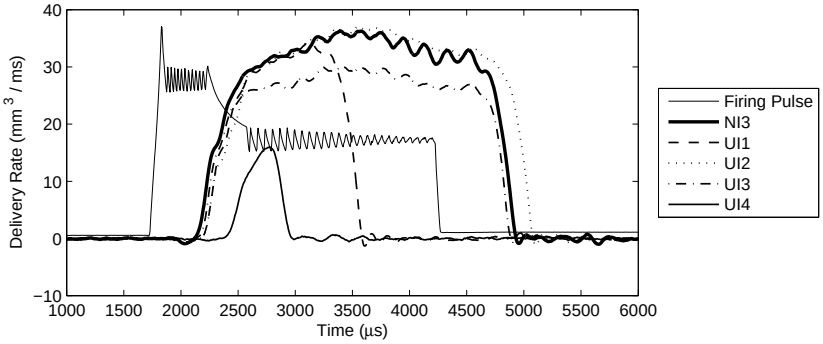

Figure C.41: Delivery rate vs time at 600 bar, 2500μs duration

C.1.3 900 bar Results

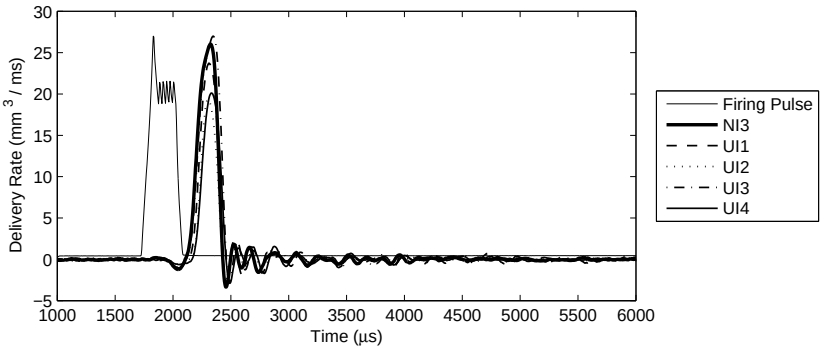

Figure C.42: Delivery rate vs time at 900 bar, 300μs duration

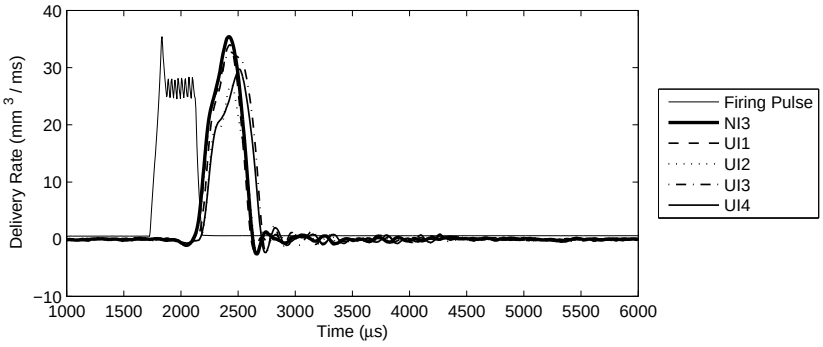

Figure C.43: Delivery rate vs time at 900 bar, 400μs duration

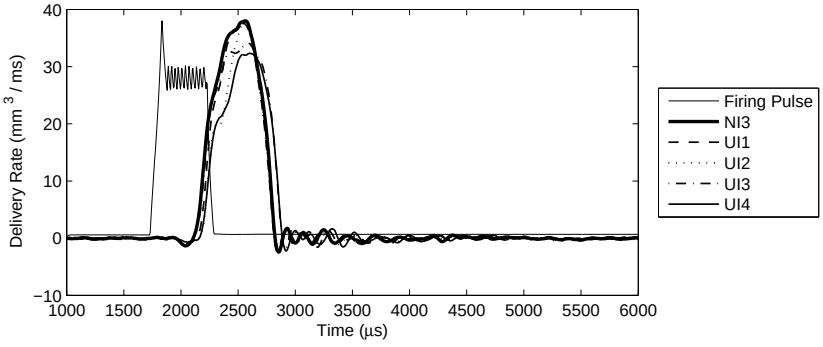

Figure C.44: Delivery rate vs time at 900 bar, 500μs duration

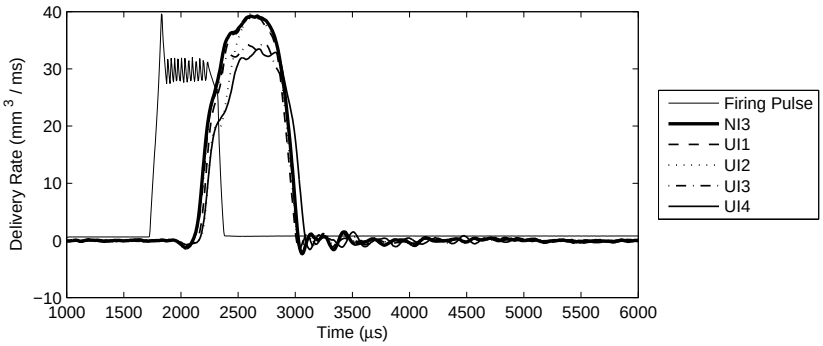

Figure C.45: Delivery rate vs time at 900 bar, 600μs duration

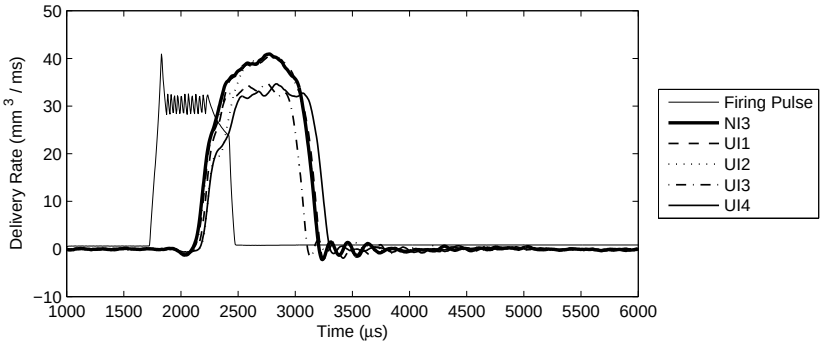

Figure C.46: Delivery rate vs time at 900 bar, 700μs duration

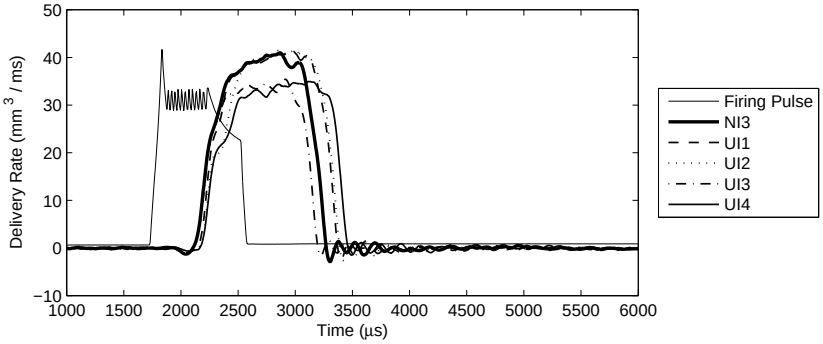

Figure C.47: Delivery rate vs time at 900 bar, 800μs duration

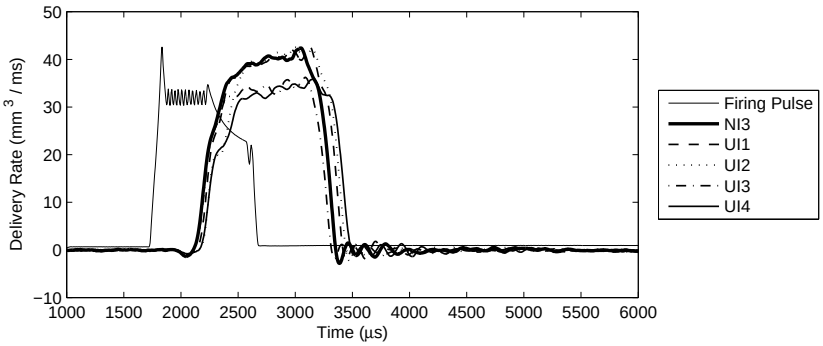

Figure C.48: Delivery rate vs time at 900 bar, 900μs duration

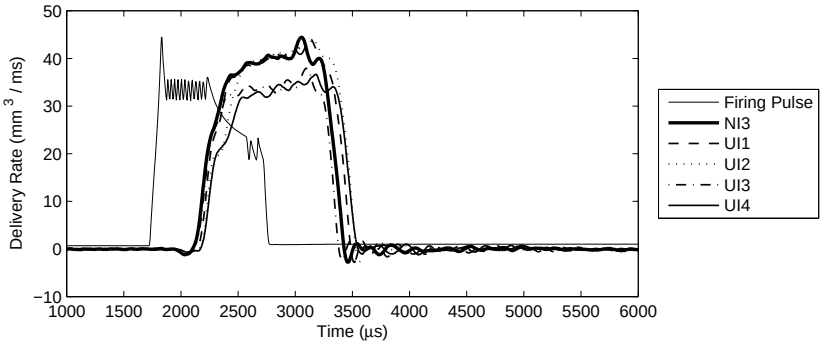

Figure C.49: Delivery rate vs time at 900 bar, 1000μs duration

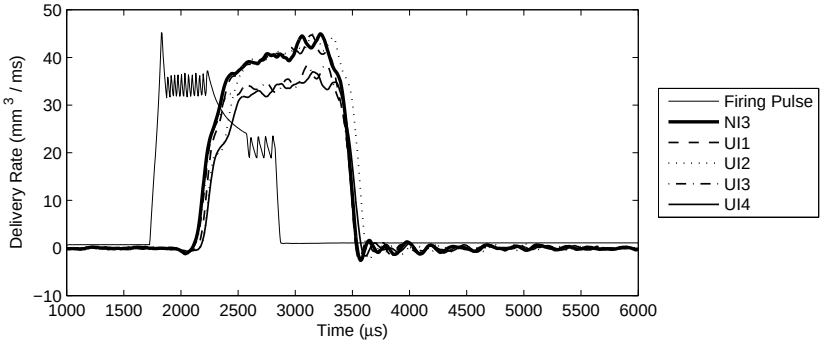

Figure C.50: Delivery rate vs time at 900 bar, 1100μs duration

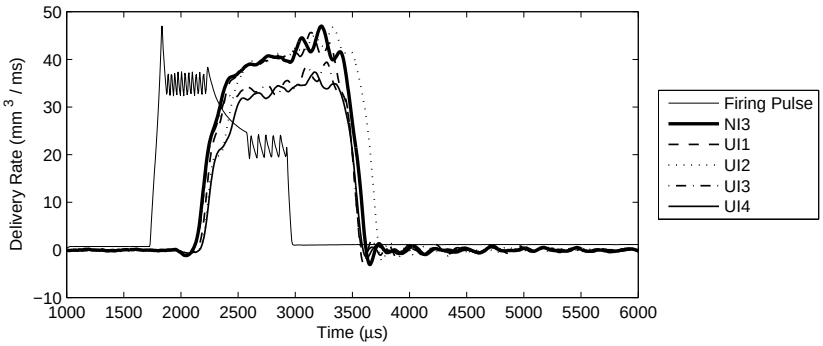

Figure C.51: Delivery rate vs time at 900 bar, 1200μs duration

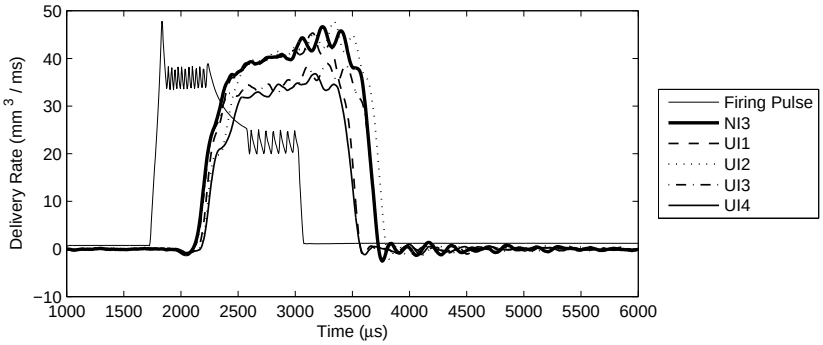

Figure C.52: Delivery rate vs time at 900 bar, 1300μs duration

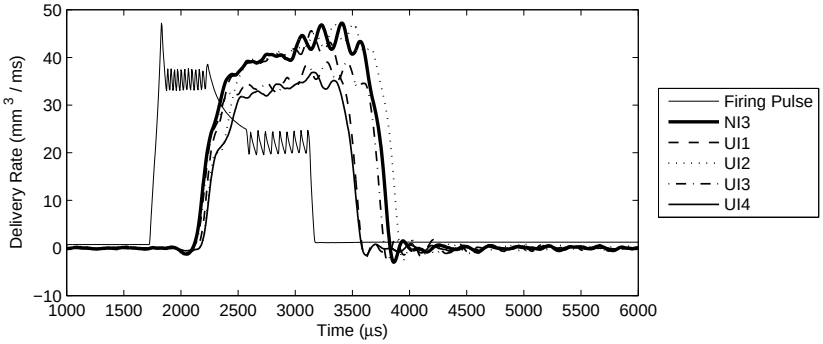

Figure C.53: Delivery rate vs time at 900 bar, 1400μs duration

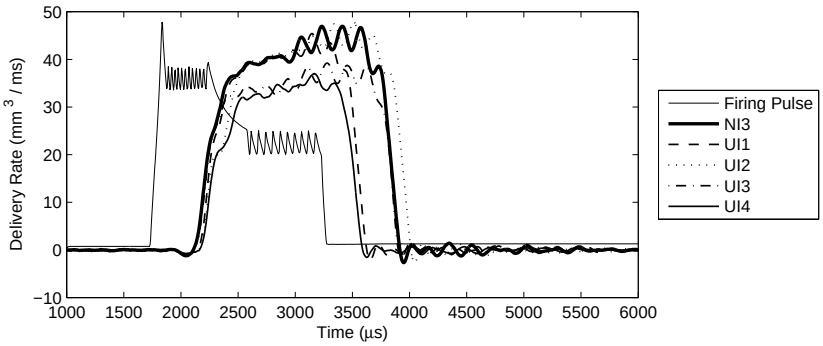

Figure C.54: Delivery rate vs time at 900 bar, 1500μs duration

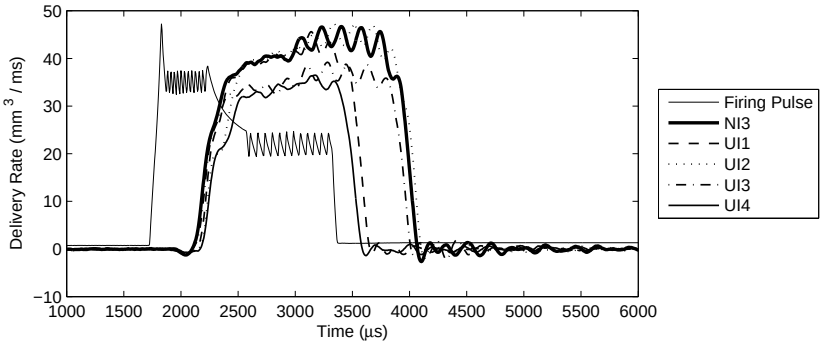

Figure C.55: Delivery rate vs time at 900 bar, 1600μs duration

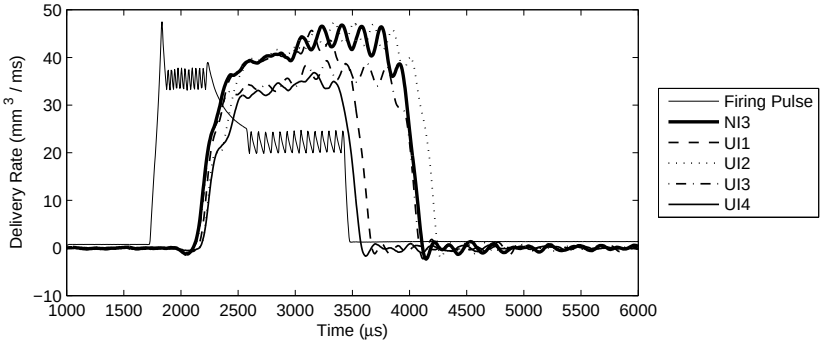

Figure C.56: Delivery rate vs time at 900 bar, 1700μs duration

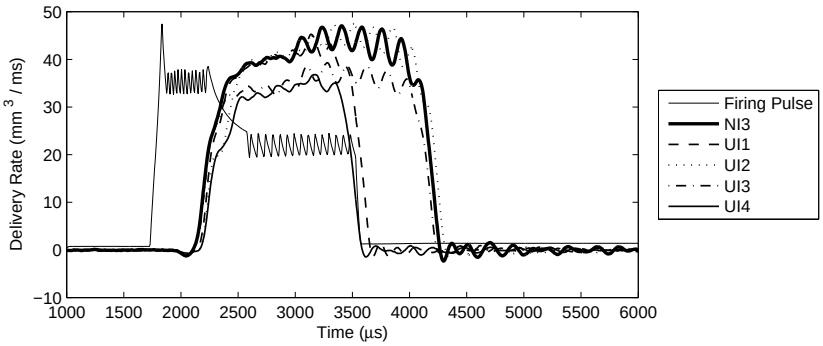

Figure C.57: Delivery rate vs time at 900 bar, 1800μs duration

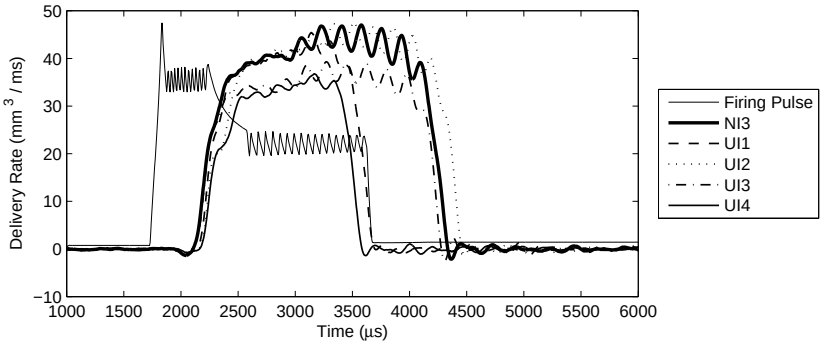

Figure C.58: Delivery rate vs time at 900 bar, 1900μs duration

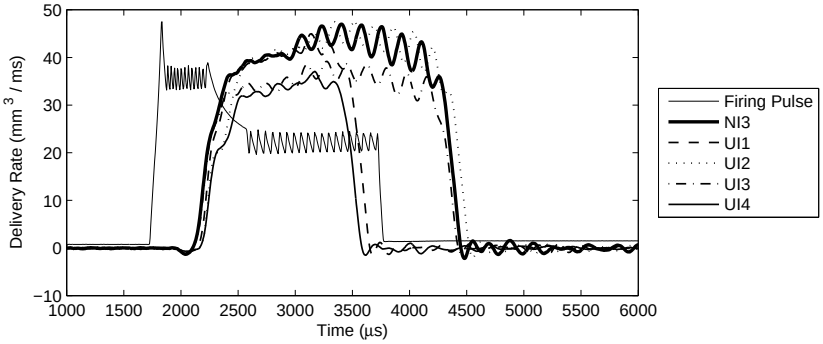

Figure C.59: Delivery rate vs time at 900 bar, 2000μs duration

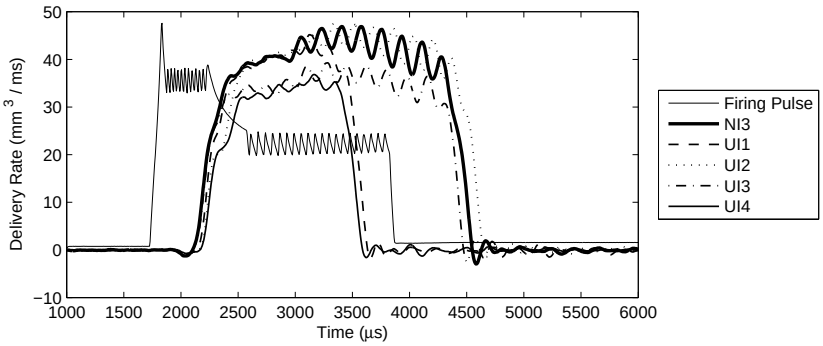

Figure C.60: Delivery rate vs time at 900 bar, 2100μs duration

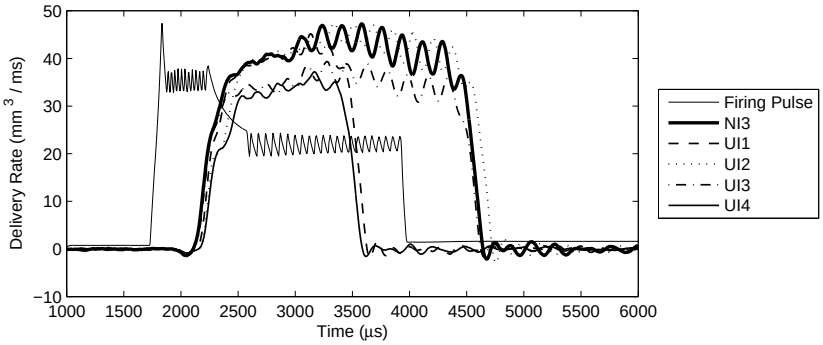

Figure C.61: Delivery rate vs time at 900 bar, 2200μs duration

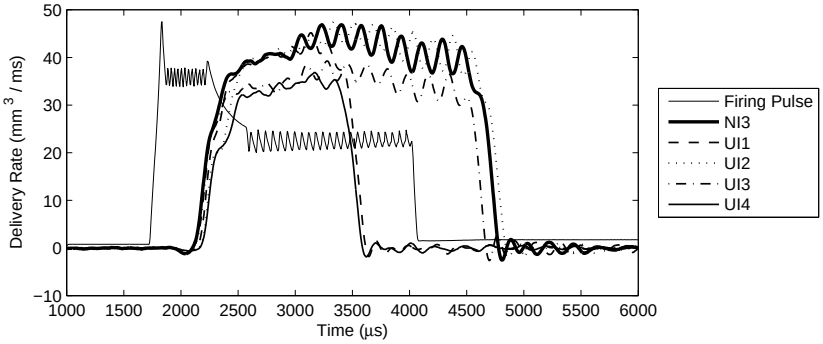

Figure C.62: Delivery rate vs time at 900 bar, 2300μs duration

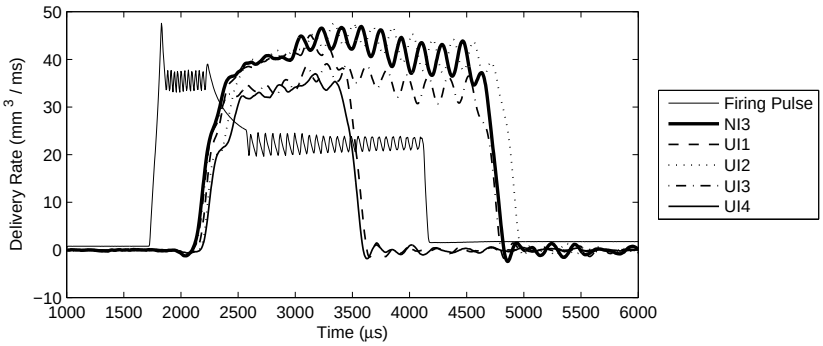

Figure C.63: Delivery rate vs time at 900 bar, 2400μs duration

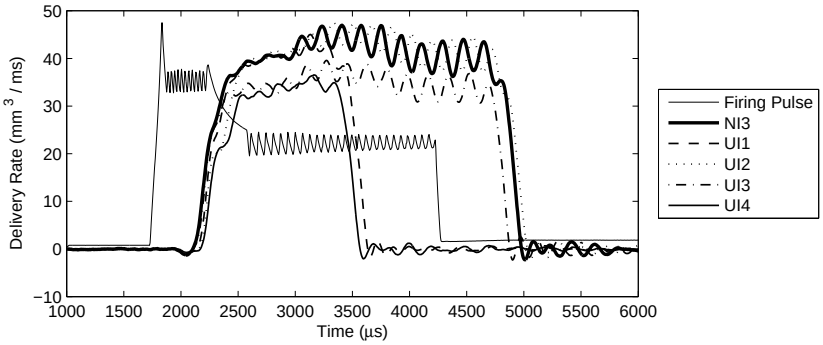

Figure C.64: Delivery rate vs time at 900 bar, 2500μs duration

C.1.4 1200bar Results

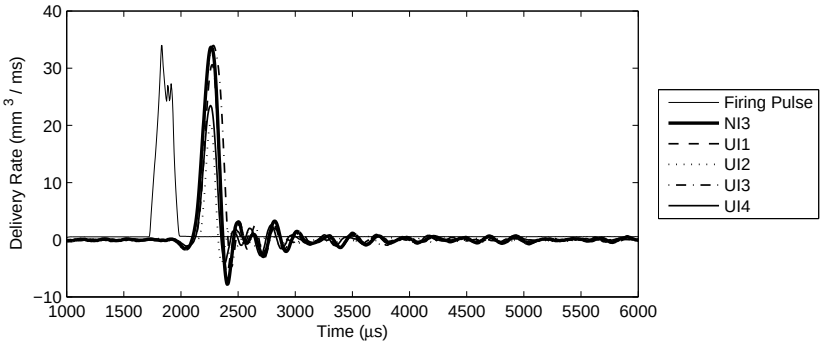

Figure C.65: Delivery rate vs time at 1200 bar, 200μs duration

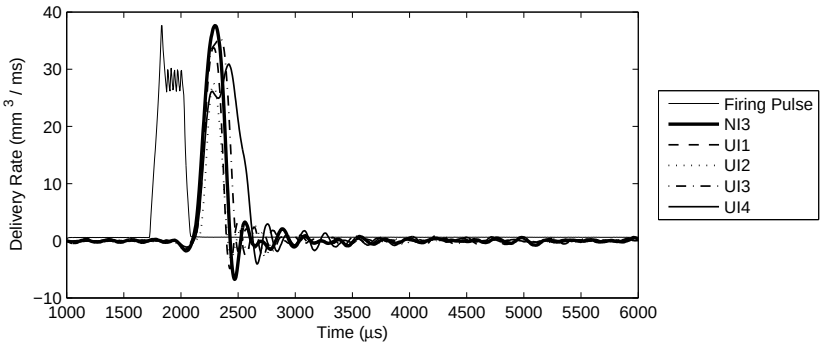

Figure C.66: Delivery rate vs time at 1200 bar, 300μs duration

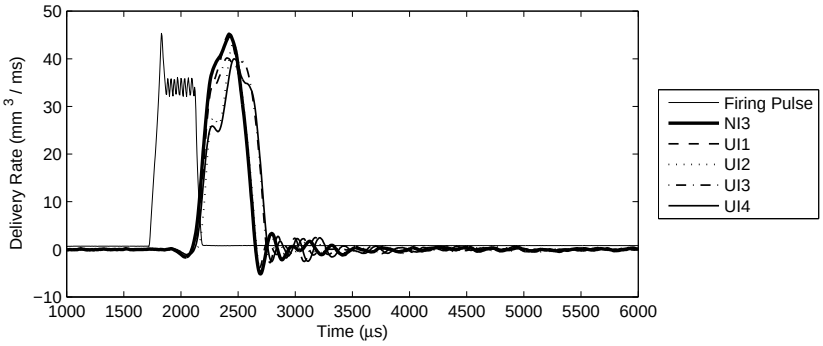

Figure C.67: Delivery rate vs time at 1200 bar, 400μs duration

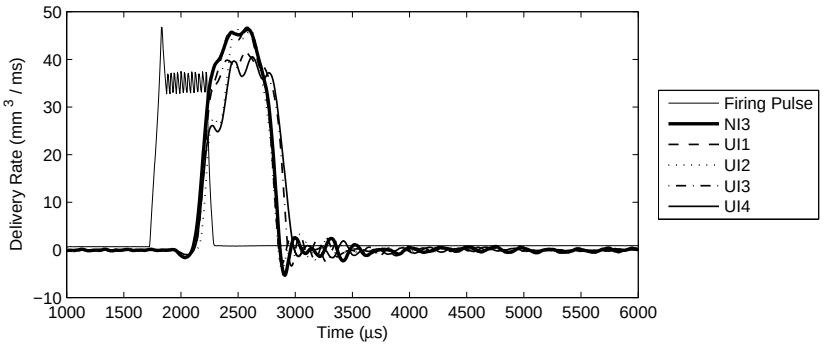

Figure C.68: Delivery rate vs time at 1200 bar, 500μs duration

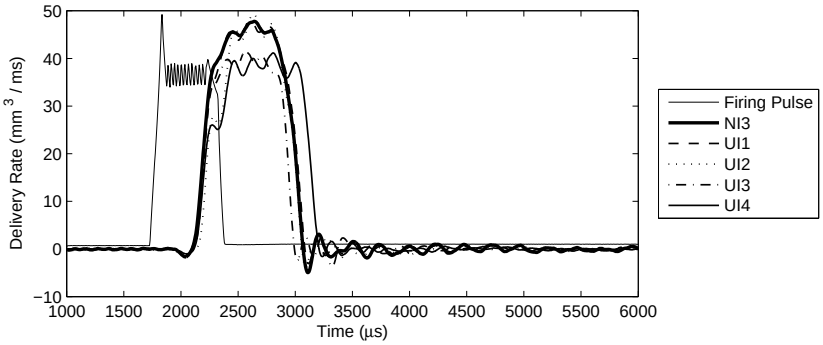

Figure C.69: Delivery rate vs time at 1200 bar, 600μs duration

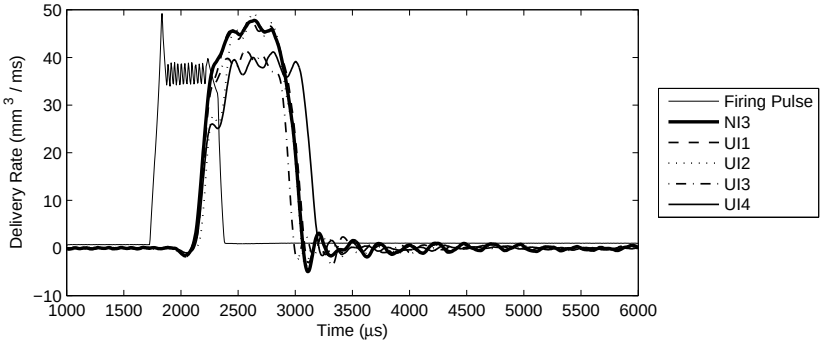

Figure C.70: Delivery rate vs time at 1200 bar, 600μs duration

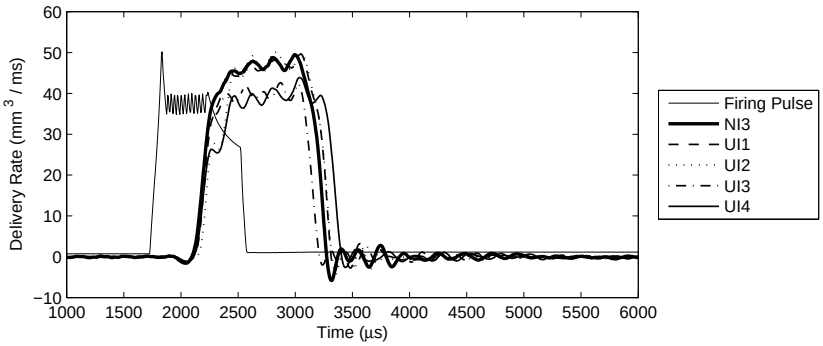

Figure C.71: Delivery rate vs time at 1200 bar, 800μs duration

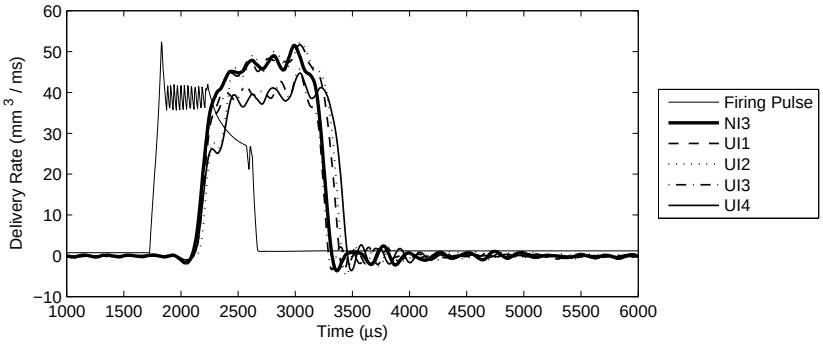

Figure C.72: Delivery rate vs time at 1200 bar, 900μs duration

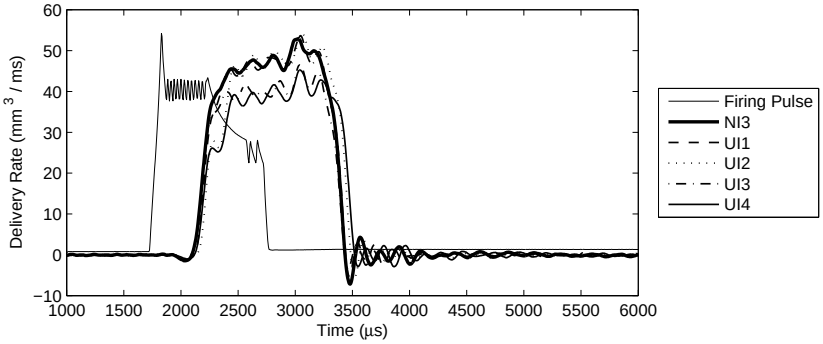

Figure C.73: Delivery rate vs time at 1200 bar, 1000μs duration

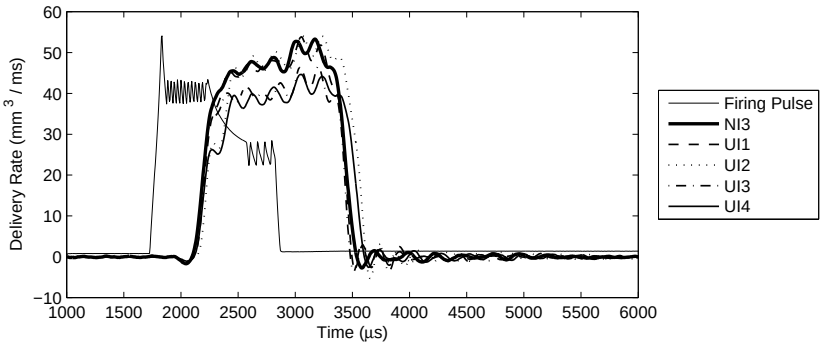

Figure C.74: Delivery rate vs time at 1200 bar, 1100μs duration

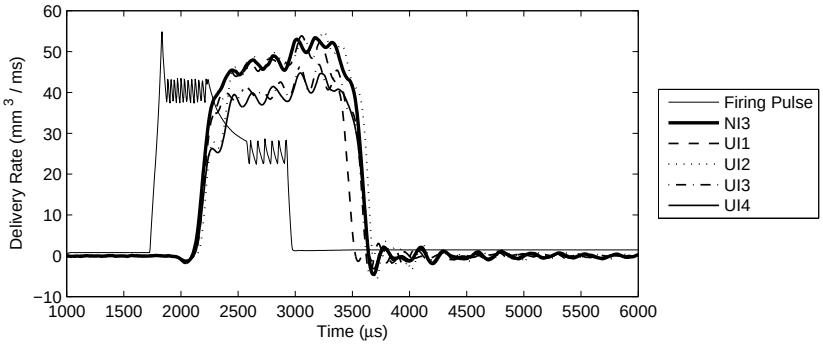

Figure C.75: Delivery rate vs time at 1200 bar, 1200μs duration

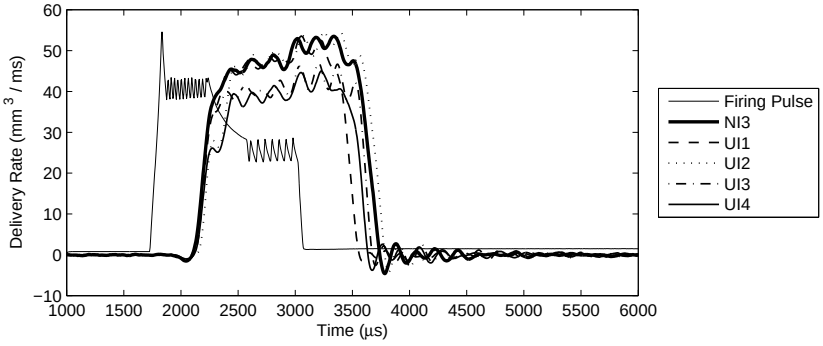

Figure C.76: Delivery rate vs time at 1200 bar, 1300μs duration

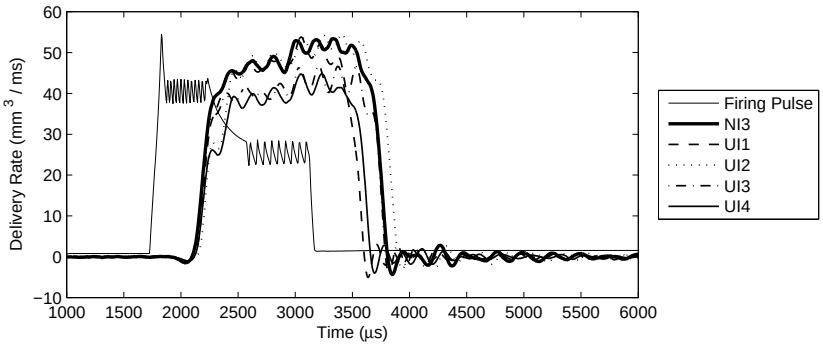

Figure C.77: Delivery rate vs time at 1200 bar, 1400μs duration

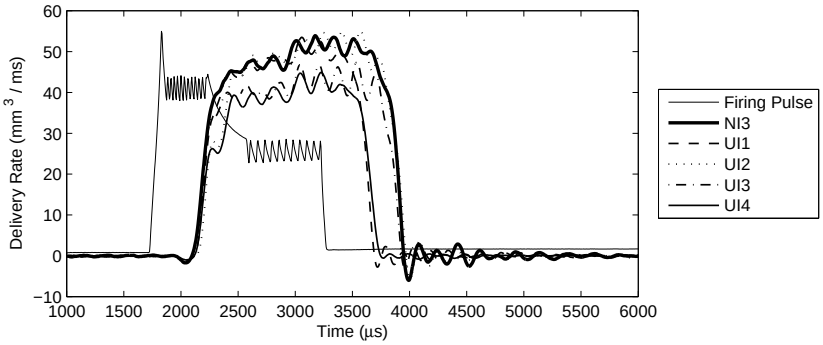

Figure C.78: Delivery rate vs time at 1200 bar, 1500μs duration

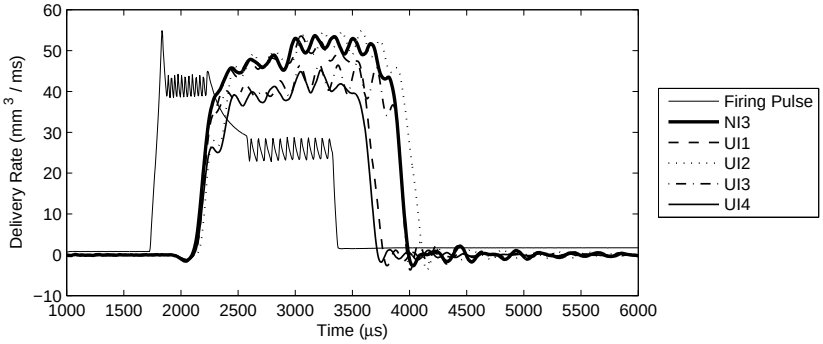

Figure C.79: Delivery rate vs time at 1200 bar, 1600μs duration

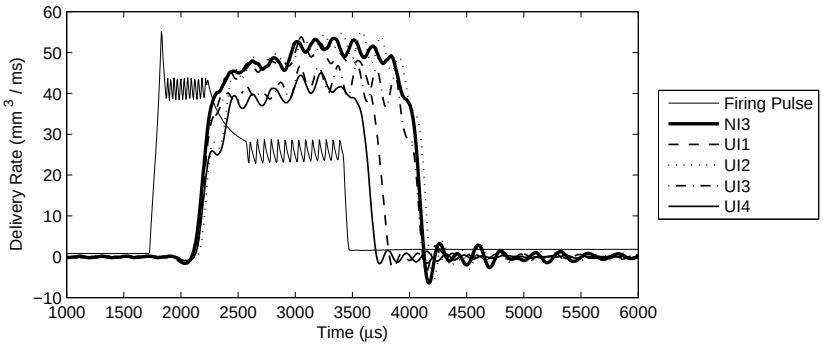

Figure C.80: Delivery rate vs time at 1200 bar, 1700μs duration

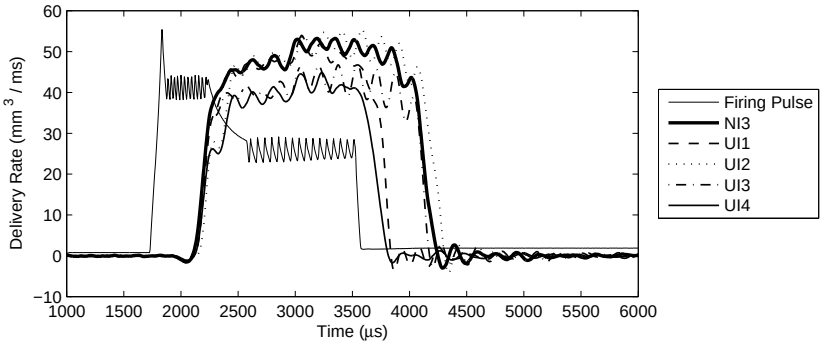

Figure C.81: Delivery rate vs time at 1200 bar, 1800μs duration

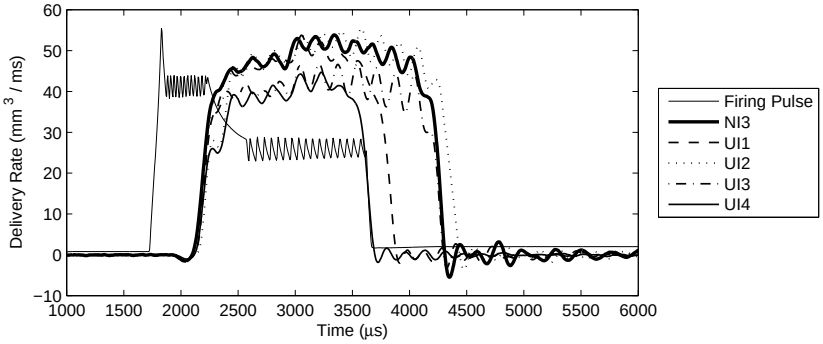

Figure C.82: Delivery rate vs time at 1200 bar, 1900μs duration

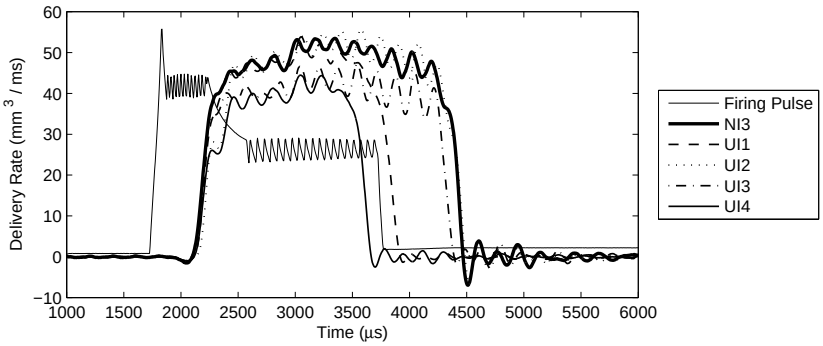

Figure C.83: Delivery rate vs time at 1200 bar, 2000μs duration

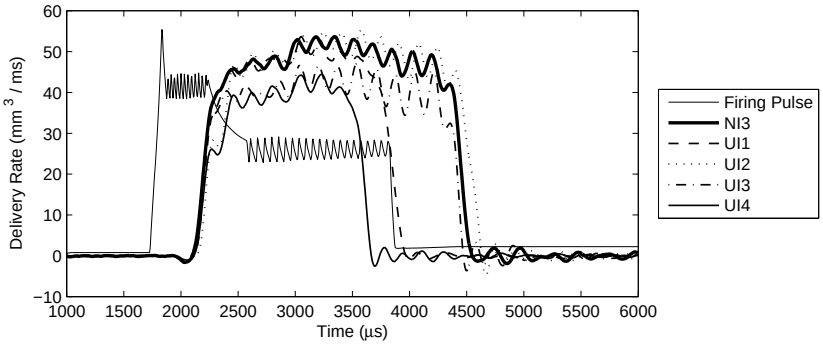

Figure C.84: Delivery rate vs time at 1200 bar, 2100μs duration

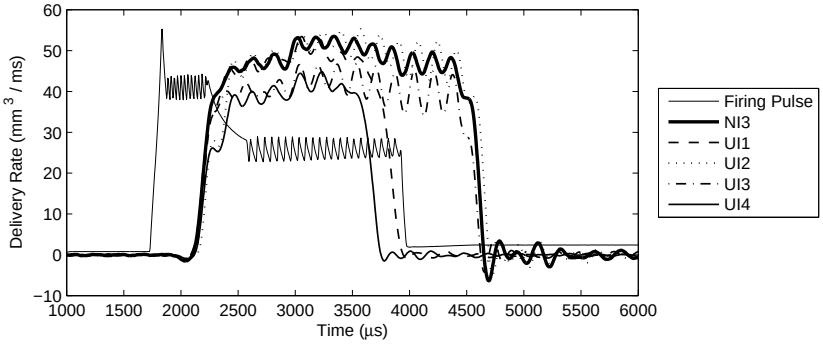

Figure C.85: Delivery rate vs time at 1200 bar, 2200μs duration

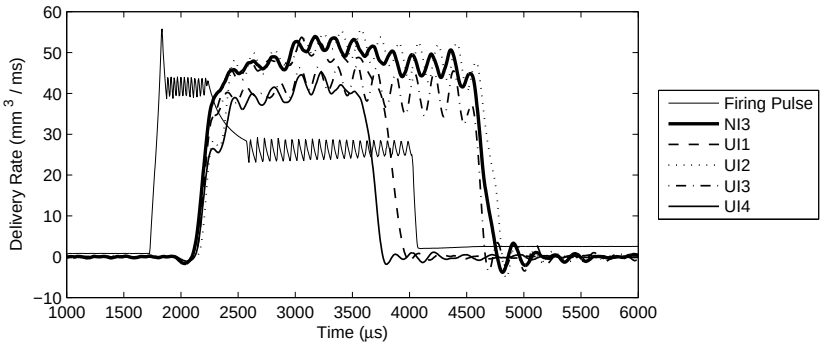

Figure C.86: Delivery rate vs time at 1200 bar, 2300μs duration

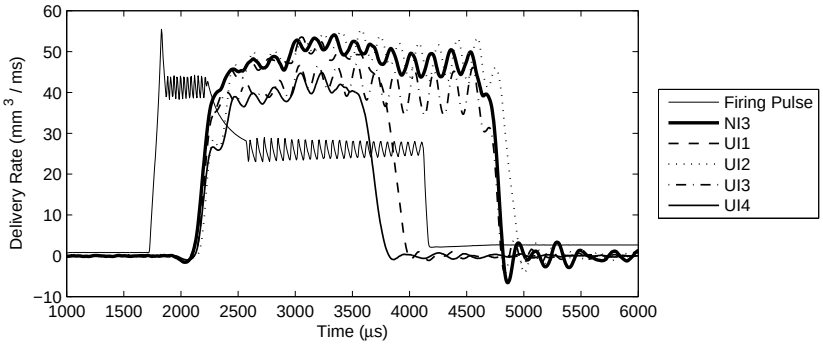

Figure C.87: Delivery rate vs time at 1200 bar, 2400μs duration

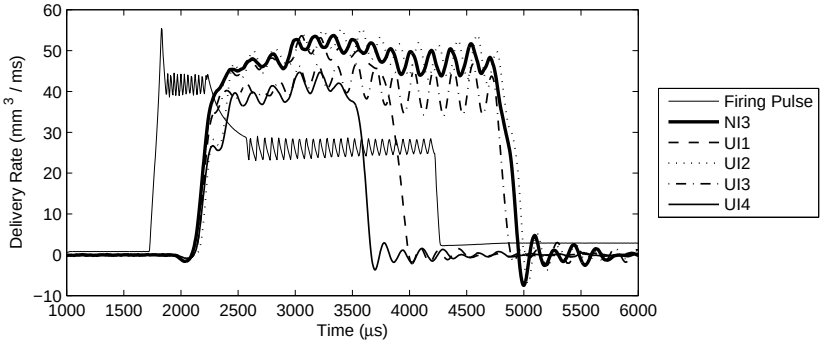

Figure C.88: Delivery rate vs time at 1200 bar, 2500μs duration

C.1.5 1400bar Results

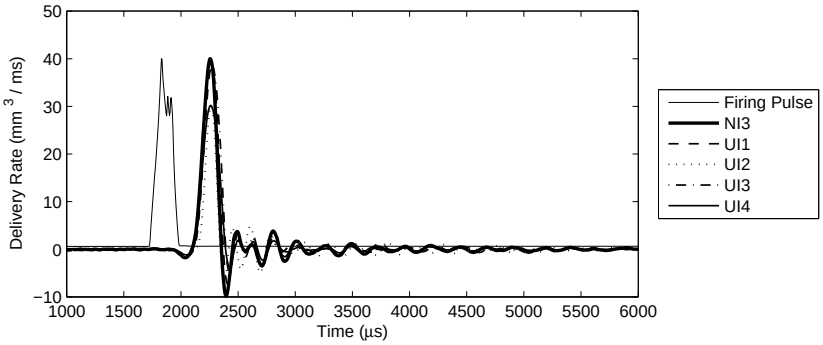

Figure C.89: Delivery rate vs time at 1400 bar, 200μs duration

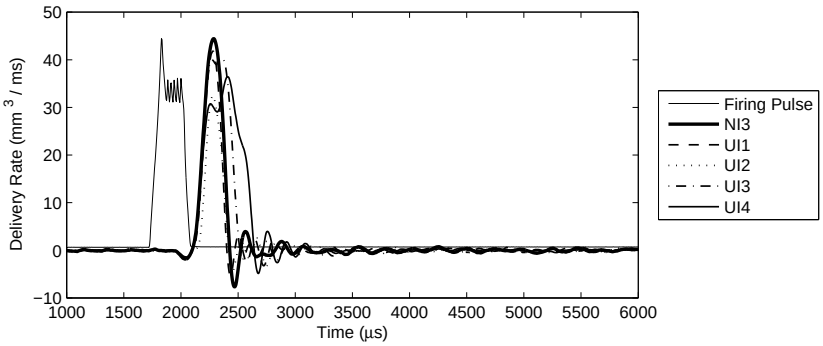

Figure C.90: Delivery rate vs time at 1400 bar, 300μs duration

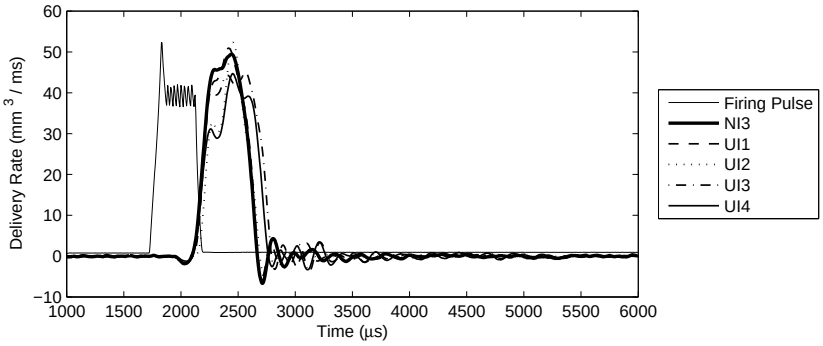

Figure C.91: Delivery rate vs time at 1400 bar, 400μs duration

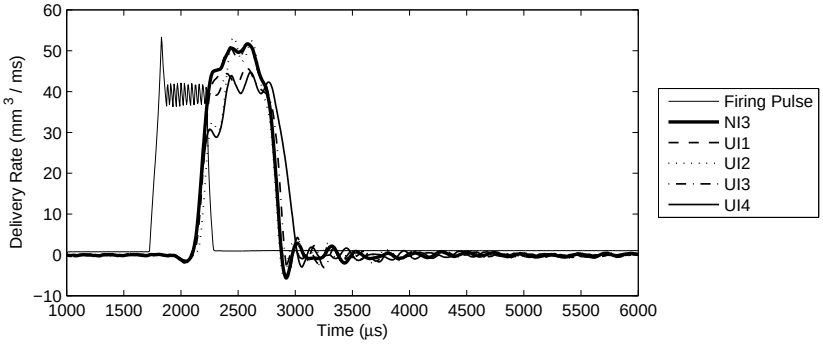

Figure C.92: Delivery rate vs time at 1400 bar, 500μs duration

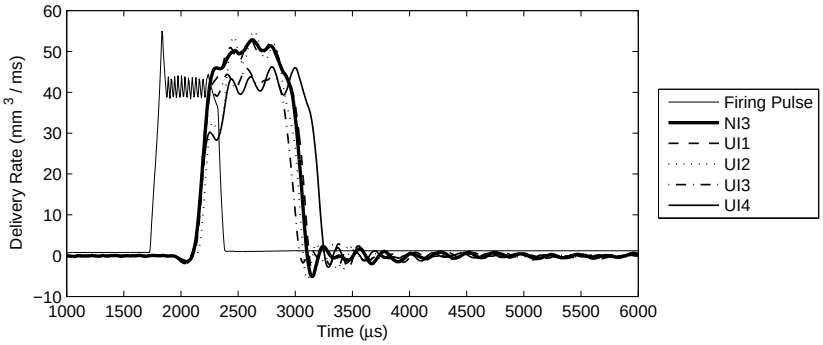

Figure C.93: Delivery rate vs time at 1400 bar, 600μs duration

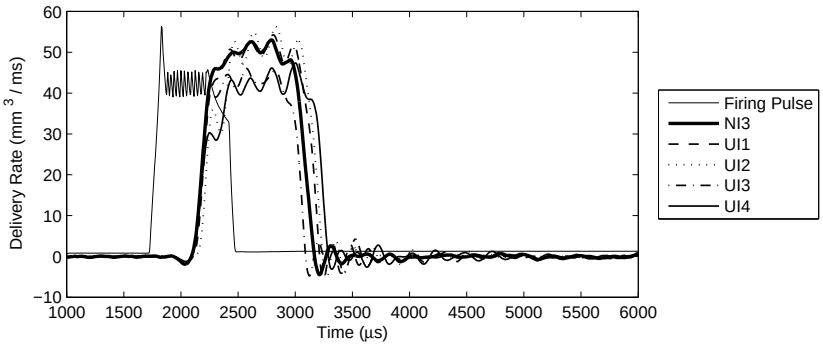

Figure C.94: Delivery rate vs time at 1400 bar, 700μs duration

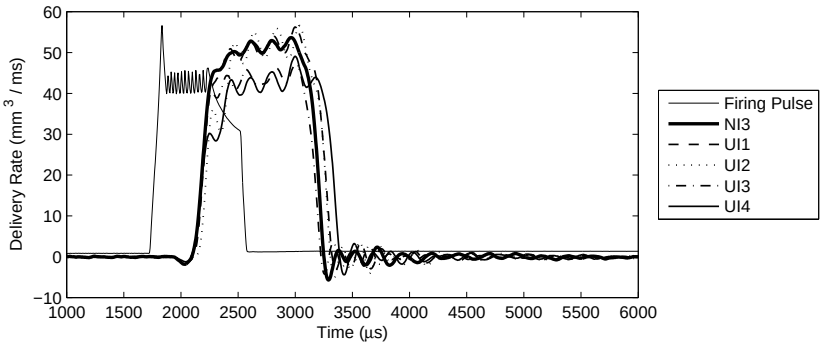

Figure C.95: Delivery rate vs time at 1400 bar, 800μs duration

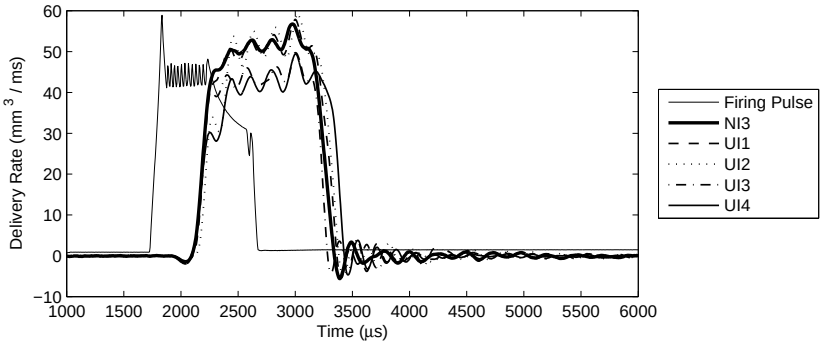

Figure C.96: Delivery rate vs time at 1400 bar, 900μs duration

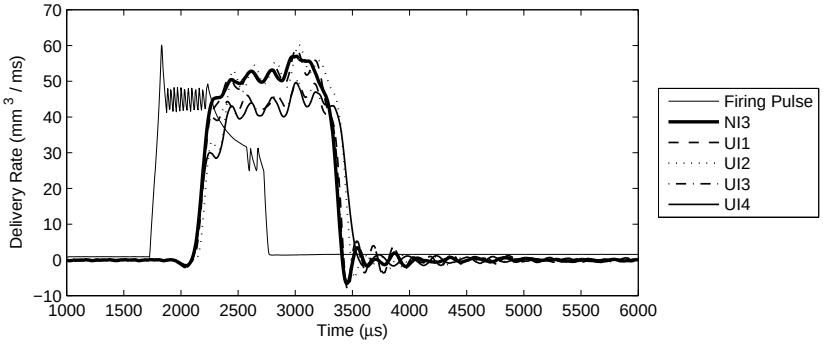

Figure C.97: Delivery rate vs time at 1400 bar, 1000μs duration

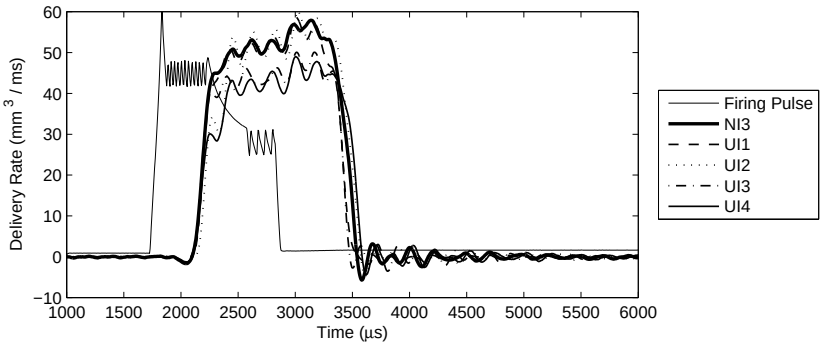

Figure C.98: Delivery rate vs time at 1400 bar, 1100μs duration

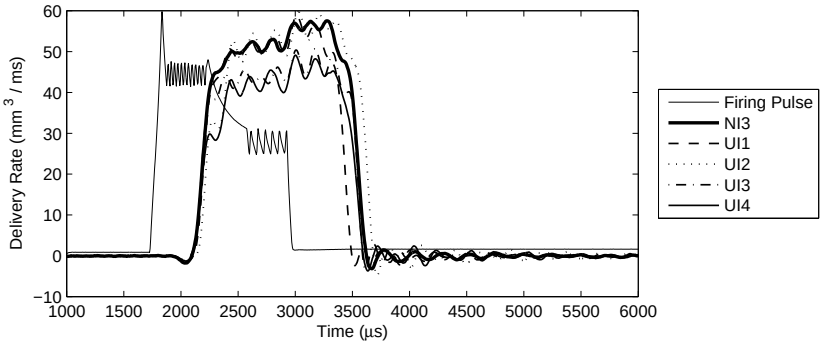

Figure C.99: Delivery rate vs time at 1400 bar, 1200μs duration

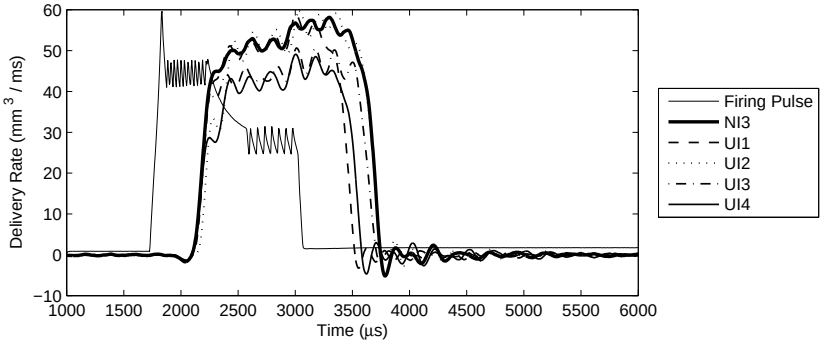

Figure C.100: Delivery rate vs time at 1400 bar, 1300μs duration

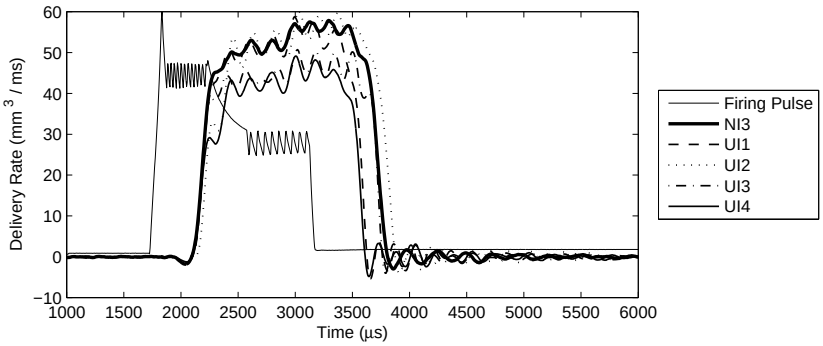

Figure C.101: Delivery rate vs time at 1400 bar, 1400μs duration

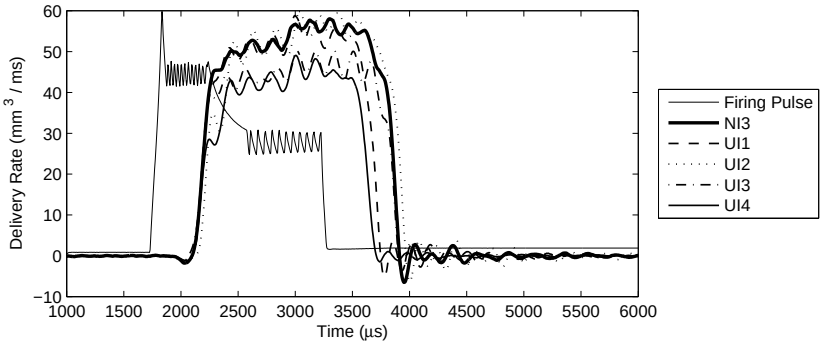

Figure C.102: Delivery rate vs time at 1400 bar, 1500μs duration

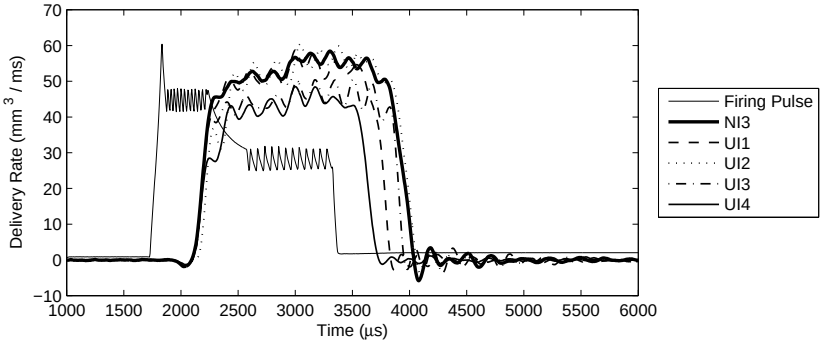

Figure C.103: Delivery rate vs time at 1400 bar, 1600μs duration

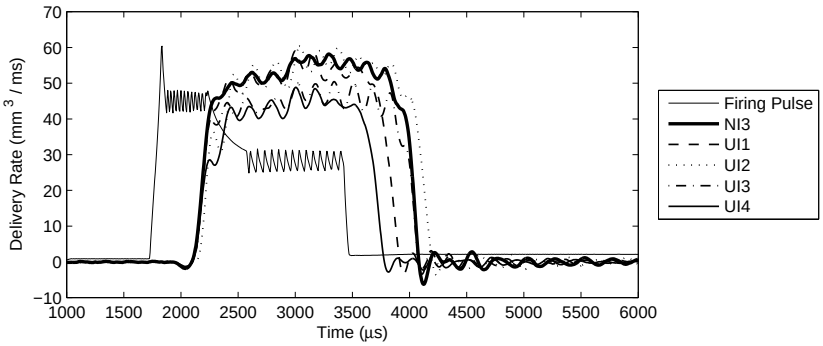

Figure C.104: Delivery rate vs time at 1400 bar, 1700μs duration

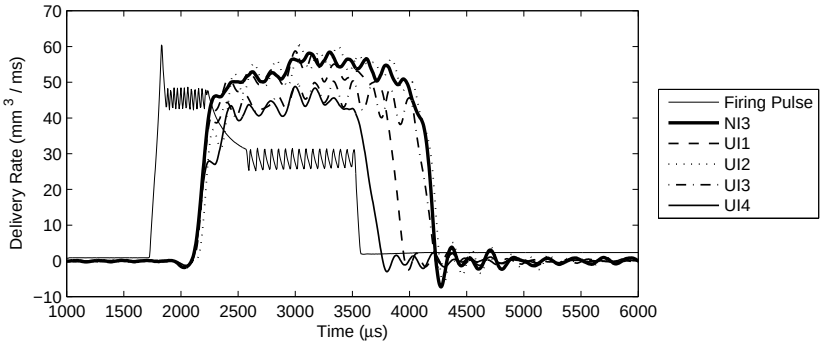

Figure C.105: Delivery rate vs time at 1400 bar, 1800μs duration

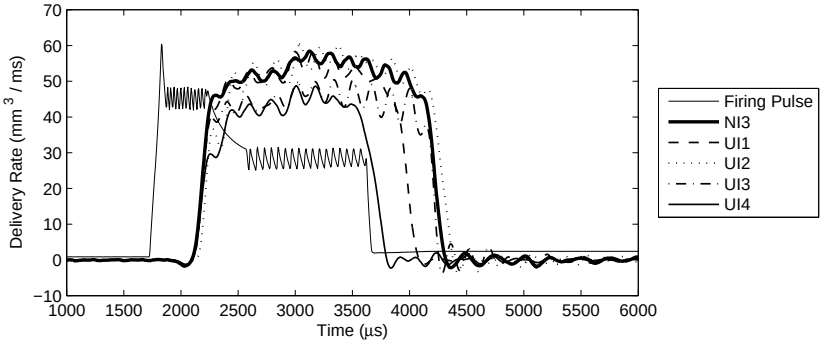

Figure C.106: Delivery rate vs time at 1400 bar, 1900μs duration

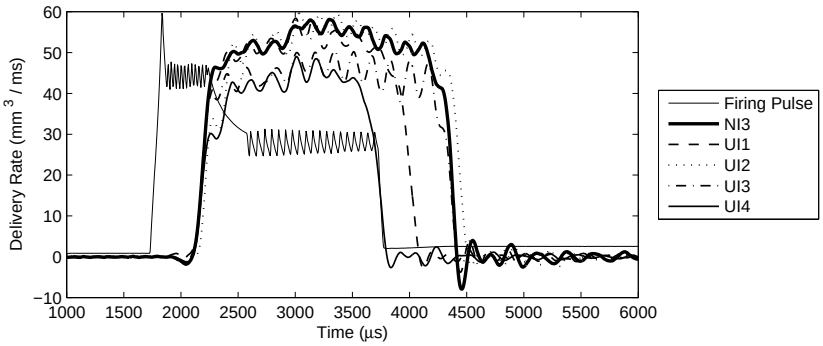

Figure C.107: Delivery rate vs time at 1400 bar, 2000μs duration

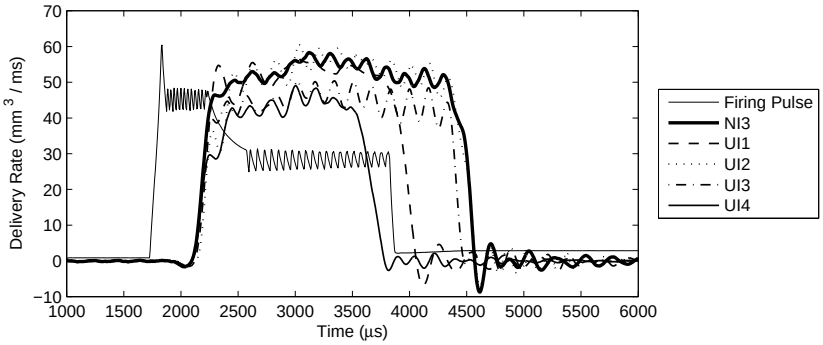

Figure C.108: Delivery rate vs time at 1400 bar, 2100μs duration

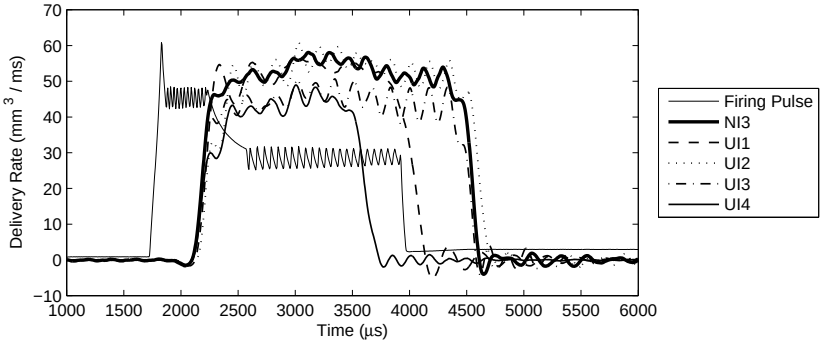

Figure C.109: Delivery rate vs time at 1400 bar, 2200μs duration

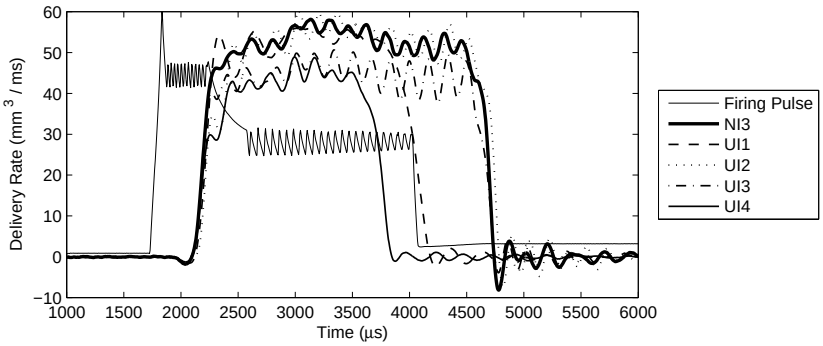

Figure C.110: Delivery rate vs time at 1400 bar, 2300μs duration

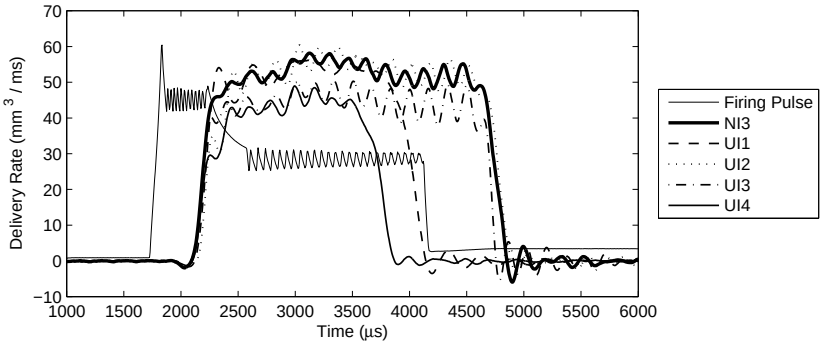

Figure C.111: Delivery rate vs time at 1400 bar, 2400μs duration

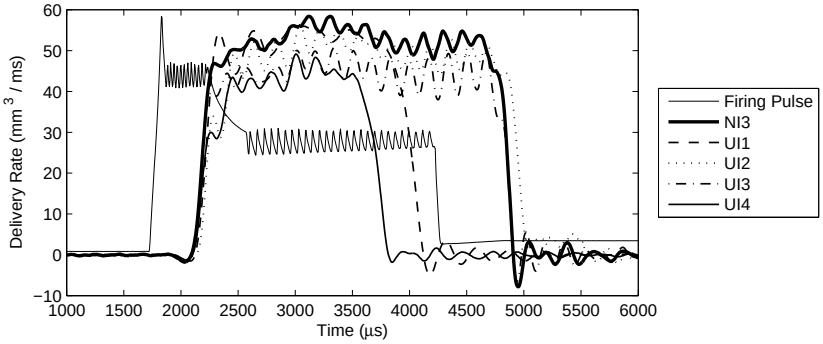

Figure C.112: Delivery rate vs time at 1400 bar, 2500μs duration

C.2 Delivery vs time Plots

C.2.1 300 bar Plots

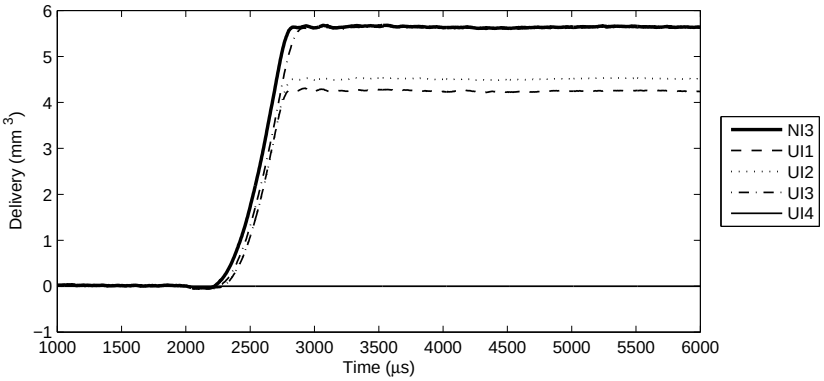

Figure C.113: Delivery vs time at 300 bar, 700μs duration

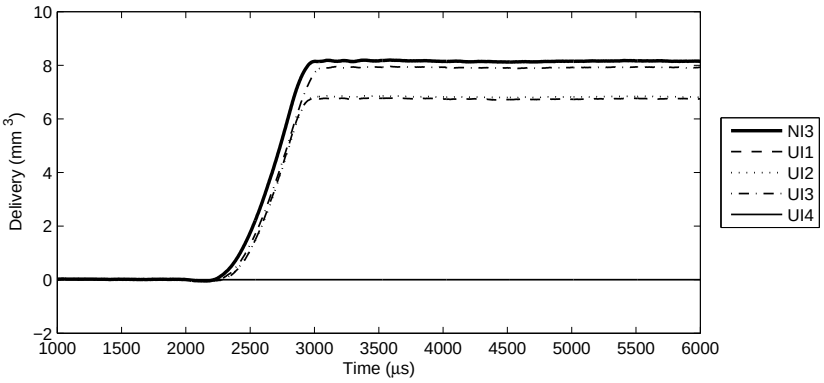

Figure C.114: Delivery vs time at 300 bar, 800μs duration

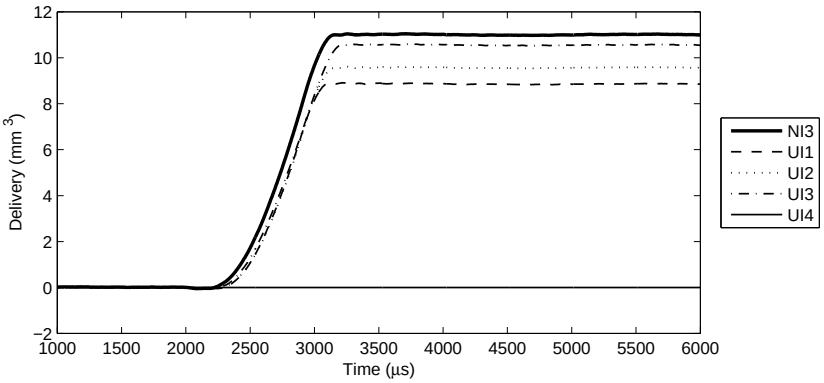

Figure C.115: Delivery vs time at 300 bar, 900μs duration

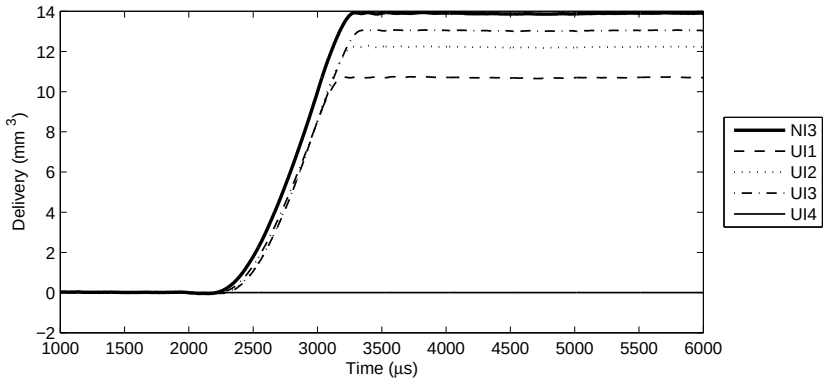

Figure C.116: Delivery vs time at 300 bar, 1000μs duration

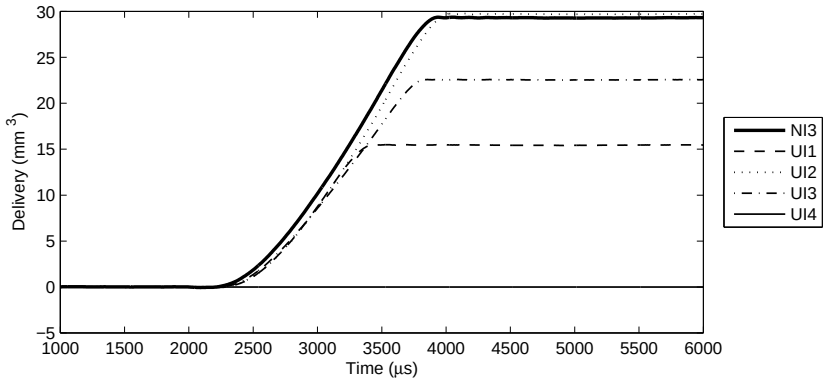

Figure C.117: Delivery vs time at 300 bar, 1500μs duration

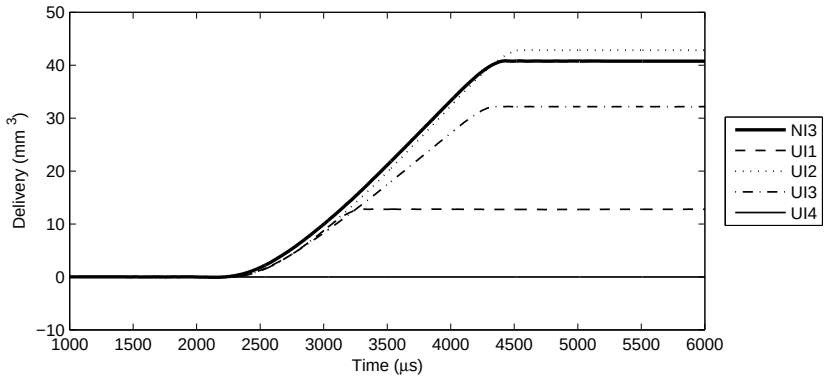

Figure C.118: Delivery vs time at 300 bar, 2000μs duration

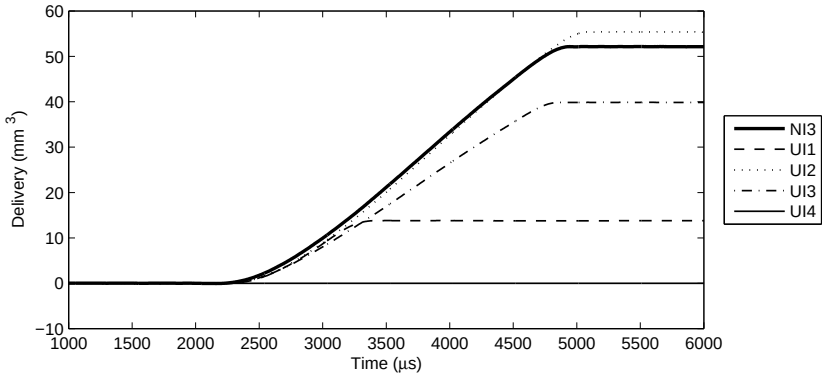

Figure C.119: Delivery vs time at 300 bar, 2500μs duration

C.2.2 600 bar Results

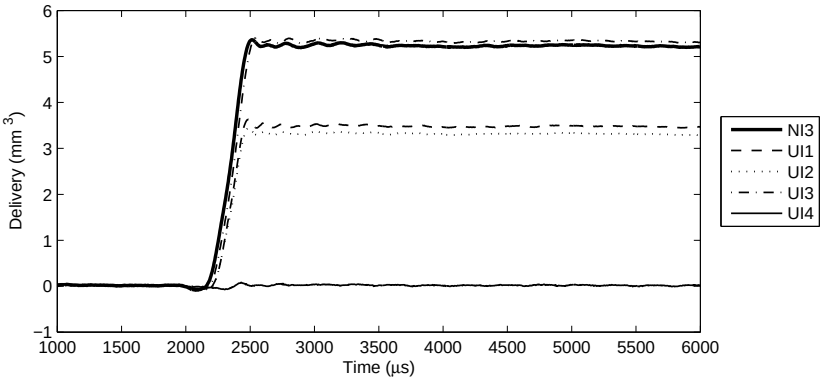

Figure C.120: Delivery vs time at 600 bar, 400μs duration

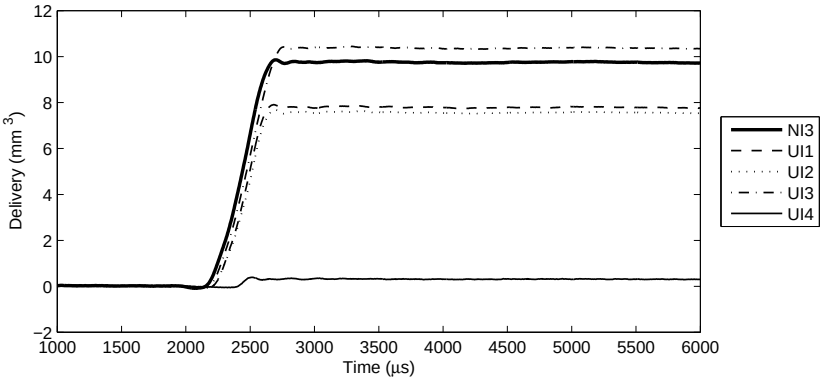

Figure C.121: Delivery vs time at 600 bar, 500μs duration

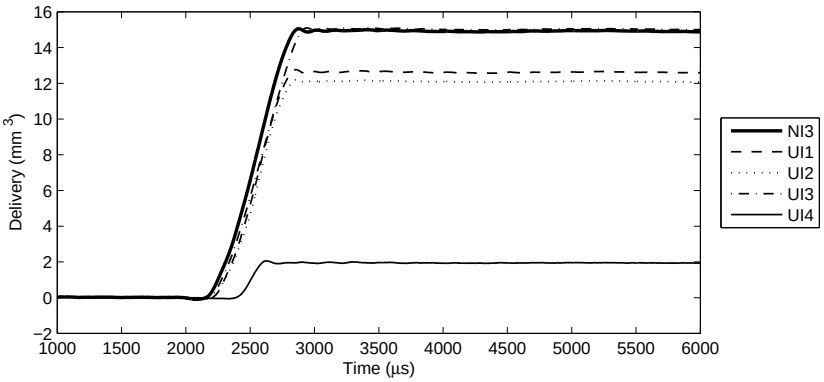

Figure C.122: Delivery vs time at 600 bar, 600μs duration

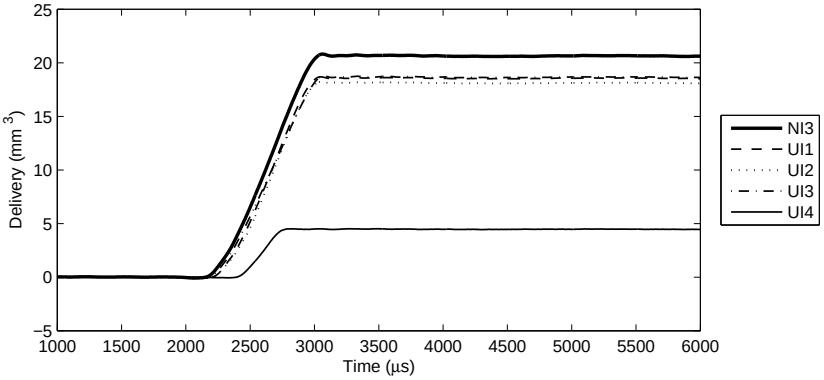

Figure C.123: Delivery vs time at 600 bar, 700μs duration

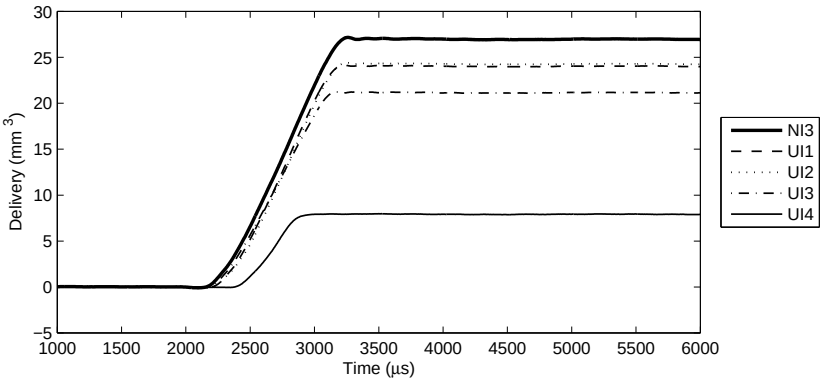

Figure C.124: Delivery vs time at 600 bar, 800μs duration

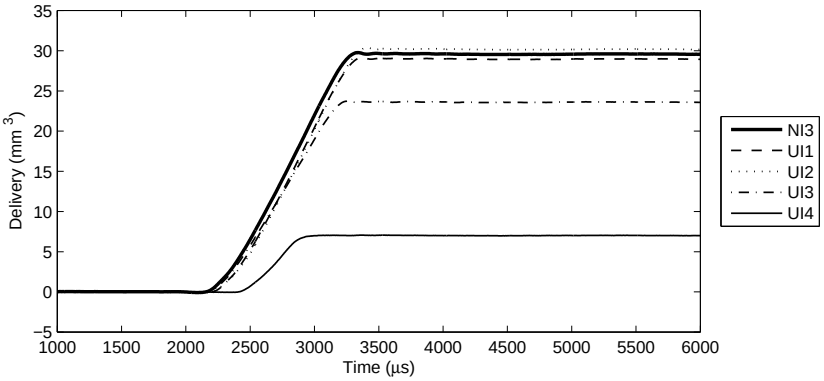

Figure C.125: Delivery vs time at 600 bar, 900μs duration

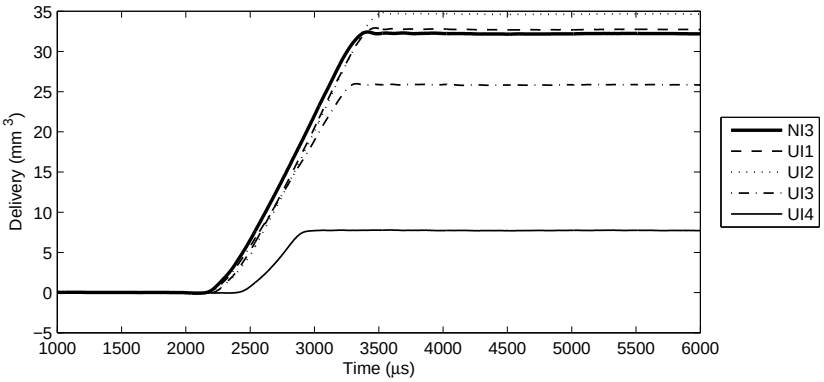

Figure C.126: Delivery vs time at 600 bar, 1000μs duration

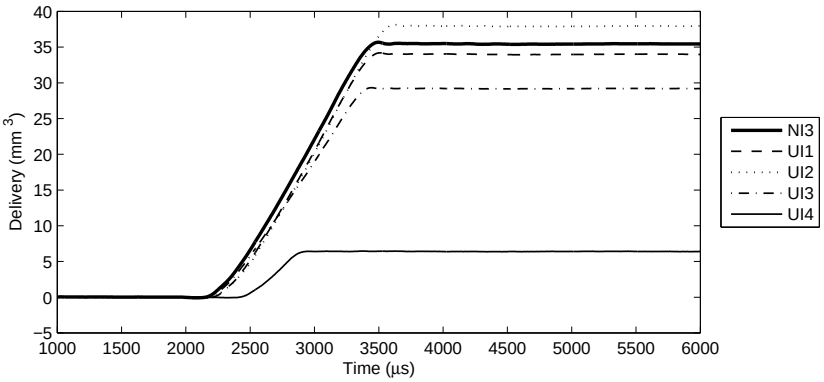

Figure C.127: Delivery vs time at 600 bar, 1100μs duration

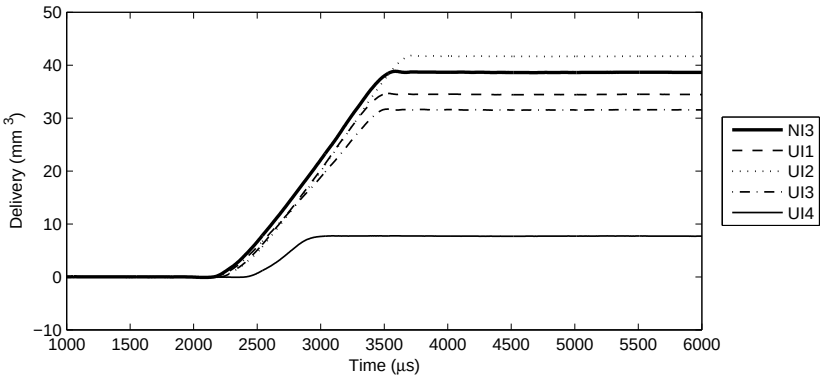

Figure C.128: Delivery vs time at 600 bar, 1200μs duration

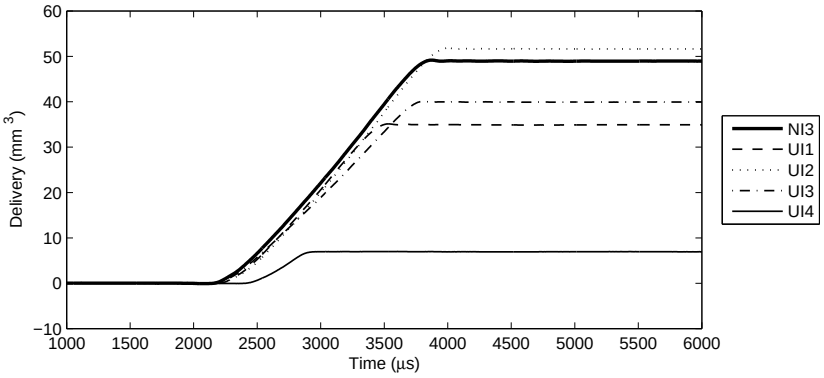

Figure C.129: Delivery vs time at 600 bar, 1500μs duration

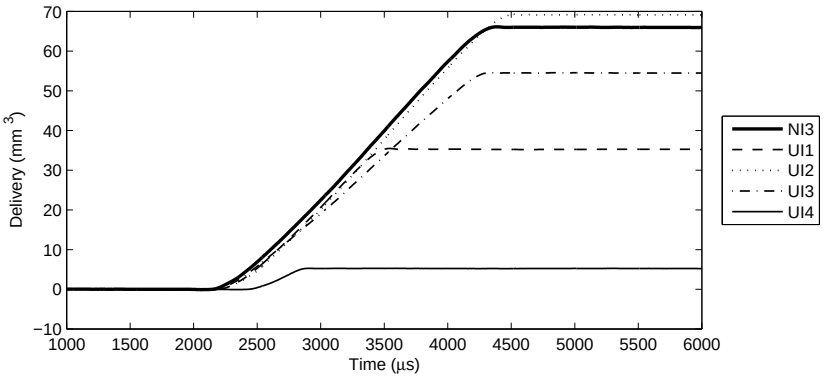

Figure C.130: Delivery vs time at 600 bar, 2000μs duration

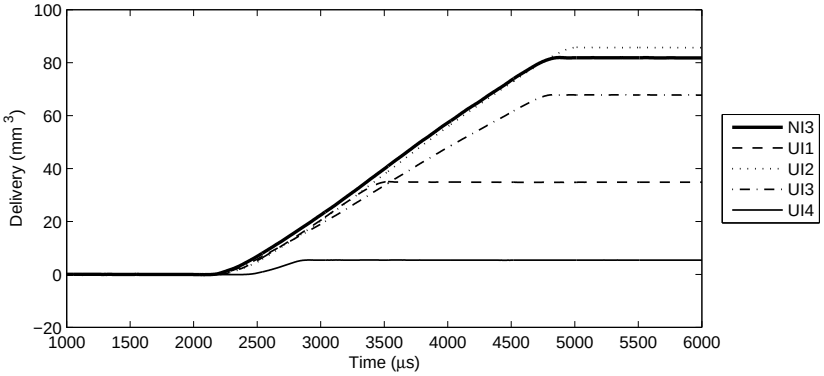

Figure C.131: Delivery vs time at 600 bar, 2500μs duration

C.2.3 900 bar Results

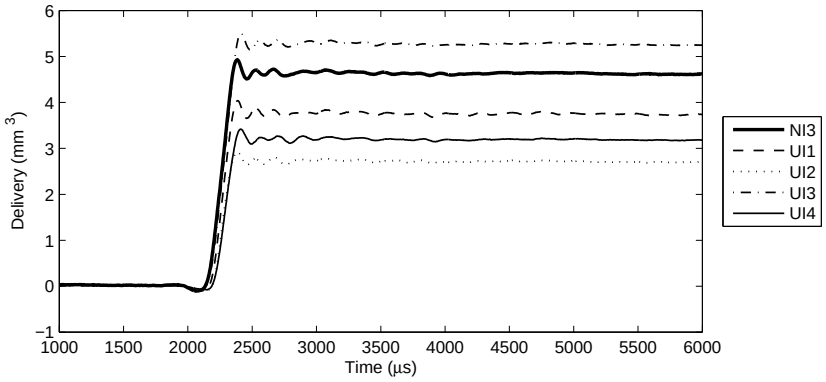

Figure C.132: Delivery vs time at 900 bar, 300μs duration

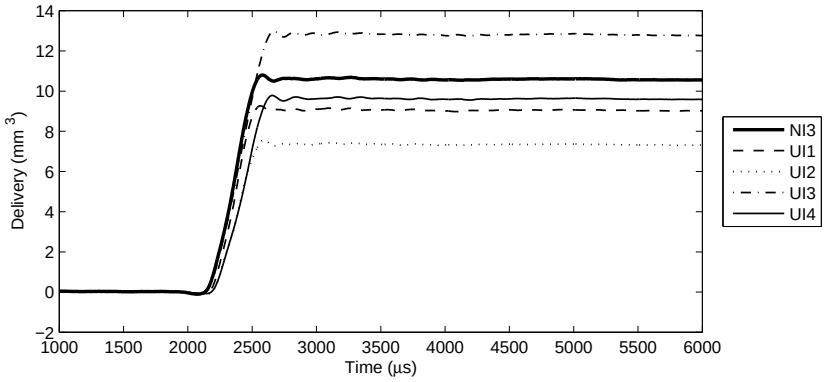

Figure C.133: Delivery vs time at 900 bar, 400μs duration

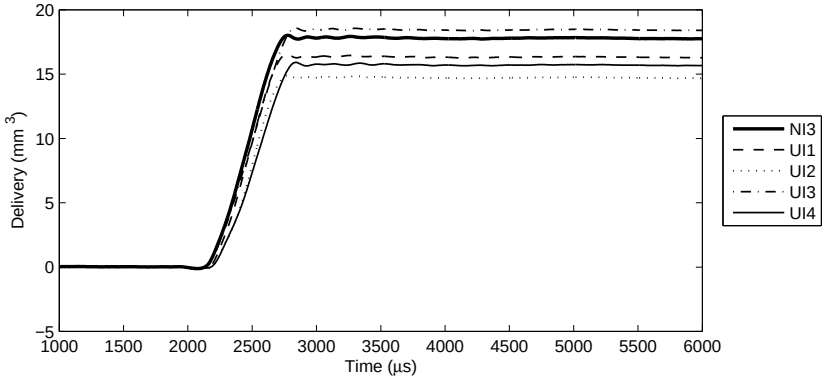

Figure C.134: Delivery vs time at 900 bar, 500μs duration

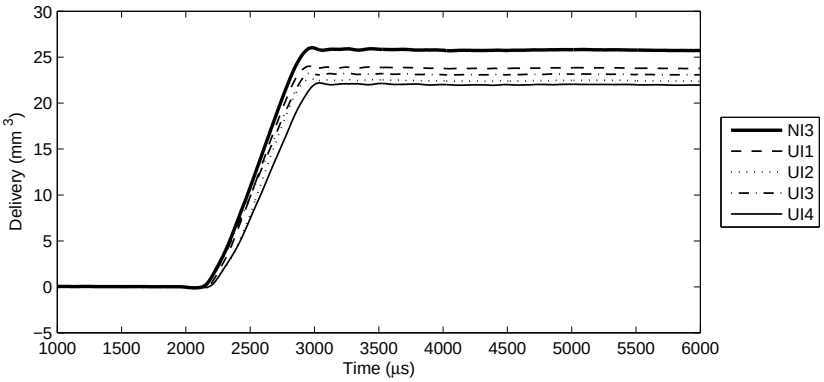

Figure C.135: Delivery vs time at 900 bar, 600μs duration

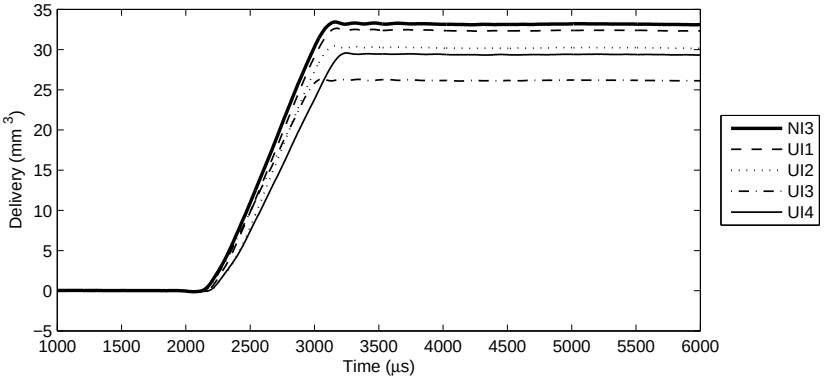

Figure C.136: Delivery vs time at 900 bar, 700μs duration

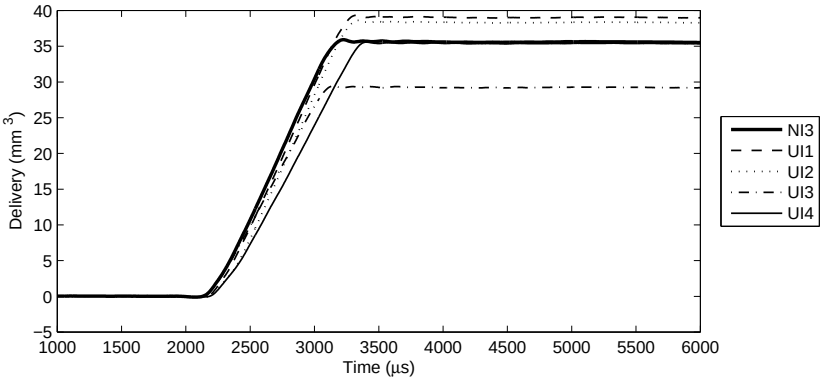

Figure C.137: Delivery vs time at 900 bar, 800μs duration

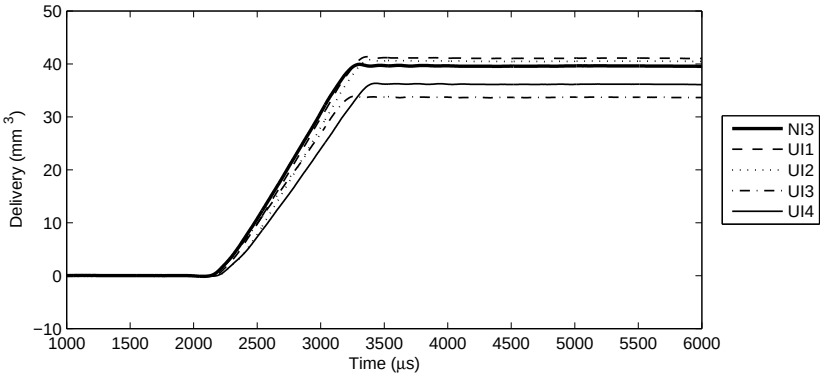

Figure C.138: Delivery vs time at 900 bar, 900μs duration

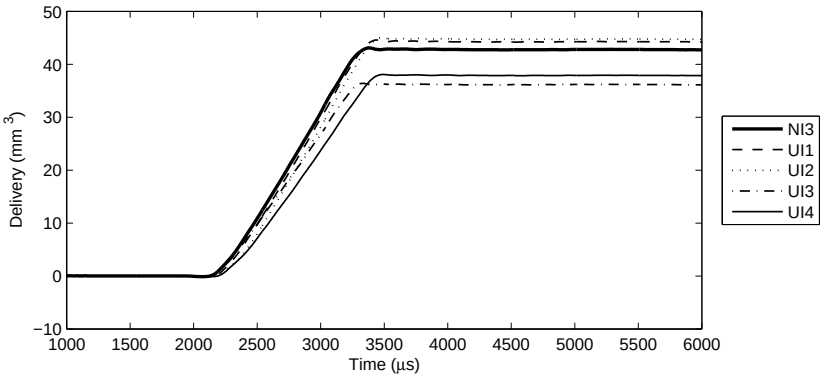

Figure C.139: Delivery vs time at 900 bar, 1000μs duration

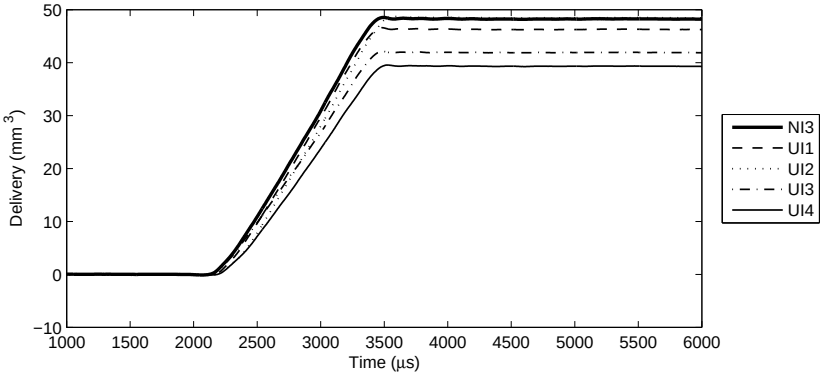

Figure C.140: Delivery vs time at 900 bar, 1100μs duration

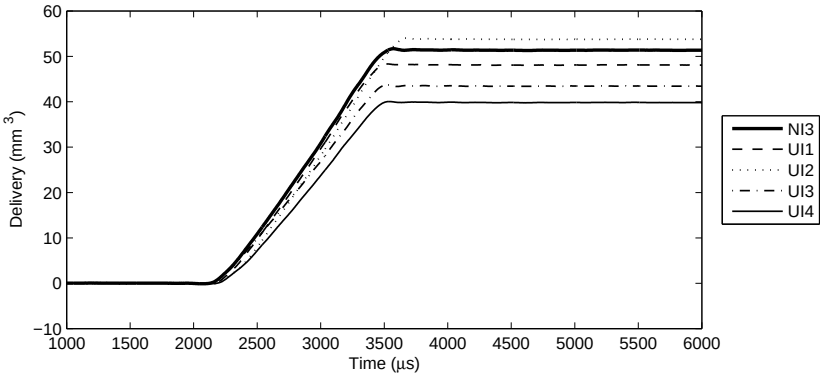

Figure C.141: Delivery vs time at 900 bar, 1200μs duration

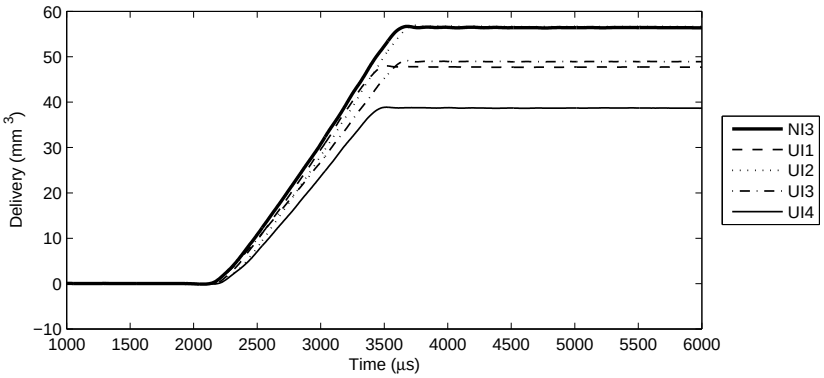

Figure C.142: Delivery vs time at 900 bar, 1300μs duration

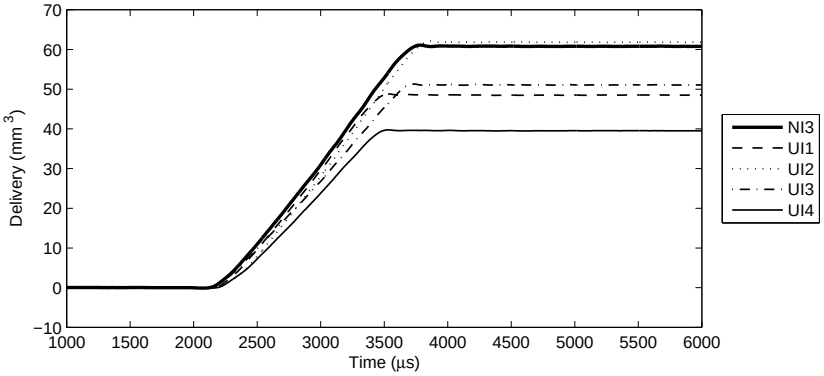

Figure C.143: Delivery vs time at 900 bar, 1400μs duration

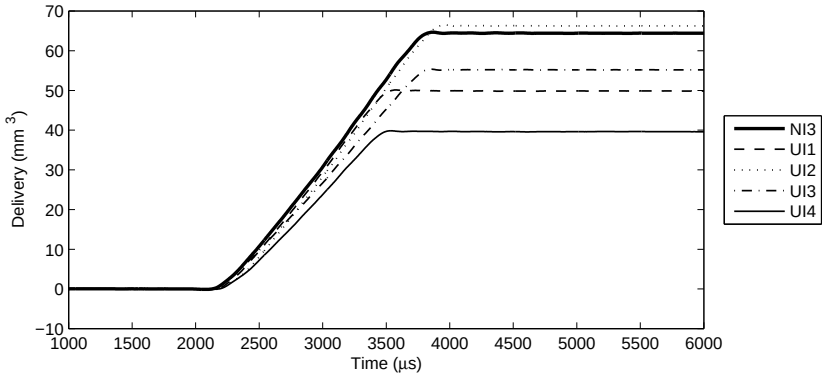

Figure C.144: Delivery vs time at 900 bar, 1500μs duration

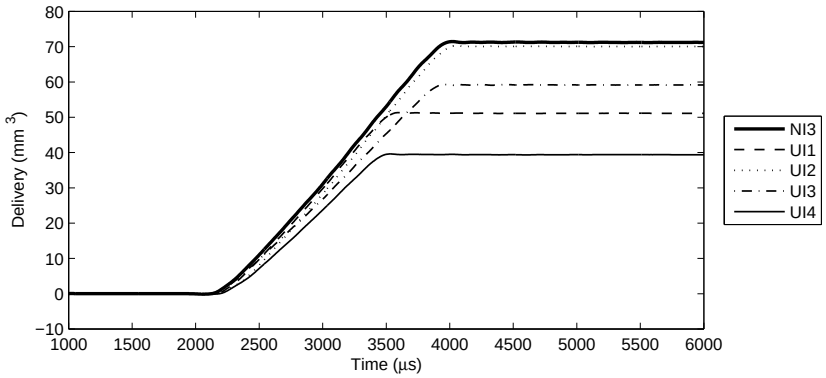

Figure C.145: Delivery vs time at 900 bar, 1600μs duration

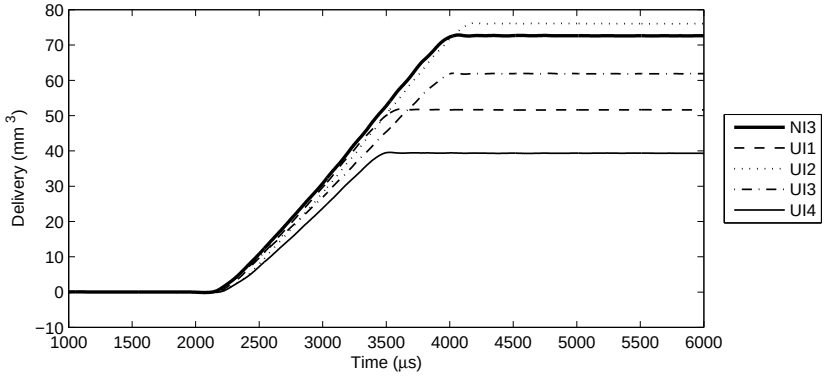

Figure C.146: Delivery vs time at 900 bar, 1700μs duration

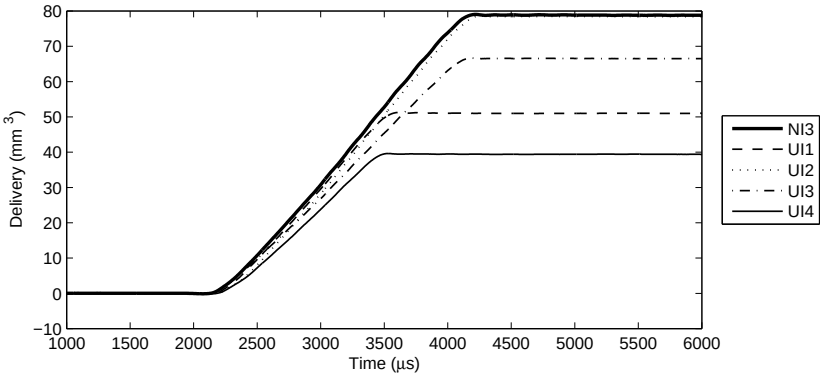

Figure C.147: Delivery vs time at 900 bar, 1800μs duration

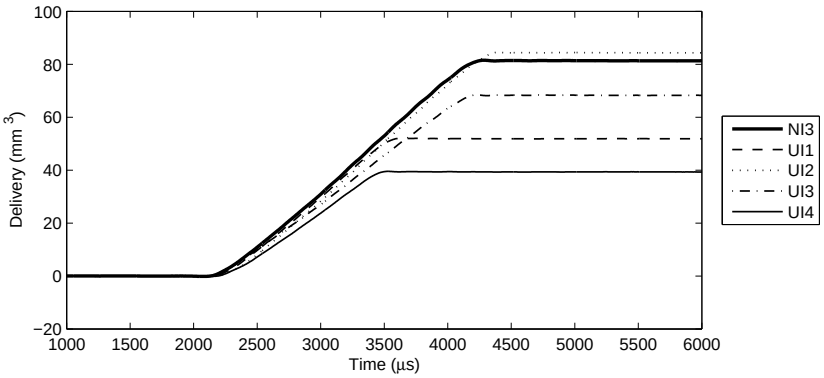

Figure C.148: Delivery vs time at 900 bar, 1900μs duration

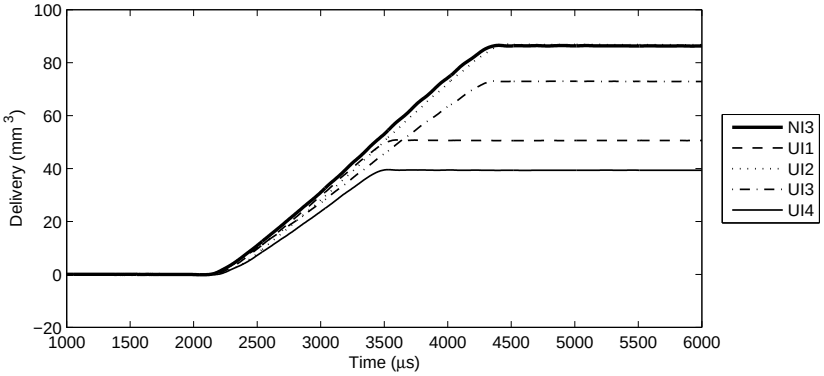

Figure C.149: Delivery vs time at 900 bar, 2000μs duration

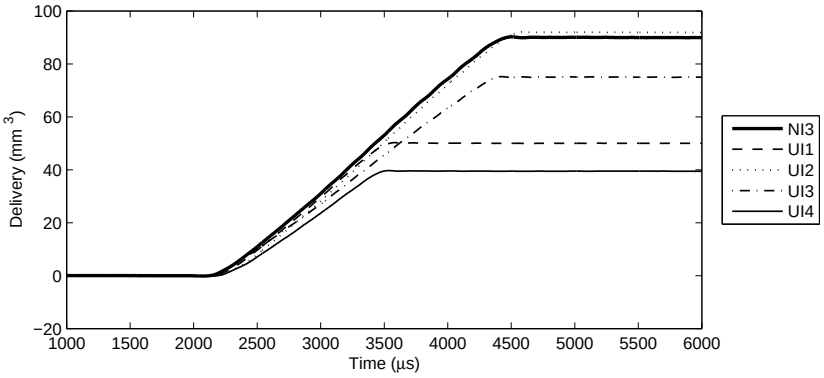

Figure C.150: Delivery vs time at 900 bar, 2100μs duration

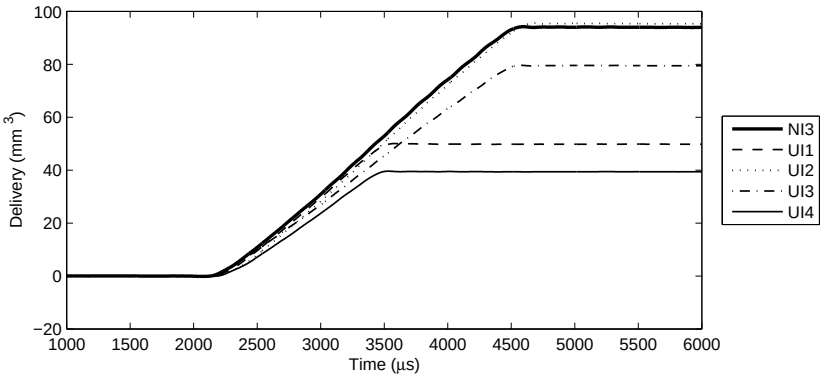

Figure C.151: Delivery vs time at 900 bar, 2200μs duration

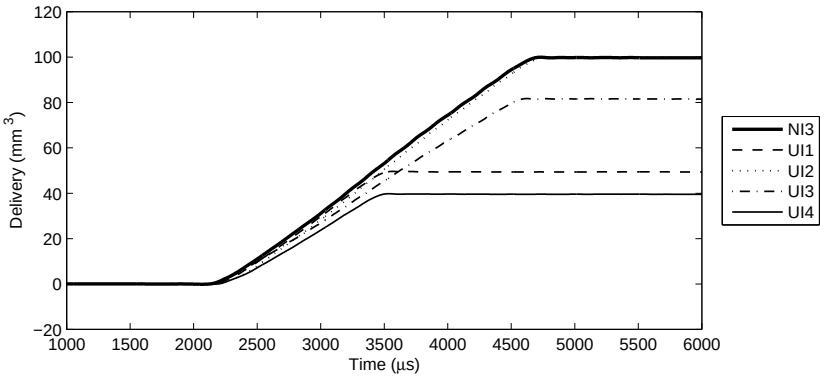

Figure C.152: Delivery vs time at 900 bar, 2300μs duration

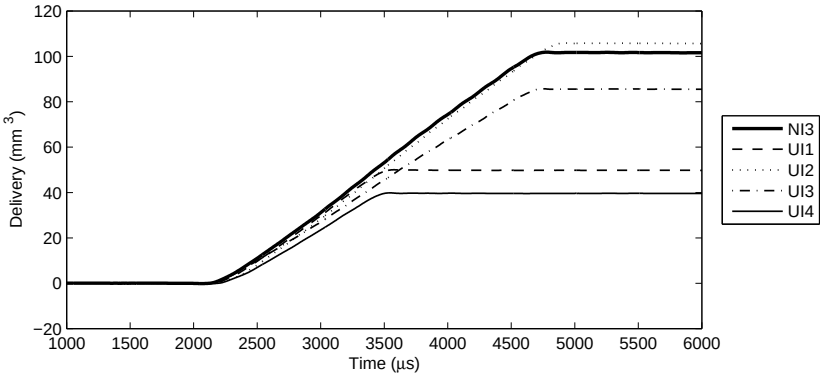

Figure C.153: Delivery vs time at 900 bar, 2400μs duration

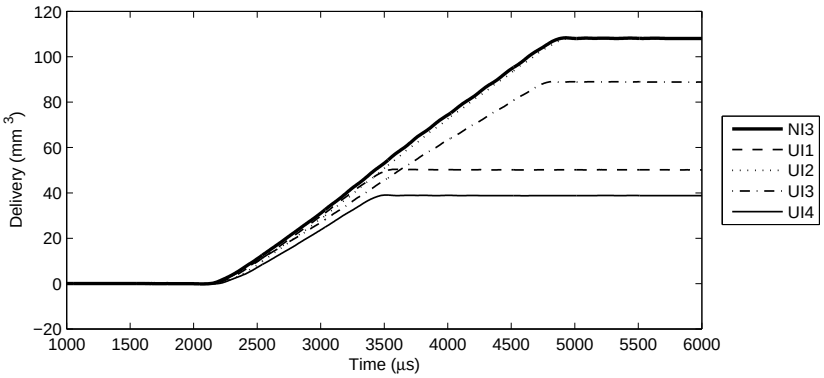

Figure C.154: Delivery vs time at 900 bar, 2500μs duration

C.2.4 1200bar Results

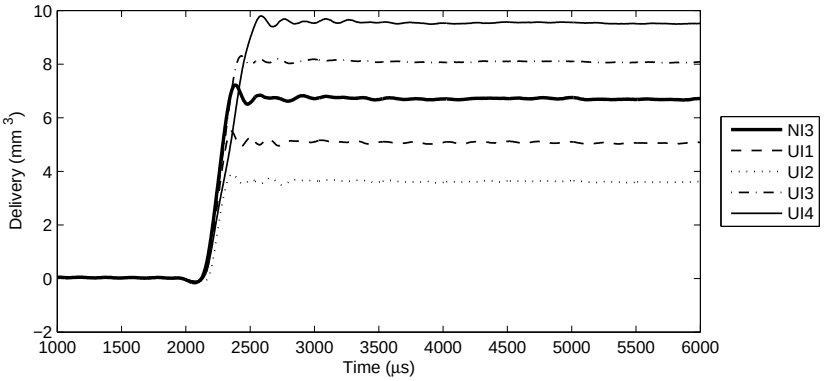

Figure C.155: Delivery vs time at 1200 bar, 300μs duration

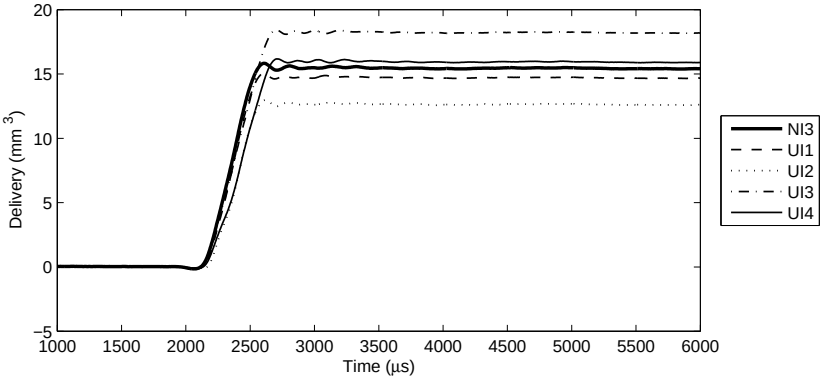

Figure C.156: Delivery vs time at 1200 bar, 400μs duration

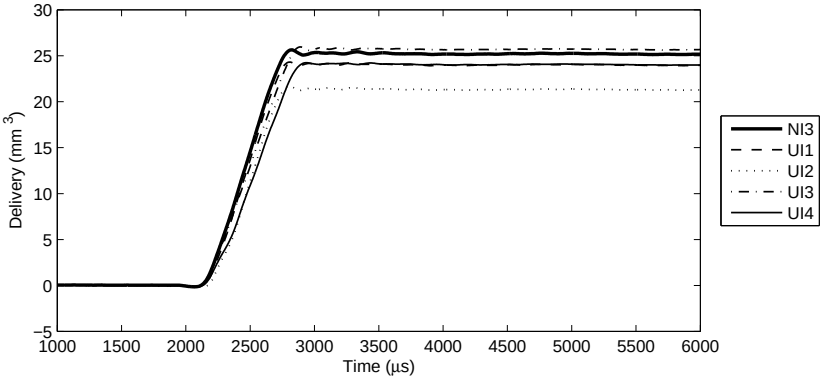

Figure C.157: Delivery vs time at 1200 bar, 500μs duration

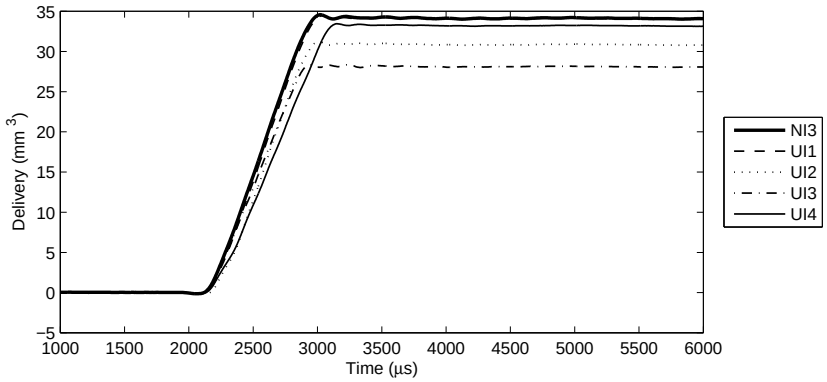

Figure C.158: Delivery vs time at 1200 bar, 600μs duration

Figure C.159: Delivery vs time at 1200 bar, 700μs duration

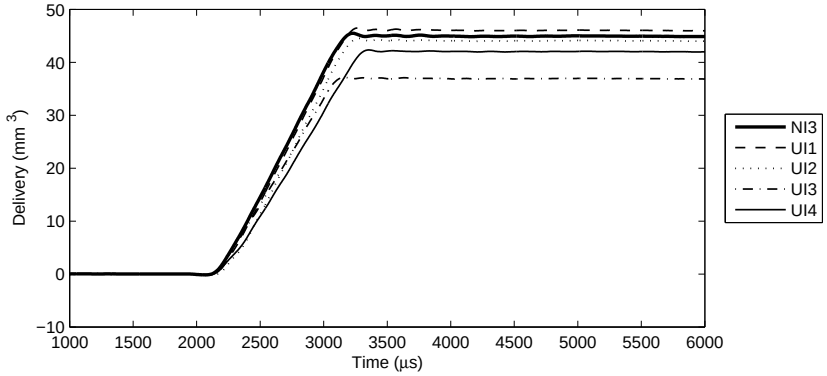

Figure C.160: Delivery vs time at 1200 bar, 800μs duration

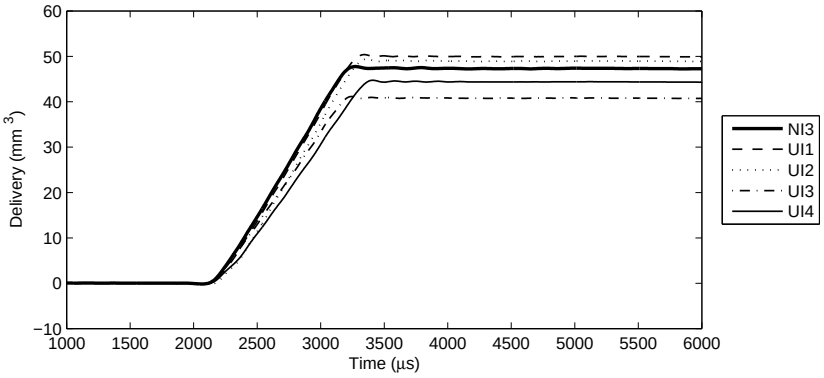

Figure C.161: Delivery vs time at 1200 bar, 900μs duration

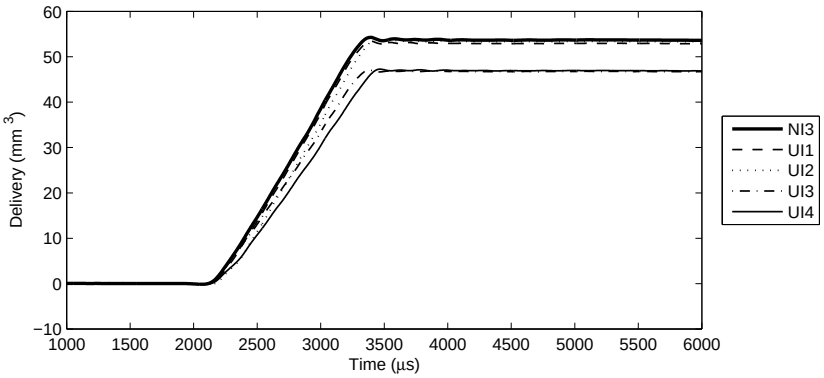

Figure C.162: Delivery vs time at 1200 bar, 1000μs duration

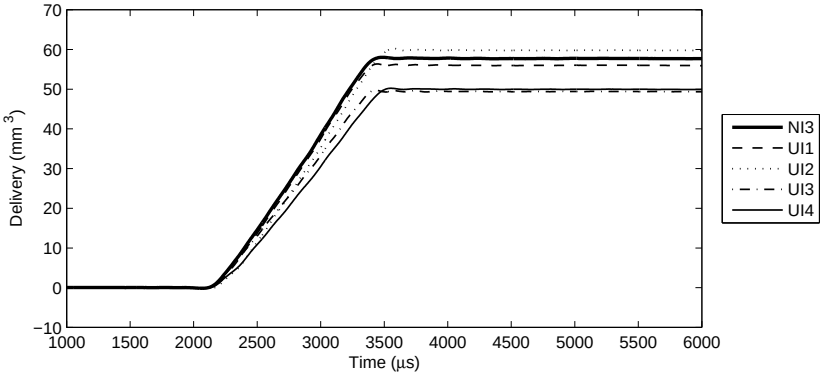

Figure C.163: Delivery vs time at 1200 bar, 1100μs duration

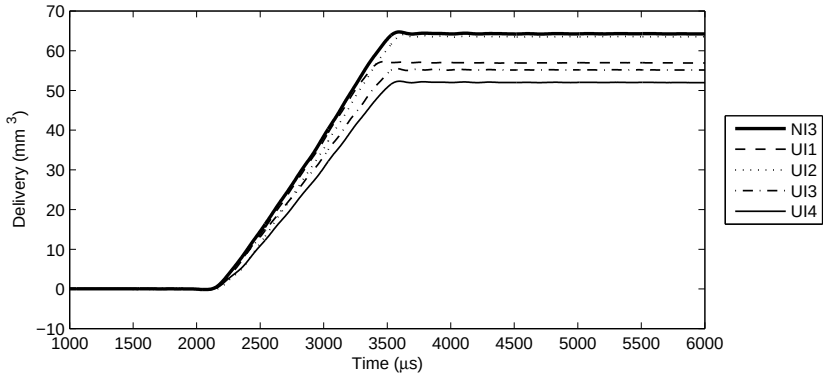

Figure C.164: Delivery vs time at 1200 bar, 1200μs duration

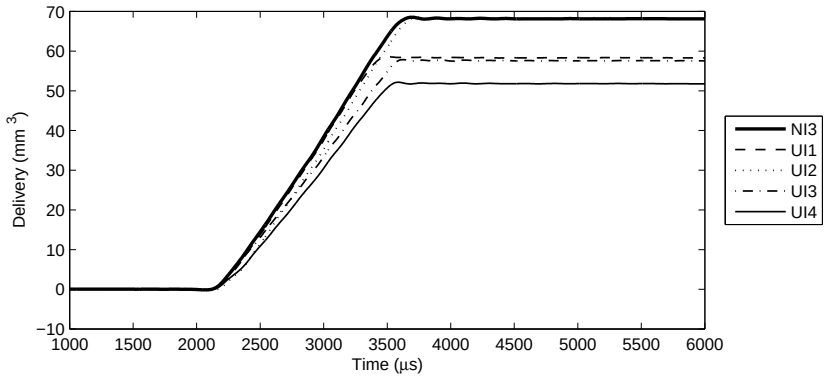

Figure C.165: Delivery vs time at 1200 bar, 1300μs duration

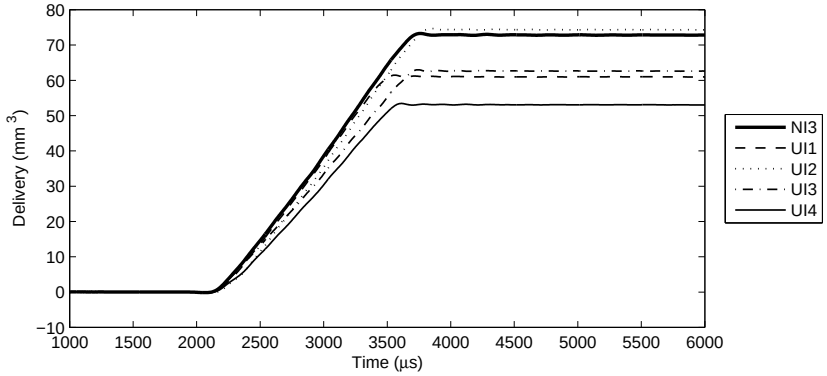

Figure C.166: Delivery vs time at 1200 bar, 1400μs duration

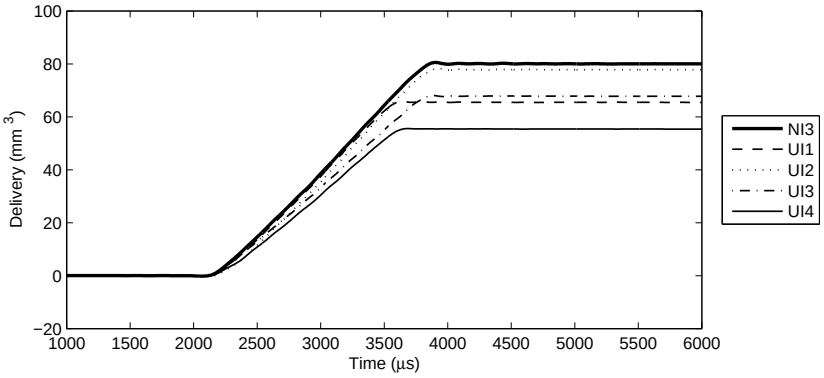

Figure C.167: Delivery vs time at 1200 bar, 1500μs duration

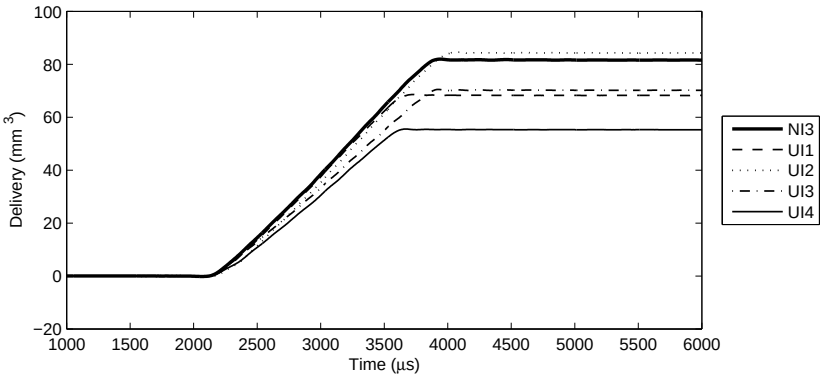

Figure C.168: Delivery vs time at 1200 bar, 1600μs duration

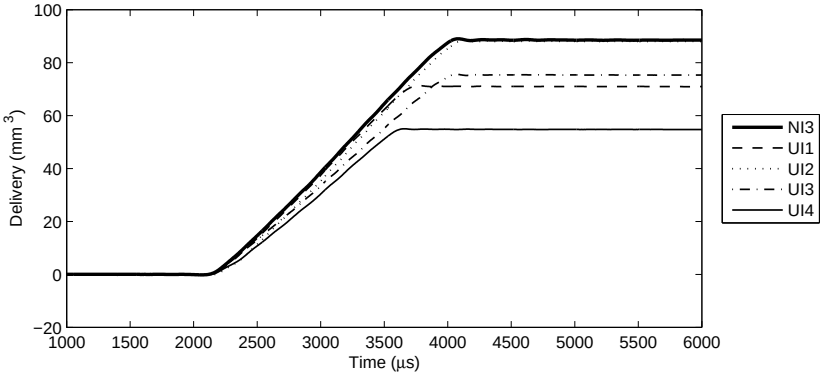

Figure C.169: Delivery vs time at 1200 bar, 1700μs duration

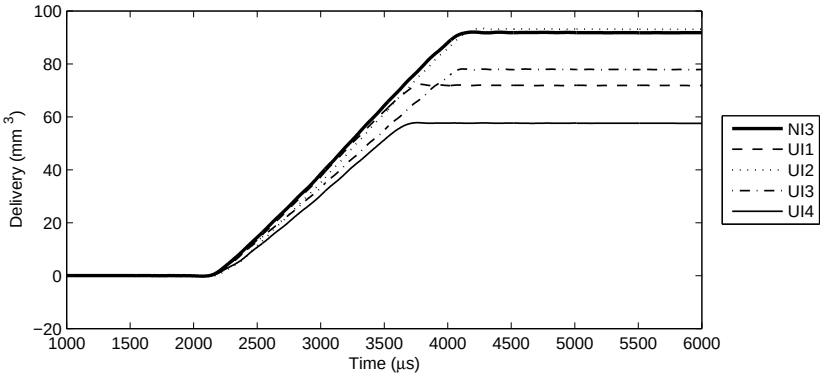

Figure C.170: Delivery vs time at 1200 bar, 1800μs duration

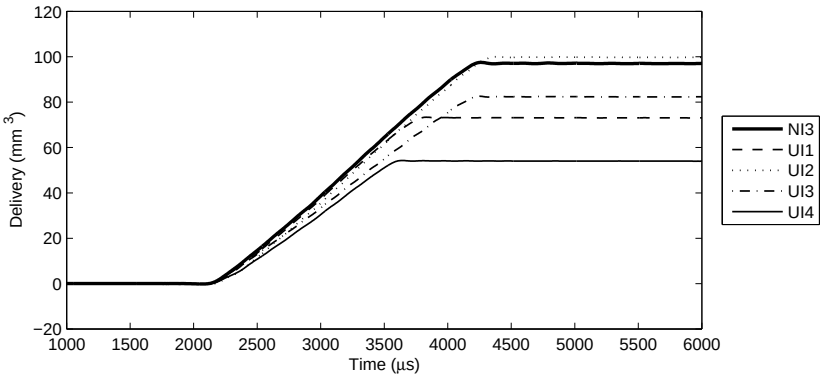

Figure C.171: Delivery vs time at 1200 bar, 1900μs duration

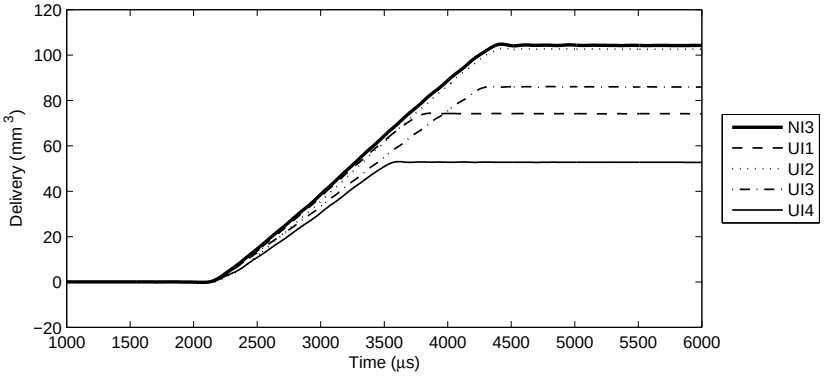

Figure C.172: Delivery vs time at 1200 bar, 2000μs duration

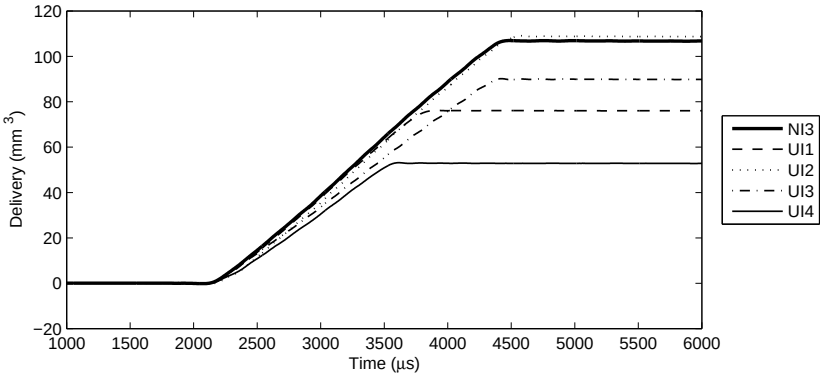

Figure C.173: Delivery vs time at 1200 bar, 2100μs duration

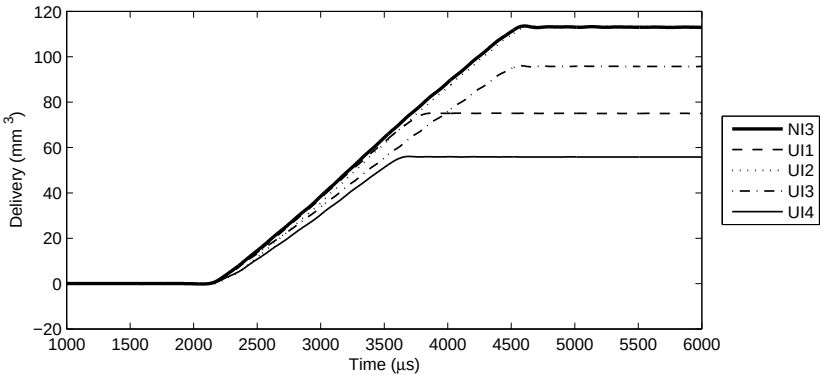

Figure C.174: Delivery vs time at 1200 bar, 2200μs duration

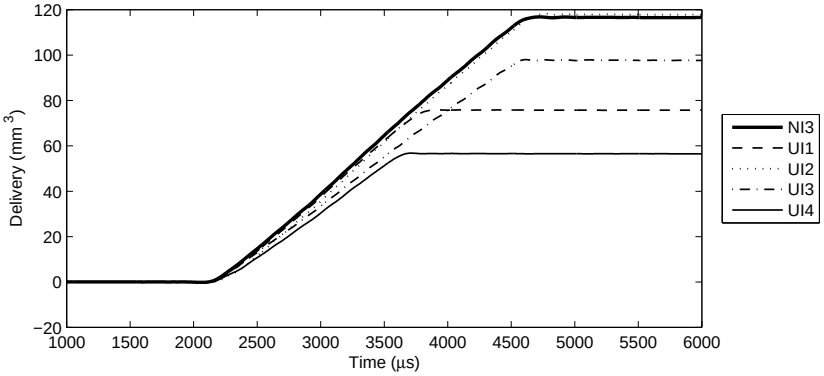

Figure C.175: Delivery vs time at 1200 bar, 2300μs duration

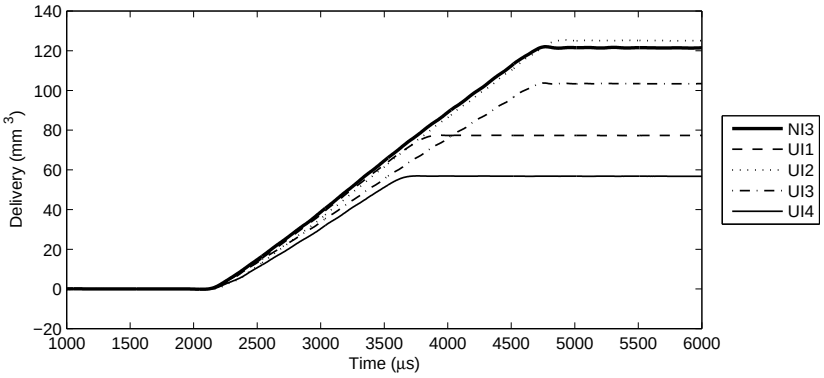

Figure C.176: Delivery vs time at 1200 bar, 2400μs duration

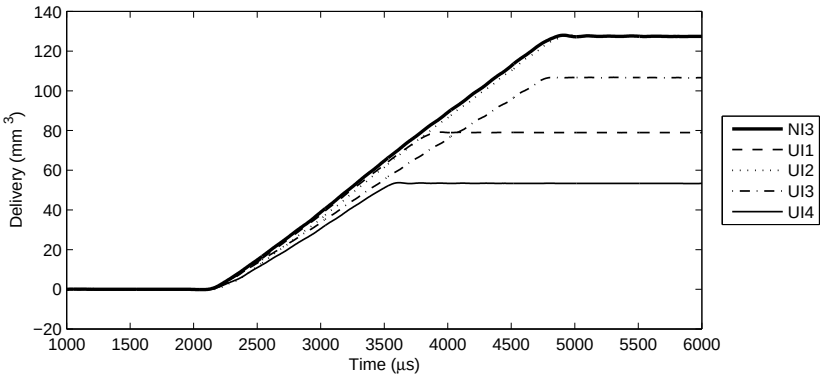

Figure C.177: Delivery vs time at 1200 bar, 2500μs duration

C.2.5 1400bar Results

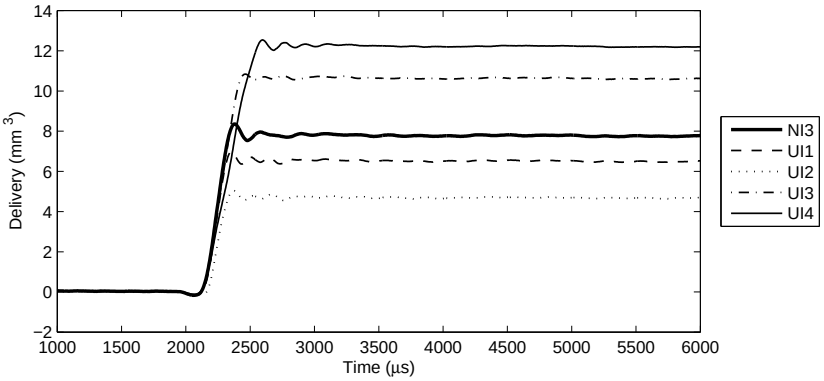

Figure C.178: Delivery vs time at 1400 bar, 300μs duration

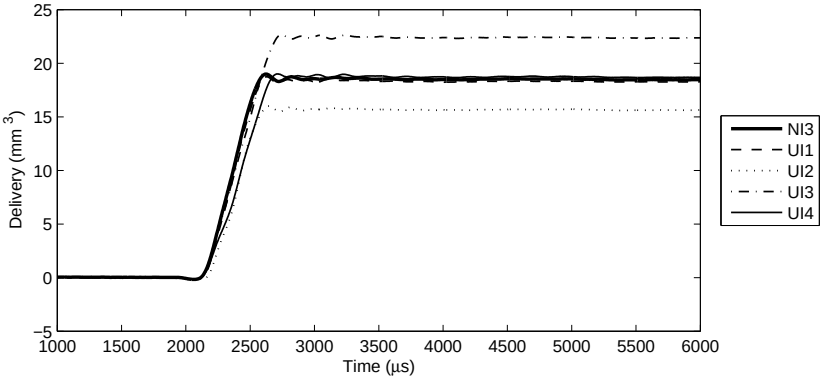

Figure C.179: Delivery vs time at 1400 bar, 400μs duration

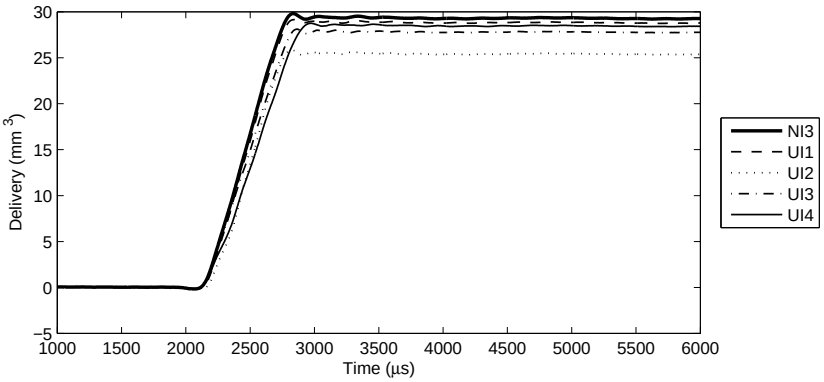

Figure C.180: Delivery vs time at 1400 bar, 500μs duration

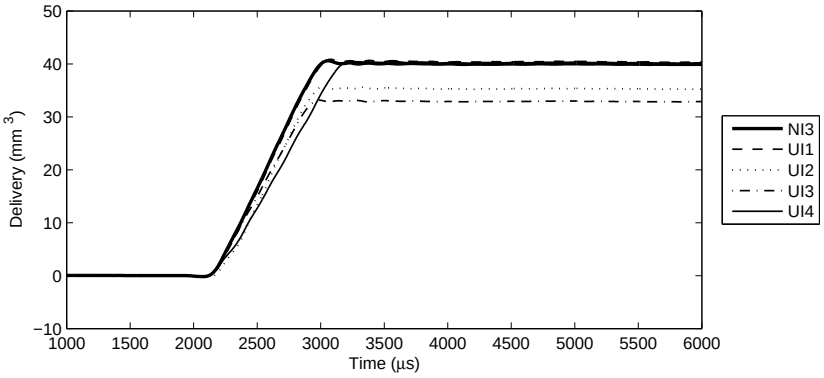

Figure C.181: Delivery vs time at 1400 bar, 600μs duration

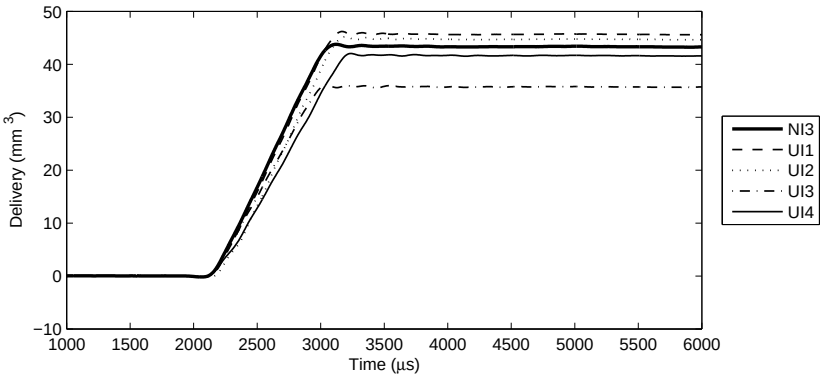

Figure C.182: Delivery vs time at 1400 bar, 700μs duration

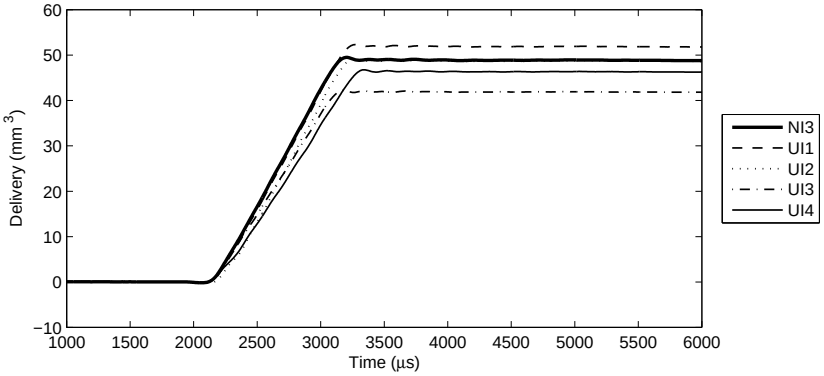

Figure C.183: Delivery vs time at 1400 bar, 800μs duration

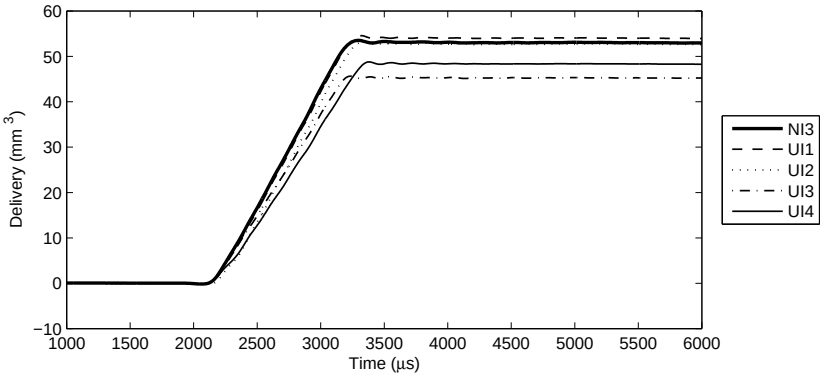

Figure C.184: Delivery vs time at 1400 bar, 900μs duration

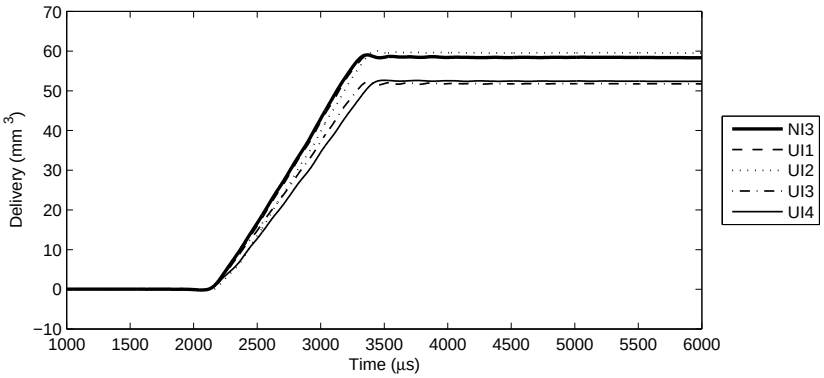

Figure C.185: Delivery vs time at 1400 bar, 1000μs duration

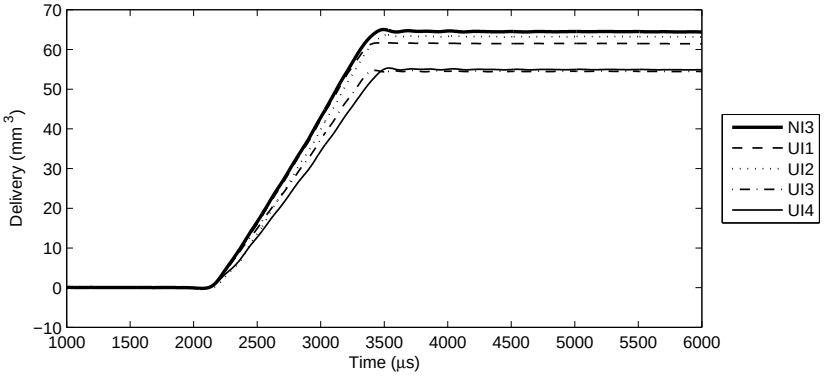

Figure C.186: Delivery vs time at 1400 bar, 1100μs duration

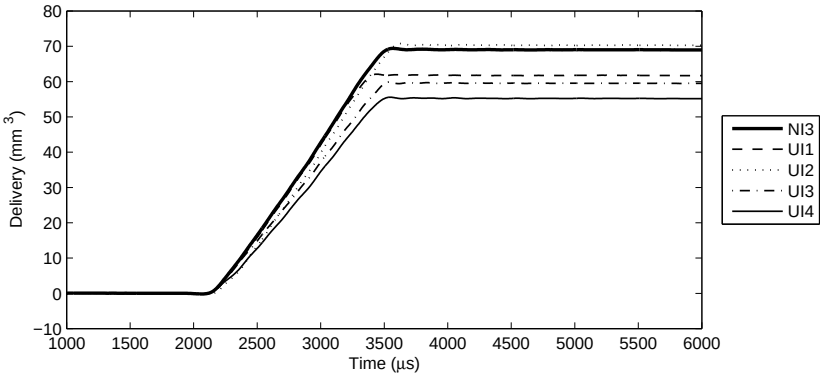

Figure C.187: Delivery vs time at 1400 bar, 1200μs duration

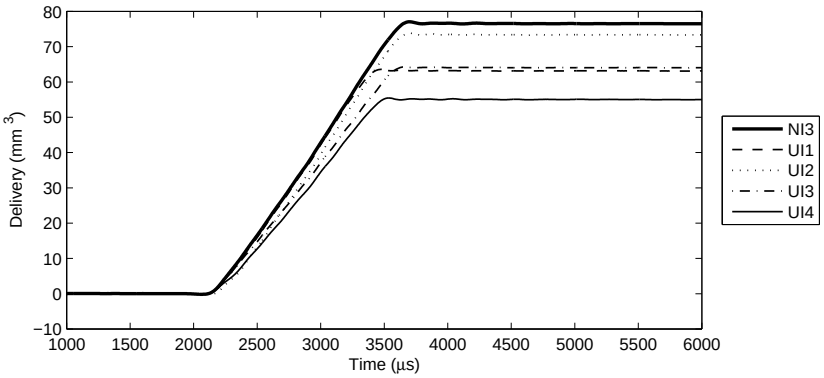

Figure C.188: Delivery vs time at 1400 bar, 1300μs duration

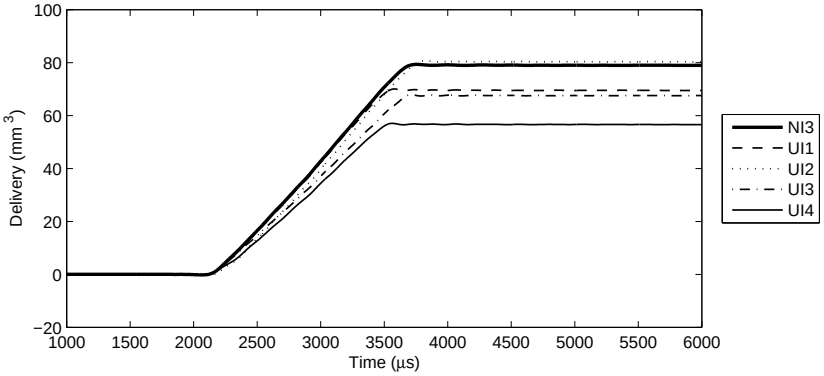

Figure C.189: Delivery vs time at 1400 bar, 1400μs duration

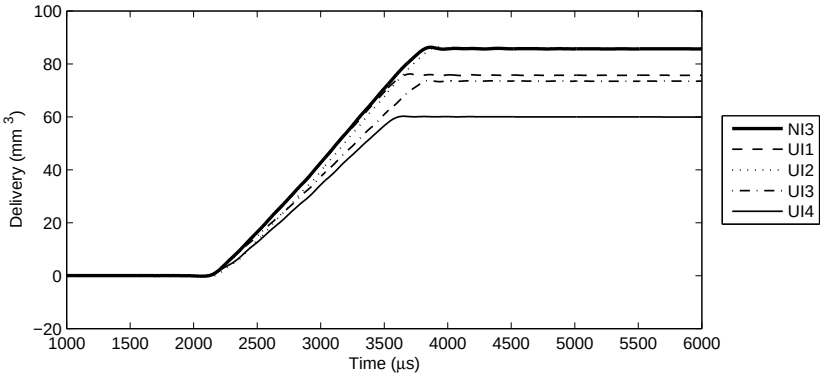

Figure C.190: Delivery vs time at 1400 bar, 1500μs duration

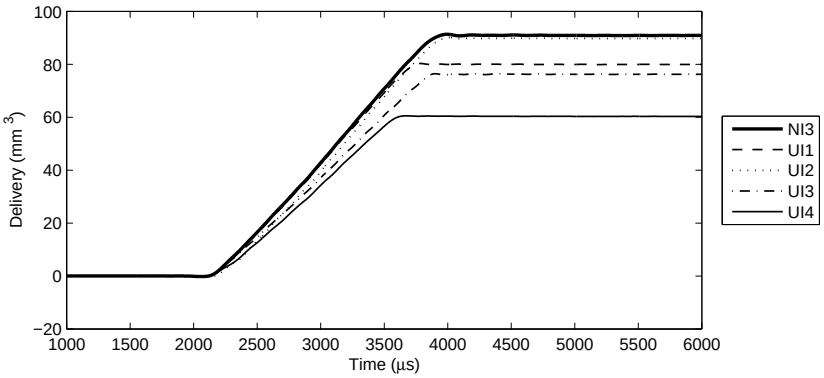

Figure C.191: Delivery vs time at 1400 bar, 1600μs duration

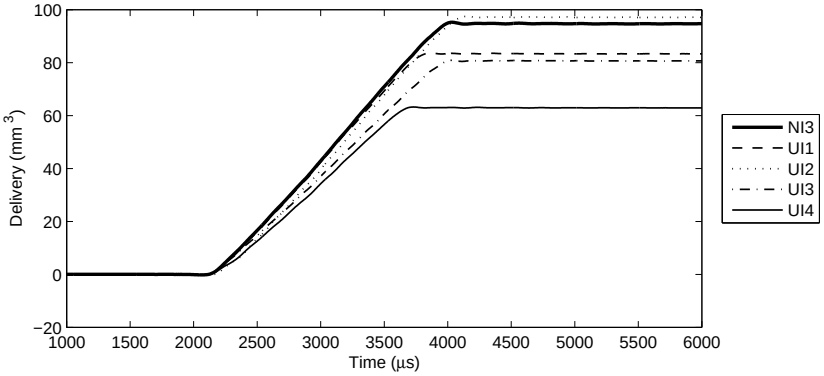

Figure C.192: Delivery vs time at 1400 bar, 1700μs duration

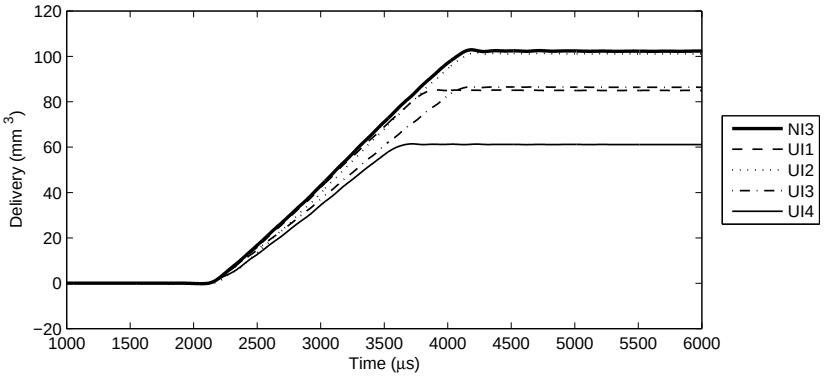

Figure C.193: Delivery vs time at 1400 bar, 1800μs duration

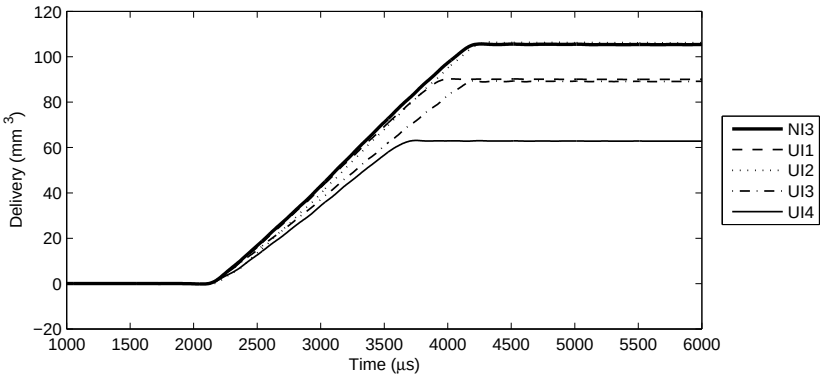

Figure C.194: Delivery vs time at 1400 bar, 1900μs duration

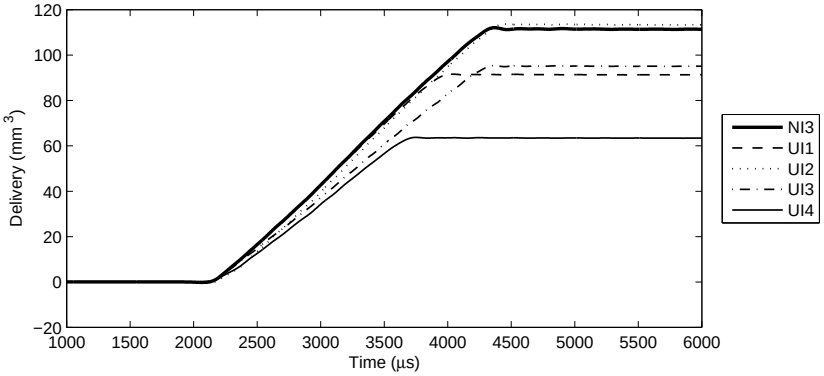

Figure C.195: Delivery vs time at 1400 bar, 2000μs duration

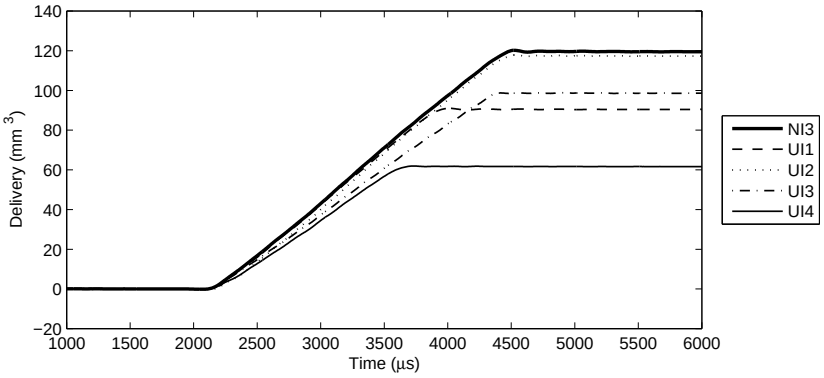

Figure C.196: Delivery vs time at 1400 bar, 2100μs duration

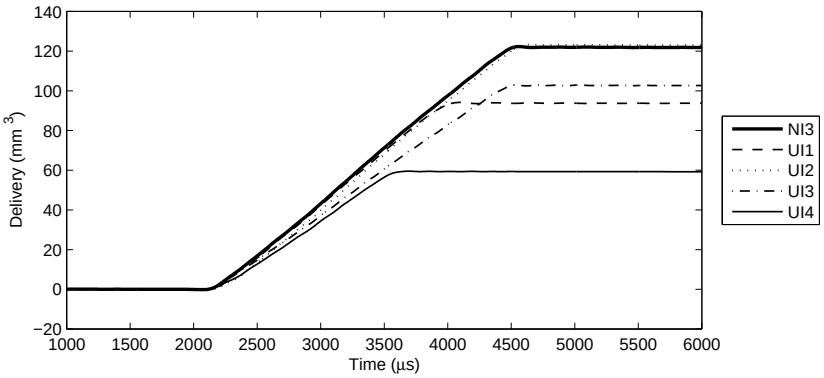

Figure C.197: Delivery vs time at 1400 bar, 2200μs duration

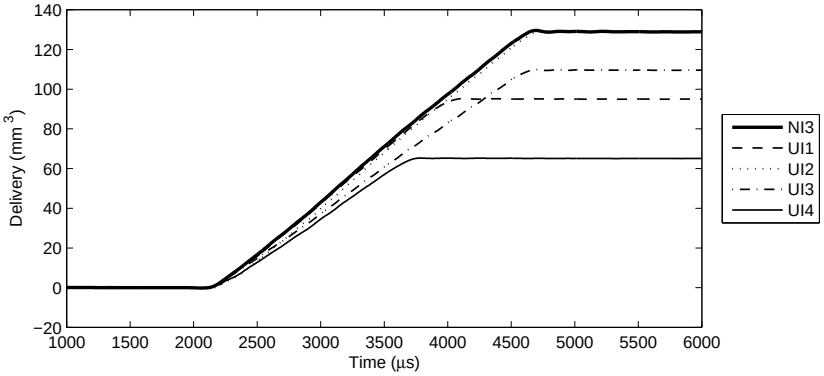

Figure C.198: Delivery vs time at 1400 bar, 2300μs duration

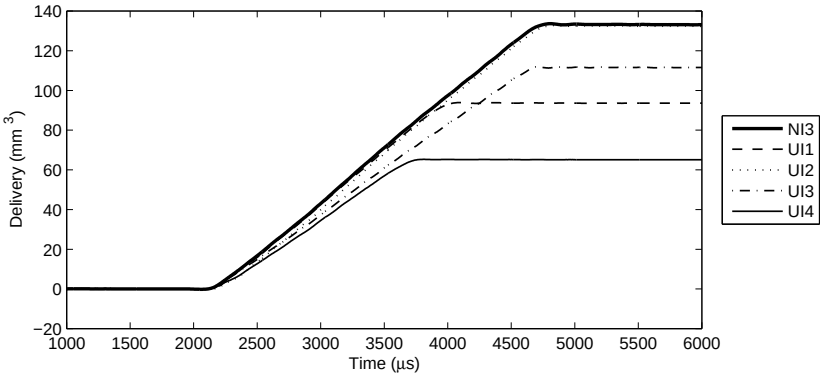

Figure C.199: Delivery vs time at 1400 bar, 2400μs duration

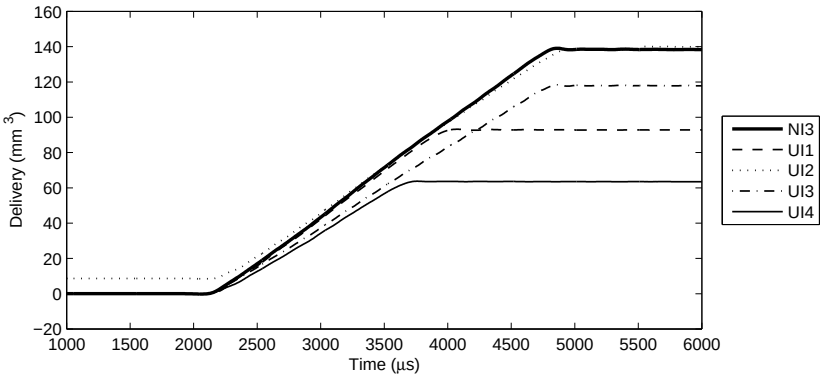

Figure C.200: Delivery vs time at 1400 bar, 2500μs duration